THE UNIVERSITY *of* EDINBURGH

The Molecular and Functional Characterisation of the Adherent Properties of H7 Flagella

Eliza Briony Kate Wolfson

THE UNIVERSITY *of* EDINBURGH

Doctor of Philosophy

The University of Edinburgh

2012

DECLARATION

I declare that this thesis and the experiments described therein are my own work unless otherwise indicated, acknowledged or referenced. No part of this thesis has been or will be submitted for any other degree or qualification at this or any other university.

Eliza Wolfson, December 2012

ABSTRACT

Enterohaemorrhagic *Escherichia coli* (EHEC) have recently emerged as significant zoonotic pathogens. O157:H7 is one of the most common EHEC serotypes associated with human disease, which is transmitted faeco-orally from a bovine reservoir. EHEC O157:H7 preferentially colonises the bovine terminal rectum (BTR). Injection of virulence factors by type-III secretion is necessary for colonisation of cattle and results in re-modelling of the host cytoskeleton. Flagella machinery is evolutionarily related to the Type III secretion apparatus and O157 strains lacking H7 flagella show reduced adherence to the BTR. Vaccination with FliC, the main component of H7 flagella, has the potential to protect cattle against *E. coli* O157:H7 infection. The focus of this work was to investigate the molecular basis for H7 flagella binding to the BTR, in order to understand the basis for $FliC_{H7}$ being an immuno-protective antigen. H7 flagella were shown to adhere across the surface and penetrate into BTR epithelial cells. Both the FliC shaft and the FliD cap components of flagella filaments showed the capacity to adhere to BTR epithelial cells. Preliminary studies indicate that the current $FliC_{H7}$ vaccination of cattle results in FliD-specific antibodies where oral challenge with O157:H7 does not. FliD is more conserved than $FliC_{H7}$, which contains a predicted 88aa structural insertion, but variation occurs along the full length of the FliD protein. There was no evidence for post-translational modification of $FliC_{H7}$. A number of actin binding proteins were identified as potential FliC and FliD binding partners from BTR epithelial cell lysates. From this, a panel of purified galectin-4, cofilin-1 and βγ-actin was used to compare binding of flagella from different pathogens. H7 flagella bound more to cofilin-1 than βγ-actin, whereas phase-1 and phase-2 flagella from *Salmonella* Typhimurium bound more to βγ-actin, than to cofilin-1. Size-exclusion chromatography indicated that cofilin-1 alters H7 flagella filament polymerisation dynamics. αβ-ctin polymerisation and depolymerisation experiments indicate that H7, phase-1 and phase-2 flagella interactions with actin affect actin dynamics.

ACKNOWLEDGEMENTS

First of all, thanks for all the chat. I've found the ideas really exciting. So thanks David Gally for inspiring me, Arvind Mahajan and anyone else who would let me bend their ear (quite a few people if I were to list them here).

Secondly, there has been a whole lot of technical assistance – to get me going in the lab (Allen, Dai, Sean and Jai), to make me feel welcome (LBEP, MPRL, CTVM crews for tea and biscuits) and to give me advice. I am indebted to Darren Shaw for his advice on statistical analyses, Trudie Gillespie for her confocal expertise, Andy Gill for his size exclusion fun times, Sutherland Maciver for getting to know Cofilin, Jo Stevens for her lovely actin polymerisation assay, Tom McNeilly for his bovine sera and advice, Edith Paxton for her wily ways with cells and handy hints, Jo Elvidge for curly horses and more, Kermit, Bertie and Dash and my friends who dragged me across the finish line – I couldn't have done this without all those people feeding me!

Thirdly, I would like to acknowledge my funders, the BBSRC and Novartis Animal Health for this CASE studentship – it was a great opportunity and hopefully worth the dosh. Also, Funds for Women Graduates awarded me with an emergency grant in 2012 and this was very gratefully received.

Hopefully I haven't forgotten anyone on these fronts. Quite a lot has happened to me and my family over the past 4 years, but I am very grateful to have the family and friends I have – they make me feel very lucky. So thanks to them all, and maybe one day I'll pretend to grow up…

TABLE OF CONTENTS

LIST OF FIGURES

LIST OF TABLES

LIST OF ABBREVIATIONS USED

°C Degrees Celsius

1y Primary

A Absorbance

A/E Attaching and effacing

aa Amino acid

AAF Aggregative adherence fimbrae

ABP Actin binding protein

ABPR Actin binding protein regulator

ACT Actin

ADP Adenosine diphosphate

AEEC Attaching and effacing Escherichia coli

AggR Regulator of AAF

ALB LB containing ampicillin

amp Ampicillin

ARF ADP-ribosylation factor

ATCC American type culture collection

ATP Adenosine triphosphate

AUC Area under curve

B1 Bleed 1

B2 Bleed 2

B3 Bleed 3

BBSRC Biotechnology and biological sciences research council

BCA Bicinchoninic acid

BFP Bundle forming pili

bp Base pairs

BSA Bovine serum albumin

BTR Bovine terminal rectum

BTRE Bovine terminal rectum epithelium/ epithelial

C Carboxy

IMPACT Confocal imaging facility

cam Chloramphenicol

cAMP Cyclic-adenosine monophosphate

CARD Caspase recruitment domain

CDS Coding sequence

CFA Colonisation Factor Antigen

CFL Cofilin

cGMP Cyclic-GMP

CL Cell lysate

CLB LB containing chloramphenicol

CnBr Cyanogen bromide

CNF1 Cytotoxic necrotising factor 1

D0 Structural domain 0

D1 Structural domain 1

D2 Structural domain 2

D3 Structural domain 3

DAEC Diffuse-adherent Escherichia coli

DAF Decay accelerating factor

DAPI 4',6-diamidino-2-phenylindole

DH-PH Dbl homology-Pleckstrin homology domains

DIG Digoxigenin-3-0-succinyl-ϵ-aminocaproic acid hydrazide

DMEM Dulbecco's minimum essential medium

DNA Deoxyribose nucleic acid

DTT Dithiothreitol

EAEC Entero-aggregative Escherichia coli

EBL Embryonic bovine lung

EBP50 ERM-binding phosphoprotein 50

ECDC European centre for disease prevention and control

ECL Enhanced chemiluminescence

EDTA Ethylenediaminetetraacetic acid

EHEC Enterohaemorrhagic Escherichia coli

Ehx Enterohaemolysin

EIEC Entero-invasive Escherichia coli

ELISA Enzyme-linked immuno-sorbent assay

EPEC Enteropathogenic Escherichia coli

ERM Ezrin/radixin/moesin

ETD Estimated time of departure

ETEC Entero-toxigenic Escherichia coli

ExPEC Extra-intestinal Escherichia coli

FAK Focal adhesion kinase

FBS Foetal bovine serum

FFAS03 Fold & Function Assignment Server 03

FITC Fluorescein isothiocynate

GAL Galectin-4

GAP Guanine activating protein

Gb3 Globotriaosylceramide

GDP Guanine diphosphate

GEF Guanine nucleotide exchange factor

GSN Gelsolin

GTP Guanine triphosphate

h Hour(s)

HACCP Hazard Analysis and Critical Control Point

HAP Hook-associated adaptor protein

HBB Hook basal body

HBSS Hank's balanced salt solution

HCP Haemorrhagic coli pilus

HEp-2 Human epidermoid cancer cells

HEPES Hydroxyethyl-Piperazine Ethanesulafonic Acid

HPLC High performance liquid chromatography

HRP Horseradish peroxidase

HUS Haemolytic uraemic syndrome

ICE Interleukin-1 converting enzyme

Ig Immunoglobulin

IL Interleukin

IM Inner Membrane

IPTG Isopropyl-β-D-thiogalactoside

IUB International union of biochemistry

JNK c-Jun N-terminal kinase

kan Kanamycin

Kb Kilo-base of DNA

kDa Kilo-Dalton

KLB LB containing kanamycin

kV Kilo-volts

LB Luria-Bertani

LEE Locus of enterocyte effacement

LIM LIN-11, Isl1 and MEC-3 zinc-finger type domain

LRR Leucine rich repeat

LT Large multi-subunit heat-labile toxin

m/z Mass:charge peaks

MALDI Matrix-assisted laser desorption/ionization

MASCOT Algorithm for protein identification by searching a sequence database using mass spectrometry data

mBCA micro bicinchoninic acid assay

MDa Megadalton

MEM Minimal essential medium

min Minute(s)

MOPS 4-Morpholinepropanesulfonic acid

MS Mass spectrometry

MUSCLE Multiple Sequence Comparison by Log-Expectation for phylogenetic tree estimation

N Amino

Naip Neuronal apoptosis inhibitory protein

NBT/X phosphate 4-nitro blue tetrazolium chloride/5-bromo-4-chloro-3-indolyl-phosphate

Nck NCK SH2/SH3 adaptor protein 1

NetNGlyc Server that predicts N-Glycosylation sites

NetOGlyc Server that produces neural network predictions of mucin type O-glycosylation sites

NF-κB Nuclear factor-κB

N-linked Asparagine-linked glycosylation

NLRC4 NOD-LRR family CARD domain-containing protein 4

NMEC Neonatal meningitis Escherichia coli

NOD Nuclotide oligomerisation domain

N-WASP Neural Wiskott-Aldrich syndrome protein

OD Optical density

OD600 Optical density at 600nm

O-linked Serine/threonine-linked glycosylation

OM Outer membrane

OPD o-phenylenediamine

P1 Phase 1 flagella/flagellin

P2 Phase 2 flagella/flagellin

PAK p21-activated kinase 1

PAMP Pathogenic-associated microbial pattern

PBS Phosphate buffered saline

PBST Dulbecco A PBS with Tween-20

PCR Polymerase chain reaction

PDB Brookhaven Protein Data Bank

pEAF EPEC adherence factor plasmid

PFA Paraformalydehyde

PG Peptidoglycan

PI Pre-immune

PI3K Phosphatidylinositol 4-phosphate 3-kinase

PNGase N-glycanase

PRR Pattern Recognition receptors

PTM Post-translational modification

RBS Ribosomal binding site

ROCK Rho-associated protein kinase

rpm Revolutions per minute

RT Room temperature

SDS Sodium dodecyl sulphate

SDS-PAGE Sodium dodecyl sulphate- polyacrylamide gel electrophoresis

SGLT-1 Sodium/glucose cotransporter 2

ShET-1 Shigella enterotoxin-1

ShET-2 Shigella enterotoxin-2

SOS Bacterial DNA-damage stress resonse

SRP Siderophore receptors and porins

ST Small heat-stable toxin

STEC Shiga toxin-producing Escherichia coli

Stx1 Shiga toxin 1

T3S Type-3 secretion/secreted

T3SS Type-3 secretion system

TBS Tris-buffered saline

Tir Translocated intimin receptor

TLR Toll-like receptor

TNF Tumour necrosis factor

TRITC Rhodamine Iso-Thiocyanate

UCSF Chimera University of California, San Francisco, Chimera software

UPEC Uropathogenic Escherichia coli

V Volts

v/v Volume per volume (%)

VrH7 Variable region of $FliC_{H7}$

VTEC Vero-toxigenic Escherichia coli

w/v Weight per volume (%)

WGA Wheat-germ agglutinin

1: Introduction

Bacterial flagella have fascinated scientists for more than 70 years. Their elegance, utility and complexity have shown that bacteria, previously thought to be very primitive, can be highly adapted to their niches. The flagellar systems of *Escherichia coli* and *Salmonella enterica* subsp. *enterica* serovar Typhimurium have served as paradigms for evolution, assembly and regulation of macromolecular machines, flagellar motility and host innate immunity. Yet despite such intensive study for many decades, there are aspects about these organelles that can still surprise us.

In parallel, advances in molecular biology and genetic engineering have allowed the study of specific contributions of different genes to bacterial pathogenesis. Again, *E. coli* has served as a model organism for studies in commensalism, host adaptation and virulence. In particular, Shiga toxin-producing *E. coli* (STEC) continues to capture the attention of researchers and the public alike with outbreaks of diarrhoeal disease, an increasing proportion of which can be fatal. Barring the large 2011 outbreak of newly emergent STEC O104:H4 in Germany, O157:H7 is the predominant serotype that causes human disease and is transmitted from a ruminant reservoir (Naylor *et al.*, 2005a). Potential control strategies are currently being targeted at the bovine reservoir (McNeilly, 2012; Sargeant *et al.*, 2007).

This study investigates the possible mechanisms of flagellar adherence to bovine cells by STEC O157:H7, with a view to understand why H7 flagella can be a protective immunogen in cattle. In doing so, the intention is to refine which parts of H7 flagella are necessary for this. By bringing this understanding of bacterial pathogenesis together with this model flagella system, it is also hoped that this study will help to establish a new paradigm in flagella-associated bacterial pathogenesis.

1.1 *Escherichia coli*

1.1.1 A brief history

First isolated as early colonisers of neonate bowels by Theodore Escherich in 1885, *Bacterium coli commune* was thought of as a normal part of human intestinal microflora, with limited nutritional or pathogenic potential (Escherich, 1884). Within

his own lifetime however, Escherich recognised that these bacteria caused acute disease in the intestinal and urinary tracts of children (Shulman *et al.*, 2007). By the time this genus was officially renamed after Escherich, specific *Escherichia coli* serotypes had been linked to outbreaks of infant diarrhoea in hospitals (Giles & Sangster, 1948; Taylor, 1952). Since then, *E. coli* has been recognised to persist in human intestinal tracts as commensals able to cause a wide range of opportunistic infections, or as pathogens that cause serious diseases after acquiring particular combinations of virulence genes (Sussman, 1997).

1.1.2 Basic properties

E. coli are facultative anaerobes that do not form spores, but grow vegetatively as single or paired short rod-shaped Gram-negative bacilli. They are normally motile, usually expressing multiple flagella uniformly on their surface (peritrichously). *E. coli* can also express multiple types of fimbrial adhesins and capsule exopolysaccharides. They are commonly serologically defined by the combination of their lipopolysaccharide outer membrane (O-antigen) and flagella (H-antigen), but are sometimes also defined by their capsule (K-antigen) and fimbriae (F-antigen) too (Kauffmann, 1947).

Despite its adaptation to the intestinal tract of mammals and reptiles, and its lack of sporulation, *E. coli* survives for long periods in the environment, in soil, liquids and on surfaces (Sussman, 1997). It is easily cultivated in or on many different kinds of simple culture media. Generally it can be phenotypically distinguished as facultatively anaerobic, non-pigmented, circular colonies of Gram negative rods that can produce indole (Madigan *et al.*, 2003). They can also generally reduce nitrite to nitrate, are oxidase negative and also unable to use citrate as a fermentative carbon source.

1.1.3 *E.coli* commensals, opportunistic pathogens and pathogens

Commensal bacteria are bacteria that are adapted to live at non-invasive sites, are the major part of their host's microflora and, in general, do not cause them harm. This is

mutually beneficial, as commensal bacteria get access to nutrients while preventing host pathogens from occupying the same niche. Additionally, the microflora appears to be essential for immune system development and even stimulates wound healing (reviewed in Abreu, 2010). However, if introduced to a site that is normally inaccessible to them, commensal bacteria can harm their host. For example, sepsis can be caused by intestinal commensal bacteria after intestinal injury (Ayres *et al.*, 2012). These commensals may lack the virulence factors necessary to be invasive, but once through the intestinal barrier, have factors that allow them to persist in the peritoneum. In this case these bacteria are also known as opportunistic or facultative pathogens.

E. coli is a major part of the aerobic microflora of the human intestinal tract, and a proportion can act as opportunistic pathogens. Generally speaking these bacteria have few virulence factors, but those they do have may allow them to persist at extra-intestinal sites (Siitonen, 1992). However, certain intestinal *E. coli* have acquired combinations of virulence genes that are more competitive in the intestine or favourable for extra-intestinal colonisation, making them specialised pathogens (Croxen & Finlay, 2010).

The pathogenesis underlying different types of disease caused by *E. coli* is multifaceted; there is no one virulence factor responsible, and many combinations of virulence factors are capable of causing each disease. For example, the K1 capsule antigen can protect *E. coli* from phagocytosis (Agüero & Cabello, 1983). 30% of *E. coli* isolates from the microflora of healthy hosts have K1 capsules (Siitonen, 1992). Therefore, K1 strains are not necessarily pathogenic. However, K1 allows neonatal meningitis *E. coli* (NMEC) or uropathogenic *E. coli* (UPEC) to survive in the blood by protecting them from the host immune response. For NMEC, this increases the likelihood of successful tropism to the brain (Kim *et al.*, 2003). However, without other virulence factors, such as type-1 fimbriae and a cytotoxin, NMEC would not be able to cross the blood brain barrier (Khan *et al.*, 2002, 2007). In contrast, UPEC that don't down-regulate the expression of type-1 fimbriae after bladder colonisation tend not to ascend to the kidneys to cause more serious disease (Connell *et al.*, 1996;

Gunther *et al.*, 2001). This illustrates the importance of not just possession of a virulence-associated factor but also its appropriate regulation.

1.1.4 Intestinal pathotypes of *E. coli*

Pathogenic *E. coli* that do not tend to cause diarrhoeal disease, such as NMEC and UPEC, are also known as extra-intestinal pathogenic *E. coli* (ExPEC, (Russo & Johnson, 2000)). Diarrhoeagenic *E. coli* have been categorised into a number of groups that refer to the type of pathology they cause and/or their HEp-2 cell adherence pattern (figure 1.1, (adapted from Croxen & Finlay, 2010; Kaper *et al.*, 2004)). The pathology caused by these *E. coli* depends on their repertoire of virulence factors. Certain virulence factors have been used as the sole defining characteristic of a pathotype, as with STEC. However, this system of classification was originally based on clinical pathology (Nataro & Kaper, 1998). Pathotypes often contain common combinations of virulence factors, which individually may be present in multiple pathotypes (figure 1.2).

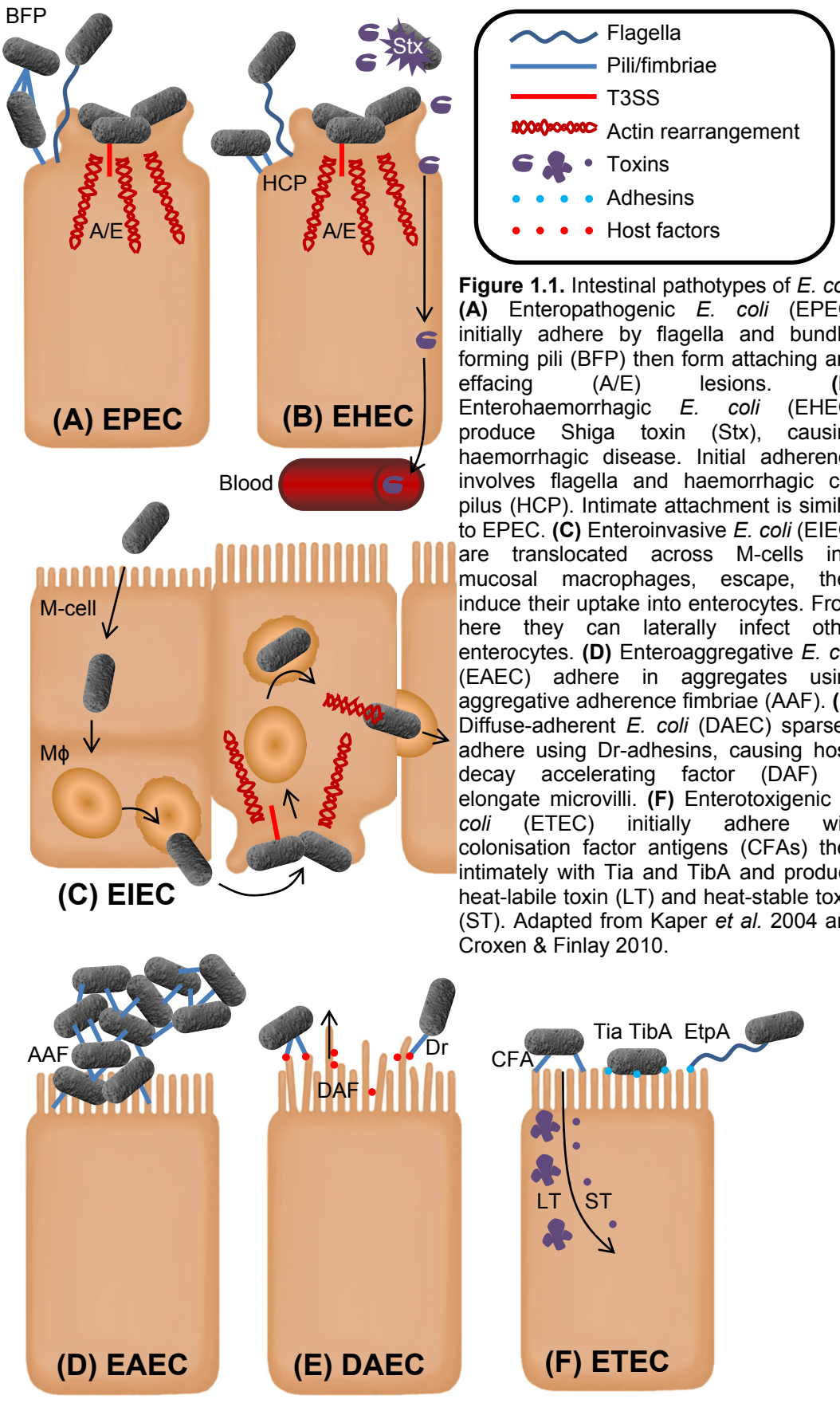

Figure 1.1. Intestinal pathotypes of *E. coli*. **(A)** Enteropathogenic *E. coli* (EPEC) initially adhere by flagella and bundle-forming pili (BFP) then form attaching and effacing (A/E) lesions. **(B)** Enterohaemorrhagic *E. coli* (EHEC) produce Shiga toxin (Stx), causing haemorrhagic disease. Initial adherence involves flagella and haemorrhagic coli pilus (HCP). Intimate attachment is similar to EPEC. **(C)** Enteroinvasive *E. coli* (EIEC) are translocated across M-cells into mucosal macrophages, escape, then induce their uptake into enterocytes. From here they can laterally infect other enterocytes. **(D)** Enteroaggregative *E. coli* (EAEC) adhere in aggregates using aggregative adherence fimbriae (AAF). **(E)** Diffuse-adherent *E. coli* (DAEC) sparsely adhere using Dr-adhesins, causing host-decay accelerating factor (DAF) to elongate microvilli. **(F)** Enterotoxigenic *E. coli* (ETEC) initially adhere with colonisation factor antigens (CFAs) then intimately with Tia and TibA and produce heat-labile toxin (LT) and heat-stable toxin (ST). Adapted from Kaper *et al.* 2004 and Croxen & Finlay 2010.

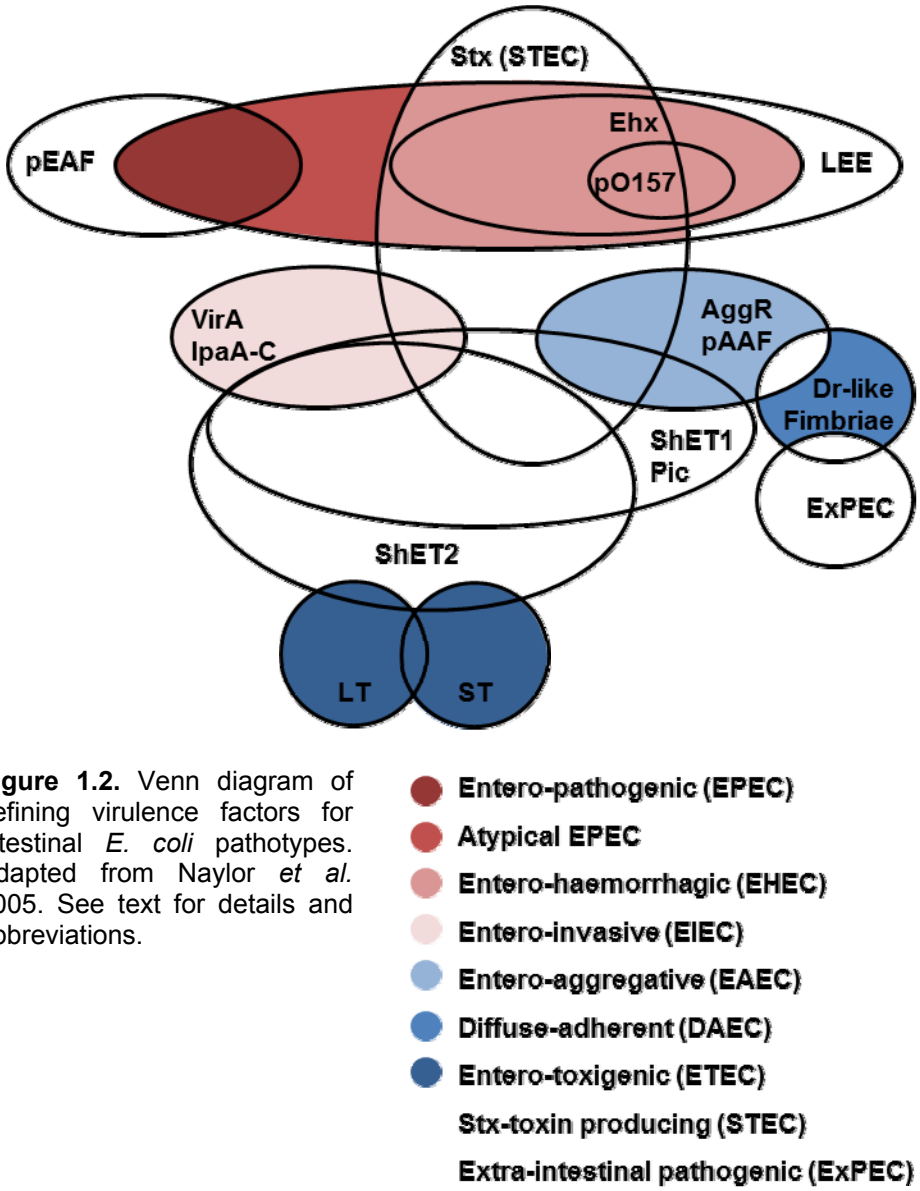

Figure 1.2. Venn diagram of defining virulence factors for intestinal *E. coli* pathotypes. Adapted from Naylor *et al.* 2005. See text for details and abbreviations.

Entero-toxigenic *E. coli* (ETEC) is a common cause of infant diarrhoea and traveller's diarrhoea in the developing world (Wennerås & Erling, 2011). ETEC can use flagella or colonisation factor antigens (CFAs) for initial adherence to enterocytes in the small intestine (Evans & Evans, 1978), then intimately attach with Tia and TibA (figure 1.1(F), (Fleckenstein *et al.*, 1996; Lindenthal & Elsinghorst, 2001)). Disease is primarily caused by production of the large multi-subunit heat-labile toxin (LT) and a small heat-stable toxin (ST) peptide (Sack, 1975). These toxins increase the intracellular levels of host cGMP, dysregulating ion secretion

channels, which causes watery diarrhoea (Field, 1979). As ETEC are defined solely by their production of LT or ST, they are a very diverse group of pathogens and therefore present a challenge to vaccine development (Roy *et al.*, 2009a).

Diffusely-adherent *E. coli* (DAEC) cause diarrhoea in young children but not infants and have been implicated in nosocomial diarrhoea in adults (Jallat *et al.*, 1993; Levine *et al.*, 1993). These bacteria are defined by their sparse pattern of adherence to HEp-2 cells (Cravioto *et al.*, 1979). In general, these strains express Dr-family fimbriae, such as F1845 (Bilge *et al.*, 1989). These fimbriae concentrate the host-expressed complement decay accelerating factor (DAF) to discrete areas of membrane, which causes elongation of microvilli (figure 1.1(E), (Betis *et al.*, 2003)).

Entero-aggregative *E. coli* (EAEC) were also defined by their adherence pattern on HEp-2 cells. This aggregative phenotype is caused by the expression of aggregative adherence fimbriae (AAF, figure 1.1(D), (Nataro *et al.*, 1992)). AAF and its master regulator AggR are co-encoded on a virulence plasmid known as pAAF (Nataro *et al.*, 1994). As a result, EAEC are another very diverse *E. coli* pathovar. They range from apparently non-pathogenic, to strains capable of causing high rates of haemolytic uraemic syndrome and mortality, depending on their repertoire of co-expressed virulence factors (Muniesa *et al.*, 2012; Nataro, 2012).

Entero-invasive *E. coli* (EIEC), which includes *Shigella* (Chaudhuri & Henderson, 2012), are defined by their ability to invade the small intestinal epithelium and cause dysentery (Nataro & Kaper, 1998). EIEC are translocated across M-cells into mucosal macrophages as part of normal antigen sampling at that site (Wassef *et al.*, 1989). Once in mucosal macrophages, EIEC can escape and induce their baso-lateral uptake into enterocytes (Croxen & Finlay, 2010). Inside enterocytes, these bacteria can escape the phago-lysosome, multiply in the cytoplasm and spread to adjacent enterocytes by polymerising host cytoskeletal proteins (figure 1.1(C), (Sansonetti *et al.*, 1986)). To invade in the manner described, EIEC use an Inv-Mxi-Spa type-III secretion system (T3SS, (Schroeder & Hilbi, 2008)). The T3SS is like a ‘molecular syringe’ that allows the translocation of effector proteins from the bacterial

cytoplasm directly into the host cytoplasm (Gauthier *et al.*, 2003). In this case, the type-III secreted (T3S) effector proteins IpaA, IpaB, IpaC and IpaD are essential for the manipulation of the host cytoskeleton necessary for the invasion phenotype (Buchrieser *et al.*, 2000). EIEC also express a selection of entero-toxins, such as Shiga toxin 1 (Stx1), ShET-1 and ShET-2 (Croxen & Finlay, 2010).

Attaching and effacing (A/E) *E. coli* are defined by their ability to cause A/E lesions. These lesions are characterised by bacteria intimately attaching to actin-rich pedestals on enterocytes with shortened or absent microvilli (Knutton *et al.*, 1987). This phenotype is due to possession of virulence factors within the locus of enterocyte effacement (LEE, (McDaniel *et al.*, 1995)). The LEE region contains genes that encode a Ssa-Esc T3SS and a number of type-III secreted effector proteins (Elliott *et al.*, 1998; Tobe *et al.*, 2006). These type-III effector proteins are secreted into enterocytes to manipulate them, effacing microvilli and disrupting tight junctions. This reduces the absorptive surface area and barrier function of the epithelium and is thought to cause diarrhoea (Dean *et al.*, 2006). The dominant pathotypes of attaching and effacing *E. coli* are entero-pathogenic *E. coli* (EPEC, figure 1.1(A)) and entero-haemorrhagic *E.coli* (EHEC, figure 1.1(B)).

Typical EPEC is distinguished from EHEC by the presence of the EPEC adherence factor plasmid (pEAF, (Knutton *et al.*, 1987)). pEAF encodes bundle-forming pili (BFP), which along with flagella, are responsible for initial attachment of EPEC to intestinal epithelial cells prior to A/E lesion formation (Girón *et al.*, 1991, 2002). Atypical EPEC is distinguished from EHEC by the absence of Shiga toxins (Stx) and particular isotypes of certain LEE-encoded effector proteins, as it does not harbour pEAF (figure 1.2, (Kaper, 1996; Naylor *et al.*, 2005b)). EPEC do not express Stx but are still an important cause of young infant diarrhoea in the developing countries (Chen & Frankel, 2005). EHEC on the other hand is more associated with diarrhoea-associated disease in developed world, as a result of contamination due to intensive farming (Valcour *et al.*, 2002). EHEC also produce entero-haemolysin (Ehx), and Stx1 and/or Stx2 of various subtypes, which cause local and systemic haemorrhagic disease (Nataro & Kaper, 1998). Initial EHEC adherence involves flagella and

fimbriae such as haemorrhagic coli pilus (HCP) prior to A/E lesion formation (Mahajan *et al.*, 2009; Xicohtencatl-Cortes *et al.*, 2007).

1.2 Entero-haemorrhagic *E. coli*

EHEC causes watery diarrhoea in humans, followed by haemorrhagic colitis, the symptoms of which include severe abdominal cramps and bloody diarrhoea. Initial symptoms are likely to be caused by the action of type-III secreted effector proteins. Haemorrhagic colitis and more serious systemic complications such as haemolytic ureamic syndrome (HUS) are due to Shiga toxin production (Richardson *et al.*, 1988). HUS is a major complication of EHEC infection and Shiga toxin release, and disease can involve multiple organs including the lungs and the brain (Richardson *et al.*, 1988). Shiga toxins bind to globotriaosylceramide (Gb3) and so targets Gb3-rich tissues such as the colonic epithelium and blood vessel endothelia, particularly of the kidneys and the brain (Jacewicz *et al.*, 1994; Lingwood *et al.*, 1987; Richardson *et al.*, 1988). HUS is defined as the combination of acute renal failure, microangiopathic haemolytic anaemia and thrombocytopaenia (Karmali, 2004). A small percentage of HUS cases are fatal and many HUS cases result in long-term morbidity. HUS mainly occurs in the old and young, and rates of HUS morbidity, fatality and resolution in EHEC outbreaks vary according to EHEC strain and Shiga-toxin type (Neupane *et al.*, 2011; Ostroff *et al.*, 1989). On average 5-10% of EHEC O157:H7 cases progress to HUS, with <10% fatality rate, and 30% of cases have serious long-term effects (Paton & Paton, 1998).

Shiga toxin is encoded on a lambdoid prophage, which can infect and integrate into the genomes over 100 serotypes of *E. coli* (Hermos *et al.*, 2011; O'Brien *et al.*, 1984). Shiga toxin is released upon bacterial lysis due to phage induction from lysogeny (Mühldorfer *et al.*, 1996). However, manipulation of host cells by T3SS is important for bacterial adherence, and the degree and success of EHEC colonisation impacts upon how much Shiga toxin is produced and therefore the severity of disease. This was aptly demonstrated by the 2011 outbreak of the LEE$^-$ STEC O104:H4, which caused high rates of HUS (22%) due to the very successful combination of EAEC AAF and AggR with Shiga toxins (Muniesa *et al.*, 2012).

EHEC O157:H7 strains have emerged in the last 30 years as important pathogens, particularly in the USA and UK, as they tend to be associated with greater prevalence and more severe outcomes in these countries. Other serotypes responsible for significant disease burden include O26, O111, O103, O121, O45 and O145 (Brooks *et al.*, 2005; USDA/FSIS, 2011). While overall incidence of haemorrhagic disease tends to be quite low, the social and economic burden is high due to the seriousness of complications and long-term effects. Supportive care and treatment of complications is very expensive (Bavaro, 2012). In the US alone, it is estimated that EHEC O157:H7 costs $405 million per year and $6.2 million for each patient that dies of HUS (Frenzen *et al.*, 2005). Additionally, the cost of screening and product recalls is high; there are costly surveillance programs across Europe and the US, and the last meat recall in the US involved 38,200 tonnes of ground beef (USDA/FSIS, 2012).

1.2.1 EHEC epidemiology

EHEC are an important set of pathogens that cause disease most notably in northern Europe, the USA, Canada, Argentina, Australia and Japan (Chase-Topping *et al.*, 2008). Around half of human cases are sporadic, with a seasonal pattern favouring summer and autumn (Lal *et al.*, 2012). However, the outbreaks that do occur can be dramatic, as with the 1996 outbreak of EHEC O157:H7 in a small community in Lanarkshire, Scotland, where there were 512 cases (279 confirmed), and 20 fatalites (Cowden *et al.*, 2001). Outbreaks of EHEC with unusual genotypes or phenotypes can be particularly problematic, as with the 2002 sorbitol-fermenting EHEC O157:H$^-$ outbreak in Germany, as it takes longer to detect and prevent its transmission, resulting in more cases (Alpers *et al.*, 2009).

EHEC is spread faeco-orally, generally from cattle sources, though transmission from other ruminant sources, like sheep, also occurs (Matthews *et al.*, 2006; La Ragione *et al.*, 2009). The infectious dose can be as low as 50 organisms (Tuttle *et al.*, 1999). Therefore transmission can occur through direct contact with ruminants, contamination of meat, milk, water, and contaminated water run-off onto fresh

produce (Rangel *et al.*, 2005). Humans appear to be incidental hosts to EHEC, as EHEC seem more adapted to persist in adult ruminants without causing disease (Naylor *et al.*, 2005b). Prevalence in cattle herds can be as high as 100% (Gyles, 2007). Due to intensive farming practices, the density of asymptomatic cattle proximal to human populations to seed EHEC infection is greater than with other ruminants, such as sheep. This may explain why EHEC is more of a problem in the developed world and why cattle are the primary reservoir of spread.

EHEC O157:H7 have been shown to preferentially colonise the last 5 cm of the intestinal tract in cattle, at the bovine terminal rectum (Naylor *et al.*, 2005a). This site presumably allows its efficient spread. There are many hypotheses for why EHEC O157:H7 shows such a specific tissue tropism in cattle. These include nutritional availability (Snider *et al.*, 2009), mechanisms or repertoire of type-III effector proteins (Girard *et al.*, 2005), regulation of type-III secretion (Roe *et al.*, 2004; Tree *et al.*, 2009), binding or regulation specificities of surface adhesins (Erdem *et al.*, 2007; Mahajan *et al.*, 2009; Mundy *et al.*, 2007), or the availability of host receptors (Mundy *et al.*, 2007; Robbe *et al.*, 2004).

1.2.2 On-farm control measures

Knowledge of the principle site and mechanisms of EHEC O157:H7 colonisation creates specific targets for control strategies in cattle, and new ways to assess their efficacy. This is necessary because proper implementation of Hazard Analysis and Critical Control Point (HACCP) principles to process beef has so far been unsuccessful in limiting transmission to humans (ECDC, 2011). Epidemiological modelling indicates that sterile immunity in cattle would not be necessary to prevent transmission to humans. Preventing faecal shedding of more than 10^4 CFU.g^{-1} could significantly reduce transmission and prevent maintenance within herds (Matthews *et al.*, 2006).

In their 2007 paper, Sargeant *et al*. concluded that targeted interventions such as probiotics, rectal washing with sodium chlorate or vaccination showed the potential to reduce cattle faecal shedding of EHEC. Practical interventions, such as additives

in feed (Callaway *et al.*, 2009) are very cheap, but their effectiveness is still debatable (Sargeant *et al.*, 2007). Targeting EHEC colonisation of cattle by vaccination has been cited as one of the most cost effective strategies to control EHEC (McNeilly, 2012). However, there are a few drawbacks to this approach. Proven vaccine efficacy has not yet been achieved, as experimental trials conducted have given variable results (Potter *et al.*, 2004; Sargeant *et al.*, 2007). As there is currently little incentive for meat producers, vaccination would also have to be low-cost for it to be adopted (McNeilly, 2012).

Vaccines and other control strategies need to be at least partially tailored to transmission routes, which are varied. For example, transmission of EHEC to children in petting zoos could be prevented simply by effective animal and human surveillance measures (HPA, 2011). Yet in the USA, pre-harvest controls would be effective in preventing spread from feedlots to meat during processing (Potter *et al.*, 2004). In contrast, an effective control strategy in Scotland would have to last throughout the lifespan of the cattle to reduce environmental contamination (Chase-Topping *et al.*, 2008).

1.2.2.1 Vaccination against EHEC in cattle

Vaccines trialled so far include those that target iron acquisition by vaccination with bacterial membrane-bound components from iron restricted cultures (Epitopix), T3S with culture supernatants (Bioniche Animal Health, (Potter *et al.*, 2004)) or recombinant LEE-encoded proteins (Dziva *et al.*, 2007; McNeilly *et al.*, 2010a) and killed bacteria (Van Diemen *et al.*, 2007). These vaccines were designed to generate mucosal antibodies, either to inhibit bacterial growth, as with Epitopix, or to prevent epithelial attachment of EHEC. These vaccines are not currently licensed for use in Northern Europe.

Vaccination strategies with T3S proteins and SRP® Epitopix technology have been shown in general to reduce faecal shedding of EHEC O157:H7 in cattle that were naturally exposed (Snedeker *et al.*, 2012). Natural exposure as a trial infection route gives a good idea of actual vaccine efficacy as this is more like pathogen exposure in

beef production. However, it does not give the quantitative proof of concept that deliberate challenges do, as times of exposure and infectious doses are unknown.

Deliberate challenges with O157:H7 have also been trialled. Antibody-mediated protection is not immediate, because it is an adaptive response, but it is also transient (Naylor *et al.*, 2007). Therefore, for vaccine strategies based on generating EHEC O157:H7 neutralising antibodies to be protective, the efficacies of different dose regimens and times between vaccination and exposure have had to be investigated. Many different schemes were used for these trials, varying the number and timing of doses. This had key implications for how such a vaccine could be used. For example, current vaccine technologies need multiple doses for full efficacy (Snedeker *et al.*, 2012), and still only provide transient protection, but they may serve as an effective pre-slaughter control in the USA.

For vaccines using T3S proteins, multiple antigens have to be used to be protective. For example, calves vaccinated with recombinant EspA or Intimin were no less colonised by EHEC than controls (Van Diemen *et al.*, 2007; Dziva *et al.*, 2007). This is one of the benefits of the T3S supernatant vaccines; many antigens are included at very little cost. However, key antigens may be variably present at different concentrations, depending on expression conditions (McNeilly *et al.*, 2010a). Also, this vaccination only includes secreted factors, not membrane-bound proteins such as intimin, which is important for intimate attachment at the bovine terminal rectum (BTR, section 1.3, (Cornick *et al.*, 2002)).

In contrast to T3S supernatants, EHEC recombinant T3S vaccines, while more expensive, allow logical antigen selection and their inclusion at defined amounts (McNeilly *et al.*, 2010a). Vaccination with the combination of recombinant Intimin, EspA and Tir has been shown to reduce colonisation rates and shedding of Stx^- EHEC O157:H7 in cattle (McNeilly *et al.*, 2010a). This strategy is known as sequential antigen targeting, as it targets antibodies towards 3 sequentially involved proteins required to initiate A/E lesion formation. Expanding on this theme, H7

flagella were later added to this vaccine, because flagella can be produced cheaply and are involved in initial colonisation of the BTR (Mahajan *et al.*, 2009).

1.3 Bovine terminal rectum colonisation model

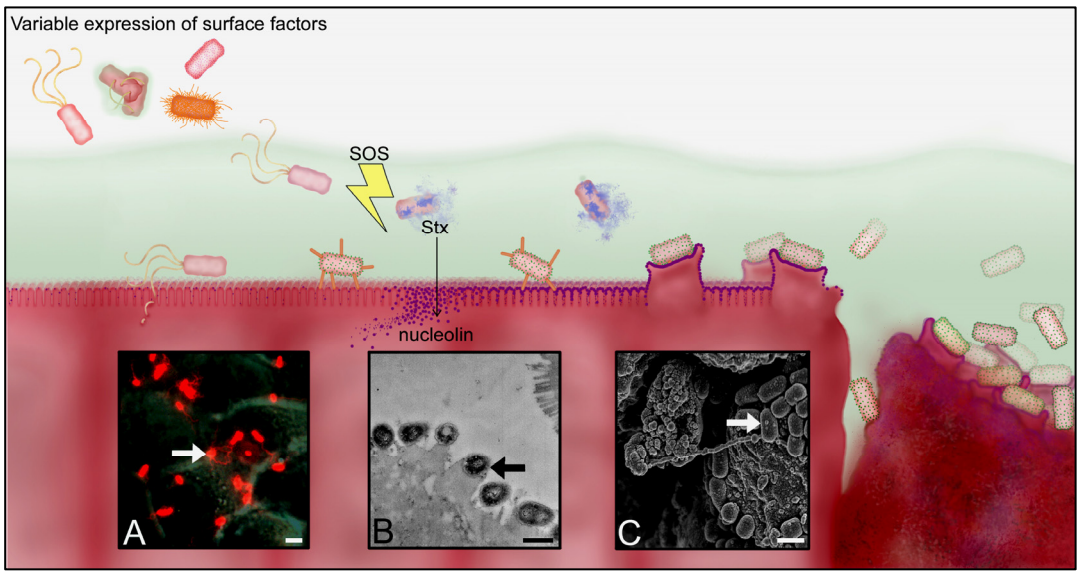

Figure 1.3. A current model of EHEC colonisation of the bovine terminal rectum (for full review please see Tree *et al.* 2009). Briefly, heterogeneous expression of surface factors allows initial attachment of EHEC and stress induces the Stx-phage dependent lysis of a subset of bacteria. Shiga toxin (Stx) induces surface expression of host receptors that EHEC is able to bind to intimately during A/E lesion formation. Type-III effectors also disrupt tight junctions and cause effacement of the intestinal epithelium as cells are shed. A) Widefield fluorescent micrograph of EHEC O157:H7 adhering to bovine rectal epithelial cells. B) Transmission electron micrograph of EHEC O157:H7 A/E lesion formation in an experimentally infected calf. C) Scanning electron micrograph of EHEC O157:H7 microcolony formation on primary bovine rectal epithelial cells. Arrows indicate bacteria, scale bars = 1μm. Diagram prepared by this author for the manuscript of Tree *et al.* 2009.

The current model of EHEC bovine colonisation involves flagellar-based motility to the BTR, where flagella and other suface factors mediate initial attachment (figure 1.3, (Tree *et al.*, 2009)). The BTR is an epithelial site, organised into villi. Villi are made of intestinal epithelial cells that are differentiated from crypt somatic stem cells in villi troughs (reviewed in (Abreu, 2010)). Therefore epithelial cells at the bottom of villi are young and as they mature, they end up at the tips, before sloughing off after about 5 days. In addition to absorptive epithelial cells, villi contain different secretory cells, which secrete mucus, hormones and antimicrobial peptides, and antigen-sampling microfold (M) cells.

This initial attachment of bacterial surface factors to villi is then superseded by T3S-based adherence (Mahajan *et al.*, 2009). At the same time, bacterial stress triggers an SOS response in a subset of bacteria close to the intestinal epithelium (Tree *et al.*, 2009). This induces Stx-phage activation, production of Shiga toxin (Stx), bacterial lysis and release of Stx from this subset of bacteria (Toshima *et al.*, 2007). Stx enriches the host apical membrane with Intimin receptors such as nucleolin (Robinson *et al.*, 2006). Intimin is a member of the auto-transporter family of secreted proteins and is targeted to the outer membrane of the bacterium. Surface localised Intimin binds nucleolin and annexin II (Sinclair & O'Brien, 2002; Zobiack *et al.*, 2002), and meanwhile the T3SS delivers translocated Intimin receptor (Tir) and other effector proteins into host cells to manipulate the cytoskeleton (Dziva *et al.*, 2004). This results in a characteristically intimate attachment to the intestinal epithelium. Intimin binding clusters Tir, causing the formation of actin-rich A/E lesions in the cytoplasm under bacteria, which are tightly tethered to the host membrane by this interaction (Chen & Frankel, 2005). However, type-III secreted proteins not only allow EHEC to bind effectively, but also to persist and cause enough pathology to allow shedding into the lumen, facilitating its spread (Smith *et al.*, 2002).

The selective advantages of a T3SS in EHEC bovine colonisation models have been demonstrated by reduced colonisation of LEE4, *escN* and type-III secreted effector mutants (Dziva *et al.*, 2004; Naylor *et al.*, 2005a; Ritchie & Waldor, 2005). More recently, possession of specific Stx2 sub-types have been suggested to be advantageous for colonisation of the BTR due to the positive regulation of host receptors, delayed down-regulation of virulence factors and host inflammation (Moxley, 2004; Robinson *et al.*, 2006; Xu *et al.*, 2012). However, the role of flagella is less clear. While H7 flagella have been shown to mediate initial adherence of EDL933 to the bovine terminal rectum *in vitro* (Mahajan *et al.*, 2009), isogenic *fliC* mutants in ATCC 43894 have a selective advantage over WT in experimentally co-infected cattle (Dobbin & Hovde, 2006). It is likely that this reflects a balance between the selective advantages of motility, adherence and modulation of pro-

survival signalling, against the disadvantages of energetic costs and immune surveillance.

In addition to remodelling the apical membrane of host epithelial cells, EHEC type-III effector proteins affect numerous other cell functions. For example, Map affects tight-junction integrity (Dean & Kenny, 2004), EspZ affects cell survival (Shames *et al.*, 2010), and NleB reduces innate immune signalling (Newton *et al.*, 2010). Table 1.1 details the general complement of type-III effector proteins in EHEC and their known binding partners and functions.

Table 1.1. Summary of EHEC type-III effector protein functions, adapted from (Wong *et al.*, 2011). Shaded areas indicate non-LEE encoded effectors (Nle). Guanine exchange factor (GEF), p21 activated kinases (PAK), integrin-linked kinase (ILK). Other abbreviations are standard protein names viewable at www.uniprot.org.

T3SS effector	Cellular location	Identified interactants	Homologues (pBLAST)	Known functions
EspB	Cytosol, Plasma membrane	α_1-antitrypsin, α-catenin, Myosin-1c	YopD	Translocation pore component, apical junction disruption, binds myosins to inhibit phagocytosis
Tir	Plasma membrane	14-3-3tau, α-actinin, cortactin, CK18, IQGAP1, IRTKS, IRSp53, Nck, PI3K, Talin, Vinculin	None known	Receptor for intimin adherence, actin pedestal formation, downregulates Map-dependent filopodia formation, SGLT-1 inactivation
EspF	Mitochondria, Cytosol, Nucleus, Tight junction, Apical membrane, Lateral membrane	14-3-3ζ, ABCF2, actin, Arp2, CK18, N-WASP, Profilin, SNX9, ZO-1/ZO-2	TccP/EspF$_u$	Mitochondrial disruption, NHE3 inactivation, SGLT-1 inactivation, tight junction disruption, disrupts nucleolus, disrupts intermediate filaments, activates SNX9 to induce membrane remodelling, binds and activates N-WASP, inhibits PI3K-dependent phagocytosis
Map	Mitochondria	EBP50 (NHERF1), NHERF2, Cdc42	IpgB, SopE	Cdc42 GEF that induces transient filopodia formation, mitochondrial disruption, SGLT-1 inactivation, tight junction disruption
EspG	Cytosol, Golgi	Tubulin, Arf1/6, PAK1/2/3	VirA	Disrupts microtubules, blocks ARF GTPase signalling and stimulates PAKs to inhibit endomembrane trafficking
EspH	Plasma	DH-PH	None known	Blocks Rho GTPase signalling

T3SS effector	Cellular location	Identified interactants	Homologues (pBLAST)	Known functions
	membrane, Pedestal	RhoGEFs		and antibody-mediated phagocytosis, promotes actin pedestal length
EspZ	Plasma membrane	CD98	None known	Enhances β1-integrin and FAK signalling to inhibit apoptosis and cellular cytotoxicity
EspI/NleA	Golgi, Plasma membrane	Syntrophin, Sec23/24, MALS3, PDZK11, SNX27, TCOF1, EBP50 (NHERF1), NHERF2, MAGI-3, SAP97, SAP102, PSD-95	None known	Inhibits COPII-dependent protein export from endoplastic reticulum, tight junction disruption
EspJ	Cytosol, Mitochondria	Unknown	HopF	Inhibits antibody-mediated and complement-mediated *trans*-phagocytosis
EspK	Unknown	Unknown	GogB	Unknown
EspL	Pedestal	Annexin 2	OspD	Enhances F-actin bundling activity of Annexin-2
EspP	Plasma membrane, Cytosol	RhoA	IpgB, SopE	RhoA GEF that induces stress fibre formation
EspN	Unknown	Unknown	SARI_01330, SARI_01464, SeAg_B1500, CNF1	Unknown
EspO	Unknown	ILK	OspE	Unknown
EspR	Unknown	Unknown	SF1757	Unknown
EspV	Cytosol	Unknown	AvrA1	Modulates cytoskeleton
EspW	Unknown	Unknown	HopPlasma membraneaA, HopW1	Unknown
EspX	Unknown	Unknown	Sd1012_0237, SSON_0027	Unknown
EspY	Unknown	Unknown	SopD	Unknown
NleB	Cytosol	Unknown	SseK	Inhibits TNF-induced NF-κB activation
NleC	Cytosol, Nucleus	p65 (RelA), p50, c-Rel, IκB	AIP56	Metallo-protease that cleaves p65 (RelA), c-Rel, p50 and IκB to inhibit NF-κB activation

T3SS effector	Cellular location	Identified interactants	Homologues (pBLAST)	Known functions
NleD	Cytosol	JNK	HopAP1, HopH1	Metallo-protease that cleaves JNK to inhibit AP-1 activation
NleE	Cytosol	Unknown	OspZ	Blocks IκB degradation to inhibit NF-κB activation
NleF	Unknown	Unknown	None known	Unknown
NleG/NleI	Cytosol	UBE2D2	STY1076	U-box E3 ubiquitin ligase
NleH	Endoplastic reticulum, Plasma membrane, Cytosol	Bax-inhibitor 1, NHERF2, RPS3	OspG	Binds Bax-inhibitor 1 to block apoptosis, sequesters RPS3 to inhibit NF-κB signalling
$EspF_u$	Cytosol	N-WASP, IRTKS, IRSp53, Cortactin	EspF	Relieves N-WASP autoinhibition to trigger actin pedestal formation

1.4 Subversion of the actin cytoskeleton by bacterial proteins

Like EHEC, other pathogenic Gram-negative bacteria use type-III secreted effector proteins to create niches. For example, *Pseudomonas syringae*, *Shigella flexneri*, *S.* Typhimurium, *Chlamydia trachomatis*, *Xanthomonas campestris*, *Burkholderia pseudomallei*, *Yersinia pestis* and *Vibrio parahaemalyticus* all contain related T3SS (Büttner, 2012). The actin cytoskeleton is fundamental to many of the cellular processes manipulated by the bacterium. As such it is heavily targeted by secreted effector proteins, both directly and indirectly, to efficiently colonise mammalian epithelial cells.

1.4.1 Actin

The actin cytoskeleton is made up of cytoplasmic actin and the factors that regulate it. Actin has three isotypes; cytoplasmic actin is a mixture of beta and gamma actin isotypes (Dos Remedios *et al.*, 2003). Monomeric actin is globular and referred to as G-actin, whereas polymeric actin is filamentous, and referred to as F-actin. G-actin and F-actin exist in a dynamic equilibrium with one another, and it is well established that this equilibrium is fundamental to the function of actin (Papakonstanti *et al.*, 2000). F-actin takes the form of a twisted double stranded helix

with polarity; the faster growing end is known as the barbed or (+) end and the slower growing end is known as the pointed or (-) end (Hanein *et al.*, 1998; Tilney & Kallenbach, 1979).

Mature F-actin filament formation involves nucleation, elongation and steady states or phases. Spontaneous actin nucleation most likely involves two steps - formation of dimers that can easily dissociate, followed by formation of stable trimers (figure 1.4(A), (Jégou *et al.*, 2011)). These steps are distinct but both thermodynamically unfavourable and therefore rate limiting. As a result, nucleation is also known as the lag phase. Once trimers, or 'critical nuclei', are formed, the addition of monomer to the ends of the actin polymer is thermodynamically favourable, allowing elongation (figure 1.4(A), (Jégou *et al.*, 2011)). This is also known as the growth phase. The steady state occurs when equilibrium is reached between actin polymerisation and depolymerisation and is also known as the equilibrium phase. Because of the polarity of the actin filaments, the equilibrium phase generally involves net depolymerisation at the pointed end and net polymerisation at the barbed end (figure 1.4(B), (Pinder & Gratzer, 1983)). The length of filament remains the same, in a dynamic equilibrium of directional subunit flux known as actin tread-milling. The concentration of free monomers at which this occurs is known as the critical concentration (Dos Remedios *et al.*, 2003).

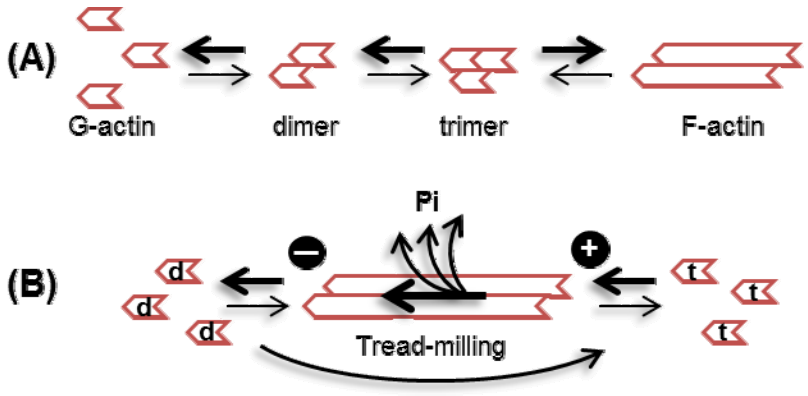

Figure 1.4. Actin assembly and filament dynamics. **(A)** Nucleation of an actin trimer from monomers (G-actin) is a rate-limiting step in assembly of actin filaments (F-actin. **(B)** F-actin filament polarity and tread-milling; see text for details. Thickness of arrows indicates favoured state. Figure is adapted from Jegou *et al.* 2011 and Alberts *et al.* 2007.

Actin tightly binds to ATP or ADP and divalent cations, such as Ca^{2+} and Mg^{2+} (Grazi & Trombetta, 1985). When G-actin is bound to Mg^{2+} it binds ATP more easily. G-actin-ATP is favoured for polymerisation due to the increased stability afforded by the third phosphate (Korn *et al.*, 1987). After polymerisation, Actin-ATP is quickly hydrolysed into actin-ADP-Pi (figure 1.4(B)). Dissociation of the inorganic phosphate occurs more slowly, at random (Jégou *et al.*, 2011). However, once this happens, F-actin-ADP is much less rigid and more likely to dissociate from actin filaments (Dos Remedios *et al.*, 2003). F-actin is unable to exchange ADP for ATP, whereas G-actin is, which allows monomers to be recycled (figure 1.4(B), (Hegyi *et al.*, 1988)). F-actin is therefore generally a mixture of newly polymerised actin-ATP at the barbed end, capped by older actin-ADP-Pi which is increasingly unstable at the pointed end due to Pi release (Jégou *et al.*, 2011). These properties, and how they are regulated, are responsible for the polarity of actin filaments (Dos Remedios *et al.*, 2003).

1.4.2 Host actin regulatory proteins

Actin is regulated by a number of host proteins, in order to co-ordinate and harness actin filaments for use in host-cell processes. Actin-binding proteins control actin dynamics and arrangement by binding to G-actin and/or F-actin. Another layer of regulatory control is added by changing the levels of expression, activation and bio-availability of the actin-binding proteins and their regulators (Scott & Olson, 2007). This allows global and spatial fine-tuning of actin dynamics at a cellular level, which is necessary for such eukaryotic processes as adherence, motility and cytokinesis (Van Troys *et al.*, 2008).

Figure 1.5 shows different examples of how actin-binding proteins interact with actin for local control of actin arrangement and dynamics. There are many proteins that interact with actin to change the arrangement or anchorage of its filaments (figure 1.5, bottom). Actin can be bundled into stress-fibres, spikes or cables (Fimbrin, α-actinin and myosins respectively), cross-linked into lattices (Filamin), or branched into meshes (Arp2/3) (Brown & McKnight, 2010; Hirokawa *et al.*, 1982; Korn &

Hammer, 1988; Maciver *et al.*, 1991). Actin can be anchored to plasma membranes by ERM proteins, (ezrin, radixin and moesin (Arpin *et al.*, 2011)), and in the case of microvilli, myosin-I with Calmodulin (Mooseker, 1989). Actin is also anchored to tight-junctions (via cadherins, (Brooke *et al.*, 2012)) and the cellular matrix (via integrins, (Wehrle-Haller, 2012)).

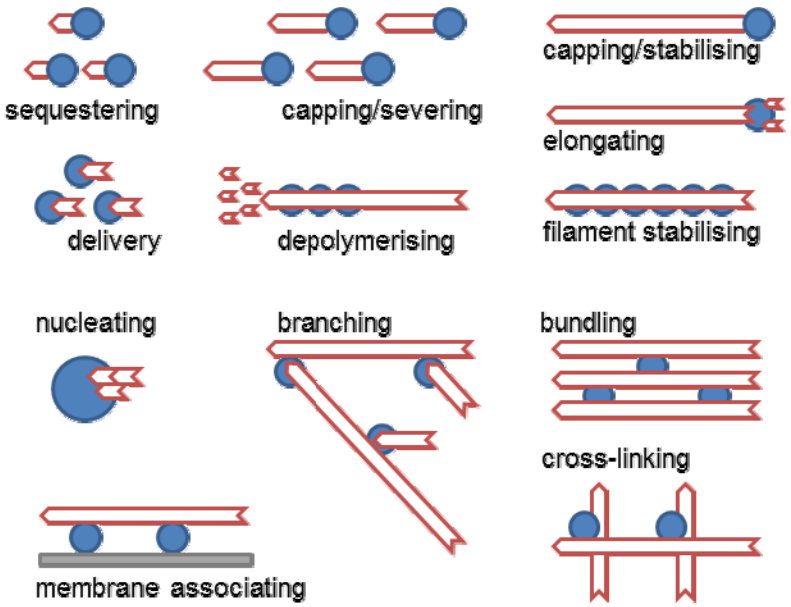

Figure 1.5. Regulation of actin (red) by actin-binding proteins (blue). Polarity of actin is indicated by pointed ends (-) and barbed, spiky (+) ends. Figure is adapted from Alberts *et al.* 2007.

Some actin-binding proteins regulate actin by changing its filament dynamics. Actin-sequestering proteins (figure 1.5, top-left) reduce the pool of free G-actin, limiting its assembly, as with thymosin (Dominguez, 2007). Other proteins that interact with G-actin have the opposite effect. For example, nucleation promoting factors, such as Arp2/3, decrease the free-energy required for actin nucleation, reducing the lag-phase in actin assembly (Goley & Welch, 2006). Also, Profilin-binding to G-actin increases the efficiency of F-actin elongation by delivering G-actin to the barbed ends of filaments (Firat-Karalar & Welch, 2011).

F-actin binding proteins can affect the efficiency of polymerisation by binding to barbed ends of F-actin. Formin caps barbed ends and interacts with profilin to

increase the efficiency of filament growth (Paul & Pollard, 2009). Conversely, Gelsolin severs filaments before nucleating fragments, resulting in actin disassembly then assembly (Sun *et al.*, 1999). In contrast to capping proteins, certain actin-binding proteins can bind along the length of F-actin. This prevents other protein interactions, resulting in either stabilised filaments, as with Tropomyosin (Ursitti & Fowler, 1994), or severed filaments, as can occur with ADF/cofilin (Andrianantoandro & Pollard, 2006).

ADF/cofilin is ubiquitously expressed in mammals and is a key regulatory player in actin dynamics. Mammalian ADF/cofilin has 3 isoforms - cofilin-1, cofilin-2 and actin-depolymerising factor (ADF) - with overlapping but not identical roles (Vartiainen *et al.*, 2002). Cofilin-1, also known as non-muscle cofilin, is ubiquitous and is crucial for embryonic development (Gurniak *et al.*, 2005). As with all ADF/cofilins, its role in actin dynamics is complex, depending on its stoichiometric ratio to actin and pH (figure 1.6).

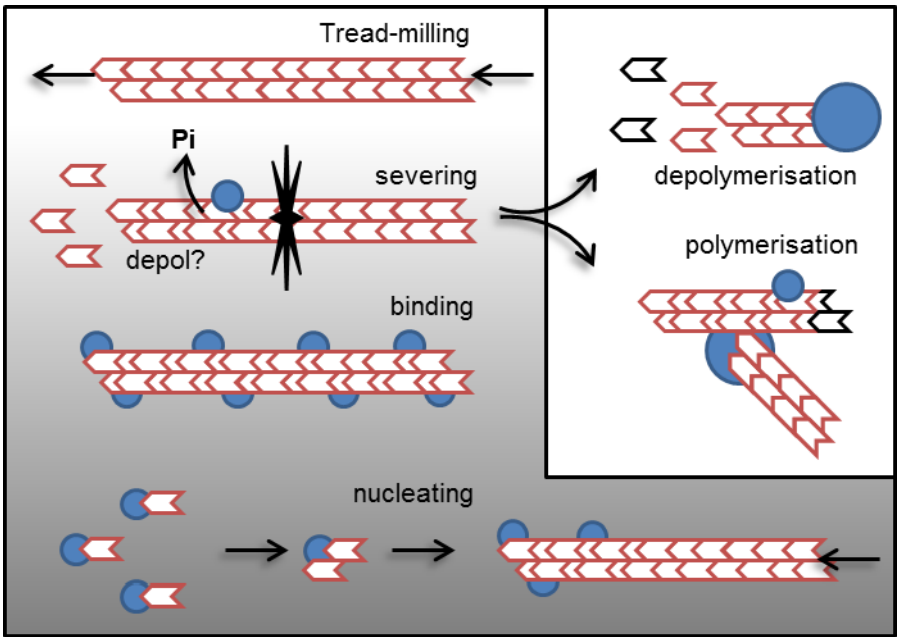

Figure 1.6. Regulation of actin, (red) dynamics by cofilins, (small blue circles). Cofilin concentration is indicated by grey gradient. As the ratio of cofilin to actin is increased, the action of cofilin changes from severing, to binding, to nucleating. Inset gives two possible outcomes of filament severing on actin dynamics, which is dependent on the presence of other factors (big blue circles). Black ends indicate where filament was severed. Polarity of actin is indicated by pointed ends (-) and barbed, spiky (+) ends. Figure is adapted from Van Troys *et al.* 2008.

Cofilins can bind filamentous or monomeric actin, but have a preference for ADP-actin (Van Troys *et al.*, 2008). When cofilins bind to F-actin, they introduce a tighter helical twist into the filament (McGough *et al.*, 1997). At low concentrations, this causes filament severing due to the tension between areas of the filaments that are tightly twisted by cofilins and areas that are not (Bobkov *et al.*, 2006). This can result in actin filament disassembly if the barbed end is capped, or assembly due to an increased number of barbed ends (figure 1.6). Increasing the number of barbed ends is enhanced in the presence of branching factors and G-actin-ATP (Andrianantoandro & Pollard, 2006). Because cofilins preferentially bind to ADP-actin, older actin filaments tend to be targeted for this severing (Van Troys *et al.*, 2008). At higher concentrations cofilins bind along the whole length of filaments. This is actually stabilising because there is no torsional tension as the whole filament is bound by cofilin (Andrianantoandro & Pollard, 2006). At actin-saturating concentrations of cofilins, they bind actin monomers and act as nucleation factors, promoting filament assembly (figure 1.6).

Cofilins are also regulated by specific mechanisms and more generally by physiological pH. Higher pH enhances actin-severing activity, while lower pH enhances actin-binding activity (Pavlov & Muhlrad, 2006). Cofilins are inhibited by phosphorylation at serine 3 by LIM-kinase, and activated by dephosphorylation by Slingshot (Huang *et al.*, 2006). Additionally, active cofilins are sequestered in the inner leaflet of the cytoplasmic membrane by polyphosphoinositide-4,5-bisphosphate and are released by the action of phospholipase C (Zhan *et al.*, 2003).

Actin-binding proteins are responsible for local actin regulation and in turn are regulated locally by actin-binding regulatory proteins. However, there are mechanisms for more global co-ordination of actin dynamics. For example, small GTPases of the Rho family (Cdc42, Rac, Rho) regulate actin-binding proteins and their regulators in response to extracellular stimuli (figure 1.7, (Hall, 1992; Ridley & Hall, 1992)). Figure 1.7 is a very simplified example of a well-established model of Rho-family regulation. In this model, actin dynamics are regulated through Rho-

family activity on actin-binding proteins and their regulators. For example, Rho activates formin (mDia), which results in long F-actin filaments (Kovar, 2006). It also activates Myosin II via Rho kinase (ROCK, (Somlyo & Somlyo, 2000)), allowing stress fibre formation by actin bundling.

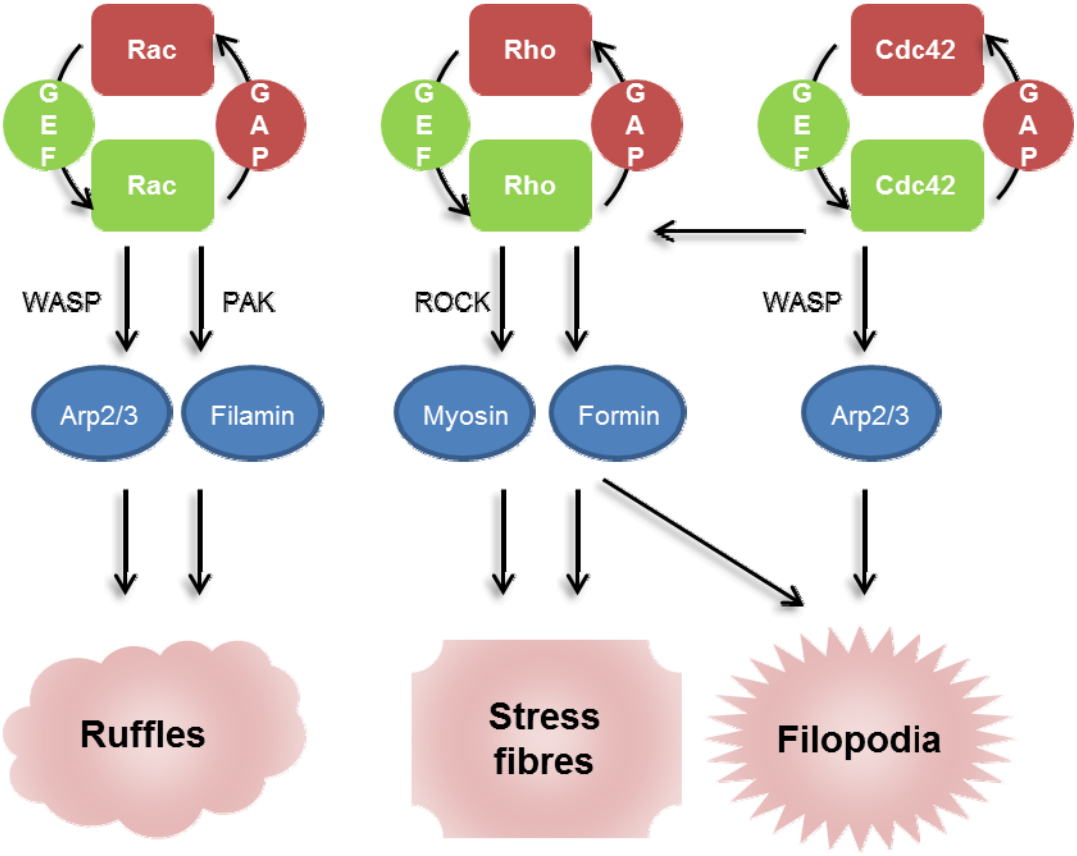

Figure 1.7. Global regulation of actin dynamics by Rho-family GTPases Rac, Rho and Cdc42. Actin-binding proteins are blue, GTPases are active when GTP bound (green) and inactive when GDP bound (red). Cell phenotype of activation of example Rho-family GTPases is indicated on the bottom. These GTPases themselves are activated by guanine nucleotide exchange factors (GEFs) and inactivated by GTPase activating proteins (GAPs). Wiskott-Aldrich syndrome protein (WASP), p21 activated kinase (PAK), Rho kinase (ROCK). Figure is adapted from Alberts *et al.* 2007.

On top of this regulatory tier, there are activators and inhibitors of Rho-family GTPases, which are only active when bound by GTP, not GDP. Guanine nucleotide exchange factors (GEFs) replace GDP with GTP, activating the regulators, while GTPase activating proteins (GAPs) cause GTP hydrolysis and consequent deactivation of these regulators (Hall, 1992). These extra levels of control shown in

figure 1.7 briefly illustrate the complexity of actin dynamics signalling cascades and the many levels that it is possible to manipulate.

1.4.3 Bacterial actin regulatory proteins

Bacteria can hijack elements of the actin cytoskeleton, taking advantage of its ability to move and shape cells according to stimuli, and to engulf, divide and traffic intracellular and extracellular contents. All these properties can be exploited by bacteria where it is advantageous to carve a niche on or inside cells, multiply there and spread (Wong *et al.*, 2011). To do this, bacteria manipulate actin regulatory cascades at multiple points.

For a bacterial niche on the outside of cells, it is advantageous to manipulate the actin cytoskeleton to promote tight binding and regulate bacterial uptake. Both EHEC and EPEC Tir proteins cause tight attachment in A/E lesions by activating the same pathway in different ways. Tir_{EPEC} is clustered by binding to intimin and then tyrosine-phosphorylated by host proteins (Phillips *et al.*, 2004). Nck binds to phosphorylated Tir_{EPEC} and recruits N-WASP (a regulator of actin-nucleation proteins), resulting in Arp2/3-dependent nucleation of actin (Garmendia *et al.*, 2004). Tir_{EHEC} is functional in the absence of Nck. Lacking the key tyrosine residue for Nck recruitment, Tir_{EHEC} is instead bound by a non-LEE encoded T3S protein, $EspF_u$. $EspF_u$ clusters N-WASP, activating Arp2/3-dependent actin nucleation (Campellone *et al.*, 2004). Activation of Arp2/3 promotes A/E lesion formation, which tightly anchors bacteria to the actin cytoskeleton through the host cell membrane.

To regulate bacterial uptake, EHEC and EPEC secrete EspH into cells. EspH inhibits many mammalian Rho family-GEFs, preventing host activation of Rho-family GTPases (Wong *et al.*, 2012). This inhibition allows bacteria to take control of membrane modelling by actin with their own Rho-family GEF mimics (Dong *et al.*, 2010). Map is a GEF mimic that activates Cdc42, resulting in short-lived filopodia formation. This activity is transient because Tir, which additionally mimics Cdc42-GAPs, antagonises Map activity and Map is quickly targeted to mitochondria (Wong *et al.*, 2012). EspT is another Rho-family GEF mimic, that when secreted, induces

bacterial uptake, resulting in a vacuolar A/E lesion (Bulgin *et al.*, 2009). This action is contrary to what might be expected of an extracellular pathogen. However, EspT is only rarely present in EPEC strains, and the effect this has on EPEC pathogenesis remains to be seen (Arbeloa *et al.*, 2009).

Other bacteria routinely manipulate the actin cytoskeleton to deliberately invade host cells. This is a rapid but complex process, regulated both in space and time by T3S effector proteins. *Shigella* IpaC, a component of the T3SS translocon pore, directly nucleates actin, highlighting that subversion of actin dynamics can happen at the earliest opportunity (Kueltzo *et al.*, 2003). In contrast, another *Shigella* T3S effector, IpaA, causes actin depolymerisation by interacting with vinculin-containing actin-membrane anchors (Bourdet-Sicard *et al.*, 1999). *S.* Typhimurium also secretes effector proteins of opposing function, to allow temporal regulation of actin dynamics. SopE, another bacterial protein that mimics Rho-GEFs, activates Cdc42 and Rac1 (Bulgin *et al.*, 2010). This induces membrane ruffles that are stabilised by SipA inhibition of cofilin function (Wong *et al.*, 2012; Zhou *et al.*, 1999). Large membrane ruffles are formed, and these engulf bacteria, allowing their entry into host cells. However, *S.* Typhimurium also secretes SptP, which mimics Rho-family GAPs and antagonises SopE (Kubori & Galán, 2003). SptP has a longer half-life than SopE, allowing the bacteria to dramatically but reversibly remodel host membranes for invasion.

However, it is not just T3S effectors that are involved in bacterial manipulation of the actin cytoskeleton. Specific membrane-bound proteins expressed at bacterial poles can harness actin dynamics to move bacteria through the cytoplasm of host cells. *Burkholderia psuedomallei* BimA, *Listeria monocytogenes* ActA, *Rickettsia* Sca2 and *Shigella* IcsA all mediate this actin-based intracellular motility (Haglund & Welch, 2011). The first bacterial actin-based motility discovered was that of ActA from *L. monocytogenes*, and was known as actin-rocketing. ActA binds directly to Arp2/3 independently of N-WASP, which then nucleates and branches polymerising actin filaments behind the bacteria, rocketing it forwards (Welch *et al.*, 1998). Sca2 from *Rickettsia* directly nucleates actin into tails of long bundled actin cables in

cooperation with profilin and fimbrin (Haglund *et al.*, 2010). Shigella IcsA nucleates actin less directly than ActA, by binding N-WASP to recruit Arp2/3 (Egile *et al.*, 1999), resulting in similar actin rockets to *Listeria*.

This example of three types of actin-based motility highlights the diversity of mechanisms that bacteria use to subvert the actin cytoskeleton. To take advantage of the same principle, nucleation of actin filaments at one pole to propel them forward, these bacteria activate the same process at three different tiers of actin regulation (Haglund & Welch, 2011). Figure 1.8 highlights this, in the context of the other examples given.

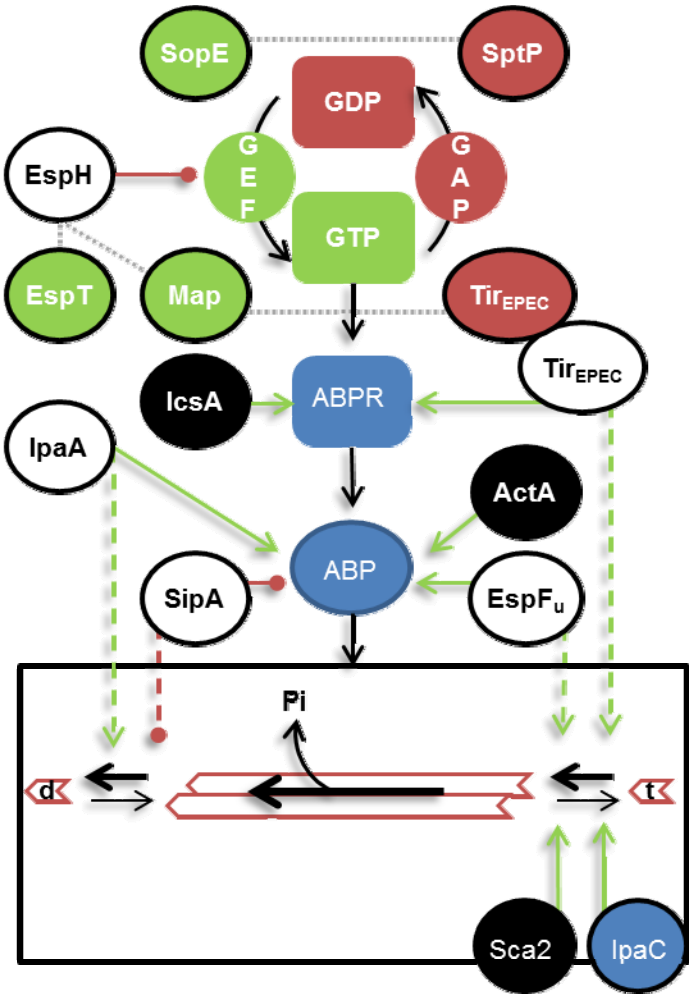

Figure 1.8. Bacterial proteins, (outlined in black), subvert actin dynamics at multiple regulatory levels. Bacterial proteins affect GEF activity, mimic GEF and GAP proteins, and bind to actin-binding proteins and their regulators with differential outcomes in actin dynamics. Effects on actin dynamics are illustrated in the bottom square, but this does not include proteins that alter Rho-family GTPase activity, as this depends on which GTPase is affected. Bacterial proteins can also bind directly to actin and cause actin polymerisation. Bacterial proteins that act antagonistically with one another are indicated by a faint grey broken line. Bacterial proteins that mediate actin-based motility are filled black. Bacterial proteins that mimic host GEFs, GAPs or actin-binding proteins (ABP) are filled with green, red or blue respectively. Rho-GTPases (red and green squares) are active when GTP bound (green) and inactive when GDP bound (red). Actin-binding proteins (ABP) and their direct regulators (ABPR) are blue.

1.5 Bacterial flagella

As mentioned in section 1.3, H7 flagella are involved in initial adherence of EHEC O157:H7 to the bovine terminal rectum (Mahajan *et al.*, 2009). Flagella can be arrayed on bacterial cells in a number of ways. They can be singly expressed (monotrichous) or multiply expressed (lophotrichous). This can be either at one pole (polar), both poles (amphitrichous), laterally, or all over (peritrichous). *E. coli* and *Salmonella* have one flagellar system that is expressed peritrichously.

1.5.1 Structure of flagella

In *E. coli* and *Salmonella*, a flagellum consists of a long capped extracellular filament, attached to a hook via hook-associated adaptor proteins (HAPs) FlgK and FlgL (Büttner, 2012). Flagella filament length varies, depending on secretion efficiency, growth conditions and mechanical stress, but they are on average between 5-10 μm long in *E. coli* (Turner *et al.*, 2012). The hook is in turn attached to the basal body in the cell wall via a rod (figure 1.9). The basal body contains an L-ring in the outer membrane, a P-ring in the peptidoglycan layer, an MS-ring in the inner membrane and a C-ring in the cytoplasm (Berg, 2003). The rod passes through the L and P rings, and connects to a secretin and the MS ring. The secretin is part of a flagellar T3SS which is housed in the MS and C rings, and the C-ring portion serves as a docking site for secretion substrates (Büttner, 2012). The MS ring is made of FliF, and is connected to the motor/stator complex via the C-ring rotor/switch complex (Ueno *et al.*, 1992). Figure 1.9 shows a schematic diagram of which proteins make up the different components of the flagellar apparatus.

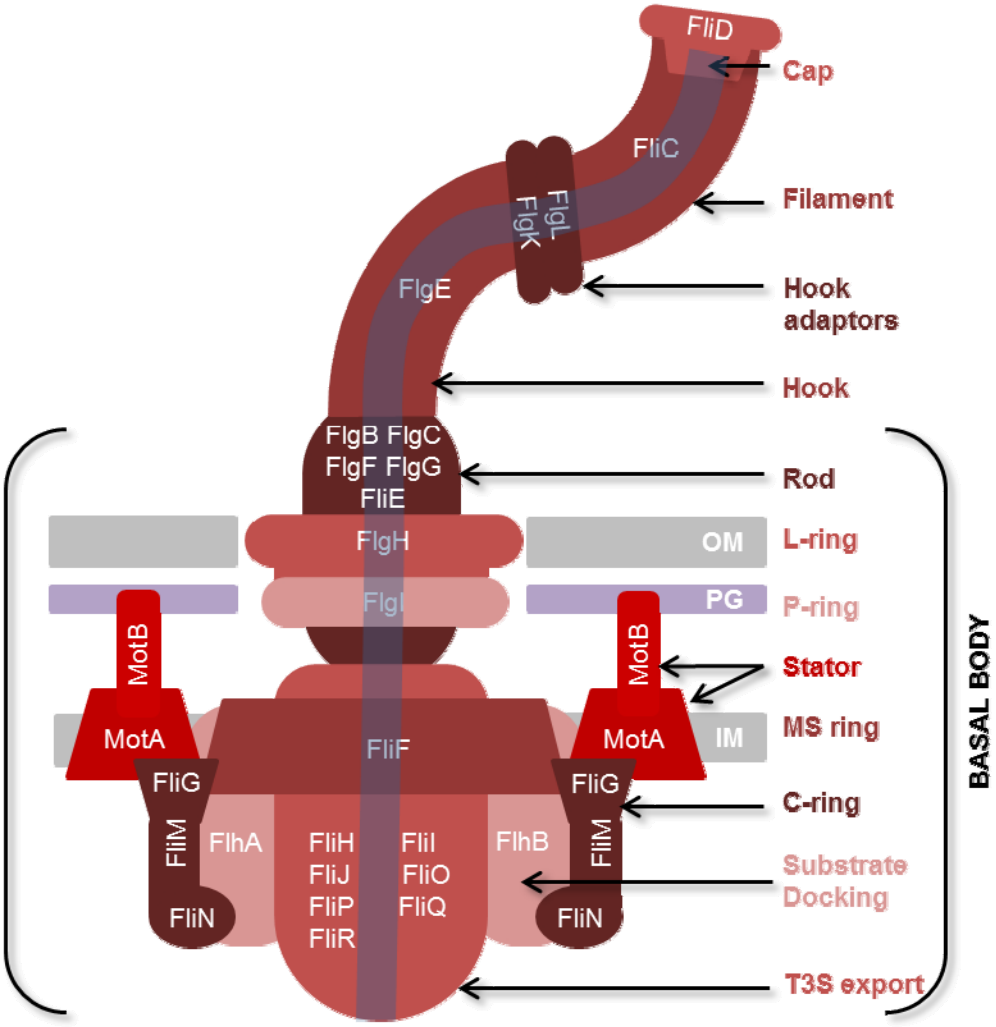

Figure 1.9. The components of the flagellar apparatus in *E. coli* and *Salmonella*. The blue line indicates that the T3S export system acts as a gateway to a uninterrupted channel that leads to the tip of the flagellum. Outer-membrane (OM), peptidoglycan (PG), inner-membrane (IM). Adapted from Berg 2003 and Büttner 2012.

1.5.1.1 Flagellin

Flagellin is major component of the flagella filament, and in *E. coli* is called FliC (Reid *et al.*, 1999). *Salmonella* has two flagellins, FliC and FljB, and while they are expressed one at a time, *Salmonella* can switch between types in a process known as phase variation (Kutsukake *et al.*, 2006). Structurally, flagellins fold back on themselves, like an elaborate hairpin, with the termini associated with one another. The termini are conserved and contain rigid helical D0 and D1 structural domains (figure 1.10, (Yonekura *et al.*, 2003)). These domains are within the flagella

filament, and are necessary for polymerisation and therefore motility (Andersen-Nissen *et al.*, 2005; Kuwajima, 1988).

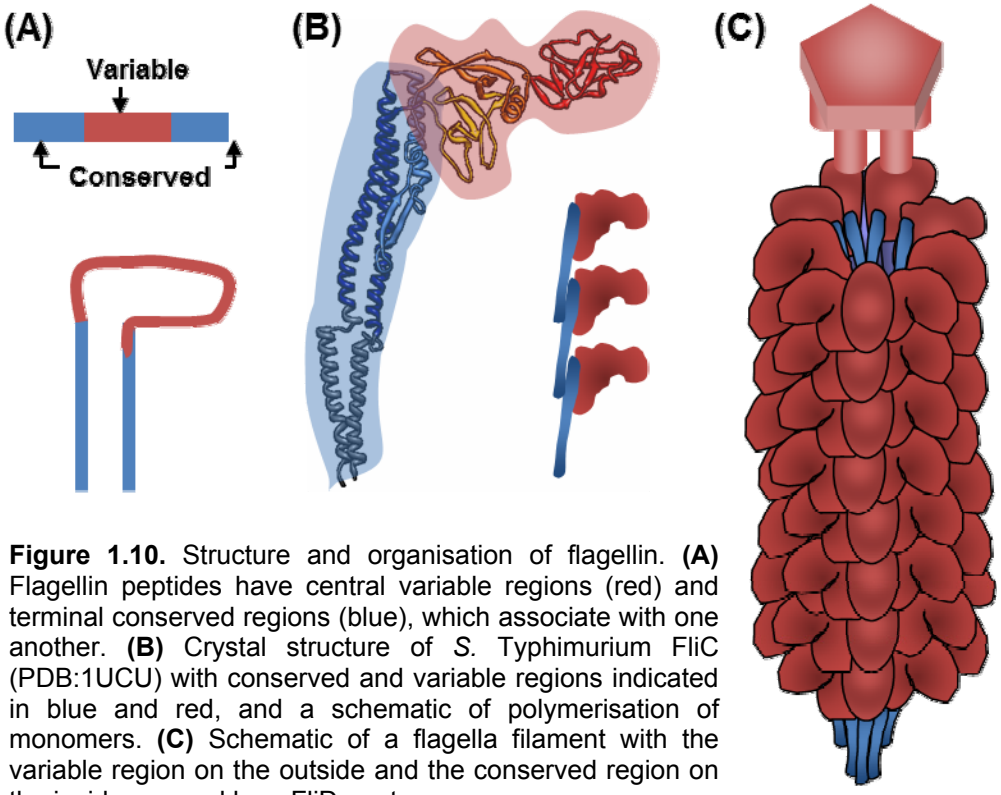

Figure 1.10. Structure and organisation of flagellin. **(A)** Flagellin peptides have central variable regions (red) and terminal conserved regions (blue), which associate with one another. **(B)** Crystal structure of *S.* Typhimurium FliC (PDB:1UCU) with conserved and variable regions indicated in blue and red, and a schematic of polymerisation of monomers. **(C)** Schematic of a flagella filament with the variable region on the outside and the conserved region on the inside, capped by a FliD pentamer.

The central portion of flagellin is variable, and contains D2 and D3 structural domains (Kwang *et al.*, 1996; Reid *et al.*, 1999; Yonekura *et al.*, 2003). These domains form the surface of the flagella filament (figure 1.10(C)) and exposed regions of flagellin can be post-translationally modified. For example, *S.* Typhimurium FliC and FljB surface-exposed lysine residues are methylated (Tronick & Martinez, 1971). Among many examples of flagellin glycosylation, *Campylobacter jejuni* FlaA, *Helicobacter pylori* FlaA and FlaB, *Pseudomonas aeruginosa* FliC and *Listeria monocytogenes* FliC are all glycosylated via serine and threonine residues (reviewed in Logan, 2006). This can alter the properties of flagella filament surfaces, which can be involved in binding.

1.5.2 Flagella assembly

The regulation of flagella assembly is complex and hierarchical (figure 1.11). There are 3 sets of co-ordinately regulated genes, which are expressed in phases (Kalir *et al.*, 2001). *flhDC* is expressed first, as the master regulator. The *flhDC* promoter integrates environmental stimuli with cross-regulatory inputs, like cAMP, to control *flhDC* expression (Brown *et al.*, 2009; Chilcott & Hughes, 2000). Due to the energetic costs of assembling and running flagella systems, and their recognition by host immune systems, *flhDC* expression is tightly regulated (Soutourina & Bertin, 2003). *flhDC* expression is influenced by growth phase (RpoS, (Dong & Schellhorn, 2009)) quorum sensing of bacterial density (QseBC, (Clarke & Sperandio, 2005)), pH and temperature (HN-S and CRP, (Soutourina *et al.*, 1999)). Additionally, coordination of flagella expression with other surface factors, to avoid steric hindrance and allow temporal expression during colonisation, also occurs. For example *E. coli* flagella are inversely regulated with type-1 fimbriae (Lehnen *et al.*, 2002), and T3SS (Iyoda *et al.*, 2006).

Expression of *flhDC* is required to produce flagella, because $FlhD_2C_2$ drives transcription of mid-phase genes (figure 1.11). Mid-phase genes encode proteins for the hook/basal body (HBB), HAPs (FlgK, FlgL, FliD), their T3S chaperones, a specific flagellar sigma factor (σ^{28}), its anti-sigma factor (FlgM) and a hook length regulator, FliK (Brown *et al.*, 2009). The mid-phase genes are expressed in a hierarchy that corresponds to HBB assembly, according to the affinity of $FlhD_2C_2$ to the different promoters (Chilcott & Hughes, 2000). The proteins encoded by mid-phase genes are required to regulate late-phase gene expression and protein secretion. Additionally, σ^{28} prevents $FlhD_2C_2$ auto-inhibition, resulting in more early to mid-phase transcription if conditions are still stimulatory (Brown *et al.*, 2009). FlgM inhibits the σ^{28}-driven expression of late-phase genes, until FlgM is secreted through the complete basal body (figure 1.11, (Chilcott & Hughes, 2000)).

Genes under late-phase control encode the HAPs, filament, T3S chaperone, motor and chemotaxis proteins (figure 1.11). FlhB, part of the flagellar T3SS, does not recognise late-phase proteins as secretion substrates until the hook is ~55 nm long

(Brown *et al.*, 2009). This process is regulated by the secretion rate of the mid-phase protein FliK. At ~55 nm, FliK secretion rate through the HBB is slow enough to allow it to interact with FlhB (Hughes, 2012). This causes a conformational change in FlhB that changes its recognition specificities, allowing the secretion of the late-phase proteins (Büttner, 2012).

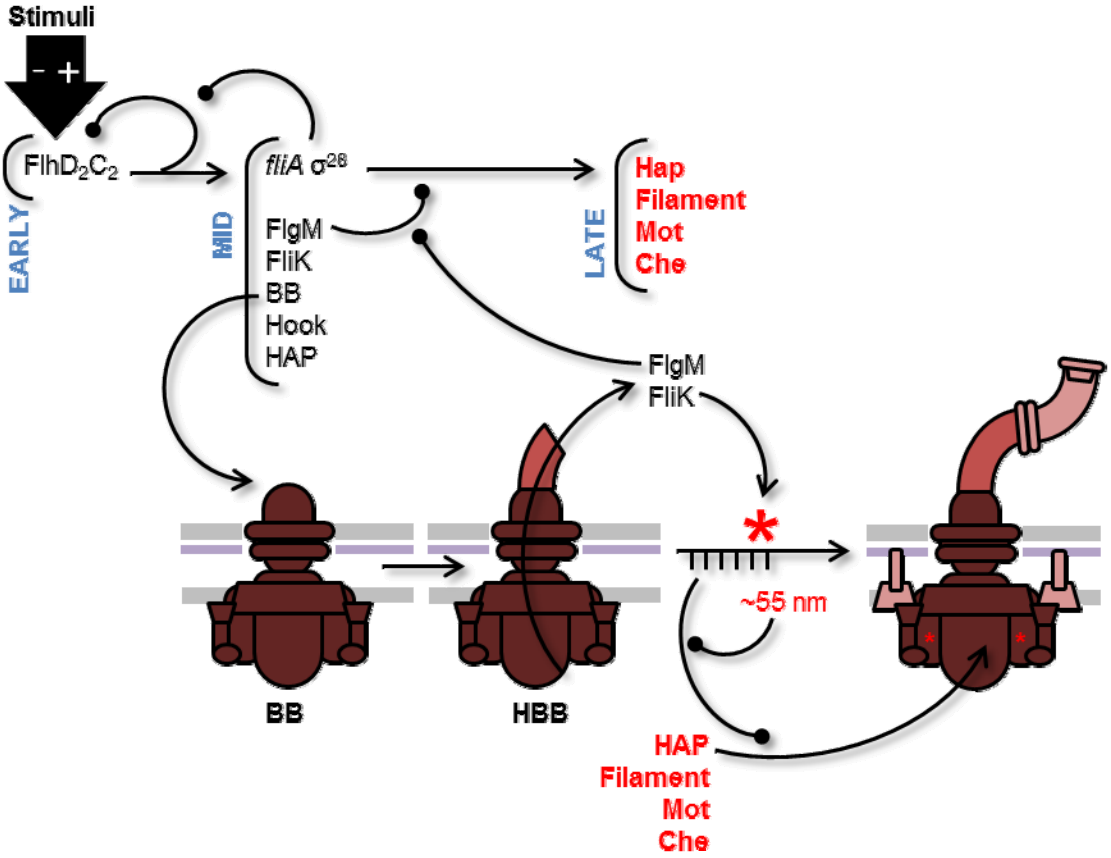

Figure 1.11. Regulation of flagellar apparatus assembly in *E. coli* and *Salmonella* (as discussed in the main text). Phases of genes in blue, late phase components in red. Substrate-specificity switch (*), Basal body (BB), hook-basal body complex (HBB). Adapted from Chillcot & Hughes 2000 and Brown *et al.* 2009.

HAPs FlgK, FlgL and FliD are secreted first, in that order, because they are also under mid-phase regulation and so present before the other late-phase proteins. Additionally, there are specific chaperones for FlgK, FlgL, FliD and FliC, which also regulate late-phase protein secretion (Chilcott & Hughes, 2000). Secreted FliD drives filament formation by increasing the polymerisation efficiency of flagellin. It does

this by capping the tip of the apparatus, slowing and guiding flagellin secretion. Flagellin is secreted in a partially unfolded state, in order to pass through the 30Å channel (Yonekura, 2000). FliD gives flagellin a chance to refold and make contacts with adjacent FliC, one at a time. With each FliC subunit added, FliD twists to the next site ready for a new FliC subunit. This results in FliD twisting in discrete steps at the end of the growing filament (Yonekura, 2000).

1.5.3 Flagellar rotation

Bacterial flagella can rotate, and this torque propels bacteria forwards (Blair, 2009). This form of motility is known as swimming and is powered by motor/stator complexes. These complexes surround the interface between C and MS rings, and are responsible for conducting proton motor force to the rotor/switch complex to generate rotation (Büttner, 2012). Each complex is made of four MotA subunits with two central MotB subunits and forms two channels (Braun *et al.*, 2004). It is likely that the passage of hydrogen ions through these channels changes specific ionic interactions between MotB and MotA. MotB is anchored to the peptidoglycan layer while MotA is not, causing more pronounced conformational changes in MotA subunits (Blair, 2009).

MotA movement is turned into rotation by its electrostatic interactions along the charged ridges of the rotor/switch complex (Blair, 2009). The rotor/switch complex connects the motor/stators to the MS ring and potentiates the rotation through the flagellum via FliG (Brown *et al.*, 2007). Other components of the rotor/switch complex can change the direction of rotation in response to stimuli by altering the conformation of FliG (Blair, 2009).

1.5.4 Swimming motility

Flagellar rotation, which occurs like a ship's propeller, can be used to push bacteria forward through liquids. This is known as swimming motility. There are other kinds of motility; swarming motility on solid substrates also uses flagella, while gliding motility does not (Merino & Tomas, 2009). Flagella filaments are predominantly

rigid left-handed helices and their rigidity is important for developing forward motion (Macnab & Ornston, 1977). However, flagella filaments have to be flexible enough to resist shearing forces, and it is their flexibility that allows peritrichous flagella to bundle behind moving bacteria (Arkhipov *et al.*, 2006). In this way bacteria can swim in a straight line, which is known as 'running'.

Bacteria change direction randomly, by 'tumbling'. Tumbling is induced by changing the direction of the flagellar rotation, by altering the conformation of the switch complex protein, FliG (Larsen *et al.*, 1974). This causes flagella to flay out from their bundle, twisting the bacterium. The altered conformation of the switch proteins resets very quickly, returning the direction of flagellar rotation back into running mode (Larsen *et al.*, 1974). As a result, the bacterium swims away in a straight line, in a new but random direction (Arkhipov *et al.*, 2006). In the absence of any chemoattractants or chemorepellents, this switching between running and tumbling modes occurs stochastically (Berg, 2003).

Chemotaxis describes the process of cells moving in the direction of an increasing or decreasing chemical gradient, depending on whether the chemical is attractive or repellent. Bacteria control the direction of swimming by altering the frequency of tumbling by phosphorylating chemotaxis proteins like CheY, which can then bind to FliM in the motor switch (Wadhams & Armitage, 2004). If bacteria are moving along a chemical gradient, then they tumble less frequently. If bacteria are not swimming along a chemical gradient, they tumble more frequently until they are.

1.5.5 Homology of flagella to T3SS

Flagella are so complex that they are often used as an example in both sides of an on-going debate between evolutionists and creationists. Creationists believe that something so irreducibly complex had to have been designed, while evolutionists think that for flagellar machines to be so complex, they must have evolved over billions of years. The icing on the cake for evolutionists came with technological advances in genomics. Bioinformatic analysis revealed a degree of sequence

homology between flagellar and translocation T3SSs across a range of bacteria that indicated a common ancestral origin (Pallen & Matzke, 2006).

Even without sequence data, the homology between flagella and T3SS is clear at many levels (Abby & Rocha, 2012). The superstructure of both macromolecular machines is similar, from the pore that runs through their entire length, membrane rings housing the substrate docking site and secretion apparatus, to the caps on the homo-multimeric filaments projecting from the cell (table 1.2, (Hughes, 2012)). In *E. coli* O157:H7 T3S filaments are made of EspA, which is structurally homologous to $FliC_{H7}$ from flagella filaments (Crepin *et al.*, 2008). Also, the tip complexes of the EHEC H7 flagella filament and T3S needle are both pentameric, encoded by the structurally homologous proteins $FliD_{H7}$ and EspD respectively (Büttner, 2012).

Table 1.2. Structural homology of T3SS proteins with flagellar components. Table is adapted from Hughes 2012.

Type III system	***Escherichia* LEE**	***Yersinia***	***Salmonella* Spi1**	***Salmonella* Spi2**	***Shigella***	**Flagella**
Secretin	EscC	YscC	InvG	SsaC	MxiD	FlgHI
M ring	EscD	YscD	PrgH	SsaD	MxiG	FliG
MA core	EscRST	YscRST	SpaPQR	SsaRST	SpaPQR	FliPQR
M/C core	EscV	YscV	InvA	SsaV	MxiA	FlhA
IM ring	EscJ	YscJ	PrgK	SsaJ	MxiJ	FliF
M/C core	EscU	YscU	SpaS	SsaU	SpaS	FlhB
C ring	EscQ	YscQ	SpaO	SsaQ	SpaO	FliN
Inner rod	EscI	YscI	PrgJ	SsaI	SpaM	FlgBCFG
Length control	EscP	YscP	InvJ	SsaP	Spa32	FliK
Needle/hook	EscF	YscF	PrgI	SsaG	MxiH	FlgE
ATPase complex	EscLN	YscKLN	OrgB, InvCI	SsaKNO	MxiK, Spa47	FliHIJ

The similarity between these two systems goes beyond their constituent parts. Flagella and T3SSs are also assembled and regulated in a similar manner (Büttner, 2012). Both are assembled by inserting the inner-membrane ring into the membrane first, followed by the outer-membrane ring, the central rod-like structure and finally the filament (Suzuki *et al.*, 1978). Both systems show secretion hierarchies and use chaperone proteins to correctly fold, prevent degradation of and deliver secretion substrates (Büttner, 2012).

Of course, there are some obvious differences between flagella and T3SSs too. Flagella filaments are much longer than EspA filaments, and wider, with a larger central channel (Crepin *et al.*, 2008). This is likely due to FliC being larger than EspA. Also, flagella have a hook, where T3SSs have a needle. Flagella rotate and are connected to a motor, while T3SSs are static. The IM ring in T3SSs is more complex. T3SSs diverged from flagella and adapted to different tasks some time ago (Abby & Rocha, 2012). Given this is the case however, it is striking how much overlap between these bacterial machines there still is.

1.5.6 Immune recognition of flagella

1.5.6.1 Innate immune recognition

Flagella are a pathogen-associated microbial pattern (PAMP) recognised by pattern recognition receptors (PRRs) of the host innate immune system. There are extracellular and intracellular PRRs that recognise flagellin. PRRs recognise monomeric flagellin and only poorly recognise filamentous flagellin. This is because they recognise conserved regions necessary for filament formation and motility, normally hidden within the filament (Smith *et al.*, 2003). Toll-like receptor 5 (TLR5) is an extracellular PRR, and NLRC4 (Nucleotide oligomerisation domain (NOD)-leucine-rich repeat (LRR) family containing caspase-recruitment domain (CARD) protein 4) is part of an intracellular PRR (Miao *et al.*, 2007). On recognition of flagellin, these PRRs quickly activate non-specific pro-inflammatory signalling.

TLR5 is generally expressed baso-laterally at epithelial sites but apical expression of TLR5 occurs in epithelial cells proximal to M cells (Abreu, 2010). Binding of flagellin to the LRR region of TLR5 allows TLR5 to dimerise and activate downstream NF-kB signalling pathways, producing pro-interleukin (IL)-1β and pro-IL-8 (Rumbo *et al.*, 2006). Apically expressed TLR5 is less reactive to flagellin (Rhee *et al.*, 2005). Despite this, apically applied $FliC_{H7}$ flagellin does result in basolateral IL-8 secretion (Berin *et al.*, 2002).

IL-8 is a chemokine which recruits monocytes and neutrophils to the site of activation and is induced strongly in response to flagella expressed by pathogenic bacteria proximal to intestinal epithelial cells (Khan *et al.*, 2008; Samanta *et al.*, 1989; Sampaio *et al.*, 2009). In addition to IL-8, bacterial flagellin induces production of CCL20, which recruits dendritic cells (Sierro *et al.*, 2001). Recruitment of monocytes leads them to differentiate into macrophages. Both neutrophils and macrophages are phagocytes, engulfing extracellular pathogens before killing them. Both macrophages and dendritic cells process the antigens they are exposed to and present them to adaptive immune cells. These adaptive cells then mount a specific response and generate immunological memory (Harris & Ronchese, 1999).

Some flagellated bacteria have evolved to escape TLR5 recognition and have still retained their motility (Anderssen-Nissen 2006). Mutations of conserved TLR5-recognition sites in flagellin have been co-selected with other compensatory mutations that allow appropriate flagellin folding. However, this has only been discovered in α and ε proteobacteria species and is not the case for γ-proteobacteria such as *E. coli* and *Salmonella*, likely due to different selection pressures. With this in mind, there is also the possibility that TLR5 signalling can be of benefit to attached bacteria. TLR5 signalling can be cyto-protective by preventing apoptosis, ensuring colonised cells remain viable (Vijay-Kumar *et al.*, 2006). Of course, this has to be weighed against the obvious disadvantage of flagellin recognition before bacterial attachment. However, there is even some debate about whether TLR5 recognition is relevant in the bovine host, due to non-synonymous single nucleotide

polymorphisms in the signalling domain which may prevent downstream signalling (Smith *et al.*, 2012).

Intracellular recognition of flagellin occurs through NLRC4 inflammasome formation (Zhao *et al.*, 2011). An inflammasome is a multi-protein complex that causes the activation of pro-inflammatory caspases, such as Caspase-1 (Miao *et al.*, 2006). NLRC4 was previously known as interleukin-1 converting enzyme (ICE)-protease activating factor (Ipaf) or CARD12. NLRC4 activation of Caspase-1 results in cleavage of pro-IL-1β, pro-IL-6, pro-IL-8 into their mature forms (Ayres *et al.*, 2012). This implies co-operation between TLR5 signalling, which prepares inflammatory cytokines, and NLRC4 signalling, which processes these cytokines for their release (Miao *et al.*, 2010). This adds another layer of regulation – two conserved regions of flagellin are sensed by the host, at different places and in sequence, to mount an innate response and help direct adaptive responses (Fontana & Vance, 2011).

Neuronal apoptosis inhibitory proteins (Naip) are key candidates for initiating NLRC4 inflammasome activation (Vinzing *et al.*, 2008). NLRC4 is also activated in response to T3S components from a number of bacteria, including *E. coli* (Zhao *et al.*, 2011). It is likely that specific Naip proteins adapt different targets to NLRC4, as with Naip5 for *Legionella pneumophila* flagellin in macrophages (Lightfield *et al.*, 2008). However, little is known specifically about intracellular innate detection of *E. coli* flagellin in intestinal epithelial cells. Naip5 did not recognise flagellin from *E. coli* but a flagella expressing opportunistic *E. coli* caused sepsis due to NLRC4 inflammasome dysregulation ((Ayres *et al.*, 2012; Wilmanski *et al.*, 2008)

1.5.6.2 Adaptive immune recognition

There is also an adaptive immune response to flagella, which results in the production of neutralising antibodies or ‘immunoglobulins' (Ig) and memory to flagella antigens. Antibodies are generated by the activation and differentiation of B cells upon recognition of flagella antigens by specific B cell receptors (Nempont & Cayet, 2008). B cell receptor recognition of flagella surface epitopes is the basis for

H-serotyping; B cell receptors are a membrane bound form of the antibodies that they will produce after differentiation into plasma cells. In parallel, the macrophages and dendritic cells recruited to the site by innate signalling then present flagellin peptides to T cells (Harris & Ronchese, 1999). This activates antigen-specific helper T cells, which then facilitate B cell differentiation into plasma and memory B cells. B cells start with IgM and IgD receptor expression. As B cells mature in response to local cytokines, they make different kinds of antibodies to the same antigen, in a process known as isotype-switching (Estes, 1996). These antibodies recognise the same antigen, but have different structures and binding avidities.

Systemic vaccination of cattle with purified H7 flagella results in IgA that recognises surface epitopes of $FliC_{H7}$, and IgG that recognises both surface epitopes and extensive linear epitopes (McNeilly *et al.*, 2010b). This indicates that there are different sub-populations of B cells that are recognising differentially processed flagella antigen but it is not known how this occurs. This has important practical implications for vaccination of cattle with H7 flagella. Antibodies to linear epitopes directed along the full length flagellin have the potential to block TLR5 recognition epitopes (Saha *et al.*, 2007).

1.6 Roles of flagella in pathogenesis

The specific contribution of flagella to bacterial pathogenesis can be controversial. Flagella can be shown to enhance or reduce bacterial colonisation, depending on the stage of infection tested. At early stages of infection, flagella tend to enhance colonisation through chemotaxis (section 1.5.4) and adherence (section 1.6.3). This is because the major limiting factor at this point is bacterial contact and attachment to favourable colonisation sites. However, once bacteria are attached, deleterious interactions with the host immune response can take precedence. In some scenarios though, flagella modulate these responses to maintain attachment. Deletion of flagella from *Salmonella* resulted in reduced NF-κB activation but also increased cleavage of caspase-3, resulting in more severe inflammation (Vijay-Kumar *et al.*,

2006). Activation of NF-κB was more self-limiting due to modulation of host caspase activity.

1.6.1 Immuno-modulation by flagellin secretion

Flagella filaments can be naturally depolymerised, snapped or sheared, releasing flagellin (as discussed in chapter 6). These flagellin monomers are more sensitively detected by the innate immune system than polymerised flagellin (section 1.5.6.1). Despite the obvious advantages of limiting the exposure of TLR5-binding epitopes, some pathogens have been shown to actively secrete flagellin monomers as potent immuno-modulators. Internalised *S.* Typhimurium secretes FliC flagellin via its T3SS from the *Salmonella*-containing vacuole into the cytosol (Miao *et al.*, 2006). It is likely that this is made possible due to the common origin of the T3SS apparatus and flagella (section 1.5.5). Type-III secretion of flagellin into cells is pro-inflammatory, resulting in NLRC4 inflammasome activation (Zhao *et al.*, 2011). If this inhibits the colonisation of extracellular bacterial competitors, it may be advantageous to the bacterium.

Lysophospholipid release by host cells can trigger the production and secretion of flagellin by extracellular *S. typhi* in order to detect it more easily (Subramanian & Qadri, 2006). This could be advantageous for bacteria too, as it recruits immune cells to the site of infection that are necessary for their dissemination. EPEC is also physically capable of secreting FliC through its T3SS (Badea *et al.*, 2009). This suggests that *E. coli* in general may also possess the ability to secrete flagellin, but that it is more tightly regulated (Badea *et al.*, 2009). However, T3SS of flagellin secretion by wild-type bacteria or flagellin translocation into host cells not yet been demonstrated.

1.6.2 Flagellar secretion of T3S effector proteins

The converse of T3S of flagellin through T3SS needles is that some bacteria can use their flagella to secrete type-III effector proteins. *C. jejuni* lacks a functional translocation-type T3SS, but is still able to secrete multiple type-III effectors

(Guerry, 2007). CiaB has been found inside the cytoplasm of eukaryotic cells. The mechanism of translocation has not been demonstrated, but a fully intact flagellum is required for this phenotype (Konkel *et al.*, 2004). Deletion of some of these effectors, such as FlaC, reduces invasion of the mutant strain, while FspA is cytotoxic when applied to cell lines (Poly *et al.*, 2007; Song *et al.*, 2004). Taken together, this indicates that proteins with effector function, that are not known to be part of the flagellar apparatus, are being secreted by flagella, perhaps directly into cells.

With the above in mind, it is interesting to note that both phase-types of *Salmonella* flagella have been shown to enhance invasion of porcine intestinal tissue culture models by deletion mutagenesis (Elvidge, 2012). Motility was thought to play an important role, but when bacteria were centrifuged onto cells there was still a flagellin-dependent invasion defect. The mechanism, whether secretory, mechanical or immune-modulatory, is still unknown.

1.6.3 Flagellar adherence

The role of flagella in adherence has received more attention over the years, as researchers have realised that there are phenotypes that require flagella other than motility. Flagella have been shown to mediate initial adherence to host cells for ETEC, EPEC, EHEC, various *Salmonella* species, *Clostridium difficile* and *P. aeruginosa*, (Best & Ragione, 2005; Feldman *et al.*, 1998; Girón *et al.*, 2002; Mahajan *et al.*, 2009; Tasteyre *et al.*, 2001). Additionally, through initial, reversible adherence to both inanimate and live surfaces, flagella play an important role in biofilm formation, and final dispersal from mature biofilms to another site (Van Houdt & Michiels, 2006).

A number of pathogens use their flagella for host-cell adherence, using a few mechanisms. Enteropathogenic *E. coli* flagella adhere to HeLa and cow intestinal cells by the FliC filament shaft, whereas flagellar adherence is primarily mediated by FliD caps with *P. aeruginosa* (Arora *et al.*, 1998; Girón *et al.*, 2002). For *C. difficile*, there is a cooperative effect of FliC and FliD on adherence (Tasteyre *et al.*, 2001). Tip-expressed adhesins can be secreted by the flagella apparatus as with FliD, or

secreted independently of the flagellar apparatus, as with EtpA from ETEC (Roy *et al.*, 2009b). Interestingly, the EtpA glycoprotein was found to bind the conserved terminals of FliC flagellin, shown to be inside the flagella filament (Roy *et al.*, 2009b; Yonekura *et al.*, 2003). Roy *et al.* (2009) went on to show that EtpA was only able to bind the conserved region of FliC in the absence of FliD filament caps.

This has two implications. Firstly, it suggests that the conserved regions of flagellin are occasionally surface-exposed and may be able to contribute to binding in a largely intact filament. The exposed conserved regions of FliC may be able to bind to host immune receptors such as apical TLR5 to promote adherence without immune recognition. Secondly, this demonstrates that adhesins are able to use existing structures, such as flagella, as an adaptor or platform to project considerable distances from the cell. This would increase the likelihood of their coming into contact with cell-associated ligands or facilitate proposed flagellar probing of host epithelia during initial attachment.

Host-cell binding by flagella often occurs via gangliosides and mucins, which can trigger downstream inflammatory signalling cascades. *P. aeruginosa* flagella bind asialo-GM1, triggering TLR2 and Ca^{2+}-dependent secretion of IL-8 in CHO cells and the shuttling of TLR5 to the apical surface of polarised 16HBE cells (Adamo *et al.*, 2004). Conversely, these flagella are also able to bind to and activate Muc1, which results in down-regulation of TLR5 activation and IL-8 induction (Lillehoj *et al.*, 2002; Ueno *et al.*, 2008). This may be important for *P. aeruginosa* epithelial colonisation, as $Muc1^{-/-}$ mice were also more able to clear *P. aeruginosa* than WT mice after pulmonary infection (Lu *et al.*, 2006). EPEC H6 and EHEC H7 flagella are able to bind to mucins as well (Erdem *et al.*, 2007), raising the possibility that EHEC O157:H7 could use host mucins as receptors for immuno-modulation as well as initial adherence.

1.6.4 H7 flagella adherence

The role of H7 flagella in adherence to host cells has not always been very clear. Initial studies showed that purified H7 flagella were adhesive to epithelial cells and

H6 flagella were not (Mahajan *et al.*, 2009). Additionally, EPEC H6 and H2 flagella but not EHEC H7 flagella were involved in bacterial adherence to epithelial monolayers (Girón *et al.*, 2002). However, these experiments were conducted on HeLa cell lines. Subsequent work has shown that EHEC purified H7 flagella adhere to primary cell cultures of the BTR and EPEC H11 flagella do not (Mahajan *et al.*, 2009). Additionally, BTR adhesion by flagella appeared to be H7-specific in the context of bacterial colonisation. Complementation of EHEC O157:H7 *fliC*$^{-}$ strains with *fliC*$_{H6}$ did not fully restore wild-type binding. This study did not address the mechanism of flagella-based adherence, so it is not yet known whether flagella $FliD_{H7}$ cap-binding, rotation or chemotaxis is required for EHEC adherence in this model.

Clues for defining the basis for the phenotypic differences between H6 and H7 flagella have come from the substrate-specificity experiments of Erdem *et al.* (2007). They showed that H6 but not H7 flagella bind to collagen, while EHEC H7 flagella bind more sensitively to certain commercial mucin preparations than H6 flagella. This differential mucin binding likely relates to differences in flagella filament binding avidity, as there was no difference between H6 and H7 flagellin monomers. As H6 and H7 flagella tend to be associated with particular pathotypes, differences in flagella binding-specificities may contribute to the host and tissue tropisms of EHEC and EPEC (Mundy *et al.*, 2007).

1.7 Vaccination with T3S and flagella together

H7 flagella are involved in adherence to host cells at the principle site of EHEC O157:H7 colonisation and are potent immuno-modulators. On this basis, the use of H7 flagellin, $FliC_{H7}$, as part of an EHEC vaccine in cattle was patented (Gally *et al.*, 2009). Vaccinating cattle intra-muscularly with purified $FliC_{H7}$ alone reduced the number of animals colonised with *E. coli* O157:H7 after experimental challenge (McNeilly *et al.*, 2008). The mode of action was thought to be by the generation of specific IgA and IgG that could block $FliC_{H7}$ flagella BTRE binding (McNeilly *et al.*, 2008). However, protection was only partial. Faecal shedding of *E. coli* O157:H7 was initially reduced, but also prolonged in vaccinated cattle that became colonised

(McNeilly *et al.*, 2008). The mechanism of this observed effect is not fully understood but likely relates to how $FliC_{H7}$ monomers and $FliC_{H7}$ flagella are recognised by the innate immune system. Despite this drawback, the use of purified $FliC_{H7}$ in a variety of multi-component recombinant T3S protein vaccines increases their efficacy (McNeilly *et al.*, 2010a).

1.8 Aims

Control of EHEC O157:H7 by vaccination of cattle with combinations of rationally chosen antigens is a cost effective way of reducing human HUS incidence. A detailed appreciation of what might happen if a potential vaccine actually inhibits these factors is vital for this. The role of many virulence factors in EHEC O157:H7 colonisation is already understood. The exquisite mechanistic detail at a molecular level of key T3S effector protein involvement in BTR adherence has made their inclusion in a rational vaccine a natural choice.

The role of H7 flagella as an adhesin in EHEC O157:H7 colonisation at its principal site and source of infection and spread, the BTR, has only recently been established. Currently, $FliC_{H7}$ has the potential to be efficacious in such a bovine EHEC vaccine. Presumably vaccination with $FliC_{H7}$ is protective because it results in antibodies that block $FliC_{H7}$ flagella adherence. However, there are still issues with $FliC_{H7}$ vaccination. To resolve these, more work is needed to understand why blocking $FliC_{H7}$ flagella with $FliC_{H7}$ antibodies might have an impact on EHEC colonisation and pathogenesis.

The mechanism of H7 flagella adherence in EHEC colonisation is not fully understood. It is not known if the role of H7 flagella as an adhesin is solely $FliC_{H7}$-dependent, or whether other H7 flagella components such as $FliD_{H7}$ are also involved. Which specific epitopes of the $FliC_{H7}$ monomer are required for $FliC_{H7}$ flagella binding to the BTR is also unknown. Additionally, there are no known $FliC_{H7}$ flagella ligands. A precise knowledge of which interactions are involved in BTR colonisation by EHEC O157:H7 is required to better design vaccine components to block it. The nature of these ligands may underpin the mechanism of

BTR adherence, or even reveal novel contributions of H7 flagella to EHEC O157:H7 colonisation. Therefore the study described by this thesis aims to:

- Characterise H7 flagella interaction with BTR.
- Investigate the role of $FliD_{H7}$ in BTR binding.
- Define the BTR binding epitopes in $FliC_{H7.}$
- Characterise H7-H7 receptor interactions in the BTR.

It is hoped that achieving these aims will lead to improved rational bovine vaccine design and a fuller appreciation for how H7 flagella can enhance EHEC colonisation of the bovine host.

1.9 References

Abby, S. S. & Rocha, E. P. C. (2012). The Non-Flagellar Type III Secretion System Evolved from the Bacterial Flagellum and Diversified into Host-Cell Adapted Systems. *PLoS genetics* **8**, e1002983.

Abreu, M. T. (2010). Toll-like receptor signalling in the intestinal epithelium: how bacterial recognition shapes intestinal function. *Nature reviews Immunology* **10**, 131–44.

Adamo, R., Sokol, S., Soong, G., Gomez, M. I. & Prince, A. (2004). *Pseudomonas aeruginosa* flagella activate airway epithelial cells through asialoGM1 and toll-like receptor 2 as well as toll-like receptor 5. *American journal of respiratory cell and molecular biology* **30**, 627–34.

Agüero, M. E. & Cabello, F. C. (1983). Relative contribution of ColV plasmid and K1 antigen to the pathogenicity of *Escherichia coli*. *Infection and immunity* **40**, 359–68.

Alpers, K., Werber, D., Frank, C., Koch, J., Friedrich, A. W., Karch, H., An DER Heiden, M., Prager, R., Fruth, A. & other authors. (2009). Sorbitol-fermenting enterohaemorrhagic *Escherichia coli* O157:H- causes another outbreak of haemolytic uraemic syndrome in children. *Epidemiology and infection* **137**, 389–95.

Andersen-Nissen, E., Smith, K. D., Strobe, K. L., Barrett, S. L. R., Cookson, B. T., Logan, S. M. & Aderem, A. (2005). Evasion of Toll-like receptor 5 by flagellated bacteria. *Proceedings of the national academy of sciences of the United States of America* **102**, 9247–52.

Andrianantoandro, E. & Pollard, T. D. (2006). Mechanism of actin filament turnover by severing and nucleation at different concentrations of ADF/cofilin. *Molecular cell* **24**, 13–23.

Arbeloa, A., Blanco, M., Moreira, F. C., Bulgin, R., López, C., Dahbi, G., Blanco, J. E., Mora, A., Alonso, M. P. & other authors. **(2009).** Distribution of *espM* and *espT* among enteropathogenic and enterohaemorrhagic Escherichia coli. *Journal of medical microbiology* **58**, 988–95.

Arkhipov, A., Freddolino, P. L., Imada, K., Namba, K. & Schulten, K. (2006). Coarse-grained molecular dynamics simulations of a rotating bacterial flagellum. *Biophysical journal* **91**, 4589–97.

Arora, S. K., Ritchings, B. W., Almira, E. C., Lory, S. & Ramphal, R. (1998). The *Pseudomonas aeruginosa* flagellar cap protein, FliD, is responsible for mucin adhesion. *Infection and immunity* **66**, 1000–7.

Arpin, M., Chirivino, D., Naba, A. & Zwaenepoel, I. (2011). Emerging role for ERM proteins in cell adhesion and migration. *Cell adhesion & migration* **5**, 199–206.

Ayres, J. S., Trinidad, N. J. & Vance, R. E. (2012). Lethal inflammasome activation by a multidrug-resistant pathobiont upon antibiotic disruption of the microbiota. *Nature medicine* **18**, 799–806.

Badea, L., Beatson, S. a, Kaparakis, M., Ferrero, R. L. & Hartland, E. L. (2009). Secretion of flagellin by the LEE-encoded type III secretion system of enteropathogenic *Escherichia coli*. *BMC microbiology* **9**, 30.

Bavaro, M. F. (2012). *E. coli* O157:H7 and other toxigenic strains: the curse of global food distribution. *Current gastroenterology reports* **14**, 317–23.

Berg, H. C. (2003). The rotary motor of bacterial flagella. *Annual review of biochemistry* **72**, 19–54.

Berin, M. C., Darfeuille-Michaud, A., Egan, L. J., Miyamoto, Y. & Kagnoff, M. F. (2002). Role of EHEC O157:H7 virulence factors in the activation of intestinal epithelial cell NF-κB and MAP kinase pathways and the upregulated expression of interleukin 8. *Cellular microbiology* **4**, 635–648.

Best, A. & Ragione, R. (2005). Role for flagella but not intimin in the persistent infection of the gastrointestinal tissues of specific-pathogen-free chicks by Shiga toxin-negative *Escherichia coli* O157:H7. *Infection and immunity* **73**, 1836–1846.

Betis, F., Brest, P., Hofman, V., Guignot, J., Bernet-Camard, M. F., Rossi, B., Servin, A. & Hofman, P. (2003). The Afa/Dr adhesins of diffusely adhering Escherichia coli stimulate interleukin-8 secretion, activate mitogen-activated protein kinases, and promote polymorphonuclear transepithelial migration in T84 polarized epithelial cells. *Infection and immunity* **71**, 1068–1074.

Bilge, S. S., Clausen, C. R., Lau, W. & Moseley, S. L. (1989). Molecular characterization of a fimbrial adhesin, F1845, mediating diffuse adherence of diarrhea-associated *Escherichia coli* to HEp-2 cells. *Journal of bacteriology* **171**, 4281–9.

Blair, D. F. (2009). Structure and mechanism of the flagellar rotary motor. In *Pili and flagella, current research and future trends*, 1st edn., pp. 121–136. Edited by K. F. Jarrell. Norfolk: Caister Academic Press.

Bobkov, A. A., Muhlrad, A., Pavlov, D. A., Kokabi, K., Yilmaz, A. & Reisler, E. (2006). Cooperative effects of cofilin (ADF) on actin structure suggest allosteric mechanism of cofilin function. *Journal of molecular biology* **356**, 325–34.

Bourdet-Sicard, R., Rüdiger, M., Jockusch, B. M., Gounon, P., Sansonetti, P. J. & Nhieu, G. T. (1999). Binding of the *Shigella* protein IpaA to vinculin induces F-actin depolymerization. *The EMBO journal* **18**, 5853–62.

Braun, T. F., Al-Mawsawi, L. Q., Kojima, S. & Blair, D. F. (2004). Arrangement of core membrane segments in the MotA/MotB proton-channel complex of *Escherichia coli*. *Biochemistry* **43**, 35–45.

Brooke, M. A., Nitoiu, D. & Kelsell, D. P. (2012). Cell-cell connectivity: desmosomes and disease. *The Journal of pathology* **226**, 158–71.

Brooks, J. T., Sowers, E. G., Wells, J. G., Greene, K. D., Griffin, P. M., Hoekstra, R. M. & Strockbine, N. A. (2005). Non-O157 Shiga toxin-producing *Escherichia coli* infections in the United States, 1983-2002. *The Journal of infectious diseases* **192**, 1422–9.

Brown, J. W. & McKnight, C. J. (2010). Molecular model of the microvillar cytoskeleton and organization of the brush border. *PloS one* **5**, e9406.

Brown, J., Faulds-Pain, A. & Aldridge, P. (2009). The co-ordination of flagellar gene expression and the flagellar assembly pathway. In *Pili and flagella, current research and future trends*, 1st edn., pp. 99–120. Edited by K. F. Jarrell. Norfolk: Caister Academic Press.

Brown, P. N., Terrazas, M., Paul, K. & Blair, D. F. (2007). Mutational analysis of the flagellar protein FliG: sites of interaction with FliM and implications for organization of the switch complex. *Journal of bacteriology* **189**, 305–12.

Buchrieser, C., Glaser, P., Rusniok, C., Nedjari, H., D'Hauteville, H., Kunst, F., Sansonetti, P. & Parsot, C. (2000). The virulence plasmid pWR100 and the repertoire of proteins secreted by the type III secretion apparatus of *Shigella flexneri*. *Molecular Microbiology* **38**, 760–771.

Bulgin, R., Arbeloa, A., Goulding, D., Dougan, G., Crepin, V. F., Raymond, B. & Frankel, G. (2009). The T3SS effector EspT defines a new category of invasive enteropathogenic *E. coli* (EPEC) which form intracellular actin pedestals. *PLoS pathogens* **5**, e1000683.

Bulgin, R., Raymond, B., Garnett, J. A., Frankel, G., Crepin, V. F., Berger, C. N. & Arbeloa, A. (2010). Bacterial guanine nucleotide exchange factors SopE-like and WxxxE effectors. *Infection and immunity* **78**, 1417–25.

Büttner, D. (2012). Protein export according to schedule: architecture, assembly, and regulation of type III secretion systems from plant- and animal-pathogenic bacteria. *Microbiology and molecular biology reviews* **76**, 262–310.

Callaway, T. R., Carr, M. A., Edrington, T. S., Anderson, R. C. & Nisbet, D. J. (2009). Diet, *Escherichia coli* O157:H7, and cattle: a review after 10 years. *Current issues in molecular biology* **11**, 67–79.

Campellone, K. G., Robbins, D. & Leong, J. M. (2004). EspFU is a translocated EHEC effector that interacts with Tir and N-WASP and promotes Nck-independent actin assembly. *Developmental cell* **7**, 217–28.

Chase-Topping, M., Gally, D., Low, C., Matthews, L. & Woolhouse, M. (2008). Super-shedding and the link between human infection and livestock carriage of *Escherichia coli* O157. *Nature reviews Microbiology* **6**, 904–12.

Chaudhuri, R. R. & Henderson, I. R. (2012). The evolution of the *Escherichia coli* phylogeny. *Infection, genetics and evolution : journal of molecular epidemiology and evolutionary genetics in infectious diseases* **12**, 214–26.

Chen, H. D. & Frankel, G. (2005). Enteropathogenic *Escherichia coli*: unravelling pathogenesis. *FEMS microbiology reviews* **29**, 83–98.

Chilcott, G. S. & Hughes, K. T. (2000). Coupling of flagellar gene expression to flagellar assembly in *Salmonella enterica* serovar Typhimurium and *Escherichia coli*. *Microbiology and molecular biology reviews* **64**, 694–708.

Clarke, M. B. & Sperandio, V. (2005). Transcriptional regulation of *flhDC* by QseBC and sigma (FliA) in enterohaemorrhagic *Escherichia coli*. *Molecular microbiology* **57**, 1734–49.

Connell, I., Agace, W., Klemm, P., Schembri, M., Mărild, S. & Svanborg, C. (1996). Type 1 fimbrial expression enhances *Escherichia coli* virulence for the urinary tract. *Proceedings of the national academy of sciences of the United States of America* **93**, 9827–32.

Cornick, N. A., Booher, S. L. & Moon, H. W. (2002). Intimin facilitates colonization by *Escherichia coli* O157:H7 in adult ruminants. *Infection and immunity* **70**, 2704–7.

Cowden, J. M., Ahmed, S., Donaghy, M. & Riley, A. (2001). Epidemiological investigation of the central Scotland outbreak of *Escherichia coli* O157 infection, November to December 1996. *Epidemiology and infection* **126**, 335–41.

Cravioto, A., Gross, R. J., Scotland, S. M. & Rowe, B. (1979). An adhesive factor found in strains of *Escherichia coli* belonging to the traditional infantile enteropathogenic serotypes. *Current microbiology* **3**, 95–99.

Crepin, V. F., Martinez, E., Shaw, R. K., Frankel, G. & Daniell, S. J. (2008). Structural and functional properties of chimeric EspA-FliCi filaments of EPEC. *Journal of molecular biology* **378**, 243–50.

Croxen, M. a & Finlay, B. B. (2010). Molecular mechanisms of *Escherichia coli* pathogenicity. *Nature reviews Microbiology* **8**, 26–38.

Dean, P. & Kenny, B. (2004). Intestinal barrier dysfunction by enteropathogenic *Escherichia coli* is mediated by two effector molecules and a bacterial surface protein. *Molecular microbiology* **54**, 665–75.

Dean, P., Maresca, M., Schüller, S., Phillips, A. D. & Kenny, B. (2006). Potent diarrheagenic mechanism mediated by the cooperative action of three enteropathogenic *Escherichia coli* - injected effector proteins. *Proceedings of the national academy of sciences of the United States of America* **103**, 1876–81.

Van Diemen, P. M., Dziva, F., Abu-Median, A., Wallis, T. S., Van den Bosch, H., Dougan, G., Chanter, N., Frankel, G. & Stevens, M. P. (2007). Subunit vaccines based on intimin and Efa-1 polypeptides induce humoral immunity in cattle but do not protect against intestinal colonisation by enterohaemorrhagic *Escherichia coli* O157:H7 or O26:H-. *Veterinary immunology and immunopathology* **116**, 47–58.

Dobbin, H. & Hovde, C. (2006). The *Escherichia coli* O157 flagellar regulatory gene *flhC* and not the flagellin gene *fliC* impacts colonization of cattle. *Infection and immunity* **74**, 2894–2905.

Dominguez, R. (2007). The beta-thymosin/WH2 fold: multifunctionality and structure. *Annals of the New York academy of sciences* **1112**, 86–94.

Dong, N., Liu, L. & Shao, F. (2010). A bacterial effector targets host DH-PH domain RhoGEFs and antagonizes macrophage phagocytosis. *The EMBO journal* **29**, 1363–76.

Dong, T. & Schellhorn, H. E. (2009). Control of RpoS in global gene expression of *Escherichia coli* in minimal media. *Molecular genetics and genomics* **281**, 19–33.

Dziva, F., Van Diemen, P. M., Stevens, M. P., Smith, A. J. & Wallis, T. S. (2004). Identification of *Escherichia coli* O157 : H7 genes influencing colonization of the bovine gastrointestinal tract using signature-tagged mutagenesis. *Microbiology* **150**, 3631–45.

Dziva, F., Vlisidou, I., Crepin, V. F., Wallis, T. S., Frankel, G. & Stevens, M. P. (2007). Vaccination of calves with EspA, a key colonisation factor of *Escherichia coli* O157:H7, induces antigen-specific humoral responses but does not confer protection against intestinal colonisation. *Veterinary microbiology* **123**, 254–61.

ECDC. **(2011).** *European Centre for Disease Prevention and Control annual epidemiological report 2011. Reporting on 2009 surveillance data and 2010 epidemic intelligence data.* Stockholm.

Egile, C., Loisel, T. P., Laurent, V., Li, R., Pantaloni, D., Sansonetti, P. J. & Carlier, M. F. (1999). Activation of the CDC42 effector N-WASP by the Shigella flexneri IcsA protein promotes actin nucleation by Arp2/3 complex and bacterial actin-based motility. *Journal of cell biology* **146**, 1319–32.

Elliott, S. J., Wainwright, L. A., McDaniel, T. K., Jarvis, K. G., Deng, Y. K., Lai, L. C., McNamara, B. P., Donnenberg, M. S. & Kaper, J. B. (1998). The complete sequence of the locus of enterocyte effacement (LEE) from enteropathogenic *Escherichia coli* E2348/69. *Molecular microbiology* **28**, 1–4.

Elvidge, J. (2012). *Identification and characterisation of* Salmonella enterica *serovar Typhimurium factors playing a role in colonisation of the porcine gut*. University of Edinburgh.

Erdem, A. L., Avelino, F., Xicohtencatl-Cortes, J. & Girón, J. a. **(2007).** Host protein binding and adhesive properties of H6 and H7 flagella of attaching and effacing *Escherichia coli*. *Journal of bacteriology* **189**, 7426–35.

Escherich, T. (1884). The intestinal bacteria of the neonate and breast-fed infant. *Reviews of infectious diseases* **10**, 1220–5.

Estes, D. M. (1996). Differentiation of B cells in the bovine. Role of cytokines in immunoglobulin isotype expression. *Veterinary immunology and immunopathology* **54**, 61–7.

Evans, D. G. & Evans, D. J. (1978). New surface-associated heat-labile colonization factor antigen (CFA/II) produced by enterotoxigenic *Escherichia coli* of serogroups O6 and O8. *Infection and immunity* **21**, 638–47.

Feldman, M., Bryan, R., Rajan, S., Scheffler, L., Brunnert, S., Tang, H. & Prince, A. (1998). Role of flagella in pathogenesis of *Pseudomonas aeruginosa* pulmonary infection. *Infection and immunity* **66**, 43–51.

Field, M. (1979). Mechanisms of action of cholera and *Escherichia coli* enterotoxins. *The American journal of clinical nutrition* **32**, 189–96.

Firat-Karalar, E. N. & Welch, M. D. (2011). New mechanisms and functions of actin nucleation. *Current opinion in cell biology* **23**, 4–13.

Fleckenstein, J., Kopecko, D., Warren, R. & Elsinghorst, E. (1996). Molecular characterization of the *tia* invasion locus from enterotoxigenic *Escherichia coli*. *Infection and immunity* **64**, 2256–2265.

Fontana, M. F. & Vance, R. E. (2011). Two signal models in innate immunity. *Immunological reviews* **243**, 26–39.

Frenzen, P. D., Drake, A. & Angulo, F. J. (2005). Economic cost of illness due to *Escherichia coli* O157 infections in the United States. *Journal of food protection* **68**, 2623–30.

Gally, D., McNeilly, T., Smith, D., George, E., Low, C., Mahajan, A. & Naylor, S. (2009). WIPO Patent No.2009050474: Immunogenic compositions containing *Escherichia coli* H7 flagella and methods of use thereof.

Garmendia, J., Phillips, A. D., Carlier, M.-F., Chong, Y., Schüller, S., Marches, O., Dahan, S., Oswald, E., Shaw, R. K. & other authors. **(2004).** TccP is an enterohaemorrhagic *Escherichia coli* O157:H7 type III effector protein that couples Tir to the actin-cytoskeleton. *Cellular microbiology* **6**, 1167–83.

Gauthier, A., Thomas, N. A. & Finlay, B. B. (2003). Bacterial injection machines. *Journal of biological chemistry* **278**, 25273–6.

Giles, C. & Sangster, G. (1948). An outbreak of infantile gastro-enteritis in Aberdeen; the association of a special type of *Bacterium coli* with the infection. *The journal of hygiene* **46**, 1–9.

Girard, F., Batisson, I. & Frankel, G. (2005). Interaction of enteropathogenic and Shiga toxin-producing *Escherichia coli* and porcine intestinal mucosa: role of intimin and Tir in adherence. *Infection and immunity* **73**, 6005–6016.

Girón, J. A., Ho, A. S. & Schoolnik, G. K. (1991). An inducible bundle-forming pilus of enteropathogenic *Escherichia coli*. *Science* **254**, 710–3.

Girón, J. A., Torres, A. G., Freer, E. & Kaper, J. B. (2002). The flagella of enteropathogenic *Escherichia coli* mediate adherence to epithelial cells. *Molecular microbiology* **44**, 361–79.

Goley, E. D. & Welch, M. D. (2006). The ARP2/3 complex: an actin nucleator comes of age. *Nature reviews Molecular cell biology* **7**, 713–26.

Grazi, E. & Trombetta, G. (1985). Effects of temperature on actin polymerized by Ca2+. Direct evidence of fragmentation. *The biochemical journal* **232**, 297–300.

Guerry, P. (2007). *Campylobacter* flagella: not just for motility. *Trends in microbiology* **15**, 456–61.

Gunther, N. W., Lockatell, V., Johnson, D. E. & Mobley, H. L. (2001). In vivo dynamics of type 1 fimbria regulation in uropathogenic *Escherichia coli* during experimental urinary tract infection. *Infection and immunity* **69**, 2838–46.

Gurniak, C. B., Perlas, E. & Witke, W. (2005). The actin depolymerizing factor n-cofilin is essential for neural tube morphogenesis and neural crest cell migration. *Developmental biology* **278**, 231–41.

Gyles, C. L. (2007). Shiga toxin-producing *Escherichia coli*: an overview. *Journal of animal science* **85**, E45–62.

Haglund, C. M. & Welch, M. D. (2011). Pathogens and polymers: microbe-host interactions illuminate the cytoskeleton. *Journal of cell biology* **195**, 7–17.

Haglund, C. M., Choe, J. E., Skau, C. T., Kovar, D. R. & Welch, M. D. (2010). *Rickettsia* Sca2 is a bacterial formin-like mediator of actin-based motility. *Nature cell biology* **12**, 1057–63.

Hall, A. (1992). Ras-related GTPases and the cytoskeleton. *Molecular biology of the cell* **3**, 475–9.

Hanein, D., Volkmann, N., Goldsmith, S., Michon, A. M., Lehman, W., Craig, R., DeRosier, D., Almo, S. & Matsudaira, P. (1998). An atomic model of fimbrin binding to F-actin and its implications for filament crosslinking and regulation. *Nature structural biology* **5**, 787–92.

Harris, N. L. & Ronchese, F. (1999). The role of B7 costimulation in T-cell immunity. *Immunology and cell biology* **77**, 304–11.

Hegyi, G., Szilágyi, L. & Belágyi, J. (1988). Influence of the bound nucleotide on the molecular dynamics of actin. *European journal of biochemistry* **175**, 271–4.

Hermos, C. R., Janineh, M., Han, L. L. & McAdam, A. J. (2011). Shiga toxin-producing *Escherichia* coli in children: diagnosis and clinical manifestations of O157:H7 and non-O157:H7 infection. *Journal of clinical microbiology* **49**, 955–9.

Hirokawa, N., Tilney, L. G., Fujiwara, K. & Heuser, J. E. (1982). Organization of actin, myosin, and intermediate filaments in the brush border of intestinal epithelial cells. *The Journal of cell biology* **94**, 425–43.

Van Houdt, R. & Michiels, C. W. (2006). Role of bacterial cell surface structures in *Escherichia coli* biofilm formation. *Research in microbiology* **156**, 626–33.

HPA. **(2011).** *Health protection agency report on the work of the Godstone multi-agency implementation committee*. London.

Huang, T. Y., DerMardirossian, C. & Bokoch, G. M. (2006). Cofilin phosphatases and regulation of actin dynamics. *Current opinion in cell biology* **18**, 26–31.

Hughes, K. T. (2012). The LEE type III secretion-specificity switch: the devil's in the data for a common mechanism. *Journal of bacteriology* **194**, 6019–22.

Iyoda, S., Koizumi, N., Satou, H., Lu, Y., Saitoh, T., Ohnishi, M. & Watanabe, H. (2006). The GrlR-GrlA regulatory system coordinately controls the

expression of flagellar and LEE-encoded type III protein secretion systems in enterohemorrhagic *Escherichia coli*. *Journal of bacteriology* **188**, 5682–92.

Jacewicz, M. S., Mobassaleh, M., Gross, S. K., Balasubramanian, K. A., Daniel, P. F., Raghavan, S., McCluer, R. H. & Keusch, G. T. (1994). Pathogenesis of *Shigella* diarrhea: XVII. A mammalian cell membrane glycolipid, Gb3, is required but not sufficient to confer sensitivity to Shiga toxin. *Journal of infectious diseases* **169**, 538–546.

Jallat, C., Livrelli, V., Darfeuille-Michaud, A., Rich, C. & Joly, B. (1993). *Escherichia coli* strains involved in diarrhea in France: high prevalence and heterogeneity of diffusely adhering strains. *Journal of clinical microbiology* **31**, 2031–7.

Jégou, A., Niedermayer, T., Orbán, J., Didry, D., Lipowsky, R., Carlier, M.-F. & Romet-Lemonne, G. (2011). Individual actin filaments in a microfluidic flow reveal the mechanism of ATP hydrolysis and give insight into the properties of profilin. *PLoS biology* **9**, e1001161.

Kalir, S., McClure, J., Pabbaraju, K., Southward, C., Ronen, M., Leibler, S., Surette, M. G. & Alon, U. (2001). Ordering genes in a flagella pathway by analysis of expression kinetics from living bacteria. *Science* **292**, 2080–3.

Kaper, J. B. (1996). Defining EPEC. *Revista de microbiologia* **21**, 130–133.

Kaper, J. B., Nataro, J. P. & Mobley, H. L. (2004). Pathogenic *Escherichia coli*. *Nature reviews Microbiology* **2**, 123–40.

Karmali, M. A. (2004). Infection by Shiga toxin-producing *Escherichia coli*: an overview. *Molecular biotechnology* **26**, 117–22.

Kauffmann, F. (1947). The serology of the *coli* group. *Journal of immunology* **57**, 71–100.

Khan, M. a, Bouzari, S., Ma, C., Rosenberger, C. M., Bergstrom, K. S. B., Gibson, D. L., Steiner, T. S. & Vallance, B. a. (2008). Flagellin-dependent and -independent inflammatory responses following infection by enteropathogenic *Escherichia coli* and *Citrobacter rodentium*. *Infection and immunity* **76**, 1410–22.

Khan, N. A., Wang, Y., Kim, K. J., Chung, J. W., Wass, C. A. & Kim, K. S. (2002). Cytotoxic necrotizing factor-1 contributes to *Escherichia coli* K1 invasion of the central nervous system. *Journal of biological chemistry* **277**, 15607–12.

Khan, N. A., Kim, Y., Shin, S. & Kim, K. S. (2007). FimH-mediated *Escherichia coli* K1 invasion of human brain microvascular endothelial cells. *Cellular microbiology* **9**, 169–78.

Kim, K. J., Elliott, S. J., Di Cello, F., Stins, M. F. & Kim, K. S. (2003). The K1 capsule modulates trafficking of E. coli-containing vacuoles and enhances intracellular bacterial survival in human brain microvascular endothelial cells. *Cellular microbiology* **5**, 245–252.

Knutton, S., Baldini, M. M., Kaper, J. B. & McNeish, A. S. (1987). Role of plasmid-encoded adherence factors in adhesion of enteropathogenic *Escherichia coli* to HEp-2 cells. *Infection and immunity* **55**, 78–85.

Konkel, M. E., Klena, J. D., Rivera-Amill, V., Monteville, M. R., Biswas, D., Raphael, B. & Mickelson, J. (2004). Secretion of virulence proteins from *Campylobacter jejuni* is dependent on a functional flagellar export apparatus. *Journal of bacteriology* **186**, 3296–303.

Korn, E. D. & Hammer, J. A. (1988). Myosins of nonmuscle cells. *Annual review of biophysics and biophysical chemistry* **17**, 23–45.

Korn, E. D., Carlier, M. F. & Pantaloni, D. (1987). Actin polymerization and ATP hydrolysis. *Science* **238**, 638–44.

Kovar, D. R. (2006). Molecular details of formin-mediated actin assembly. *Current opinion in cell biology* **18**, 11–7.

Kubori, T. & Galán, J. E. (2003). Temporal regulation of *Salmonella* virulence effector function by proteasome-dependent protein degradation. *Cell* **115**, 333–42.

Kueltzo, L. A., Osiecki, J., Barker, J., Picking, W. L., Ersoy, B., Picking, W. D. & Middaugh, C. R. (2003). Structure-function analysis of invasion plasmid antigen C (IpaC) from *Shigella flexneri*. *Journal of biological chemistry* **278**, 2792–8.

Kutsukake, K., Nakashima, H., Tominaga, A. & Abo, T. (2006). Two DNA invertases contribute to flagellar phase variation in *Salmonella enterica* serovar Typhimurium strain LT2. *Journal of bacteriology* **188**, 950–7.

Kuwajima, G. (1988). Construction of a minimum-size functional flagellin of *Escherichia coli*. *Journal of bacteriology* **170**, 3305–9.

Kwang, J., Wilson, R., Yang, S. & He, Y. (1996). Mapping of the H7-serospecific domain of *Escherichia coli* flagellin. *Clinical and diagnostic laboratory immunology* **3**, 523–6.

Lal, A., Hales, S., French, N. & Baker, M. G. (2012). Seasonality in human zoonotic enteric diseases: a systematic review. *PloS one* **7**, e31883.

Larsen, S. H., Reader, R. W., Kort, E. N., Tso, W. W. & Adler, J. (1974). Change in direction of flagellar rotation is the basis of the chemotactic response in *Escherichia coli*. *Nature* **249**, 74–7.

Lehnen, D., Blumer, C., Polen, T., Wackwitz, B., Wendisch, V. F. & Unden, G. (2002). LrhA as a new transcriptional key regulator of flagella, motility and chemotaxis genes in *Escherichia coli*. *Molecular microbiology* **45**, 521–32.

Levine, M. M., Ferreccio, C., Prado, V., Cayazzo, M., Abrego, P., Martinez, J., Maggi, L., Baldini, M. M., Martin, W. & other authors. **(1993).** Epidemiologic studies of *Escherichia coli* diarrheal infections in a low socioeconomic level peri-urban community in Santiago, Chile. *American journal of epidemiology* **138**, 849–869.

Lightfield, K. L., Persson, J., Brubaker, S. W., Witte, C. E., Von Moltke, J., Dunipace, E. A., Henry, T., Sun, Y.-H., Cado, D. & other authors. **(2008).** Critical function for Naip5 in inflammasome activation by a conserved carboxy-terminal domain of flagellin. *Nature immunology* **9**, 1171–8.

Lillehoj, E. P., Kim, B. T. & Kim, K. C. (2002). Identification of *Pseudomonas aeruginosa* flagellin as an adhesin for Muc1 mucin. *American journal of physiology Lung cellular and molecular physiology* **282**, L751–6.

Lindenthal, C. & Elsinghorst, E. A. (2001). Enterotoxigenic *Escherichia coli* TibA glycoprotein adheres to human intestine epithelial cells. *Infection and immunity* **69**, 52–7.

Lingwood, C. A., Law, H., Richardson, S., Petric, M., Brunton, J. L., De Grandis, S. & Karmali, M. (1987). Glycolipid binding of purified and recombinant *Escherichia coli* produced verotoxin in vitro. *Journal of biological chemistry* **262**, 8834–9.

Logan, S. M. (2006). Flagellar glycosylation - a new component of the motility repertoire? *Microbiology* **152**, 1249–62.

Lu, W., Hisatsune, A., Koga, T., Kato, K., Kuwahara, I., Lillehoj, E. P., Chen, W., Cross, A. S., Gendler, S. J. & other authors. **(2006).** Cutting edge: enhanced pulmonary clearance of *Pseudomonas aeruginosa* by Muc1 knockout mice. *Journal of immunology* **176**, 3890–4.

Maciver, S. K., Wachsstock, D. H., Schwarz, W. H. & Pollard, T. D. (1991). The actin filament severing protein actophorin promotes the formation of rigid

bundles of actin filaments crosslinked with alpha-actinin. *Journal of cell biology* **115**, 1621–8.

Macnab, R. M. & Ornston, M. K. (1977). Normal-to-curly flagellar transitions and their role in bacterial tumbling. Stabilization of an alternative quaternary structure by mechanical force. *Journal of molecular biology* **112**, 1–30.

Madigan, M. T., Martinko, J. M. & Parker, J. (2003). *Brock Biology of Microorganisms*, 10th edn. New Jersey: Pearson Prentice Hall.

Mahajan, A., Currie, C. G., Mackie, S., Tree, J., McAteer, S., McKendrick, I., McNeilly, T. N., Roe, A., La Ragione, R. M. & other authors. **(2009).** An investigation of the expression and adhesin function of H7 flagella in the interaction of *Escherichia coli* O157 : H7 with bovine intestinal epithelium. *Cellular microbiology* **11**, 121–37.

Matthews, L., Low, J. C., Gally, D. L., Pearce, M. C., Mellor, D. J., Heesterbeek, J. a P., Chase-Topping, M., Naylor, S. W., Shaw, D. J. & other authors. **(2006).** Heterogeneous shedding of *Escherichia coli* O157 in cattle and its implications for control. *Proceedings of the national academy of sciences of the United States of America* **103**, 547–52.

McDaniel, T. K., Jarvis, K. G., Donnenberg, M. S. & Kaper, J. B. (1995). A genetic locus of enterocyte effacement conserved among diverse enterobacterial pathogens. *Proceedings of the national academy of sciences of the United States of America* **92**, 1664–8.

McGough, a, Pope, B., Chiu, W. & Weeds, A. (1997). Cofilin changes the twist of F-actin: implications for actin filament dynamics and cellular function. *Journal of cell biology* **138**, 771–81.

McNeilly, T. N., Naylor, S. W., Mahajan, A., Mitchell, M. C., McAteer, S., Deane, D., Smith, D. G. E., Low, J. C., Gally, D. L. & Huntley, J. F. (2008). *Escherichia coli* O157:H7 colonization in cattle following systemic and

mucosal immunization with purified H7 flagellin. *Infection and immunity* **76**, 2594–602.

McNeilly, T. N. (2012). Prevention, control and treatment of STEC/VTEC in animals [abstract]. In *8th international symposium on Shiga toxin (verocytotoxin) producing* Escherichia coli *infections 6th-9th May 2012 VTEC 2012 congress office, conference abstracts*, p. 49. Amsterdam.

McNeilly, T. N., Mitchell, M. C., Rosser, T., McAteer, S., Low, J. C., Smith, D. G. E., Huntley, J. F., Mahajan, A. & Gally, D. L. (2010a). Immunization of cattle with a combination of purified intimin-531, EspA and Tir significantly reduces shedding of *Escherichia coli* O157:H7 following oral challenge. *Vaccine* **28**, 1422–8.

McNeilly, T. N., Mitchell, M. C., Nisbet, A. J., McAteer, S., Erridge, C., Inglis, N. F., Smith, D. G. E., Low, J. C., Gally, D. L. & other authors. **(2010b).** IgA and IgG antibody responses following systemic immunization of cattle with native H7 flagellin differ in epitope recognition and capacity to neutralise TLR5 signalling. *Vaccine* **28**, 1412–21.

Merino, S. & Tomas, J. M. (2009). Lateral flagella systems. In *Pili and flagella, current research and future trends*, 1st edn., pp. 173–190. Edited by K. F. Jarrell. Norfolk: Caister Academic Press.

Miao, E. a, Alpuche-Aranda, C. M., Dors, M., Clark, A. E., Bader, M. W., Miller, S. I. & Aderem, A. (2006). Cytoplasmic flagellin activates caspase-1 and secretion of interleukin 1beta via Ipaf. *Nature immunology* **7**, 569–75.

Miao, E. a, Andersen-Nissen, E., Warren, S. E. & Aderem, A. (2007). TLR5 and Ipaf: dual sensors of bacterial flagellin in the innate immune system. *Seminars in immunopathology* **29**, 275–88.

Miao, E. a, Mao, D. P., Yudkovsky, N., Bonneau, R., Lorang, C. G., Warren, S. E., Leaf, I. a & Aderem, A. (2010). Innate immune detection of the type III

secretion apparatus through the NLRC4 inflammasome. *Proceedings of the national academy of sciences of the United States of America* **107**, 3076–80.

Mooseker, M. S. (1989). The 110-kD protein-calmodulin complex of the intestinal microvillus (brush border myosin I) is a mechanoenzyme. *Journal of Cell Biology* **108**, 2395–2400.

Moxley, R. A. (2004). *Escherichia coli* 0157:H7: an update on intestinal colonization and virulence mechanisms. *Animal health research reviews / Conference of research workers in animal diseases* **5**, 15–33.

Mühldorfer, I., Hacker, J., Keusch, G. T., Acheson, D. W., Tschäpe, H., Kane, A. V, Ritter, A., Olschläger, T. & Donohue-Rolfe, A. (1996). Regulation of the Shiga-like toxin II operon in *Escherichia coli*. *Infection and immunity* **64**, 495–502.

Mundy, R., Schüller, S., Girard, F., Fairbrother, J. M., Phillips, A. D. & Frankel, G. (2007). Functional studies of intimin in vivo and ex vivo: implications for host specificity and tissue tropism. *Microbiology* **153**, 959–67.

Muniesa, M., Hammerl, J. A., Hertwig, S., Appel, B. & Brüssow, H. (2012). Shiga toxin-producing *Escherichia coli* O104:H4: a new challenge for microbiology. *Applied and environmental microbiology* **78**, 4065–73.

Nataro, J. P. & Kaper, J. B. (1998). Diarrheagenic *Escherichia coli*. *Clinical microbiology reviews* **11**, 142–201.

Nataro, J. P., Deng, Y., Maneval, D. R., German, A. L., Martin, W. C. & Levine, M. M. (1992). Aggregative adherence fimbriae I of enteroaggregative *Escherichia coli* mediate adherence to HEp-2 cells and hemagglutination of human erythrocytes. *Infection and immunity* **60**, 2297–304.

Nataro, J. P., Yikang, D., Yingkang, D. & Walker, K. (1994). AggR, a transcriptional activator of aggregative adherence fimbria I expression in enteroaggregative *Escherichia coli*. *Journal of bacteriology* **176**, 4691–9.

Nataro, J. P. (2012). Entero-aggregative *E. coli*: an eccentric old pathogen. In *8th international symposium on Shiga toxin (verocytotoxin) producing* Escherichia coli *infections 6th-9th May 2012 VTEC 2012 congress office, conference abstracts*, p. 35. Amsterdam.

Naylor, S. W., Roe, A. J., Nart, P., Spears, K., Smith, D. G. E., Low, J. C. & Gally, D. L. (2005a). *Escherichia coli* O157 : H7 forms attaching and effacing lesions at the terminal rectum of cattle and colonization requires the LEE4 operon. *Microbiology* **151**, 2773–81.

Naylor, S. W., Flockhart, A., Nart, P., Smith, D. G. E., Huntley, J., Gally, D. L. & Low, J. C. (2007). Shedding of *Escherichia coli* O157:H7 in calves is reduced by prior colonization with the homologous strain. *Applied and environmental microbiology* **73**, 3765–7.

Naylor, S. W., Gally, D. L. & Christopher Low, J. (2005b). Enterohaemorrhagic *E. coli* in veterinary medicine. *International journal of medical microbiology* **295**, 419–441.

Nempont, C. & Cayet, D. (2008). Deletion of flagellin's hypervariable region abrogates antibody-mediated neutralization and systemic activation of TLR5-dependent immunity. *Journal of immunology* **181**, 2036–2043.

Neupane, M., Abu-Ali, G. S., Mitra, A., Lacher, D. W., Manning, S. D. & Riordan, J. T. (2011). Shiga toxin 2 overexpression in *Escherichia coli* O157:H7 strains associated with severe human disease. *Microbial pathogenesis* **51**, 466–70.

Newton, H. J., Pearson, J. S., Badea, L., Kelly, M., Lucas, M., Holloway, G., Wagstaff, K. M., Dunstone, M. A., Sloan, J. & other authors. **(2010).** The type III effectors NleE and NleB from enteropathogenic *E. coli* and OspZ from *Shigella* block nuclear translocation of NF-kappaB p65. *PLoS pathogens* **6**, e1000898.

O'Brien, A., Newland, J., Miller, S., Holmes, R., Smith, H. & Formal, S. (1984). Shiga-like toxin-converting phages from *Escherichia coli* strains that cause hemorrhagic colitis or infantile diarrhea. *Science* **226**, 694–696.

Ostroff, S. M., Tarr, P. I., Neill, M. A., Lewis, J. H., Hargrett-Bean, N. & Kobayashi, J. M. (1989). Toxin genotypes and plasmid profiles as determinants of systemic sequelae in *Escherichia coli* O157:H7 infections. *Journal of infectious diseases* **160**, 994–998.

Pallen, M. J. & Matzke, N. J. (2006). From *The Origin of Species* to the origin of bacterial flagella. *Nature reviews Microbiology* **4**, 784–90.

Papakonstanti, E. A., Vardaki, E. A. & Stournaras, C. (2000). Actin cytoskeleton: a signaling sensor in cell volume regulation. *Cellular physiology and biochemistry : international journal of experimental cellular physiology, biochemistry, and pharmacology* **10**, 257–64.

Paton, J. C. & Paton, A. W. (1998). Pathogenesis and diagnosis of Shiga toxin-producing *Escherichia coli* infections. *Clinical microbiology reviews* **11**, 450–479.

Paul, A. S. & Pollard, T. D. (2009). Energetic requirements for processive elongation of actin filaments by FH1FH2-formins. *Journal of biological chemistry* **284**, 12533–40.

Pavlov, D. & Muhlrad, A. (2006). Severing of F-actin by yeast cofilin is pH-independent. *Cell motility and the cytoskeleton* **63**, 533–542.

Phillips, N., Hayward, R. D. & Koronakis, V. (2004). Phosphorylation of the enteropathogenic *E. coli* receptor by the Src-family kinase c-Fyn triggers actin pedestal formation. *Nature cell biology* **6**, 618–25.

Pinder, J. C. & Gratzer, W. B. (1983). Structural and dynamic states of actin in the erythrocyte. *Journal of cell biology* **96**, 768–75.

Poly, F., Ewing, C., Goon, S., Hickey, T. E., Rockabrand, D., Majam, G., Lee, L., Phan, J., Savarino, N. J. & Guerry, P. (2007). Heterogeneity of a *Campylobacter jejuni* protein that is secreted through the flagellar filament. *Infection and immunity* **75**, 3859–67.

Potter, A. a., Klashinsky, S., Li, Y., Frey, E., Townsend, H., Rogan, D., Erickson, G., Hinkley, S., Klopfenstein, T. & other authors. **(2004).** Decreased shedding of *Escherichia coli* O157:H7 by cattle following vaccination with type III secreted proteins. *Vaccine* **22**, 362–369.

La Ragione, R. M., Best, A., Woodward, M. J. & Wales, A. D. (2009). *Escherichia coli* O157:H7 colonization in small domestic ruminants. *FEMS microbiology reviews* **33**, 394–410.

Rangel, J. M., Sparling, P. H., Crowe, C., Griffin, P. M. & Swerdlow, D. L. (2005). Epidemiology of *Escherichia coli* O157:H7 outbreaks, United States, 1982-2002. *Emerging infectious diseases* **11**, 603–9.

Reid, S. D., Selander, R. K. & Whittam, T. S. (1999). Sequence diversity of flagellin (*fliC*) alleles in pathogenic *Escherichia coli*. *Journal of bacteriology* **181**, 153–60.

Dos Remedios, C. G., Chhabra, D., Kekic, M., Dedova, I. V, Tsubakihara, M., Berry, D. A. & Nosworthy, N. J. (2003). Actin binding proteins: regulation of cytoskeletal microfilaments. *Physiological reviews* **83**, 433–73.

Rhee, S. H., Im, E., Riegler, M., Kokkotou, E., O'brien, M. & Pothoulakis, C. (2005). Pathophysiological role of Toll-like receptor 5 engagement by bacterial flagellin in colonic inflammation. *Proceedings of the national academy of sciences of the United States of America* **102**, 13610–5.

Richardson, M. S. E., MB, Karmali, C. M. A., Becker, M. L. E. & Smith, M. C. R. (1988). The histopathology of the hemolytic uremic syndrome associated

with verocytotoxin-producing *Escherichia coli* infections. *Human pathology* **19**, 1108–1102.

Ridley, A. J. & Hall, A. (1992). The small GTP-binding protein rho regulates the assembly of focal adhesions and actin stress fibers in response to growth factors. *Cell* **70**, 389–99.

Ritchie, J. M. & Waldor, M. K. (2005). The locus of enterocyte effacement-encoded effector proteins all promote enterohemorrhagic *Escherichia* pathogenicity in infant rabbits. *Infection and immunity* **73**, 1466–74.

Robbe, C., Capon, C., Coddeville, B. & Michalski, J.-C. (2004). Structural diversity and specific distribution of O-glycans in normal human mucins along the intestinal tract. *The biochemical journal* **384**, 307–16.

Robinson, C. M., Sinclair, J. F., Smith, M. J. & O'Brien, A. D. (2006). Shiga toxin of enterohemorrhagic *Escherichia coli* type O157:H7 promotes intestinal colonization. *Proceedings of the national academy of sciences of the United States of America* **103**, 9667–72.

Roe, A. J., Naylor, S. W., Spears, K. J., Yull, H. M., Dransfield, T. a, Oxford, M., McKendrick, I. J., Porter, M., Woodward, M. J. & other authors. (2004). Co-ordinate single-cell expression of LEE4- and LEE5-encoded proteins of *Escherichia coli* O157:H7. *Molecular microbiology* **54**, 337–52.

Roy, K., Hamilton, D., Ostmann, M. M. & Fleckenstein, J. M. (2009a). Vaccination with EtpA glycoprotein or flagellin protects against colonization with enterotoxigenic *Escherichia coli* in a murine model. *Vaccine* **27**, 4601–8.

Roy, K., Hilliard, G. M., Hamilton, D. J., Luo, J., Ostmann, M. M. & Fleckenstein, J. M. (2009b). Enterotoxigenic *Escherichia coli* EtpA mediates adhesion between flagella and host cells. *Nature* **457**, 594–8.

Rumbo, M., Nempont, C., Kraehenbuhl, J.-P. & Sirard, J.-C. (2006). Mucosal interplay among commensal and pathogenic bacteria: lessons from flagellin and Toll-like receptor 5. *FEBS letters* **580**, 2976–84.

Russo, T. A. & Johnson, J. R. (2000). Proposal for a new inclusive designation for extraintestinal pathogenic isolates of *Escherichia coli*: ExPEC. *Journal of infectious diseases* **181**, 1753–4.

Sack, R. B. (1975). Human diarrheal disease caused by enterotoxigenic Escherichia coli. *Annual review of microbiology* **29**, 333–53.

Saha, S., Takeshita, F., Matsuda, T., Jounai, N., Kobiyama, K., Matsumoto, T., Sasaki, S., Yoshida, A., Xin, K.-Q. & other authors. **(2007).** Blocking of the TLR5 activation domain hampers protective potential of flagellin DNA vaccine. *Journal of immunology* **179**, 1147–54.

Samanta, A. K., Oppenheim, J. J. & Matsushima, K. (1989). Identification and characterization of specific receptors for monocyte-derived neutrophil chemotactic factor (MDNCF) on human neutrophils. *Journal of experimental medicine* **169**, 1185–9.

Sampaio, S. C. F., Gomes, T. A. T., Pichon, C., Du Merle, L., Guadagnini, S., Abe, C. M., Sampaio, J. L. M. & Le Bouguénec, C. (2009). The flagella of an atypical enteropathogenic *Escherichia coli* strain are required for efficient interaction with and stimulation of interleukin-8 production by enterocytes in vitro. *Infection and immunity* **77**, 4406–13.

Sansonetti, P. J., Ryter, A., Clerc, P., Maurelli, A. T. & Mounier, J. (1986). Multiplication of *Shigella flexneri* within HeLa cells: lysis of the phagocytic vacuole and plasmid-mediated contact hemolysis. *Infection and immunity* **51**, 461–9.

Sargeant, J. M., Amezcua, M. R., Rajic, A. & Waddell, L. (2007). Pre-harvest interventions to reduce the shedding of *E. coli* O157 in the faeces of weaned

domestic ruminants: a systematic review. *Zoonoses and public health* **54**, 260–77.

Schroeder, G. N. & Hilbi, H. (2008). Molecular pathogenesis of *Shigella* spp.: controlling host cell signaling, invasion, and death by type III secretion. *Clinical microbiology reviews* **21**, 134–56.

Scott, R. W. & Olson, M. F. (2007). LIM kinases: function, regulation and association with human disease. *Journal of molecular medicine* **85**, 555–68.

Shames, S. R., Deng, W., Guttman, J. A., De Hoog, C. L., Li, Y., Hardwidge, P. R., Sham, H. P., Vallance, B. A., Foster, L. J. & Finlay, B. B. (2010). The pathogenic *E. coli* type III effector EspZ interacts with host CD98 and facilitates host cell prosurvival signalling. *Cellular microbiology* **12**, 1322–39.

Shulman, S. T., Friedmann, H. C. & Sims, R. H. (2007). Theodor Escherich: the first pediatric infectious diseases physician? *Clinical infectious diseases : an official publication of the Infectious Diseases Society of America* **45**, 1025–9.

Sierro, F., Dubois, B., Coste, A., Kaiserlian, D., Kraehenbuhl, J. P. & Sirard, J. C. (2001). Flagellin stimulation of intestinal epithelial cells triggers CCL20-mediated migration of dendritic cells. *Proceedings of the national academy of sciences of the United States of America* **98**, 13722–7.

Siitonen, A. (1992). *Escherichia coli* in fecal flora of healthy adults: serotypes, P and type 1C fimbriae, non-P mannose-resistant adhesins, and hemolytic activity. *Journal of infectious diseases* **166**, 1058–65.

Sinclair, J. F. & O'Brien, A. D. (2002). Cell surface-localized nucleolin is a eukaryotic receptor for the adhesin intimin-gamma of enterohemorrhagic Escherichia coli O157:H7. *Journal of biological chemistry* **277**, 2876–85.

Smith, D. G. E., Naylor, S. W. & Gally, D. L. (2002). Consequences of EHEC colonisation in humans and cattle. *International journal of medical microbiology* **292**, 169–183.

Smith, K. D., Andersen-Nissen, E., Hayashi, F., Strobe, K., Bergman, M. a, Barrett, S. L. R., Cookson, B. T. & Aderem, A. (2003). Toll-like receptor 5 recognizes a conserved site on flagellin required for protofilament formation and bacterial motility. *Nature immunology* **4**, 1247–53.

Smith, S. A., Jann, O. C., Haig, D., Russell, G. C., Werling, D., Glass, E. J. & Emes, R. D. (2012). Adaptive evolution of Toll-like receptor 5 in domesticated mammals. *BMC evolutionary biology* **12**, 122.

Snedeker, K. G., Campbell, M. & Sargeant, J. M. (2012). A systematic review of vaccinations to reduce the shedding of *Escherichia coli* O157 in the faeces of domestic ruminants. *Zoonoses and public health* **59**, 126–38.

Snider, T. a, Fabich, A. J., Conway, T. & Clinkenbeard, K. D. (2009). *E. coli* O157:H7 catabolism of intestinal mucin-derived carbohydrates and colonization. *Veterinary microbiology* **136**, 150–4.

Somlyo, A. P. & Somlyo, A. V. (2000). Signal transduction by G-proteins, Rho-kinase and protein phosphatase to smooth muscle and non-muscle myosin II. *Journal of physiology* **522**, 177–185.

Song, Y. C., Jin, S., Louie, H., Ng, D., Lau, R., Zhang, Y., Weerasekera, R., Al Rashid, S., Ward, L. A. & other authors. **(2004).** FlaC, a protein of *Campylobacter jejuni* TGH9011 (ATCC43431) secreted through the flagellar apparatus, binds epithelial cells and influences cell invasion. *Molecular microbiology* **53**, 541–53.

Soutourina, O., Kolb, A., Krin, E., Laurent-Winter, C., Rimsky, S., Danchin, A. & Bertin, P. (1999). Multiple control of flagellum biosynthesis in *Escherichia coli*: role of H-NS protein and the cyclic AMP-catabolite activator protein complex in transcription of the *flhDC* master operon. *Journal of bacteriology* **181**, 7500–8.

Soutourina, O. & Bertin, P. (2003). Regulation cascade of flagellar expression in Gram-negative bacteria. *FEMS microbiology reviews* **27**, 505–523.

Subramanian, N. & Qadri, A. (2006). Lysophospholipid sensing triggers secretion of flagellin from pathogenic *Salmonella*. *Nature immunology* **7**, 583–9.

Sun, H. Q., Yamamoto, M., Mejillano, M. & Yin, H. L. (1999). Gelsolin, a multifunctional actin regulatory protein. *Journal of biological chemistry* **274**, 33179–82.

Sussman, M. (1997). *Escherichia coli* and human disease. In Escherichia coli*: Mechanisms of virulence*, 1st edn., pp. 3–48. Edited by M. Sussman. Cambridge: Cambridge University Press.

Suzuki, T., Iino, T., Horiguchi, T. & Yamaguchi, S. (1978). Incomplete flagellar structures in nonflagellate mutants of *Salmonella typhimurium*. *Journal of bacteriology* **133**, 904–915.

Tasteyre, A., Barc, M. & Collignon, A. (2001). Role of FliC and FliD flagellar proteins of *Clostridium difficile* in adherence and gut colonization. *Infection and immunity* **69**, 7937–7940.

Taylor, J. (1952). Conservation of the generic name *Bacterium* and the family name *Bacteriaceae* - comments of the *Enterobacteriaceae* subcommittee, British advisory bacteriological nomenclature committee. *International bulletin of bacteriological nomenclature and taxonomy* **2**, 92–93.

Tilney, L. G. & Kallenbach, N. (1979). Polymerization of actin. VI. The polarity of the actin filaments in the acrosomal process and how it might be determined. *Journal of cell biology* **81**, 608–23.

Tobe, T., Beatson, S. a, Taniguchi, H., Abe, H., Bailey, C. M., Fivian, A., Younis, R., Matthews, S., Marches, O. & other authors. (2006). An extensive repertoire of type III secretion effectors in *Escherichia coli* O157 and the role of

lambdoid phages in their dissemination. *Proceedings of the national academy of sciences of the United States of America* **103**, 14941–6.

Toshima, H., Yoshimura, A., Arikawa, K., Hidaka, A., Ogasawara, J., Hase, A., Masaki, H. & Nishikawa, Y. (2007). Enhancement of Shiga toxin production in enterohemorrhagic *Escherichia coli* serotype O157:H7 by DNase colicins. *Applied and environmental microbiology* **73**, 7582–8.

Tree, J. J., Wolfson, E. B., Wang, D., Roe, A. J. & Gally, D. L. (2009). Controlling injection: regulation of type III secretion in enterohaemorrhagic *Escherichia coli*. *Trends in microbiology* **17**, 361–70.

Tronick, S. R. & Martinez, R. J. (1971). Methylation of the flagellin of *Salmonella typhimurium*. *Journal of bacteriology* **105**, 211–9.

Van Troys, M., Huyck, L., Leyman, S., Dhaese, S., Vandekerkhove, J. & Ampe, C. (2008). Ins and outs of ADF/cofilin activity and regulation. *European journal of cell biology* **87**, 649–67.

Turner, L., Stern, A. S. & Berg, H. C. (2012). Growth of flagellar filaments of *Escherichia coli* is independent of filament length. *Journal of bacteriology* **194**, 2437–42.

Tuttle, J., Gomez, T., Doyle, M. P., Wells, J. G., Zhao, T., Tauxe, R. V & Griffin, P. M. (1999). Lessons from a large outbreak of *Escherichia coli* O157:H7 infections: insights into the infectious dose and method of widespread contamination of hamburger patties. *Epidemiology and infection* **122**, 185–92.

Ueno, K., Koga, T., Kato, K., Golenbock, D. T., Gendler, S. J., Kai, H. & Kim, K. C. (2008). MUC1 mucin is a negative regulator of toll-like receptor signaling. *American journal of respiratory cell and molecular biology* **38**, 263–8.

Ueno, T., Oosawa, K. & Aizawa, S. (1992). M ring, S ring and proximal rod of the flagellar basal body of *Salmonella typhimurium* are composed of subunits of a single protein, FliF. *Journal of molecular biology* **227**, 672–7.

Ursitti, J. A. & Fowler, V. M. (1994). Immunolocalization of tropomodulin, tropomyosin and actin in spread human erythrocyte skeletons. *Journal of cell science* **107**, 1633–9.

USDA/FSIS. **(2011).** Shiga toxin-producing Escherichia coli in certain raw beef products. *Federal register* **76**, 58157–58165.

USDA/FSIS. **(2012).** Utah firm recalls beef products due to possible *E. coli* O157:H7 contamination (FSIS-RC-055-2012). *http://www.fsis.usda.gov/news/Recall_055_2012_Release/index.asp* [accessed 20/12/12].

Valcour, J. E., Michel, P., McEwen, S. A. & Wilson, J. B. (2002). Associations between indicators of livestock farming intensity and incidence of human Shiga toxin-producing *Escherichia coli* infection. *Emerging infectious diseases* **8**, 252–7.

Vartiainen, M. K., Mustonen, T., Mattila, P. K., Ojala, P. J., Thesleff, I., Partanen, J. & Lappalainen, P. (2002). The three mouse actin-depolymerizing factor/cofilins evolved to fulfill cell-type-specific requirements for actin dynamics. *Molecular biology of the cell* **13**, 183–94.

Vijay-Kumar, M., Wu, H., Jones, R., Grant, G., Babbin, B., King, T. P., Kelly, D., Gewirtz, A. T. & Neish, A. S. (2006). Flagellin suppresses epithelial apoptosis and limits disease during enteric infection. *American journal of pathology* **169**, 1686–700.

Vinzing, M., Eitel, J., Lippmann, J., Hocke, A. C., Zahlten, J., Slevogt, H., N'guessan, P. D., Günther, S., Schmeck, B. & other authors. **(2008).** NAIP

and Ipaf control *Legionella pneumophila* replication in human cells. *Journal of immunology* **180**, 6808–15.

Wadhams, G. H. & Armitage, J. P. (2004). Making sense of it all: bacterial chemotaxis. *Nature reviews Molecular cell biology* **5**, 1024–37.

Wassef, J. S., Keren, D. F. & Mailloux, J. L. (1989). Role of M cells in initial antigen uptake and in ulcer formation in the rabbit intestinal loop model of shigellosis. *Infection and immunity* **57**, 858–63.

Wehrle-Haller, B. (2012). Assembly and disassembly of cell matrix adhesions. *Current opinion in cell biology* **24**, 569–81.

Welch, M. D., Rosenblatt, J., Skoble, J., Portnoy, D. A. & Mitchison, T. J. (1998). Interaction of human Arp2/3 complex and the *Listeria monocytogenes* ActA protein in actin filament nucleation. *Science* **281**, 105–8.

Wennerås, C. & Erling, V. (2011). Prevalence of enterotoxigenic *Escherichia coli* -associated diarrhoea and carrier state in the developing world. *Journal of health, population and nutrition* **22**, 370–382.

Wilmanski, J. M., Petnicki-Ocwieja, T. & Kobayashi, K. S. (2008). NLR proteins: integral members of innate immunity and mediators of inflammatory diseases. *Journal of leukocyte biology* **83**, 13–30.

Wong, A. R. C., Pearson, J. S., Bright, M. D., Munera, D., Robinson, K. S., Lee, S. F., Frankel, G. & Hartland, E. L. (2011). Enteropathogenic and enterohaemorrhagic *Escherichia coli*: even more subversive elements. *Molecular microbiology* **80**, 1420–38.

Wong, A. R. C., Clements, A., Raymond, B., Crepin, V. F. & Frankel, G. (2012). The interplay between the *Escherichia coli* Rho guanine nucleotide exchange factor effectors and the mammalian RhoGEF inhibitor EspH. *mBio* **3**.

Xicohtencatl-Cortes, J., Monteiro-Neto, V., Ledesma, M. A., Jordan, D. M., Francetic, O., Kaper, J. B., Puente, J. L. & Girón, J. A. (2007). Intestinal adherence associated with type IV pili of enterohemorrhagic *Escherichia coli* O157:H7. *The Journal of clinical investigation* **117**, 3519–29.

Xu, X., McAteer, S. P., Tree, J. J., Shaw, D. J., Wolfson, E. B. K., Beatson, S. A., Roe, A. J., Allison, L. J., Chase-Topping, M. E. & other authors. **(2012).** Lysogeny with Shiga toxin 2-encoding bacteriophages represses type III secretion in enterohemorrhagic *Escherichia coli*. *PLoS pathogens* **8**, e1002672.

Yonekura, K. (2000). The bacterial flagellar cap as the rotary promoter of flagellin self-assembly. *Science* **290**, 2148–2152.

Yonekura, K., Maki-Yonekura, S. & Namba, K. (2003). Complete atomic model of the bacterial flagellar filament by electron cryomicroscopy. *Nature* **424**, 643–50.

Zhan, Q., Bamburg, J. R. & Badwey, J. A. (2003). Products of phosphoinositide specific phospholipase C can trigger dephosphorylation of cofilin in chemoattractant stimulated neutrophils. *Cell motility and the cytoskeleton* **54**, 1–15.

Zhao, Y., Yang, J., Shi, J., Gong, Y.-N., Lu, Q., Xu, H., Liu, L. & Shao, F. (2011). The NLRC4 inflammasome receptors for bacterial flagellin and type III secretion apparatus. *Nature* **477**, 596–600.

Zhou, D., Mooseker, M. & Galán, J. (1999). Role of the *S. typhimurium* actin-binding protein SipA in bacterial internalization. *Science* **283**, 2092–2095.

Zobiack, N., Rescher, U., Laarmann, S., Michgehl, S., Schmidt, M. A. & Gerke, V. (2002). Cell-surface attachment of pedestal-forming enteropathogenic *E. coli* induces a clustering of raft components and a recruitment of annexin 2. *Journal of cell science* **115**, 91–8.

2 : Materials and methods

2.1 Bacterial culture

Bacterial strains (table 2.1, appendix 1) were stored as saturated cultures in Luria-Bertani broth (LB) with 25% (v/v) glycerol at -70°C. Strains were revived by streaking onto LB agar (Melford) and incubating statically at 37°C for 16 h unless they contained temperature sensitive plasmids, in which case they were grown at 28-30°C. Plates were used fresh for phenotypic assays or stored at 4°C for deoxyribonucleic acid (DNA) manipulation. Single colonies from streak-plates were grown in LB at 28°C-30°C or 37°C at 200 rpm for 16 h, as stated. Bacteria were sub-cultured 1:100 into the same media at the same temperature unless otherwise stated. Plasmid-containing strains were grown in the presence of antibiotics at the following concentrations: ampicillin (amp) 100µg/ml, chloramphenicol (cam) 50µg/ml, kanamycin (kan) 50µg/ml.

Table 2.1. Strains used or constructed in this study.

Strain	Relevant features	Source
TOP10	*E.coli* cloning strain; *F- mcrA Δ(mrr-hsdRMS-mcrBC) (Φ80lacZ Δ M15 Δ lacX74 deoR recA1 araD139 Δ (ara-leu)7697 galU galK rpsL endA1 nupG*	Invitrogen
DH5α	*E. coli* plasmid storage strain	(McNeilly *et al.*, 2010)
BL21(DE3)	*E. coli* protein expression for purification strain	Novagen
JT1	*E.coli* K-12; 11 mutations, *fliC(H48)::Tn*10; *fimA::cat* derivative of *E. coli* C600	(Bachmann, 1987; Westerlund-Wikström *et al.*, 1997)
E2348/69	*E.coli* 0127:H6; sequenced.	Mark Stevens
SL1344Δ*fljB*	*S.* Typhiumurium Δ*fljB,* for purification FliC	(Arques *et al.*, 2009)
SL1344Δ*fliC*	*S.* Typhiumurium Δ*fliC,* for purification FljB	(Arques *et al.*, 2009)
Walla-1	*E. coli* O157:H7, *stx*$^{+}$	(Mahajan *et al.*, 2009)
ZAP198	*E. coli* O157:H7, *stx*$^{-}$	(McNeilly *et al.*, 2010)
TUV93-0	*E.coli* O157:H7; EDL933 (ATCC 700927) *stx*$^{-}$	(Campellone *et al.*, 2007)
TUVΔ*fliC*	TUV93-0 intermediate strain clone 10; *fliC*::*sacB::kan*^{r}	This study
TUV*fliC*$^{-}$	TUV93-0 *fliC*$^{-}$ clone 1	This study
TUV*fliC*$^{-}_{H7}$	TUVΔ*fliC*10 *cis* complement *fliC* CDSE from TUV93-0, clone 13	This study
TUV*fliC*$_{H7F}$	TUVΔ*fliC*10 *cis* complement *fliC* CDSF from TUV930, inserted with F site, clone 1.	This study
TUV*fliC*$_{H6F}$	TUVΔ*fliC*10 *cis* complement *fliC* CDSF from E2348/69, inserted with F site, clone 1.	This study
TUV*fliD*$^{-}$	TUV93-0 *fliD*$^{-}$ clone 1	This study

2.2 Motility enrichment

Freshly revived colonies were stab inoculated into motility agar plates (1% (w/v) tryptone (BD Biosciences), 0.5% (w/v) NaCl, 0.3% (w/v) granulated agar (Melford)) and incubated at 28-30°C for 16 h. Agar plugs from leading edge of the motility halos were taken using 10 µl inoculation loops, and these was used to inoculate LB broth. This was incubated at 28-30°C 200 rpm for 16 h and then sub-cultured in the desired media.

2.3 DNA manipulation

General molecular biology methods were adapted from Molecular Cloning: A Laboratory Manual (Russell & Sambrook, 2001), unless indicated otherwise.

Table 2.2. Plasmids used or constructed in this study. Plasmids in the top portion of the table were used for strain construction. Plasmids in the lower portion were used for protein expression or purification. Plasmids constructed in this study are validated in appendix 1.

Plasmid	Relevant features	Source
pIB307	Chl^r, T^oC^s replication (28ºC), single copy number	(Blomfield *et al.*, 1991)
$pIBXH7_{tuv}$	pIB307; H7downD flank; *sacB :kan*^{r} ; H7upB flank	This study
$pIBXSK_{tuv}$	pIB307; H7downD flank; H7upB flank	This study
pIBXH7KI	pIB307; H7downE flank; H7 CDS(E); H7upB flank	This study
pIBXH7KIF	pIB307; H7downF flank; H7 CDS(F); H7upB flank	This study
pIBXH6KIF	pIB307; H7downF flank; H6 CDS(F); H7upB flank	This study
pIBXFliD	pIB307; FliDdown flank; *sacB :kan*^{r} ; FliDup flank	This study
pIBXSKFliD	pIB307; FliDdown flank; FliDup flank	This study
pWSK29	*lac* operon, low copy number (<10) amp^r	(Kushner, 1991)
$pWSKH7_{tuv}$	pWSK29; amp^r; SalI-BamHI insertion of $fliC_{H7}$ (from TUV93-0); clone 33	This study
$pFliC_{H6}$	pGEM; amp^r; BamHI-BamHI insertion $fliC_{H6}$ (from E2348/69)	(Mahajan *et al.*, 2009)
pWSKH6	pWSK29; BamHI-BamHI insertion of $fliC_{H6}$ from p*fliC*H6; clone 3	This study
pBAD/*Myc*-His A	amp^r; L-arabinose-inducible expression; C-terminal 6x(His) tag	Invitrogen
$pBADFliD_{H7}$	pBAD/*Myc*-His A; NcoI-SacI insertion of $fliD_{H7}$ (from TUV93-0). For purification of $FliD_{H7}$	This study
pET22(b)+	amp^r; IPTG-inducible expression; C-terminal 6x(His) tag	Novagen
pFLrH7	pET22(b)+ with BamHI-HindIII insertion of full-length $fliC_{H7}$ (from ZAP198). For purification of $FLrH7_{1-585}$	(McNeilly *et al.*, 2010)
pVrH7	pET22(b)+ with BamHI-HindIII insertion of variable domain of $fliC_{H7}$ (from ZAP198). For purification of $VrH7_{180-496}$	(McNeilly *et al.*, 2010)
p5'rH7	pET22(b)+ with BamHI-HindIII insertion of N-terminal of $fliC_{H7}$ (from ZAP198). For purification of $NTrH7_{1-179}$	(McNeilly *et al.*, 2010)

Table 2.3. Primers used in this study. Restriction sites are underlined. Temperature in bold indicates annealing temperature used for specific primer pair. Amplification conditions are detailed in section 2.3.4.

Product	Primer Name	Primer Sequence	Source
fliC$_{H7}$ + promoter	Ct-FliC-SalI	CGGTCGACGGCAATTTGGCG TTGCCG	This study
69°C	Nt-FliC-BamHI2	CGGGATCCCGATGAAATACT TGCCATGC	This study
fliC$_{H7}$ (CDSE)	5'CtH7R.BamHI	AAGGATCCTTAACCCTGCAG CAGAGACAG	This study
68°C	3'NtH7F.BamHI	AAGGATCCATGGCACAAGTC ATTAATACC	This study
fliC$_{H6}$	JTfliC.F+.BamHI	CCGGATCCGAACTTAAATCCA GACCTGA	(Mahajan *et al.*, 2009)
n/a	JTH11fliC.R.BamHI	CCGGATCCCTAACCCTGCAG CAGAGACAG	(Mahajan *et al.*, 2009)
H7upB	5'H7upF.SacI	AAGAGCTCTATTGCCTGTGC CACTTCAC	This study
55°C	3'H7upR.BamHI	AAGGATCCTAACTGAGACTG ACGGCAAC	This study
H7downD	5'H7downF.BamHI	GGGGATCCTCCTATATTGCAA GTCGTTG	This study
55°C	3'H7downR.SalI	AAGTCGACTTCGTATCGTCTC TGGTGGT	This study
H7downE	5'H7downF2.BamHI	GCCATGGATCCTTATCCTATA TTGCAAGTCG	This study
55°C	3'H7downR.SalI	AAGTCGACTTCGTATCGTCTC TGGTGGT	This study
H7downF	H7downF3.BamHI	GGGGATCCCACCCGTCGGCT CAATCG	This study
55°C	3'H7downR.SalI	AAGTCGACTTCGTATCGTCTC TGGTGGT	This study
H7 CDSF	3'NtH7F2.BamHI	GGGGATCCCAATACGTAATC AACGACTTGC	This study
58°C	5'CtH7R.BamHI	AAGGATCCTTAACCCTGCAG CAGAGACAG	This study
H6 CDSF	3'NtH6F2.BamHI	GGGGATCCCAAAACGTAATC AACGACTTGC	(Mahajan *et al.*, 2009)
58°C	JTH11fliC.R.BamHI	CCGGATCCCTAACCCTGCAG CAGAGACAG	(Mahajan *et al.*, 2009)
FliDup	FliDupF.SacI	GGGAGCTCATGGAGTCCAGG TCAGAATC	This study
55°C	FliDupR.BamHI	GGGGATCCGCGATTTCCTTTT ATCATTCGAC	This study
FliDdown	FliDdownF.BamHI	GGGGATCCCATTATTCATCG GGAGACAG	This study
55°C	FliDdownR.XbaI	GGTCTAGAGGGTCAACCTCT TCAGTCAA	This study
FliDhis	5'NtFliDHISF.NcoI	AACCATGGCAAGTATTTCATC GCTGGGAGTC	This study
60°C	3'CtFliDHISF.SacI	AAGAGCTCTTAATGATGATGA TGATGATGCTTGGAATTACTG TTGTTTTCG	This study

sacB		GCAACTCAAGCGTTTGCGAA	(Xu *et al.*, 2012)
	SacB-5	A	
		GGCTTGTATGGGCCAGTTAA	(Xu *et al.*, 2012)
55°C	SacB-3	G	
FliC locus		AAGAGCTCTATTGCCTGTGC	This study
	5'H7upF.SacI	CACTTCAC	
		AAGTCGACTTCGTATCGTCTC	This study
55°C	3'H7downR.SalI	TGGTGGT	
FliD locus		GGGAGCTCATGGAGTCCAGG	This study
	FliDupF.SacI	TCAGAATC	
		GGTCTAGAGGGTCAACCTCT	This study
55°C	FliDdownR.XbaI	TCAGTCAA	
O157			(Paton & Paton,
specific	O157F	CGGACATCCATGTGATATGG	1998)
			(Paton & Paton,
55°C	O157R	TTGCCTATGTACAGCTAATCC	1998)
pIB307			(Flockhart *et al.*,
insert	PIBF	CCTGTCCTACGAGTTGCATG	2012)
60°C			(Flockhart *et al.*,
	PIBR	GACTCCTGCATTAGGAAGCA	2012)
pWSK29	pWSKF	CAGTCACGACGTTGTAAAAC	This study
insert			This study
55°C	pWSKR	CGTATGTTGTGTGGAATTGT	
pBAD	pBADF	AGATTAGCGGATCCTACCTG	This study
insert			This study
56°C	pBADR	TATCAGACCGCTTCTGCGTTC	

2.3.1 Agarose electrophoresis

DNA was loaded into 1% (w/v) agarose (Melford) in Tris-Borate-EDTA (TBE; 90mM Tris-borate, 1mM EDTA) gels containing Safeview (NBS Biologicals) in the presence of loading buffer (Bluejuice, Invitrogen) and 1kb or 100bp size markers (Promega, Invitrogen and Fermentas). Agarose gels were electrophoresed at 80-100 V for 20-45 min in TBE and imaged using a Bio-Rad 1000 UV gel-documentation system.

2.3.2 Plasmid preparation

Plasmids were extracted using Wizard SV plus Plasmid Mini-prep kit (Promega), GeneJet Plasmid Mini-prep Kit (Fermentas Life Sciences) or EZ-10 Plasmid Mini-prep kit (NBS Biologicals) according to their instructions with a few exceptions. 5-10 times more bacteria than suggested were used. All centrifugation was undertaken at 29000 x *g*. Cell lysates were clarified by centrifugation for 10 min rather than 5 min. Also, after washing, DNA was dried by a 3 min centrifugation, incubated with

sterile distilled water for 5 min and eluted by 2 min centrifugation. Where low or single-copy plasmids were used, multiple preparations were often eluted in a lower volume and pooled. Plasmid DNA was stored at -20°C.

2.3.3 Genomic DNA extraction

For use in cloning, genomic DNA was extracted using the Charge-switch gDNA mini-kit (Invitrogen) according to their instructions. Briefly, saturated bacterial cultures were centrifuged at 8900 x *g* for 5 min, pellets were re-suspended in proprietary re-suspension buffer with RNAse A. Bacteria were lysed with 1 mg/ml lysozyme at 37°C for 10 min followed by lysis buffer and ~200 µg/ml proteinase K for 1 h at 80°C. ChargeSwitch magnetic beads were added to this sample, mixed and proprietary binding buffer added. This lowered the pH so that DNA bound to beads. The beads were separated using magnetism, the buffer was removed. Beads were washed twice with proprietary washing buffer using magnetism to retain beads. DNA was then eluted by increasing the pH in elution buffer (10 mM Tris-HCl, pH 8.5).

For screening of strains by polymerase chain reaction (PCR, section 2.3.4), DNA was extracted from colonies by suspending them with distilled water and incubating them at 98°C for 5 min to make a colony lysate which was used in the PCR reaction. Alternatively, the colony was suspended in the PCR reaction after re-streaking.

2.3.4 Polymerase chain reactions (PCR)

For high fidelity amplification of DNA for use in cloning, Phusion DNA polymerase (Finnzymes) was used. Reaction mixtures followed manufacturers' instructions (which typically contained proprietary HF buffer, 200µM dNTPs (New England Biolabs), 1µM of each primer (Invitrogen), 0.5 µl genomic DNA and 1 U DNA polymerase). PCR reactions were undertaken in a Thermo-Hybaid PCR Express thermocycler (Thermo Fischer Scientific), with the following program: 98°C for 30 s then 30 cycles of (98°C for 10 s, annealing T°C for 30 s, 72°C 35 s/kb), 72°C for 10

min. PCR reactions were cleaned or gel purified then cleaned using a Wizard SV gel and PCR clean-up kit (Promega) according to their instructions. PCR products were gel purified if a single size product could not be obtained. In these cases, the whole PCR reaction was electrophoresed (section 2.3.1) and the band of the desired size was excised and purified using a Wizard SV gel and PCR clean-up kit.

For amplification of DNA for screening, Quick-Load 2x *Taq* DNA polymerase (New England Biolabs) was used. Reaction mixtures contained Quick-Load *Taq* master mix, 1µM of each primer and 1 µl colony lysate or 0.5 µl genomic DNA. PCR reactions were undertaken in a thermocycler as above, with the following program: 95°C for 5 min, then 35 cycles of (95°C for 15 s, annealing T°C for 30 s, 68°C 1 min/kb), 68°C for 5 min.

2.3.5 Restriction digests

Plasmid or PCR amplified DNA was digested using specified restriction endonucleases purchased from New England Biolabs or Roche according to their instructions. Restriction digests typically contained a compatible proprietary buffer, 10 µg/ml bovine serum albumin (BSA), DNA diluted 3:2 and 20 U of each restriction enzyme. These reactions were incubated for 1-2 h at 37°C. Where appropriate, to prevent self-ligation, digested plasmids were dephosphorylated by shrimp alkaline phosphatase (Promega) at 37ºC for 30 min. Restriction digests were cleaned up using a Wizard SV gel and PCR clean-up kit (Promega) according to their instructions.

2.3.6 Ligations

DNA was ligated using the T4 DNA ligase (Promega) according to their instructions. Briefly, DNA to be ligated of varying ratios of plasmid:insert, were added to 8 U of ligase, and incubated at 16ºC for 16 h. Ligation mixtures were used directly in chemical transformations (section 2.3.8).

2.3.7 Preparation of chemically competent bacteria

Saturated cultures of bacteria were sub-cultured 1:100 in LB until the culture reached an optical density at 600nm (OD_{600}) of 0.6-0.8. The culture was incubated on ice for 0.5-1 h then centrifuged at 8900 x *g* at 4°C for 30 min. The pelleted cells were re-suspended in transformation buffer 1 (30mM potassium acetate, 10mM $CaCl_2$, 100mM KCl, 500mM $MnCl_2$, 15% (v/v) glycerol). This was then centrifuged at 8900 x *g* at 4°C for 15 min and re-suspended in transformation buffer 2 (100mM 4-Morpholinepropanesulfonic acid (MOPS), 75mM $CaCl_2$, 10mM KCl, 15% (v/v) glycerol). Cells were then either used fresh or stored at -70°C in single-use aliquots.

2.3.8 Chemical transformation

Plasmids (or ligation reactions) and chemically competent cells were incubated on ice for 5 min. Plasmid DNA was added to 1:20 to chemically competent cells (section 2.3.7), and incubated on ice for 2 min. This was then heat-shocked at 42°C for 35 s, cooled on ice for 1 min then 4:1 LB was added. The cells were then recovered for 1 h at 37°C or 2 h at 28°C at 100 rpm as indicated and plated onto LB agar containing appropriate antibiotics. Plates were incubated at the same temperature for 16 or 36 h respectively. Single transformants were re-streaked and mixed into a screening PCR reaction mixture (section 2.3.4) or sub-cultured into LB with antibiotics for 16 h for restriction digest confirmation (section 2.3.5).

2.3.9 Preparation of electro-competent bacteria

Saturated cultures of bacteria were sub-cultured 1:100 in LB until the culture reached an OD_{600} of 0.6-0.8. The culture was incubated on ice for 0.5-1 h then centrifuged at 8900 x *g* at 4°C for 30 min. The pelleted cells were re-suspended in 10% (v/v) ice-cold glycerol. This mixture was centrifuged a further 4 times as previously but re-suspended in successive half volumes of 10% (v/v) ice cold glycerol. These cells were either used fresh or stored at -70°C in single use aliquots.

2.3.10 Electro-transformation

Plasmids (or ligation reactions, section 2.3.6) and electro-competent cells (section 2.3.9) were incubated on ice for 5 min. Plasmid DNA was added to 1:40 to electro-competent cells and incubated on ice for 1 min. This mixture was then pulsed with 2.5 kV for 0.1 s over 2 mm. LB was immediately added 9:1 and cells were incubated for 1 h at 37°C or 2 h at 28°C at 100 rpm. This was plated onto LB agar containing appropriate antibiotics. Plates were incubated at 37°C for 16 h or 28°C for 36 h. Single transformants were used fresh where transformation was performed with a validated plasmid.

2.3.11 Sequencing

After delivery of samples according to their instructions, di-deoxy-termination sequencing was carried out at The GenePool (UK) using ABI 3730 Sanger with BigDye reagents.

2.3.12 Allelic exchange

Allelic exchange was performed using the method published by (Blomfield *et al.*, 1991). This method involved the exchange of a counter-selectable *sacB-kan*^{r} cassette with the gene of interest. DNA that was homologous to the flanking regions of *fliC*$_{H7}$ or *fliD*$_{H7}$ from TUV93-0 was cloned into pIB307, on either side of the *sacB-kan*^{r} cassette, to allow homologous recombination with TUV93-0. pIB307 is a low copy number cam^r plasmid, which is temperature sensitive (table 2.2). Growth at 42ºC in cam caused integration of pIB307 into the chromosome at regions of homology, to allow allelic exchange. Then growth at 28ºC in kan cured the strain of the exchange plasmid and the original allele (figure 2.1). For example, this was done with TUV93-0, to replace *fliC*$_{H7}$ with a *sacB-kan*^{r} cassette, to make TUVΔ*fliC* (figure 2.3, appendix 1). This intermediate strain was then used in a second round of exchange with other *fliC* genes or to make a clean *fliC*$_{H7}$ deletion in a similar manner (figure

2.3, appendix 1). The main difference was that in exchanging with the *sacB-kan*^{r} cassette, unsuccessful resolution was selected against with sucrose, toxic to strains containing *sacB* (figure 2.1). After allelic exchange, all strains were confirmed to be O157^{+} by PCR and immunofluorescence (table 2.3, section 2.3.4 and 2.7.1, and appendix 1).

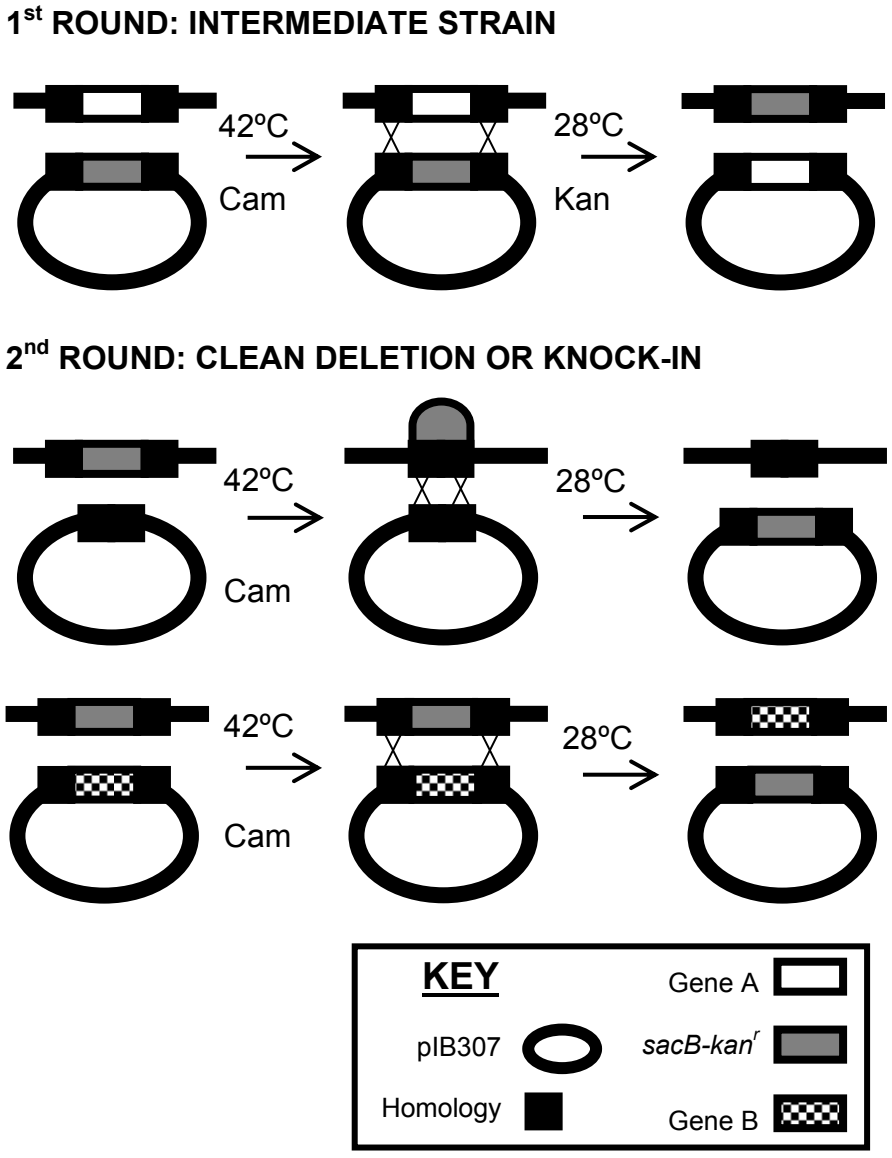

Figure 2.1. Allelic exchange strategy as described in Blomfield *et al* 1991. The 1st round involves allelic exchange of a gene with the *sacB-kan*^{r} cassette to create an intermediate mutant strain. This is then used to create a knock-out and/or knock-in in a 2nd round.

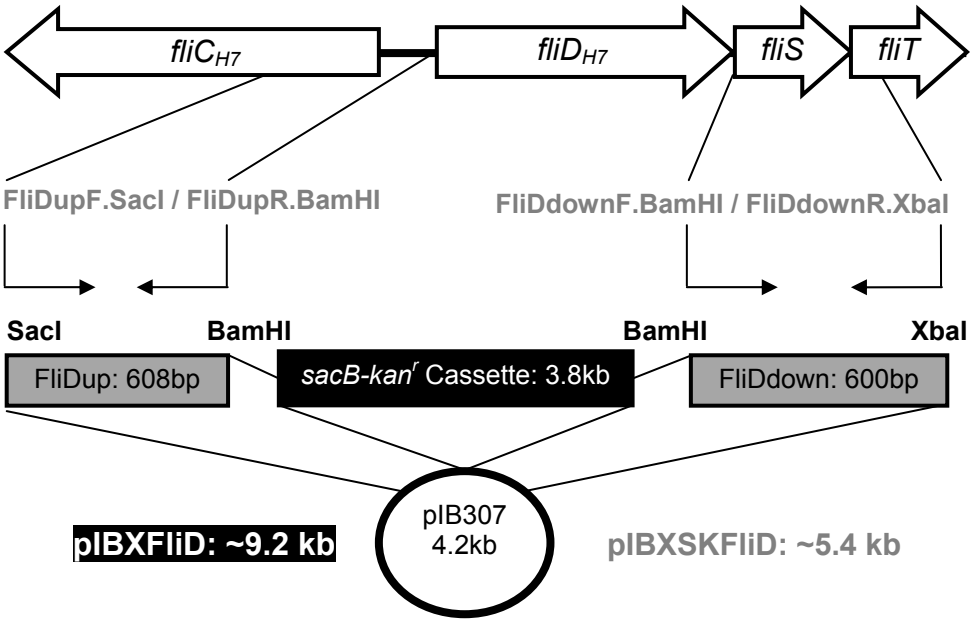

Figure 2.2. Cloning strategy for construction of exchange vectors to make *fliD*$_{H7}$ mutants in TUV93-0. TUVΔ*fliD* was made using pIBXFliD, which was like pIBXSKFliD but with a *sacB-kan*^{r} cassette between FliDup and H7down. TUV*fliD*$^-$ was made from TUVΔ*fliD* using pIBXSKFliD. See table 2.3 for primers and appendix 1 for validation.

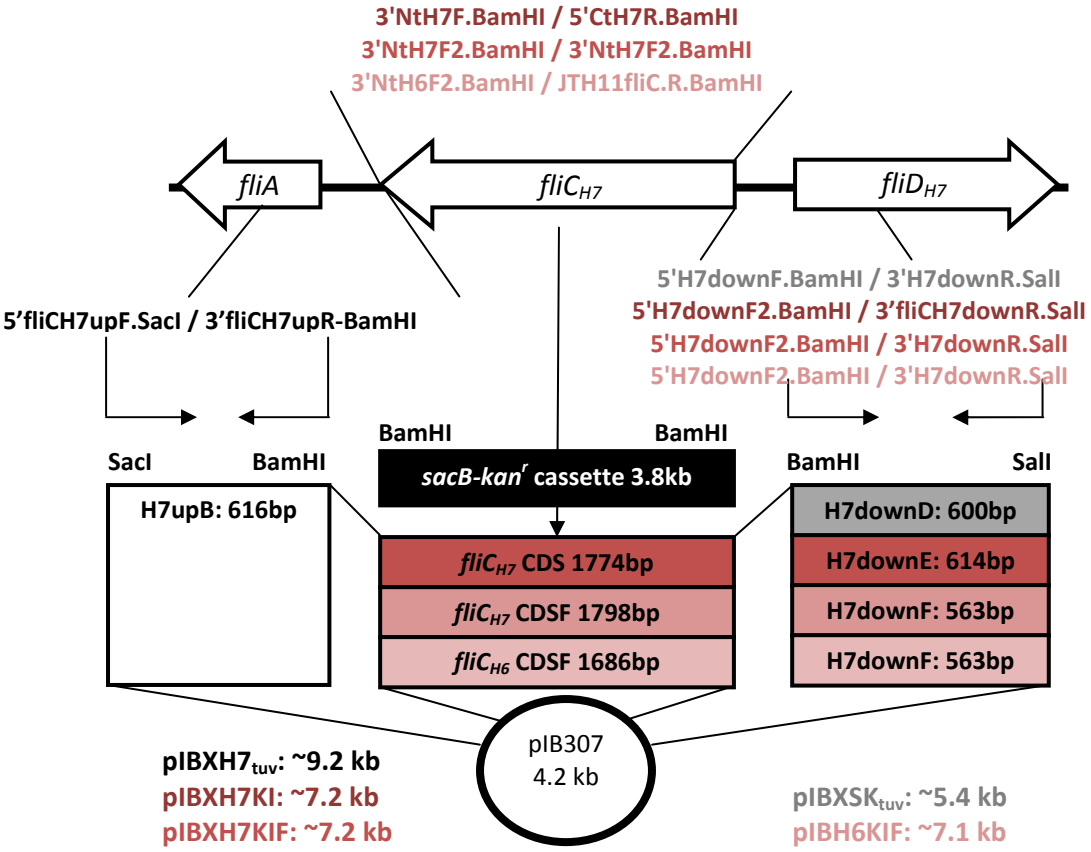

Figure 2.3. Cloning strategy for construction of exchange vectors to make *fliC* mutants in TUV93-0. TUVΔ*fliC* was made using pIBXH7$_{tuv}$, which was like pIBXSK$_{tuv}$ but with a *sacB::kan*^{r} cassette between H7upB and H7downD. TUV*fliC*$^-$ was made from TUVΔ*fliC* using pIBXSK$_{tuv}$. TUV*fliC*$^-_{H7}$, TUV*fliC*$_{H7F}$ and TUV*fliC*$_{H6F}$ were made from TUVΔ*fliC* using pIBH7KI, pIBH7KIF and pIBH6KIF respectively. See table 2.3 for primers and appendix 1 for validation.

2.3.12.1 TUVΔ*fliC* and TUVΔ*fliD*

pIBXFliD$_{tuv}$ and pIBXH7$_{tuv}$ (figures 2.2 and 2.3, table 2.2, appendix 1) were transformed into electro-competent TUV93-0 and incubated at 28ºC on LB agar with cam (CLB) for 48 h. Five transformants were used for allelic exchange of *fliC*$_{H7}$ or *fliD*$_{H7}$ with *sacB-kan*^{r} to create intermediate strains (see figure 2.1). These were streak-plated onto CLB agar and incubated for 16 h at 42ºC. Single colonies were then re-streaked onto CLB agar and incubated for 8 or 16 h at 42ºC a further three times. The five lineages were pooled in LB broth with kanamycin (KLB) and incubated for 16 h at 28ºC 200 rpm. The broth was sub-cultured 1:1000 into KLB and incubated for 8 or 16 h at 28ºC 200 rpm a further three times, after which 8 serial 1:10 dilutions in PBS were made. Dilutions 10^{-5}-10^{-8} were plated onto KLB agar plates and incubated at 28ºC for 48 h. Colonies were plated onto KLB (presence of *sacB-Kan*^{r}), CLB (absence of pIB307) and LB agar and incubated at 28ºC for 24 h. Colonies with the correct resistance profile (kan^{r}, cam^{s}) were screened for the presence of *sacB*, the absence of *fliD*$_{H7}$ coding sequence (CDS) or *fliC*$_{H7}$ (CDS)E and the size of the region by PCR (table 2.3). Non-motile clones with the correct PCR profile was classified as intermediate strains TUVΔ*fliC*10 and TUVΔ*fliD*1 (appendix 1).

2.3.12.2 TUV*fliD*$^{-}$, TUV*fliC*$^{-}$, TUV*fliC*$_{H7}$, TUV*fliC*$_{H7F}$ and TUV*fliC*$_{H6F}$

TUVΔ*fliD*1 was used for allelic exchange of *sacB-kan*^{r} with pIBXSKFliD to make a clean *fliD*$_{H7}$ deletion. TUVΔ*fliC*10 was similarly used for allelic exchange of *sacB-kan*^{r} with pIBXSKtuv to make a clean *fliC*$_{H7}$ deletion, or with pIBH7KI, pIBH7KIF or pIBH6KIF to complement the mutation with *fliC*$_{H7}$ or *fliC*$_{H6}$ (figure 2.2 and 2.3). The above exchange vectors were transformed into electro-competent TUVΔ*fliD*1 or TUVΔ*fliC*10, plated onto CLB agar and incubated for 48 h at 28ºC. The allelic exchange was performed as in section 2.3.12.1 with eight transformants, using CLB agar for four 42ºC passages and LB broth for four 28ºC passages. Dilutions 10^{-5}-10^{-8} were plated onto 6% (w/v) sucrose LB agar plates and incubated at 28ºC for 48 h. Sucrose^{r} colonies were patch-plated onto KLB (absence of *sacB-kan*^{r}), CLB (absence of pIB307) and LB agar and incubated at 28ºC for 24 h.

Colonies with the correct resistance profile (sucrose^r, kan^s, cam^s) were screened for the absence of *sacB*, the absence or presence of $fliD_{H7}$ CDS or $fliC_{H7}$ (CDS)E and the size of the region by PCR (table 2.3). Clones with the correct PCR profile and motility phenotype were stained with H-type specific polyclonal anti-sera to determine flagella expression, and classified as TUV*fliD*$^-$1, TUV*fliC*$^-$1, TUV$fliC^-_{H7}$, TUV$fliC_{H7F}$1 or TUV$fliC_{H6F}$1 accordingly (appendix 1).

2.3.13 Expression plasmids

2.3.13.1 pWSKH6

$fliC_{H6}$, the $fliC_{H6}$ CDS and native promoter from E2348/69, (~200bp upstream of the ATG), were sub-cloned from $pFliC_{H6}$ to pWSK29 as a BamHI fragment. Direction of insertion was screened by sequencing. As the functional importance of directionality was unknown, two clones with $fliC_{H6}$ in opposite directions were assessed for their ability to complement *fliC* mutants JT1 and TUV*fliC*$^-$ in motility assays.

2.3.13.2 pWSKH7$_{tuv}$ and pBADFliD$_{H7}$

Primers were designed to amplify the corresponding $fliC_{H7}$ CDS and promoter region or $fliD_{H7}$ CDS (table 2.3) from TUV93-0 genomic DNA. Digested PCR products (SalI-BamHI and NcoI-SacI respectively) were then cloned into pWSK29 or pBAD/*Myc*-His A (table 2.2). The presence of inserts was confirmed by restriction digest (section 2.3.5), sequencing (section 2.3.11) and complementation of *fliC* mutants JT1 and TUV93-0 or *fliD* mutant *TUVfliD*$^-$ in motility assays (section 2.9.2).

2.4 Bioinformatics

Cloning strategies and primers were designed using Vector NTI v.10 (Invitrogen). Primers were checked for specificity using NCBI nblast against relevant genome sequences (table 2.1 and 2.4). EDL933 was used for $fliC_{H7}$ alignments and primer

design as TUV93-0 is a *stx*$^-$ derivative of EDL933. Sequences were viewed using Chromas 2.33 (Techneleysium Pty Ltd) and identity confirmed using nblast (NCBI). All presentation of crystallographic protein structures was performed using UCSF Chimera (Pettersen *et al.*, 2004).

Table 2.4. Sequences used in sequence and structural alignments. Accession numbers refer to current version of used sequence, but corresponding sequences were accessed 03/2012.

Protein & H-type	Strain & O-type	Uniprot Accession Number
$FliC_{H6}$; H6	E2348/69; O126	B7USU2
$FliC_{H7}$; H7	EDL933; O157	Q7DBI0
$FliC_{H11}$; H11	DEC/10D; O26	Q5ECK7
$FliC_{H21}$; H21	serogroup O113:H21	Q0GJI9
$FliC_{H48}$; H48	MG1655; OR	P04949
$FliC_{P1}$; Hi (phase-1)	LT2; O4	P06179
$FliD_{H6}$; H6	E2348/69; O126	B7USU3
$FliD_{H7}$; H7	EDL933(TUV93-0 stx$^+$); O157	P58297
$FliD_{H11}$; H11	11368; O26	C8TTK5
$FliD_{H21}$; H21	serogroup O113:H21	Q0GJI8
$FliD_{H48}$; H48	MG1655; OR	P24216

2.4.1 RNA modelling

BamHI site insertion effects on *fliC* mRNA secondary structure were modelled using RNAdraw (v1.1b2). Sequences of $fliC_{H6}$ (from E2348/69) and $fliC_{H7}$ (from EDL933) with 100bp upstream of the ATG site were aligned using NCBI blast. Again EDL933 was used as it is a sequenced strain and TUV93-0 is a *stx*$^-$ derivative of EDL933. Upstream sequence that was found to be conserved was used as model mRNA. Modelling different sized portions of sequence made no difference to the predicted conformation of the RBS and start site. 2-3 bp changes were made in the conserved *fliC* mRNA sequence to introduce the BamHI sites for TUV$fliC^-_{H7}$, TUV$fliC_{H7F}$ and TUV$fliC_{H6F}$. These theoretical mRNAs were modelled using default parameters at 28°C and 37°C (figure 2.4).

Models of wild-type sequence predicted an open RBS and transcriptional start site (figure 2.4(B)). Changing 3bp to introduce the BamHI site as in TUV$fliC^-_{H7}$, the RBS and start site were predicted to be inside a stem loop structure (figure 2.4(C)). This was not overcome by modelling the structure at a lower temperature. This helped explain the poor flagella expression in the $fliC_{H7}$ knock-in. No 3 bp changes in the

upstream region of the model mRNA were predicted to be tolerated. Figure 2.4(D) shows the location (F) where 2 bp could be tolerated to introduce a BamHI site in this model, and this was used to design new *fliC*$_{H6F}$ and *fliC*$_{H7F}$ knock-ins.

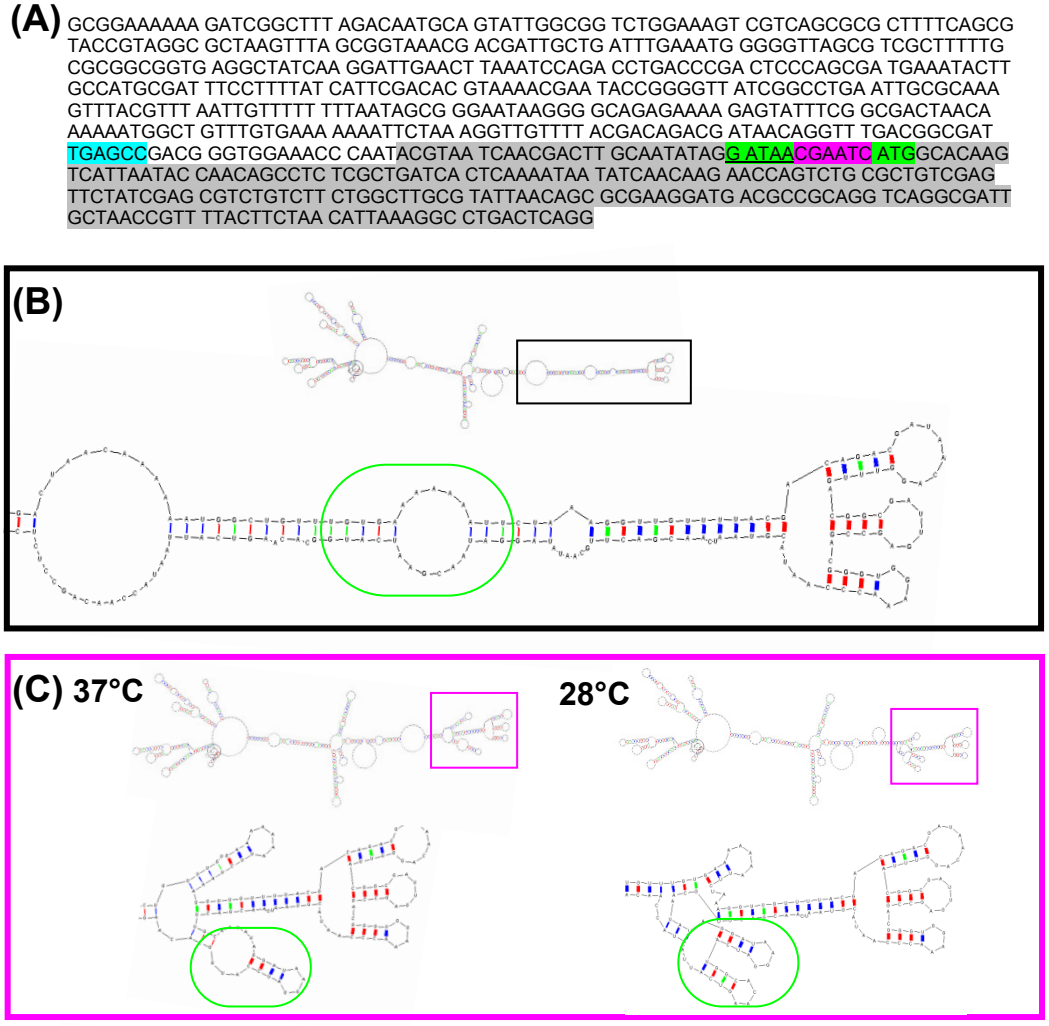

Figure 2.4. Modelling BamHI site insertion effects on *fliC*$_{H7}$ mRNA secondary structure. **(A)** Conserved upstream sequence used as model mRNA; identical in EDL933 and E2348/69 (grey), <5bp variation (unhighlighted). RBS and start site (green). Models show model mRNA and enlarged boxed promoter regions at 37ºC unless indicated, and thickness of pairing indicates probability. **(B)** EDL933 WT. **(C)** BamHI insertion in TUV*fliC*$^{-}_{H7}$ (purple in (A)). **(D)** Proposed BamHI insertion F (blue in (A)).

2.4.2 Multiple sequence alignments

FliC and FliD amino-acid sequences (table 2.4) were aligned using MUSCLE, a multi-sequence alignment program shown to be more accurate than other conventional methods (Edgar, 2004). The E2348/69 and DEC/10D FliC sequences were corrected by predicted translation of DNA sequence files as the sequences were incorrectly annotated and didn't include all of the expressed protein sequences. Structural alignments were carried out using FFAS03 via PDB0408 (Jaroszewski *et al.*, 2005). Only one crystallographic structural template for flagellin exists, for *S.* Typhimurium SJW1655 (PDB#:1ucu), so the three FliC of different H-types were structurally aligned individually to this. These were merged manually, imposing gaps against all other proteins where one protein was predicted an insertion compared to the template structure.

Alignment quality was judged by three criteria. Firstly, as the DNA sequence of the terminals is highly conserved (data not shown; (Reid *et al.*, 1999)), the alignment was judged by whether or not both terminals were aligned for all proteins. Secondly, the region of $FliC_{H7}$ known to confer H7-serospecificity (N352-P374; (Kwang *et al.*, 1996)) was expected to be part of an insertion sequence. In addition to this, numbers and type of insertions in defined secondary structure for PDB 1ucu were compared. Secondary structure elements are usually more highly conserved than turns and coils, therefore insertions in the former are more likely to indicate a poor quality alignment.

2.4.3 Mass-spectrometry fragment PTM analysis

All programs used were accessed on-line through the Expasy bioinformatics resource portal. $FliC_{H6}$ and $FliC_{H7}$ sequences were input into NetOGlyc and NetNGlyc to predict possible O-linked and N-linked glycosylation. This was used as a guideline to assess mass-spectrometry fragment analysis.

Mass spectrometry was undertaken on the two sodium dodecyl sulphate-polyacrylamide gel electrophoresis (SDS-PAGE) species of acid depolymerised $FliC_{H7}$ flagella, and sheared $FliC_{H7}$ flagella (section 2.5.2 and 2.5.5 respectively). Peptide-mass fingerprinting using MASCOT was used to assign peptide identities within each sample (section 2.5.7). Identified peptides gave a sequence coverage that ranged between 61.5-71.8% of $FliC_{H7}$. Unassigned mass:charge (m/z) values were put through GlycMod, FindMod and FindPept programs to predict possible post-translational modifications.

2.5 Protein manipulation

Table 2.5. Proteins used in this study.

Protein	Source	Storage/handling
95% pure human platelet actin (β/γ)	Cytoskeleton Inc.	Lyophilised 4°C Solution snap-frozen in single-use aliquots and stored -70°C.
99% pure human platelet actin (β/γ)	Cytoskeleton Inc.	Lyophilised 4°C Solution snap-frozen in single-use aliquots and stored -70°C.
99% pure rabbit skeletal actin- Pyrene (β/α)	Cytoskeleton Inc.	Lyophilised 4°C Solution snap-frozen in single-use aliquots and stored -70°C.
Cofilin-1 human recombinant	Cytoskeleton Inc.	Lyophilised 4°C Solution -70°C or -20°C temporarily
Arp2/3 complex from bovine brain	Cytoskeleton Inc.	Lyophilised 4°C Solution snap-frozen in single-use aliquots and stored -70°C.
Galectin-4 human recombinant	R&D	-20°C.
Gelsolin from bovine plasma	Sigma	-20°C.
Porcine-gastric mucin II	Sigma	Lyophilised 4°C
$FliC_{H6}$	Flagella purified from TUV*fliC*$_{H6F}$ by shearing or acid depolymerisation	-20°C.
$FliC_{H7}$	Flagella purified from TUV*fliC*$_{H7}$ by shearing or acid depolymerisation	-20°C.
$FliC_{P1}$	Flagella purified from SL1344Δ*fljB* by shearing	-20°C.
$FljB_{P2}$	Flagella purified from SL1344Δ*fliC* by shearing	-20°C.
$VrH7_{180-496}$ (6x(His)-tagged)	Purified from DH5a::pVrH7his recombinant purified in native conditions	-20°C.

$FLrH7_{1-585}$ (6x(His)-tagged)	Purified from DH5a::pFLrH7his recombinant purified in native conditions	-20°C.
$NTrH7_{1-179}$ (6x(His)-tagged)	Purified from DH5a::p5'rH7his recombinant purified in native conditions	-20°C.
$FliD_{H7}$ (6x(His)-tagged)	Purified from TOP10::pBAD*fliD*$_{his}$ recombinant purified in native conditions	-20°C.

Table 2.6. Antibodies used in this study.

Primary Antibody	**Details**	**Company**	**Dilution Used**
α-H6	polyclonal rabbit IgG	Mast Assure	1:1000
α-H7	Polyclonal rabbit IgG	Mast Assure	1:1000
α-Hi (phase-1 flagella from *S.* Typhimurium)	Polyclonal rabbit IgG	Mast Assure	1:100
α-H2 (phase-2 flagella from *S.* Typhimurium)	Polyclonal rabbit IgG	Difco	1:500
α-O157	Polyclonal rabbit IgG	Mast Assure	1:100
α-O157	Monoclonal mouse IgG3	AbD SeroTec	1:1000
α-C-terminal 6x(His)	Monoclonal mouse IgG1	Invitrogen	1:5000
Pre-immune serum	Polyclonal rabbit serum	SNBTS	1:100
α-FliD bleed 1	Polyclonal rabbit serum	SNBTS	as indicated
α-FliD bleed 2	Polyclonal rabbit serum	SNBTS	as indicated
α-FliD bleed 3	Polyclonal rabbit serum	SNBTS	as indicated
pre-T3S+H7 vaccination bovine serum	Polyclonal bovine serum	Tom McNeilly	1:100
post-T3S+H7 vaccination bovine serum	Polyclonal bovine serum	Tom McNeilly	1:100
pre-*E. coli* O157:H7 challenge bovine serum	Polyclonal bovine serum	Tom McNeilly	1:100
post- *E. coli* O157:H7 challenge bovine serum	Polyclonal bovine serum	Tom McNeilly	1:100
α-cofilin-1	monoclonal mouse IgG	AbDSeroTec	1:500
α-galectin-4	polyclonal goat IgG	R&D	1:1000
Secondary Antibodies	**Details**	**Company**	**Dilution Used**
α-rabbit IgG-HRP	Polyclonal goat IgG	R&D Systems	1:1000
α-rabbit IgG-FITC	Polyclonal goat IgG	Sigma	1:1000
α-mouse IgG-HRP	Polyclonal goat	R&D Systems	1:1000 (α-O157)

	IgG		or 1:5000 (α-his)
α-bovine IgG-HRP	Polyclonal mouse IgG	AbD SeroTec	1:1000
α-goat IgG-HRP	Polyclonal rabbit IgG	R&D Systems	1:1000
Staining	**Details**	**Company**	**Dilution Used**
DAPI		Various	1:1000
WGA-texas red		Invitrogen	1:1000
Phalloidin-texas red		Invitrogen	1:250
Phalloidin-AlexaFluor588		Molecular Probes	1:1000
Phalloidin-AlexaFluor647		Invitrogen	1:250

2.5.1 Protein concentration estimation

Cell lysates were tested by A_{280} and micro bicinchoninic acid assay (mBCA) methods. Purified proteins were tested by mBCA, A_{280} and densitometry from protein stained SDS-PAGE gels. Densitometry was useful in testing flagella preparations as flagellin does not generally contain many aromatic residues, causing inaccurate estimation with other methods. With A_{280}, an absorbance of 1.0 = 1.0 mg/ml, but with all other methods, a standard curve with BSA was used to estimate protein concentration.

2.5.1.1 mBCA

Using the method established by (Wiechelman *et al.*, 1988), protein standards or samples were dispensed in duplicate into 96-well plates and diluted 1:10 in working BCA reagent (Novagen; contains bicinchroninic acid, sodium bicarbonate, sodium carbonate and sodium tartrate pH 11.25, with 0.08% (v/v) cupric sulphate). Samples were incubated at 37°C for 15-30 min. A_{590} was measured using a Synergy HT plate-reader (BioTek).

2.5.1.2 Bradford assay

Using the method established by (Bradford, 1976), protein standards or samples were diluted 1:100 in Bradford reagent (AppliChem) and incubated at room temperature (RT) for 5 min. A_{595} was measured using an Ultrospec 2100pro spectrophotometer (Amersham Biosciences).

2.5.1.3 Densitometry

Using SDS-PAGE, protein standards and samples were run through 4-12% polyacrylamide gels. Gels were stained using the Imperial protein stain (Thermo Fischer), destained and imaged by scanning. They were then analysed by densitometry in GeneTools software (Syngene).

2.5.2 SDS-PAGE

Samples were diluted in Laemmli sample buffer (Laemmli, 1970), then incubated at 95-100°C for 5 min unless indicated. The samples were then loaded into a 4-12, 15 or 20% (v/v) polyacrylamide, 1% (w/v) SDS gels as indicated. 0.75, 1 and 1.5 mm polyacrylamide gels were run in 25mM Tris, 192mM glycine, 0.1% (w/v) SDS. 4-12% gels were run at 120 V for 90-120 min, 4-15% and 4-20% gels were run at 120V for 120-150 min.

2.5.2.1 Protein staining

SDS-PAGE gels were stained for proteins using coomassie G250, Imperial Protein Stain (Thermo Fischer) or by silver staining at RT. Coomassie staining was carried out by incubating gels in G250 solution, rocking for 16 h then de-staining in distilled water, with rocking for 6 h. Imperial protein staining was done as with coomassie staining for high sensitivity, or for rapid detection, gels were incubated in the stain for 1-2 h rocking, and de-stained as above for 2 h.

Silver staining was done using SDS-PAGE (section 2.5.2). Gels were incubated with rocking for 1h in fixing solution (30% (v/v) ethanol, 10% (v/v) acetic acid). Gels were then incubated with rocking for 1 h in sensitising solution (500mM sodium acetate trihydrate, 30% (v/v) ethanol, 4% (v/v) of 5% (w/v) sodium thiosulphate, and 0.12% (v/v) glutaraldehyde). After sensitisation, gels were washed 4 times in H_2O at 15 min intervals, rocking. Gels were then incubated for 1 h rocking, in silver staining

solution (0.25% (w/v) silver nitrate, 0.04% (v/v) formaldehyde). Gels were washed with H_2O twice at exactly 1 min intervals, developed in 2.5% (w/v) sodium carbonate, 0.01% (v/v) formaldehyde until bands were stained and stopped with 50mM EDTA. Gels were imaged using a gel-documentation system or a scanner.

2.5.3 Western-blotting

Proteins in SDS-PAGE gels (section 2.5.2) were Western-blotted onto nitrocellulose (Amersham, GE Healthcare) using the standard Bio-Rad wet and semi-dry methods. The wet method was carried out on ice in Towbin buffer (25mM Tris, 192mM glycine, 20% (v/v) methanol pH 8.3), at 60V for 1.5 h or 10V for 16 h. The semi-dry method was carried out at RT in Schaeffer-Nielsen buffer (48mM Tris, 39mM glycine, 20% (v/v) methanol, 0.04% (v/v) SDS, pH 9.2), and transferred with 15V for 30-60 min, depending on the gel thickness (mm).

Blots were blocked in Carbofree (VectorLabs) or 5% (w/v) skimmed milk powder (Sigma, Marvel), 0.1% (v/v) $Tween_{20}$ (Sigma) in Dulbecco A PBS (PBST) at RT for at least 2 h or 4°C for at least 16 h. Blots were washed three times between steps in 0.1% (v/v) PBST for 15 min intervals at RT, with rocking. Primary antibodies were added at the desired concentration (table 2.6), either straight into the blocking buffer, or after washing as above, then adding it to 1% (w/v) skimmed milk powder, 0.1% (v/v) PBST. Primary antibodies were incubated with blots for at least 1 h at RT, rocking, and then the blots were washed as above. Horseradish peroxidase (HRP)-conjugated secondary antibodies were added to 1% (w/v) skimmed milk powder, 0.1% (v/v) PBST at the desired concentration (table 2.6) and incubated with blots for at least 1 h RT, rocking, and then the blots were washed as above.

Blots were developed using chemi-luminescence (with either enhanced chemi-luminescence (ECL) solution A (2.5mM luminol (Fluka), 400µM *p*-Coumaric acid (Sigma) in 100mM Tris-HCl pH 8.5) and ECL solution B (0.2% (v/v) H_2O_2 in 100mM Tris-HCl pH 8.5) or Pico-West SuperSignal ECL reagents from Thermo

Fischer. Blots were either exposed onto chemi-luminescence film (Amersham, GE Healthcare) or captured on the G:box (Syngene) using GeneSnap (Syngene). If blots were exposed to film, they were incubated in the ECL reagents for 5 min at RT, rocking. They were then sealed, exposed to film, and developed (Kodak). If blots were captured on the G:Box, they were placed on an acetate sheet and covered with a thin layer of ECL reagent in the G:box. The G:box settings used were a focus of 62 at a distance of 575mm, at the highest quality.

2.5.3.1 Far Western-blotting

Far Western blots were performed like Western blots, but with an extra detection step. Instead of detecting proteins on nitrocellulose membranes directly with antibodies, blotted membranes were probed with protein solutions, and their binding to the blotted membranes was detected with specific antibodies. This made it possible to use this method to screen for protein:protein interactions.

80 µg BTRE freeze-thawed cell lysates 5 µg 95% pure human platelet actin or 1 µg purified receptor candidates were Western-blotted onto nitrocellulose membranes and blocked according to section 2.5.3. These membranes were washed three times in 0.1% (v/v) PBST at RT, rocking, at 15 minute intervals. Membranes were then probed with 1 µg/ml PBS of $FliC_{H7}$ flagella or recombinant $FliD_{H7}$ for 3 h at RT, rocking and washed as above. $FliC_{H7}$ flagella or recombinant $FliD_{H7}$ were labelled using α-H7 rabbit IgG and a-his mouse IgG, and detected with appropriate horse radish peroxidase (HRP)-conjugated antibodies as detailed in section 2.5.3 and table 2.6.

To assess the involvement of glycosylation in protein interactions detected, Carbofree (VectorLabs) blocked membranes were treated with PNGase-F or O-glycosidase prior to protein binding. 25 mU (IUB) PNGase-F (New England Biolabs) or 2.5 mU (Roche) O-Glycosidase F (Roche) in enzyme buffer (50mM Na_2HPO_4, 50mM NaH_2PO_4, 0.02% (v/v) Nonidet P-40 (New England Biolabs) pH

7.5) were incubated with membranes at 37°C for 16 h. Membranes were then washed three times in 0.1% (v/v) PBST at RT, rocking, at 15 minute intervals before protein binding was performed.

2.5.4 DIG-labelled glycan detection

Proteins were Western-blotted onto nitrocellulose membranes (section 2.5.3) and a digoxigenin-3-0-succinyl-ϵ-aminocaproic acid (DIG)-labelling Glycan Detection kit (Roche) was used according to manufacturer's instructions. This method was described in (Haselbeck & Hosel, 1990). Briefly, blotted proteins were washed twice in PBS then oxidised by incubation with 10mM sodium metaperiodate in 100mM sodium acetate pH 5.5 for 20 min at RT, rocking. Membranes were then washed three times in PBS at RT rocking, with 10 minute intervals. Membranes were then DIG-labelled by incubating them with DIG-hydrazide diluted 1:5000 in 100mM sodium acetate pH 5.5 for 1 h at RT, rocking. Membranes were washed three times in tris-buffered saline (TBS) at RT, rocking, at 10 min intervals then blocked with the blocking reagent supplied with the kit for 1 h at RT, rocking. After washing as above, membranes were incubated with α-DIG FAb-alkaline phosphatase diluted 1:1000 in TBS for 1 h at RT, rocking. Membranes were washed as above once more then stained with NBT/X-phosphate (4-nitro blue tetrazolium chloride/5-bromo-4-chloro-3-indolyl-phosphate) diluted 1:500 in staining buffer (100mM Tris, 50mM $MgCl_2$, 100mM NaCl, pH 9.5) until bands appeared. The staining reactions were then stopped by rinsing membranes with H_2O and imaged on a gel-documentation system (G:box, Syngene).

2.5.5 Purification of bacterial flagella

2.5.5.1 Acid depolymerisation

Fresh colonies were motility-enriched and grown in LB broth at 30°C 200 rpm to an OD_{600} of 1-1.5. Cultures were then centrifuged at 10000 x *g* for 15 min at 4°C. The supernatant was discarded and pellets were re-suspended in PBS at 1:20 of the initial

culture volume for 16 h at 4°C. Re-suspended pellets were adjusted to pH 2.0 with 1M HCl and incubated for 30 min rocking at RT to depolymerise flagella. They were then centrifuged at 5000 x *g* for 30 min at 4°C, pelleting the bacteria. The supernatants were separated and adjusted to pH 7.0 with 1M NaOH to re-polymerise flagella. Flagella were precipitated with 2.67M ammonium sulphate at 4°C for 16 h. They were centrifuged at 15000 x *g* for 15 min at 4°C and supernatants kept aside for SDS-PAGE analysis. The pellets were re-suspended in PBS, 1:500 of the initial culture volume. These preparations were then dialysed 1:1000 against sterile PBS four times in succession at 4°C (for 8 h then 16 h, twice) and analysed by SDS-PAGE and mBCA (section 2.5.1 and 2.5.2) for purity and concentration.

2.5.5.2 Shearing

Fresh colonies were motility-enriched and grown in LB broth at 30°C 200 rpm to an OD_{600} of 0.8-1.2. These cultures were then centrifuged at 4100 x *g* at 4°C for 30 min to pellet cells. The supernatants were discarded and pellets were re-suspended in PBS 1:5 of the initial culture volume for 16 h at 4°C. Re-suspended pellets were diluted 1:2 with cold PBS and sheared at top speed for 2 min on ice using an IKA T-10 homogeniser (Ultra-Turrax). Culture supernatants were then centrifuged at 4100 x *g* at 4°C for 15 min and transferred to fresh tubes multiple times, until there were no visible pellets. To completely clear the supernatants of bacterial cells, they were then centrifuged at 16000 x *g* 4°C for 10 min. The top 80% of supernatants were transferred into fresh tubes and centrifuged at 20500 x *g* at 4°C for 1.5 h to pellet flagella. Pellets were re-suspended in PBS 1:500 to initial culture volume. Re-suspension by pipetting or vortexing was carried out for 2 min, incubated on ice for 10 min, then re-suspended for another 2 min. Samples were stored at 4°C until protein concentration (section 2.5.1) and purity (section 2.5.2) were assessed. Samples were then aliquoted and stored at -20°C.

2.5.6 Purification of His-tagged proteins

Plasmids containing desired 6x(His) tagged proteins were electroporated into electro-competent *E. coli* BL21(DE3), except for $FliD_{H7}$, where TOP10 was used. Fresh amp^r transformants were used to inoculate LB broth with amp (ALB), which were incubated at 37°C 200 rpm for 16 h. These were sub-cultured 1:100 into ALB, incubated at 37°C 200 rpm to an OD_{600} of 0.6. Cultures were then induced with a final concentration of 1mM isopropyl β-D-1-thiogalactopyranoside (IPTG, Promega) and incubated in the same conditions for a further 3-4 h. Cultures were centrifuged at 4100 x *g* 30 min to pellet bacteria. Cell pellets were stored for 16 h at -20°C.

Pellets were then thawed on ice for 30 min and re-suspended in lysis buffer (50mM NaH_2PO_4, 300mM NaCl, 10mM imidazole, pH8.0) 1:500 to initial culture volume. 1 mg/ml lysozyme (Sigma) was added and preparations were incubated on ice for 30 min. Lysates were then sonicated on ice using 6 200 W 10 s bursts with 10 s intervals. Lysates were drawn in and out of narrow-gauge needles 5 times and centrifuged at 10000 x *g* at 4°C for 30 min for lysate clarification. Lysate supernatants were used for further protein purification.

Ni-NTA resin (Novagen) was washed 3 times with lysis buffer by gentle centrifugation (100 x *g* for 1 min) to create 50% slurries. 50% slurries were added 1:4 to clarified lysate supernatants in capped columns. These were then incubated for 30 min RT rocking. The columns were then fixed in place, un-capped and allowed to flow through. Resins were washed twice with 4:1 volumes of wash buffer (50mM NaH_2P04, 300mM NaCl, 20mM imidazole, pH 8.0). Proteins were then eluted from the column resin 1:1 with elution buffer 4 times (50mM NaH_2P04, 300mM NaCl, 250mM imidazole, pH 8.0), in four fractions.

Fractions were analysed by SDS-PAGE and Western-blotting with α-his mouse IgG and α-mouse IgG-HRP (table 2.6, section 2.5.3) to assess elution fractions for yield

and purity. High yield fractions of acceptable purity were assayed for protein concentration and aliquoted for storage.

2.5.7 Mass spectrometry

Mass-spectrometry, tandem mass-spectrometry and peptide mass fingerprinting were undertaken by Kevin Mclean at the Moredun Research Institute Proteomics Facility. Protein bands from Imperial protein stained SDS-PAGE gels were excised and delivered to Kevin Mclean for trypsinisation, enrichment, clean-up and mass spectrometry according to their protocols. Spectra were then input into MASCOT peptide mass fingerprinting software (Matrix Science) to generate protein identities.

2.5.7.1 Accurate MW determination by mass-spectrometry

$FliC_{H7}$ was analysed by online HPLC-MS by Andy Gill in the facilities of Proteomics and Metabolomics at the Roslin Institute. A sample of sheared $FliC_{H7}$ flagella was diluted to ~1 pmole/µl in 0.1 % (v/v) formic acid and ~20 pmole was applied to a microbore HPLC column (Dionex Acclaim C_{18}, 4.6 mm i.d., 150mm length, 5 µm beads, 120 Å pore size) pre-equilibrated with 0.1 % (v/v) formic acid by use of a Ultimate HPLC system (Dionex). Bound components were eluted with a gradient of 0.1 % (v/v) formic acid in acetonitrile into the electrsopray source of an amaZon ETD ion trap mass spectrometer (Bruker Daltonics, Germany). The mass spectrometer acquired full scan mass spectra with final spectra being an average of 8 trap fills of a maximum averaging time of 200 ms. Signals corresponding to intact H7 protein were summed, the raw data was smoothed and background subtracted and then de-convoluted by use of the Burker proprietary algorithm.

2.5.8 $FliD_{H7}$ antibodies

All serum was collected and stored in 50% (v/v) Alsever's solution. Rabbits were screened for exposure to $FliD_{H7}$ by probing $FliD_{H7}$ Western blots with their blood serum and a naïve rabbit was selected. This rabbit was vaccinated with 150 µg

recombinant $FliD_{H7}$ at 1 mg/ml in 25% (v/v) Freund's complete adjuvant in PBS, by four small injections – 2 intra-muscularly in hind-legs, 2 sub-cutaneously over each scapula. Further booster doses of $FliD_{H7}$ were given with 25% (v/v) Freund's incomplete adjuvant as above, at 28-day intervals. Before each dose of recombinant $FliD_{H7}$, serum was collected (pre-immune serum (PI), bleed 1, 2 and 3). Sera from the rabbit were monitored throughout by testing it for recognition of recombinant $FliD_{H7}$ by Western blotting and enzyme-linked immuno-sorbent assay (ELISA). ELISAs were done by coating 1 µg of recombinant $FliD_{H7}$ in 100mM bicarbonate buffer pH 9.6 for 16 h at 4°C and blocking it with 3% (w/v) BSA (fraction V, Sigma) in 0.1% (v/v) PBST for 2 h RT, rocking. Rabbit sera were added at different dilutions in 3% (w/v) BSA, washed in 0.1% (v/v) PBST, and detected with a-rabbit IgG-HRP diluted in 3% (w/v) BSA and ECL reagents as in section 2.9.1.1. Rabbits were exsanguinated and serum was stored at -70°C.

2.6 Primary culture of BTR epithelial cells

2.6.1 Isolation of BTRE

This method was performed by Edith Paxton for the majority of cells. Abbattoir-derived bovine rectal canals were collected. These were cut longitudinally and washed in H_2O. The terminal rectal canals were isolated as the ~5 cm of tissue proximal to the recto-anal junction. The underlying bulk of connective tissue was cut away and terminal rectums were thoroughly mixed in washing media (Hank's Balanced Salt Solution (HBSS), Sigma) containing 25 µg/ml Gentamicin (Sigma), 5 µg/ml Fungizone (Invitrogen), 100 U/ml penicillin and 30 µg/ml streptomycin (Invitrogen)) and incubated for 30 min at RT. Epithelial mucus was then removed from tissue by lightly scraping epithelia with sterile glass slides. The epithelial layers were then isolated from the sub-mucosa by firmly scraping the tissue with sterile glass slides. Epithelia were collected in this way and shaken vigorously in HBSS to disrupt tissue. These were then centrifuged at 300 x *g* for 2 min at RT, carefully discarding the supernatant, until supernatants were clear.

Digestion medium (Dulbecco's Minimum Essential Medium (DMEM, Sigma), 1% (v/v) foetal bovine serum (FBS, Sigma), 25 μg/ml Gentamicin (Sigma), 100 U/ml penicillin and 30 μg/ml streptomycin) was added to cell pellets (<10 ml), then 75 U/ml Collagenase (Sigma) and 20 μg/ml Dispase I (Roche) were added. These were mixed vigorously and incubated at 37°C 200 rpm for 1 h 20 min.

Digested tissues were centrifuged at 300 x *g* for 2 min at RT. Pellets were re-suspended in HBSS and this process was repeated until the top of supernatants were free of crypts. At this stage, 1:5 less HBSS was added with each re-suspension until all of the supernatants were clear. Pellets were then washed with HBSS and re-suspended in primary cell culture medium (DMEM, 2% (v/v) FBS, 2mM L-glutamine (Invitrogen), 25 μg/ml gentamicin (Sigma), 100U/ml penicillin (Invitrogen), 30 μg/ml streptomycin (Invitrogen), 10 ng/ml epidermal growth factor (Sigma), 0.25 U Insulin (Sigma)) to a concentration of ~5000 crypts/ml.

2.6.2 Primary BTRE growth

500-700 crypts/well were seeded in primary cell culture medium on Collagen (Nutacon) coated plates. Primary cell cultures were incubated at 37°C, 5% CO2, 80% humidity for 1-2 days, then half of the media was replaced with feeding medium (as primary cell culture medium but 5% (v/v) FBS). Media was then completely replaced every 2 days until cells were confluent.

2.6.3 Primary BTRE cell lysate preparation

Confluent cells were harvested for freeze-thawed cell lysates by washing them twice in PBS then incubating them with TripLE Express (Gibco) at 37°C 5% CO2 80% humidity for 10 min. The TripLE Express on cells was then diluted 1:2 with PBS, cells were scraped off, collected and centrifuged at 300 x *g* at RT for 2 min. They were then washed by re-suspending and centrifuging as above in PBS or HBSS, twice. The cell pellet was re-suspended in 1 ml PBS or HBSS and subjected to 5

cycles of snap-freezing in ethanol and dry-ice and thawing at RT. These lysates were clarified by centrifugation at 18000 x *g* for 10 min at 4°C to remove cellular debris. For cell lysates prepared using Triton X-100, cells were washed twice in PBS then incubated with lysis buffer (3% (v/v) Triton X-100 (Sigma), 20mM Tris, 150mM NaCl, 1mM EDTA) for 5 min RT. Cells were then scraped off and mixed by pipetting.

2.7 Wide-field immunofluorescence microscopy

Samples were visualized using a Leica DM-LB epi-fluorescence microscope (Leica Microsystems), photographed using a Hamamatsu ORCA-ER B/W CCD digital camera (Hamamatsu Photonics K.K.) and analysed using OpenLab 4.0 (Improvision; UK). A minimum of three fields of view were sampled per duplicate.

2.7.1 Imaging of flagella expression in bacterial cultures

Fresh colonies of TUV93-0 and its derivatives were grown in LB broth at 30°C 200 rpm for 16 h. These saturated cultures were fixed by diluting them 1:10 in 4% (w/v) paraformaldehyde (PFA) on ice for 30 min, and were stored at 4°C. Samples were heat-fixed at 37ºC to multispot glass slides (C.A.Henley Essex Ltd) in duplicate. These were stained using H-type specific polyclonal rabbit IgG (table 2.6, diluted with 1% BSA in PBS) at RT for 30 min in a dark, slow-rocking humidified chamber. After washing the slides three times in PBS, they were incubated with anti-rabbit fluorescein isothiocynate (FITC)-conjugated goat IgG (diluted 1:1000 with 1% (w/v) BSA in PBS) for a further 30 min at RT. Slides were washed again in PBS and dried at 37ºC before mounting with DAKO (a fluorescent mounting medium, Sigma). Slides were left for a minimum of 2 days before viewing and were stored at 4ºC in the dark.

2.7.2 A/E lesion formation

This was undertaken by Xuefang Xu as in (Xu *et al.*, 2012). Confluent embryonic bovine lung (EBL) cells grown in glass 4-well chamber slides were washed and incubated with minimal essential medium (MEM) with the Hydroxyethyl-Piperazine Ethanesulafonic Acid (HEPES) modification 1 h prior to infection with TUV93-0. 2 x 10^6 bacteria were incubated with EBL cells at an MOI of 10 at 37°C 5% CO2 80% humidity for 3 h. Cells were washed twice with PBS, fixed in 2.5% (w/v) PFA in PBS for 20 min at RT, then permeabilised for 5 min with 0.1% (v/v) Triton X-100 in PBS at RT. Cells were washed three times in PBS and α-O157 rabbit IgG (Mast Assure) diluted 1:50 in 1% (w/v) BSA (PBS) were added for 35 min. Slides were then washed three times in PBS, and incubated with anti-mouse IgG-AlexaFluor$_{568}$ (Molecular Probes) diluted 1:1000 in 1% (w/v) BSA (PBS) for 30 min in the dark. The cells were then washed three times in PBS and stained with 1 µg/ml phalloidin-FITC (fluoroscein isothiocyanate, Sigma) in PBS for 30 min in the dark. Slides were then washed twice with PBS and mounted with DAKO mounting medium. The slides were imaged by fluorescent microscopy after at least 16 h to allow the mountant to set.

2.8 Confocal microscopy

2.8.1 Bacterial infection

Semi-confluent primary BTRE cells (section 2.6.2) grown in 4 well chamber slides were washed twice with PBS then incubated for with MEM-HEPES 1-2 h prior to infection with TUV93-0. Fresh colonies of TUV93-0 were grown in LB broth at 30°C 200 rpm for 16 h then were centrifuged at 4100 x *g* for 5 min at RT and the pellet was re-suspended in MEM-HEPES to an OD_{600} of 0.3-0.4. 1 x 10^7 bacteria were added to each well and cells were incubated for 1 h at 37°C 5% CO2 80% humidity as in (Mahajan *et al.*, 2009).

2.8.2 Bacterial staining

Cells were washed with PBS three times then fixed with 2% (w/v) PFA in PBS for >5 min. If wheat-germ agglutin (WGA)-Texas red (Invitrogen) was added, it was at this point prior to permeabilisation, diluted 1:1000 in PBS for 30 min, kept dark. Cells were permeabilised with 0.1% (v/v) Triton X-100 in PBS for 2 min then washed three times with PBS. Cells were then labelled with α-H7 rabbit IgG diluted 1:1000 in PBS for 16 h at 4°C, washed three times in PBS, then labelled with α-O157 rabbit IgG diluted 1:100 in PBS for 1 h at RT. After washing three times in PBS, α-rabbit IgG-FITC was added, diluted 1:100 in PBS, for 1 h RT in the dark onwards if not already kept in the dark. Cells were then washed three times in PBS.

2.8.3 BTRE staining

If wheat-germ agglutinin-Texas red had been used, phalloidin-AlexaFluor647 was used to label actin. If not, then Texas red conjugated phalloidin was used instead. In either case, the phalloidin was added, diluted 1:250 in PBS, for 1 h at RT, and cells were then washed three times with PBS. If 4,6-diamidino-2-phenylindole (DAPI) was used, it was added, diluted 1:1000 in PBS for 30 min at RT. Slides labelled with wheat-germ agglutin were mounted using VectorShield (VectorLabs) mountant, the rest were mounted using ProLong Gold (Invitrogen) mountant. Slides were stored for at least 5 days to set before imaging.

2.8.4 Confocal imaging

Imaging was undertaken at the Roslin Institute Bioimaging Facility on a Zeiss LSM5-Pascal confocal microscope with 488 nm, 543 nm HeNe lasers and an 633 nm argon laser (Lasos GmBH), using Axiovert software, or performed by Trudie Gillespie at the IMPACT facility in the Centre for Integrative Physiology at the University of Edinburgh. At the IMPACT facility, slides were imaged using a Zeiss LSM510 confocal system with a 488 nm Argon Kryton laser, 514 nm HeNe laser, a Titanium:Sapphire multi-photon laser and Axiovert software. Images were presented using ImageJ.

2.9 Assays

2.9.1 Enzyme-linked immuno-sorbent assays (ELISAs)

2.9.1.1 Mucin II ELISA

96-well MaxiSorb ELISA plates (Nunc) were coated with 100 µg/well of porcine gastric mucin fraction II (Sigma) in 100mM bicarbonate buffer pH 9.6 at 4°C for 16 h. TUV93-0 that had been fixed with 4% (w/v) PFA (section 2.8.2) was coated onto the plate as a positive control. Coating was removed and wells were blocked with 1% (w/v) BSA at 37°C for 1 h. Wells were washed with 0.1% (v/v) PBST three times.

Strains were grown at 28°C in LB broth 200 rpm for 16 h. Saturated cultures were centrifuged at 8900 x *g* and cell pellets were re-suspended in PBS to an OD_{600} of 1.0. Strains were added to wells in 1:2 serial dilutions, incubated at 37°C for 1 h, and washed three times with 0.1% (v/v) PBST.

Bound bacteria were labelled with α-O157 rabbit IgG, diluted 1:100 in PBS, for 1 h at 37°C, and were then washed three times with 0.1% (v/v) PBST. HRP-conjugated α-rabbit IgG antibodies were diluted 1:1000 in PBS and incubated in wells for 1 h at 37°C before washing again as above. Bacteria were detected using OPD-fast (Sigma); after 15 min at RT, the reaction was stopped using 1M H_2SO_4 and A_{492} was read in a Fluostar Optima plate reader.

2.9.1.2 Far ELISAs

96-well MaxiSorb ELISA plates (Nunc) were coated with 1 µg/well of galectin-4, cofilin-1 or 95% pure human platelet actin in 100mM bicarbonate buffer pH 9.6 at 4°C for 16 h. 1 µg/well of purified flagella proteins were coated onto the plate for positive and negative detection controls. Coating was removed and wells were blocked with Carbofree (VectorLabs) for 2 h at RT. Wells were washed with 0.1%

(v/v) PBST three times then 1000, 500, 100 or 0 ng/well of purified flagella proteins in PBS were added to wells for 3 h at RT, rocking, then washed again.

Bound flagella proteins were labelled with specific antibodies (table 2.6), diluted in 0.1% (v/v) PBST for 1 h at RT, rocking, before washing three times in 0.1% (v/v) PBST. These rabbit and mouse IgG were then detected with specific HRP-conjugated secondary antibodies (table 2.6), diluted in 0.1% (v/v) PBST, for 1 h at RT, rocking. After washing as above, bound protein was detected using SuperSignal West Pico ECL reagents (Thermo-Fischer) in the G:box using GeneSnap (Syngene), as with Western blots (section 2.5.3).

Binding results were then quantified in GeneTools (Syngene) by densitometry of the inverted chemi-luminescence image using a spot radius of 25. Data from three independent experiments were normalised using the formula *Relative binding = 100 x [(Test-0P)/(PC-0P)],* where 0P = 0 ng flagella protein, PC = positive detection control. Statistical analysis was carried out in Minitab 16. Data residuals were assessed for normality using a Kolmogorov-Smirnov test ($p>0.05$). A general linear model was used to assess the statistical significance of results, where the response was relative binding, and the model included experiment as a confounding factor and receptor candidate (galectin-4, cofilin-1 and actin) and protein concentration (1000, 500, 100 ng/well) as factors. Post-hoc Tukey pairwise comparisons of the interaction between protein concentration and receptor candidate terms were then performed on the data, with a p-value of <0.05 being taken as significant.

2.9.1.3 Cell-based ELISAs

Cell-based ELISAs were used to detect protein binding to BTRE cells or to assess α-FliD-inhibition of *E. coli* O157:H7 binding to BTRE cells. In each case, BTRE primary cell culture was performed as described in section 2.6.2, then 1-2 h before protein or strain co-incubation, cells were washed twice with PBS then incubated with MEM-HEPES (Sigma).

2.9.1.4 Protein-binding cell-based ELISAs

Primary BTRE cells were incubated with 10 μg/well protein (sheared $FliC_{H7}$ flagella, recombinant $FliD_{H7}$, $VrH7_{180-496}$) for 3 h at 37°C 5% CO_2 80% humidity. Cells were washed three times in PBS and fixed with 2% (w/v) PFA for 20 min at RT with 0.1% (v/v) Triton X-100, except for experiments with sheared $FliC_{H7}$ flagella. Endogenous peroxidase activity was quenched with 1% (v/v) H_2O_2 in methanol at RT for 20 min, except for experiments with sheared $FliC_{H7}$ flagella. After washing cells three times with PBS, they were blocked with 3% (w/v) BSA (fraction V, Sigma) in PBS at 4°C for at least 16 h.

After blocking buffer was removed, α-6x(His) mouse IgG (Invitrogen) was added 1:5000 to 3% (w/v) BSA and incubated with cells for 1 h at RT, except with $FliC_{H7}$ flagella, where α-H7 rabbit IgG was used at a 1:1000 dilution. Cells were washed three times in PBS then α-mouse IgG-HRP (BD) was added 1:5000 to 3% (w/v) BSA and incubated and washed as above, except with $FliC_{H7}$ flagella, where α-rabbit IgG-HRP was used at a 1:1000 dilution.

Binding was detected using SuperSignal West Pico ECL reagents (Thermo-Fischer) in a G:Box (Syngene) with a 62 focus at 575mm in GeneSnap (SynGene). Densitometry was performed on inverted images in GeneTools (SynGene) using a 65 spot radius. Cells were then washed three times in PBS and 0.1% (v/v) crystal violet stain was added to measure BTRE cell coverage, except with $FliC_{H7}$ flagella. This was incubated at 4°C for 30-45 min then washed three times in PBS. 20% (v/v) acetone in ethanol was added, incubated for 30 min at RT, rocking, and A_{590} was read in a Synergy HT plate reader (BioTek).

Binding data from 2 experiments with 3-5 technical replicates was assessed for quality using no BTRE and no primary antibody controls, then analysed using the

formula *BTRE binding* = (R_t/CV_t)- $\bar{x}(R_{no1y}/CV_{no1y})$ where R = raw pixel volume, CV = crystal violet value, t = test, No1y = no primary antibody control. With $FliC_{H7}$ flagella there were no CV values, but otherwise analysis was the same. Molecular binding efficiencies were calculated using the formula *Molecular binding efficiency = Binding index/(protein concentration in nM* x *1000)*, where *Binding index = (BTRE binding at 10 µg/ml)/(BTRE binding at 0 µg/ml)*. This gives BTRE binding/nmol of protein.

2.9.1.5 Antibody inhibition cell-based ELISAs

Freshly revived TUV93-0 was grown in LB broth at 30°C 200 rpm for 16 h. TUV93-0 was then sub-cultured 1:50 in LB broth at 30°C 200 rpm until it reached an OD_{600} of 0.3. Cultures were centrifuged at 8900 x *g* for 5 min and pellets re-suspended in MEM-HEPES (Sigma). Pre-immune, α-H7 and α-FliD rabbit antisera (table 2.6) were mixed 1:10 with separate bacterial cultures and incubated at RT statically for 30 min. 1 x 10^7 bacteria were added to cells and incubated for 1 h at 37°C 5%CO2 80% humidity. BTRE cells were then washed three times in PBS, fixed with 2% (w/v) PFA for 15 min at RT then permeabilised with 0.1% (v/v) Triton X-100 for <1min. Cells were washed three times in PBS, peroxide treated, washed and blocked as in section 2.9.1.3.

After blocking buffer was removed, α-O157 mouse IgG (AbDSeroTec) was added 1:1000 to 3% (w/v) BSA and incubated with cells for 1 h at RT. Cells were washed three times in PBS then α-mouse IgG-HRP (BD) was added 1:1000 to 3% (w/v) BSA and incubated and washed three times in PBS. Binding was detected, densitometry and crystal violet staining was performed as in section 2.9.1.4. Binding data from two experiments with 5 technical replicates was assessed for quality and normalised using the same formula as in section 2.9.1.3.

2.9.2 Motility assays

Motility assays were used to phenotypically validate the construction of *fliC* expression vectors and mutants. Fresh streak plates or electro-transformants were stab inoculated once into dried semi-solid agar plates (1% (w/v) tryptone, 0.5% (w/v) NaCl, 0.3% (w/v) granulated agar). Antibiotics were added prior to plate-pouring where appropriate. Inoculated plates were incubated at 28ºC for 16 or 24 h, as indicated. Assays were carried out with 4 replicates where possible and repeated at least once for confirmation. Motility assays are very variable, even with wild-type flagellated strains. As such, motility was regarded as complemented where motility halos of mutants were within limits of typical wild-type variation.

2.9.2.1 Antibody inhibition of motility

Colonies from freshly revived TUV93-0 were stab inoculated into motility agar containing 1:1000 dilutions of pre-immune rabbit serum, α-H7 and α-FliD bleed 1, α-FliD bleed 3, α-H7+ α-FliD bleed 1 or α-H7+α-FliD bleed 3 (sera was added when agar was cooling). Plates were incubated at 30°C for 24 h and motility was quantified by scanning plates and measuring relative halo radius in GeneTools (SynGene). Where halos were not circular, halo radius was considered to be the radius of the largest circle that could fit within the halo. Motility inhibition was assessed as a percentage of motility in the presence of pre-immune serum. Analysis was performed on data from two independent experiments with 3 technical replicates (except with bleed 3, which only had 3 technical replicates).

2.9.3 Co-immunoprecipitation of $FliC_{H7}$ flagella with BTRE cell lysates

Pierce protein A/G agarose 50% slurry (Thermo Scientific) was used according to manufacturer's instructions. Briefly, slurries were washed twice by centrifugation at 10000 x *g* for 1 min and re-suspension in equal volume of TBS. Resin was centrifuged as above then re-suspended in 250 µg of BTRE cell lysate (Triton X-100 method, section 2.6.3) for 2 h at 4°C, rocking. Beads were then centrifuged as above and supernatants were used as pre-cleared cell lysates for co-immunoprecipitation.

Sheared $FliC_{H7}$ flagella or an equivalent volume of TBS were added to pre-cleared cell lysates for 16 h at 4°C rocking. Fresh Pierce protein A/G agarose beads were washed as above and α-H7 was added, diluted 1:4 in TBS, for 1 h at 4°C, rocking. This α-H7/A/G agarose was then washed as above and added to pre-cleared cell lysates +/- $FliC_{H7}$ flagella for 2 h at 4°C, rocking. The beads were washed again and 2xSDS-PAGE sample buffer added for 5 min at 100°C. The eluted proteins were separated from the A/G beads by centrifugation as above. Supernatants were analysed by 12% SDS-PAGE and coomassie staining.

2.9.4 CnBr-Sepharose pull-downs

2.9.4.1 Bead preparation

Cyanogen bromide (CnBr) activated sepharose 4B lyophilised beads (GE Healthcare) were used according to manufacturer's instructions. They were dissolved to 2% (w/v) bead re-suspension buffer (1mM HCl, pH 3.0) and centrifuged at 3600 x *g* for 5min at RT. The beads were re-suspended as above in bead re-suspension buffer three more times. The fourth time, the beads were re-suspended as a 50% slurry in re-suspension buffer and stored at 4°C.

2.9.4.2 Pull-downs

Slurries were touch-spun down and re-suspended in coupling buffer (100mM $NaHCO_3$, 500mM NaCl, pH 8.3). 50 µg protein (flagella proteins or receptor candidates) was added 2:1 to CnBr beads for 16 h at 4°C, rocking, except galectin-4, where only 1:3 was added. Excess protein was washed off beads by five cycles of centrifugation at 17900 x *g* for 30 s and re-suspension of beads in the same volume of coupling buffer. The above was done with receptor candidates, except at 100 x *g* for 10 s. The beads were centrifuged as above once more, but re-suspended in blocking buffer (100mM Tris-HCl, 500mM NaCl, pH 8.0) and incubated for 2 h static at RT. CnBr beads were then washed ten times by centrifugation as above,

with alternate cycles of re-suspension in coupling buffer or wash buffer (100mM acetic acid, 100mM sodium acetate, 500mM NaCl, pH 4.0). On the final centrifugation, beads were re-suspended in 180 µg BTRE freeze-thawed cell lysate in HBSS (section 2.6.3) or 5-10 µg sheared flagella in PBS. These were incubated for 16 h at 4°C, rocking.

2.9.4.3 Elution and analysis

CnBr beads were centrifuged at 17900 x *g* for 30 s if incubated with cell lysates or at 100 x *g* for 10 s if incubated with sheared flagella. Beads were then washed by three cycles of centrifugation as above and re-suspension in 0.1% (v/v) PBST. Beads were centrifuged a final time and eluted as in co-immunoprecipitation (section 2.9.3), then analysed by 12% SDS-PAGE and imperial protein staining. For pull-downs with BTRE cell lysates, bands only apparent in the presence of flagella proteins and equivalent cell lysate bands were excised and identified by mass spectrometry (section 2.5.7). For pull-downs with receptor candidates, Western blots (section 2.5.3) for all constituents were performed.

2.9.5 Flagella co-sedimentation assays

2.9.5.1 Purified flagella

1:1 molar ratios of sheared $FliC_{H7}$ flagella and cofilin-1 were incubated in interaction buffer (10mM Tris-HCl, 50mM NaCl, 1mM dithiothretol (DTT), pH 6.8 or 8.0) for 30 min at RT static. Reactions were diluted 1:3 in interaction buffer and ultra-centrifuged at 172600 x *g* for 1.5 h at 4°C. Supernatants were kept aside for SDS-PAGE analysis. Pellets were re-suspended in an equal volume of interaction buffer. Equal volumes of pellet and supernatant samples were added to 5xSDS-PAGE sample buffer and were analysed by SDS-PAGE. Results were quantified using densitometry in GeneTools and normalised by the formula *Protein recovery* = $(R_f/R_{tot}) \times 100$ where R_f = raw pixel volume of fraction and R_{tot} = total raw pixel volume of both fractions.

2.9.5.2 Bacteria-associated flagella

Freshly revived TUV93-0 and TUV*fliC*$^{-}$ were inoculated into LB broth and incubated at 30°C 200 rpm for 16 h. Saturated cultures were centrifuged at 8900 x *g* for 5 min at RT and cell pellets were re-suspended in interaction buffer (section 2.9.5.1). 1 nmol of cofilin-1 was added to each strain for 1 h at RT statically, and then samples were centrifuged at 17900 x *g* for 2 min. As pellets were very delicate, a fixed volume from the top two thirds of the supernatant were taken as the supernatant fraction, the middle bit discarded, and the pellet re-suspended in an equal volume of interaction buffer. Fractions were then prepared for SDS-PAGE and Western-blotting for $FliC_{H7}$ and cofilin-1. Results were quantified as in section 2.9.5.1.

2.9.6 Size exclusion chromatography

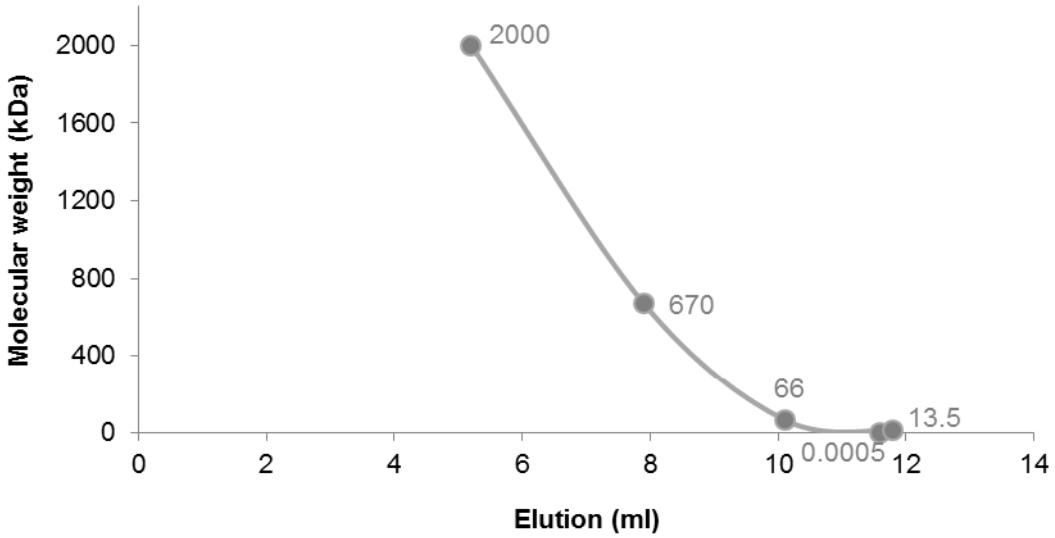

Figure 2.5. Size calibration of TSK G4000SWXL HPLC column. Molecular weight expressed in kDa, and sizes of standards are labelled. Standards were applied to the column one at a time and their elution value was taken as the volume eluted at the top of the peak.

Samples were applied to an HPLC column (Sigma TSK G4000SWXL, 4.6 mm i.d., 300mm length, 8 µm beads, 450 Å pore size) pre-equilibrated with 100mM Tris-HCl, 200mM NaCl, 1mM DTT, pH 8.0, by use of an Ultimate HPLC system (Dionex).

Columns were calibrated with molecular weight standards (Blue Dextran 2.5 MDa, Thyroglobulin 670 kDa, BSA 66 kDa, Ribonuclease A 13.5 kDa, ATP 0.5 Da, figure 2.5).

For $FliC_{H7}$ flagella-cofilin-1 interactions, proteins were mixed at 1:0, 1:1 and 1:4 molar ratios in 10mM Tris-HCl, 50mM NaCl, 1mM DTT pH 8.0, immediately before first application to column. Each ratio was run ten times at 30 min intervals, and A_{220} over ml was recorded. Data was analysed by calculating the area under curve (AUC) for each run, for large filaments (4.5-6.75 ml ≈ >2 MDa- ~1.4 MDa), small filaments (6.75-9 ml ≈ ~1.4 MDa- ~300 kDa) and 'monomers' (9-11.25 ml < ~300 kDa) with the formula $AUC = [(A_1+A_2)/2] \times (T_2-T_1)$, where A = absorbance at 220 nm and T = time. Data were normalised by using a percentage of the sum of large filaments, small filaments and monomer AUCs. Differences in % AUC for the above groups between different molar ratios of cofilin-1 to $FliC_{H7}$ flagella were analysed for statistical significance using a Kruskal-Wallis test in Minitab 16.

2.9.7 Actin polymerisation assays

2.9.7.1 G-actin preparation

G-actin was prepared by re-suspending lyophilised pyrene conjugated-rabbit skeletal muscle actin (Cytoskeleton) in G-buffer (10mM Tris, 200µM $CaCl_2$, 200µM adenosine triphosphate (ATP), 1mM DTT, pH 7.5) for 1 h on ice in the dark to depolymerise. This was then ultra-centrifuged at 100000 x *g* for 2 h at 4°C to pellet nucleated actin. The top 80% of the supernatant was kept on ice in the dark for further use.

2.9.7.2 Test protein preparation

Test proteins were all dialysed into 50mM Tris-HCl pH 7.5 using U-tube concentrators according to manufacturer's instructions (Novagen). Molar concentrations of all protein components were calculated using the Bradford assay

(densitometry was used to adjust these values for $FliC_{H6}$ and $FliC_{H7}$ flagella) with BSA standards.

2.9.7.3 Actin polymerisation

To normalise the polymerisation capability of G-actin preparations, a gain value was applied to all wells (calculated using pyrene-actin +/- 0.25x polymerisation buffer (12.5mM KCl, 500µM $MgCl_2$, 250µM ATP) read after 1 h incubation at RT in the dark). Assays were carried out in black opaque 96-well plates. Cofilin-1 or sheared flagella were added to wells, followed by 1µM actin, and then polymerisation was initiated with 0.25x polymerisation buffer. Samples were excited at 365nm, and emission data was measured 407nm for 1 h, at 30 s intervals.

Maximum velocity of reactions (V_{max}) were calculated with the formula $V_{max} = (A_2-A_1)/(T_2-T_1)$, where A = absorbance at 407nm and T = time. Differences due to addition of flagella with different concentrations of cofilin-1 were assessed for statistical significance using a general linear model in Minitab 16. In this model, V_{max} was the response, experiment was a confounding factor, and flagella type ($FliC_{H6}$, $FliC_{H7}$, $FliC_{P1}$, $FljB_{P2}$) and cofilin-1 concentration (250uM, 500uM) as factors. Tukey pairwise comparisons of flagella type were carried out with p-values of <0.05 being taken as significant.

2.9.8 Actin depolymerisation assays

Lyophilised 99% pure human platelet actin was re-suspended in G-buffer and pyrene conjugated-rabbit skeletal muscle was added to it at a ~1:10 dilution. 0.25x polymerisation buffer was added for 1 h at RT to prepare F-actin. ~5µM F-actin was added to wells in black opaque 96-well plates. Samples were excited at 365nm, and emission data was measured 407nm for 1 h at 1 min intervals. After 3 min ~1µM sheared $FliC_{H7}$ flagella and cofilin-1 were added.

2.10 References

Arques, J. L., Hautefort, I., Ivory, K., Bertelli, E., Regoli, M., Clare, S., Hinton, J. C. D. & Nicoletti, C. (2009). *Salmonella* induces flagellin- and MyD88-dependent migration of bacteria-capturing dendritic cells into the gut lumen. *Gastroenterology* **137**, 579–87, 587.e1–2.

Bachmann, B. (1987). Derivations and genotypes of some mutant derivatives of *Escherichia coli* K-12. In Escherichia coli *and* Salmonella typhimurium*: cellular and molecular biology*, pp. 1190–1219. Washington D.C.: American society for microbiology.

Blomfield, I. C., Vaughn, V., Rest, R. F. & Eisenstein, B. I. (1991). Allelic exchange in *Escherichia coli* using the *Bacillus subtilis sacB* gene and a temperature-sensitive pSC101 replicon. *Molecular microbiology* **5**, 1447–57.

Bradford, M. (1976). A rapid and sensitive method for the quantitation of microgram quantities of protein utilizing the principle of protein-dye binding. *Analytical biochemistry* 248–254.

Campellone, K. G., Roe, A. J., Løbner-Olesen, A., Murphy, K. C., Magoun, L., Brady, M. J., Donohue-Rolfe, A., Tzipori, S., Gally, D. L. & other authors. **(2007).** Increased adherence and actin pedestal formation by *dam*-deficient enterohaemorrhagic *Escherichia coli* O157:H7. *Molecular microbiology* **63**, 1468–81.

Edgar, R. C. (2004). MUSCLE: a multiple sequence alignment method with reduced time and space complexity. *BMC bioinformatics* **5**, 113.

Flockhart, A. F., Tree, J. J., Xu, X., Karpiyevich, M., McAteer, S. P., Rosenblum, R., Shaw, D. J., Low, C. J., Best, A. & other authors. **(2012).** Identification of a novel prophage regulator in *Escherichia coli* controlling the expression of type III secretion. *Molecular microbiology* **83**, 208–23.

Haselbeck, A. & Hosel, W. (1990). Description and application of an immunological detection system for analyzing glycoproteins on blots. *Glycoconjugate journal* **7**, 63–74.

Jaroszewski, L., Rychlewski, L., Li, Z., Li, W. & Godzik, A. (2005). FFAS03: a server for profile--profile sequence alignments. *Nucleic acids research* **33**, W284–8.

Kushner, S. R. (1991). Construction of versatile low-copy-number vectors for cloning, sequencing and gene expression in *Escherichia coli*. *Gene* **100**, 195–199.

Kwang, J., Wilson, R., Yang, S. & He, Y. (1996). Mapping of the H7-serospecific domain of *Escherichia coli* flagellin. *Clinical and diagnostic laboratory immunology* **3**, 523–6.

Laemmli, U. K. (1970). Cleavage of structural proteins during the assembly of the head of bacteriophage T4. *Nature* **227**, 680–685.

Mahajan, A., Currie, C. G., Mackie, S., Tree, J., McAteer, S., McKendrick, I., McNeilly, T. N., Roe, A., La Ragione, R. M. & other authors. **(2009).** An investigation of the expression and adhesin function of H7 flagella in the interaction of *Escherichia coli* O157 : H7 with bovine intestinal epithelium. *Cellular microbiology* **11**, 121–37.

McNeilly, T. N., Mitchell, M. C., Nisbet, A. J., McAteer, S., Erridge, C., Inglis, N. F., Smith, D. G. E., Low, J. C., Gally, D. L. & other authors. **(2010).** IgA and IgG antibody responses following systemic immunization of cattle with native H7 flagellin differ in epitope recognition and capacity to neutralise TLR5 signalling. *Vaccine* **28**, 1412–21.

Paton, A. W. & Paton, J. C. (1998). Detection and characterization of Shiga toxigenic *Escherichia coli* by using multiplex PCR assays for *stx1*, *stx2*, *eaeA*, enterohemorrhagic *E. coli hlyA*, *rfbO111* and *rfbO157*. *Journal of clinical microbiology* **36**, 598–602.

Pettersen, E. F., Goddard, T. D., Huang, C. C., Couch, G. S., Greenblatt, D. M., Meng, E. C. & Ferrin, T. E. (2004). UCSF Chimera--a visualization system for exploratory research and analysis. *Journal of computational chemistry* **25**, 1605–12.

Reid, S. D., Selander, R. K. & Whittam, T. S. (1999). Sequence diversity of flagellin (*fliC*) alleles in pathogenic *Escherichia coli*. *Journal of bacteriology* **181**, 153–60.

Russell, D. W. & Sambrook, J. (2001). *Molecular Cloning. A laboratory manual.*, 3rd edn. New York: Cold Spring Harbor Press.

Westerlund-Wikström, B., Tanskanen, J., Virkola, R., Hacker, J., Lindberg, M., Skurnik, M. & Korhonen, T. K. (1997). Functional expression of adhesive peptides as fusions to *Escherichia coli* flagellin. *Protein engineering* **10**, 1319–26.

Wiechelman, K. J., Braun, R. D. & Fitzpatrick, J. D. (1988). Investigation of the bicinchoninic acid protein assay: Identification of the groups responsible for color formation. *Analytical biochemistry* **175**, 237–231.

Xu, X., McAteer, S. P., Tree, J. J., Shaw, D. J., Wolfson, E. B. K., Beatson, S. A., Roe, A. J., Allison, L. J., Chase-Topping, M. E. & other authors. **(2012).** Lysogeny with Shiga toxin 2-encoding bacteriophages represses type III secretion in enterohemorrhagic *Escherichia coli*. *PLoS pathogens* **8**, e1002672.

3 : H7 Flagella binding interaction with the BTRE

3.1 H7 flagella adherence

As shown in the paper by Mahajan and colleagues (Mahajan *et al.*, 2009), H7 flagella play a role in initial colonisation of *E. coli* O157:H7 at the BTR. They proposed that H7 flagella do this by binding to rectal epithelial cells. However, the Mahajan study raised many questions. For instance, what is the nature of this adhesion? What parts of the flagella and flagellin are involved in binding? Is it a protein-protein interaction, or do flagella interact with sugars or lipids? Does the binding involve specific or non-specific receptors? Or is this binding a more physical phenomenon, involving hydrophobic or physical forces? This body of work follows on directly from that study. An initial aim of the work was to develop, if possible, a simplified binding assay and use this to investigate the molecular basis of the interaction.

The role of H7 flagella in initial adhesion is unlikely to be restricted to $FliC_{H7}$. While $FliC_{H7}$ is the main structural component, other proteins form extracellular parts of the flagella filament. The flagella hook and its adaptors are made up of 3 proteins (Büttner, 2012). Flagella assemble distally in a clear hierarchy, the final stage being the assembly of FliC into the filament, a process directed by the FliD tip pentamer (section 1.5.2, (Yonekura, 2000)). *fliC* mutants therefore still have extracellular flagella basal bodies, with hooks and tips. This may be one reason that the differences in adhesion between wild-type *E. coli* O157:H7 and its $fliC_{H7}$ mutant (Mahajan *et al.*, 2009) were subtle. Complementation of the $fliC_{H7}$ mutant with $fliC_{H6}$ by Mahajan *et al.* did not fully restore wild-type levels of binding to bovine terminal rectum epithelial cells (BTRE), indicating that $FliC_{H6}$ flagella has a reduced adhesive capacity compared to $FliC_{H7}$ flagella. However, along the same lines as with the $fliC_{H7}$ mutant, the variation with the $fliC_{H6}$ complement and the $fliC_{H7}$ was such that there was still some overlap between $FliC_{H6}$ and $FliC_{H7}$ flagella-associated bacterial binding levels. These results therefore indicate that there may be adhesins other than $FliC_{H7}$ involved in initial adhesion and there is no reason to exclude other flagella proteins.

3.2 Vaccination with $FliC_{H7}$ flagella

Intra-muscular vaccination of cattle with purified $FliC_{H7}$ flagella was partially protective against *E. coli* O157:H7 challenge (McNeilly *et al.*, 2008). In this study, fewer cattle were colonised following oral challenge after vaccination compared to non-vaccinated controls. Specific $FliC_{H7}$ flagella-neutralising IgA and IgG were thought to block initial BTRE binding of EHEC (McNeilly *et al.*, 2008). However, in the vaccinated cattle that were colonised by *E. coli* O157:H7, total faecal shedding was not reduced. Instead, after an initial delay, there was a prolonged period of *E. coli* O157:H7 shedding (McNeilly *et al.*, 2008). This partial protection was still shown to be the case when $FliC_{H7}$ flagella were used as part of a multi-component recombinant vaccine (McNeilly *et al.*, 2010a).

The prolonged shedding in colonised animals was thought to be due to IgG, but not IgA, that recognised $FliC_{H7}$ TLR5-binding epitopes, blocking TLR5 activation (McNeilly *et al.*, 2010b). H7-specific IgA and IgG would block $FliC_{H7}$ flagella binding and prevent or delay initial colonisation of *E. coli* O157:H7. However, if *E. coli* O157:H7 were still able to colonise cattle, H7-specific IgG could then block its detection by the innate immune system. This would increase the time taken for the bovine host to clear *E. coli* O157:H7 and therefore prolong bacterial shedding.

$FliC_{H7}$ flagella still have the potential to increase the efficacy of vaccines against *E. coli* O157:H7. This is because including $FliC_{H7}$ flagella in bovine vaccines results in antibodies that block flagella binding. Theoretically, if a vaccine component could be designed that retains the ability to elicit antibodies that block $FliC_{H7}$ flagella binding, but does not raise antibodies that also block innate immune recognition, it should be protective.

3.3 $FliD_{H7}$ adherence

The role of $FliD_{H7}$ in H7 flagella-based adhesion was not ruled out by Mahajan *et al.* in their 2009 paper. $FliD_{H7}$ is likely to play a role as it is right at the tip of the flagella filament, and therefore has the largest 'reach' from the bacterial cell. FliD has been shown to be involved in adhesion in *Pseudomonas aeruginosa* (Arora *et al.*, 1998;

Scharfman & Arora, 2001) and *Clostridium difficile* (Tasteyre *et al.*, 2001). Some of these results must be interpreted with caution though. Reduced binding by *fliD* mutant strains could either be due to their lack of FliD, or the resulting inability to produce fully-formed flagella filaments. However, there is evidence in the 2009 article by Mahajan *et al*. that in some cases flagella tips are adhering to the BTRE (figure 3.1).

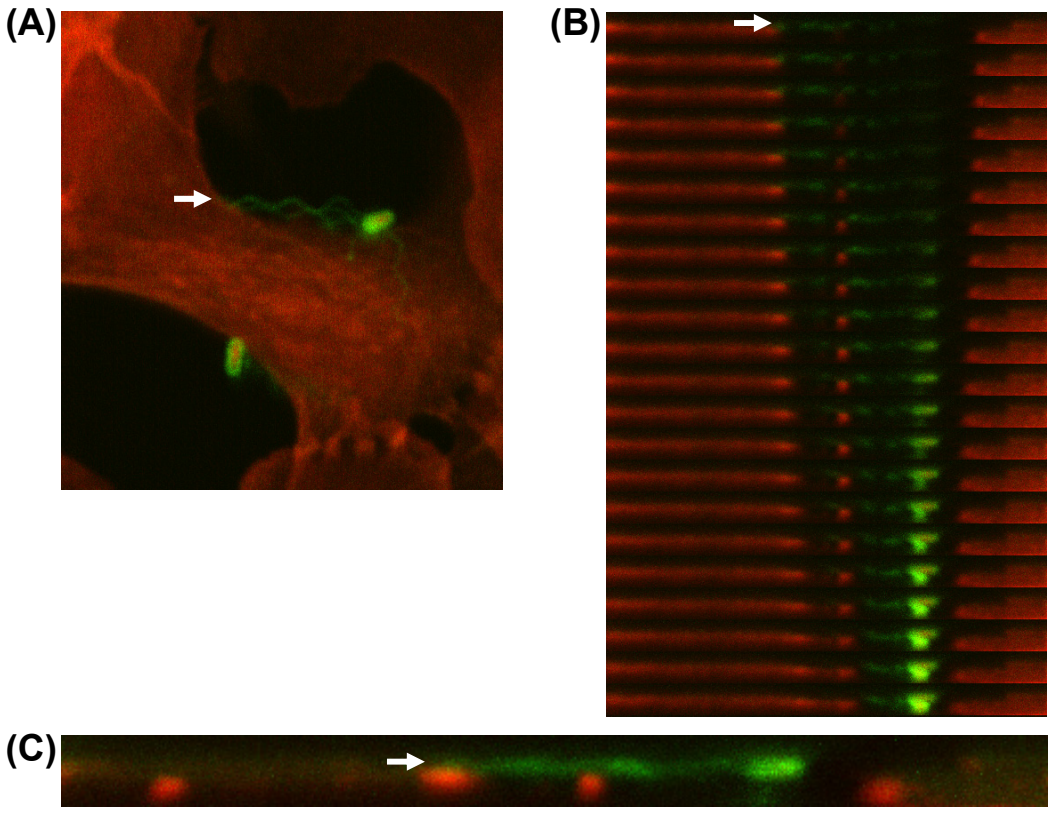

Figure 3.1. Confocal micrographs of *E. coli* O157:H7 adhering to a BTRE cell with the tips of H7 flagella after 1 h post infection. **(A)** *E. coli* O157:H7 adhering to a BTRE cell with the tips of H7 flagella (arrow) in 1 XY slice. **(B)** Flagella adherence to a BTRE cell via its tip (arrow) in a series of XZ slices. **(C)** Projection of the standard deviation of values in the XZ slices shown in **(B)** shows the tip of the H7 flagella adhering to the BTRE cell (arrow). Actin is stained in red (Phalloidin-TRITC) and bacteria and flagella are stained in green (α-O157 and α-H7 rabbit IgG, followed by α-rabbit IgG-FITC goat IgG). These images were constructed from the raw data, obtained by Arvind Mahajan, which was used to prepare images in Mahajan *et al.* 2009.

It is not known if $FliD_{H7}$ is immunogenic in cattle. It is also unknown whether there is any innate recognition of $FliD_{H7}$, or if vaccination with purified $FliD_{H7}$ would

result in $FliD_{H7}$-neutralising antibodies. If $FliD_{H7}$ was involved in initial binding (and therefore *E. coli* O157:H7 colonisation), but not recognised by TLR5, it would be a promising candidate to include as part of a multi-component vaccine.

3.4 Aims

- To repeat previous observations of $FliC_{H7}$ flagella interacting with the BTRE.
- To investigate the potential role of $FliD_{H7}$ in BTRE binding.
- To investigate the implications of $FliD_{H7}$ involvement on vaccine development.

3.5 Results

3.5.1 H7 Flagella interactions with the BTRE

Confocal microscopy was undertaken to observe the interaction of H7 flagella with primary cultures of BTRE first-hand. Observations at 1 h post-infection for the most part showed flagella adhering along the majority of the filament. Figure 3.2 shows two bacteria and their flagella (green) adhering to the BTRE membrane (red). This is an example of two of the three major types of flagella-based adherence that were observed. The flagellum of the bacterium shown in the YZ projection appears to be binding via lateral adhesion. That is to say, it is adhering along its length, flat on one face, with its bends occurring laterally in the XY plane. The flagellum of the bacterium shown in the XZ projection appears to be binding via perpendicular adhesion. That is to say it is adhering to the membrane at discrete points along its length, as its kinks occur in the XZ plane, perpendicular to the membrane (in the XY plane).

A point to note is that in this primary epithelial culture system the wheat-germ agglutinin labelling is fairly non-specific, staining internal membranes as well as external membranes, despite the lack of permeabilisation. However, the external membrane is still visible in this instance as a linear concentration of staining in the

XZ and YZ stacks (arrow, figure 3.2). Flagellum staining in the XZ projection is partially occluded where the flagellum crosses this line.

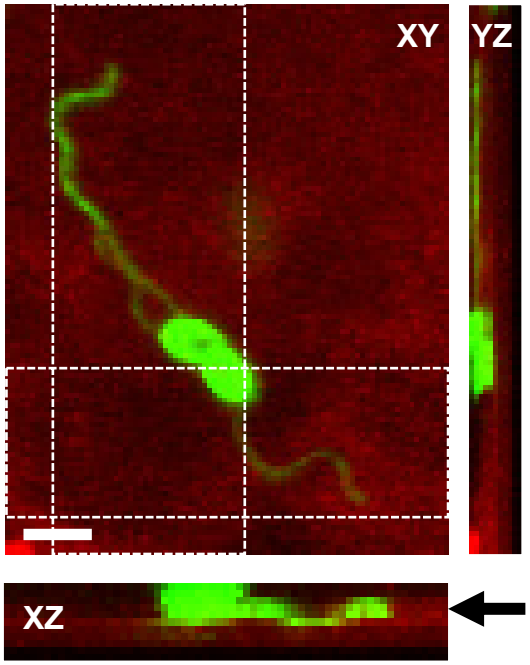

Figure 3.2. Confocal micrograph projections of *E. coli* O157:H7 interacting with BTRE membranes (methods 2.8). All projections are of maximum values, XZ and YZ projections are of areas indicated. Membranes are red (Wheatgerm-agglutinin-Texas Red) and bacteria are green (α-O157 and α-H7 rabbit IgG followed by α-rabbit IgG-FITC). Arrow indicates concentration of membrane staining. Images are representative of 2 independent experiments, with 5-10 fields of view captured. Images were captured using a Zeiss LSM5 pascal at the Roslin Institute in the University of Edinburgh, and presented in ImageJ. Scale bar indicates 2μm.

The third major type of flagella-based adherence is penetrative. Figure 3.3 shows the first z-stack in which this was captured. In this micrograph, the bacterium and its flagellum are stained green and actin is stained blue. The XY montage of z-slices starts from above the cell, where the bacterium is, and goes downwards into the cell. The flagellum appears to be right inside an area of actin staining, coincident in at least 3 z-slices. A YZ projection shows the bacterium in the edge of or outside a cell, with a green flagella filament penetrating deep inside it.

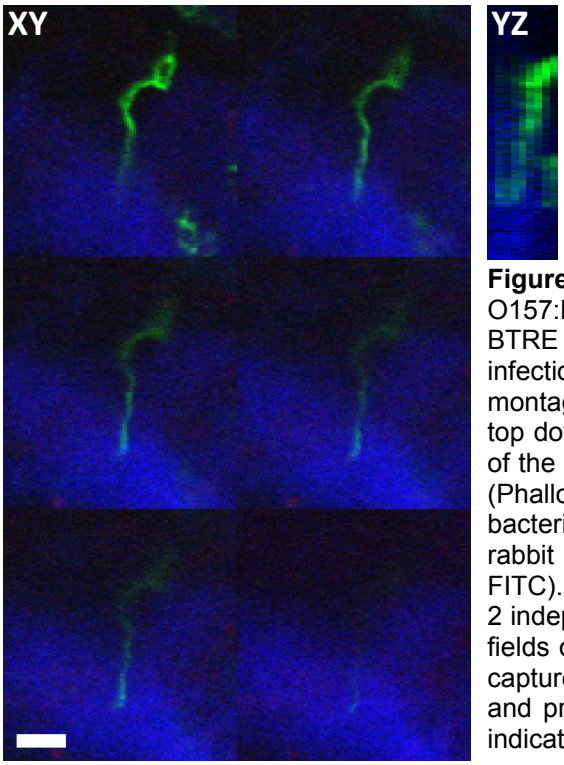

Figure 3.3. Confocal stack of *E. coli* O157:H7 flagella interaction with BTRE primary cell culture, 1 h post-infection. The XY view is shown in a montage of the 6 uppermost z slices, top downwards. The YZ projection is of the complete z stack. Actin is blue (Phalloidin-AlexaFluor$_{647}$) and bacteria are green (α-O157 and α-H7 rabbit IgG followed by α-rabbit IgG-FITC). Images are representative of 2 independent experiments with 5-10 fields of view captured. Images were captured using a Zeiss LSM pascal and presented in ImageJ. Scale bar indicates 3μm.

To further investigate penetrative adherence by H7 flagella, additional samples were taken to Trudi Gillespie at the IMPACT facility in the Centre for Integrative Physiology, University of Edinburgh (figure 3.4 and 3.5, methods 2.8.4). The impact facility has an upright Zeiss LSM510 confocal system coupled to a Titanium:Sapphire multi-photon laser, from which it is possible to get very clear high-resolution confocal micrographs. This is particularly important when imaging flagella, as they are only ~20 nm thick (Büttner, 2012). Whilst not occurring with every flagellated bacterium, and despite probably being a dynamic process, clear examples of penetrative flagella were readily imaged with every attempt using this system.

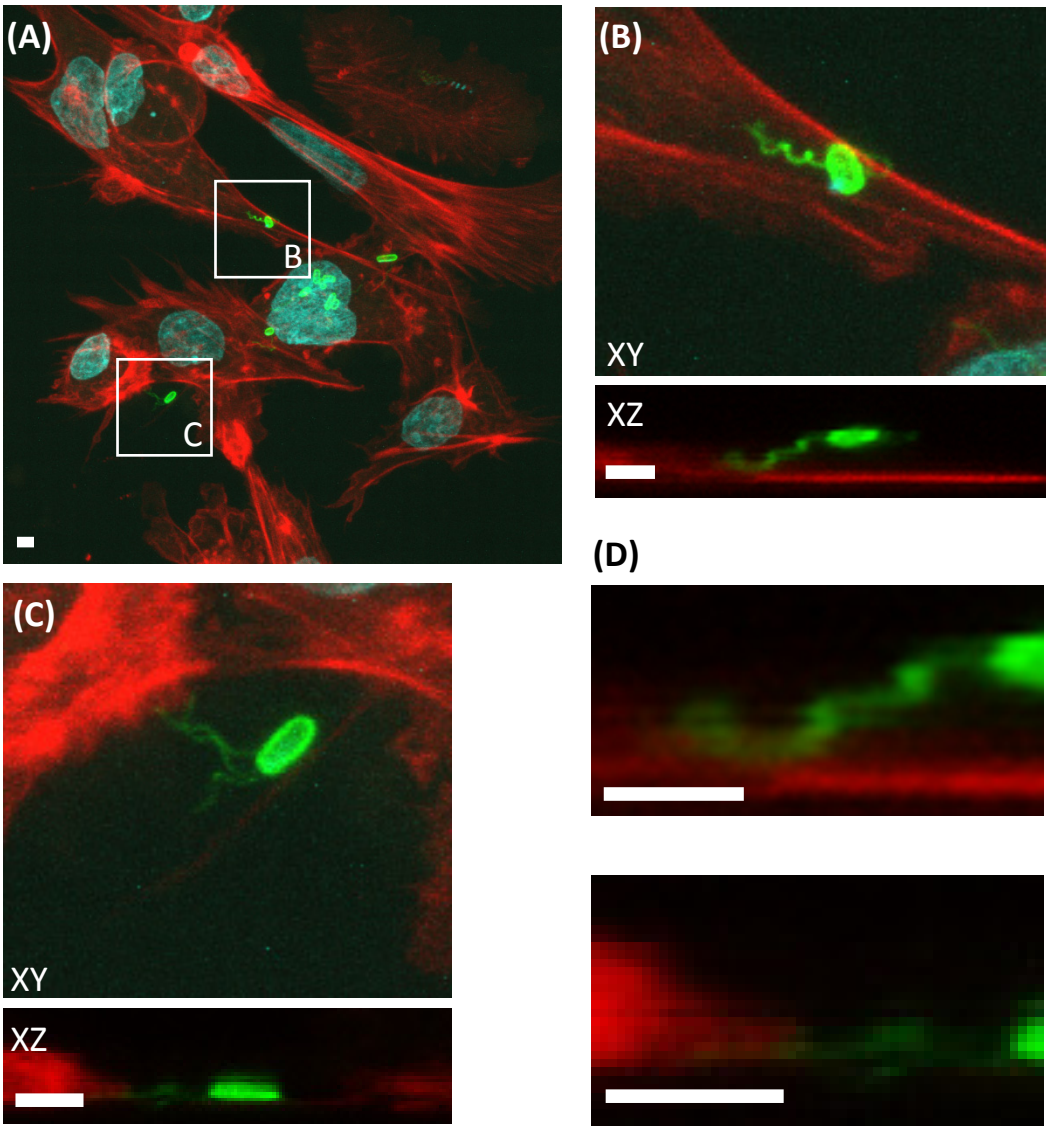

Figure 3.4. Co-incidence of *E. coli* O157:H7 flagella with actin in primary BTRE cells after 1 h. **(A)** A confocal z-stack with insets B **(B)** and C **(C)**. Insets show an XY and corresponding XZ image. **(D)** Close up images of inset XZ images, where H7 flagella appear to be co-incident with actin. Actin is red (Phalloidin-Alexa Fluor 647) and bacteria are green (α-O157 and α-H7 rabbit IgG followed by α-rabbit IgG-FITC). Images are representative of 2 independent experiments with 5-10 fields of view captured. Images were captured using a Zeiss LSM510 at the IMPACT facility in the University of Edinburgh by Trudi Gillespie, and presented in ImageJ. All scale bars indicate 2μm.

Fluorophore-labelled phalloidin is much smaller than an antibody pair would be in indirect immunofluorescence, and it has a very high affinity for F-actin, so the area of staining is very specific (Faulstich *et al.*, 1983, 1988). As this staining is so specific and the actin cytoskeleton is only present inside eukaryotic cells, any coincidence of flagellum staining with actin suggests that the flagellum is inside the cell. Figure 3.4 highlights 2 examples of where flagellum staining is coincident with

actin staining (insets B and C, (B)-(D)). Figure 3.4(D) shows magnified XZ projections of both examples where flagella appear to be inside BTRE cells. Figure 3.5 shows what appears to be a bacterial flagellum coincident with cortical actin. This can be seen in montages of z-slices of the XY plane (figure 3.5(B)) or y-slices of the XZ plane (figure 3.5(C)).

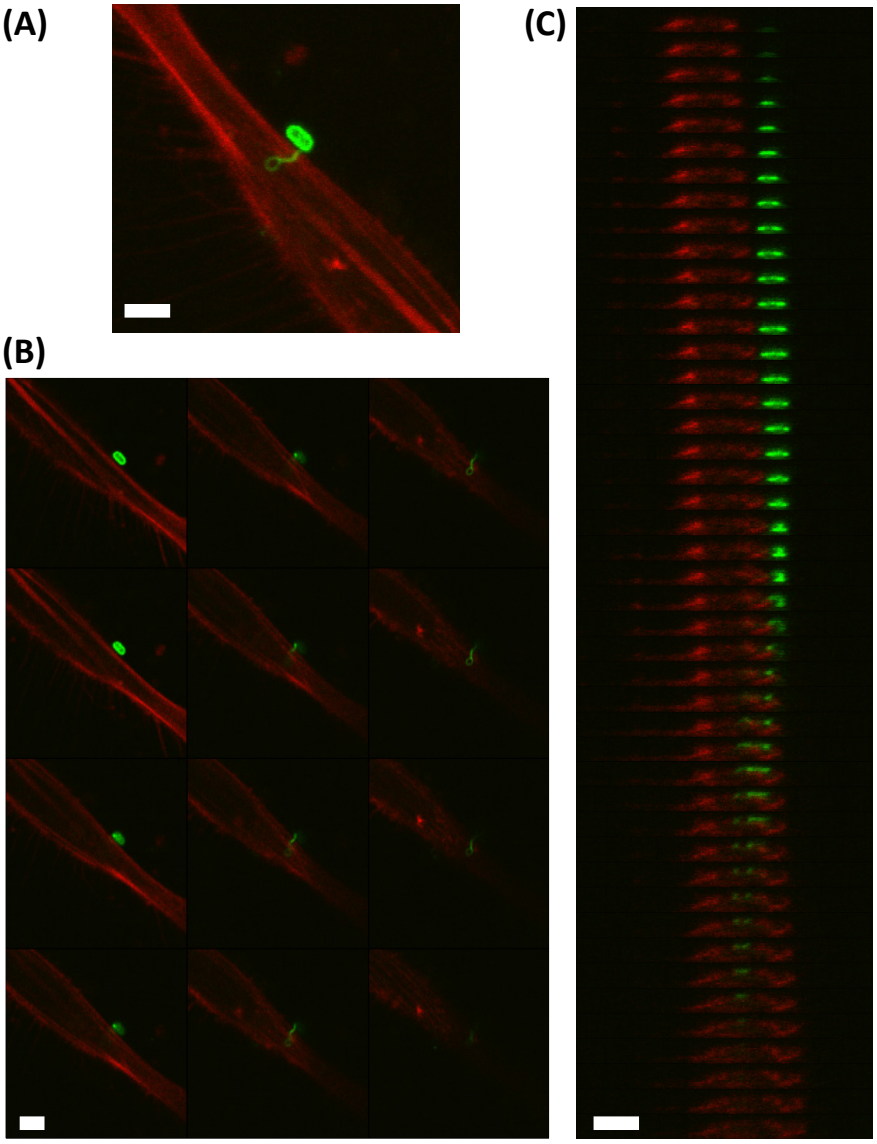

Figure 3.5. *E. coli* O157:H7 and flagella interaction with actin cortex of primary cell cultures from the BTRE after 1 h of infection (section 2.8). **(A)** Projection of a confocal z-stack. **(B)** Montage of XY z-slices, reading from left downwards. **(C)** Montage of XZ y-slices. Actin is red (Phalloidin-Alexa Fluor 647) and bacteria are green (α-O157 and α-H7 rabbit IgG followed by α-rabbit IgG-FITC). Images are representative of 2 independent experiments with 5-10 fields of view captured. Images were captured using a Zeiss LSM pascal at the IMPACT facility in the University of Edinburgh by Trudi Gillespie, and presented in ImageJ. All scale bars indicate 3μm.

Observing H7 flagella penetrate into host cells led to a re-assessment of micrographs previously captured by another PhD student, Xuefang Xu (figure 3.6). Multiple $O157^+$ slightly curved filaments appear to be inside actin-rich A/E lesions. Xuefang Xu acquired these images at 3 h post-infection of embryonic bovine lung (EBL) cells using a Leica DMLB widefield fluorescence microscope. Images are therefore two-dimensional, so it is impossible to say that these filaments are definitely inside the A/E lesions. However, the O157 staining appears to occlude actin staining, indicating the filaments are where actin is expected to be.

Bearing in mind host cell penetration by H7 flagella, figure 3.6 raises an interesting possibility. Perhaps the $O157^+$ filaments are flagella. It is possible that the polyclonal O157 anti-serum is recognising another filamentous protein, such as EspA. However, the filaments are morphologically similar to flagella and the polyclonal O157 anti-serum recognises $FliC_{H7}$ epitopes independently of the O157 antigen (figure 3.7). Figure 3.7 shows α-O157 recognition of ~ 2μg denatured $FliC_{H7}$ flagella purified from strains +/- O157 LPS and native $FliC_{H7}$ flagella on *E. coli* O157:H7. If these filaments were $FliC_{H7}$ flagella, this suggests that, having already penetrated host cell membranes, they are now embedded within an A/E lesion.

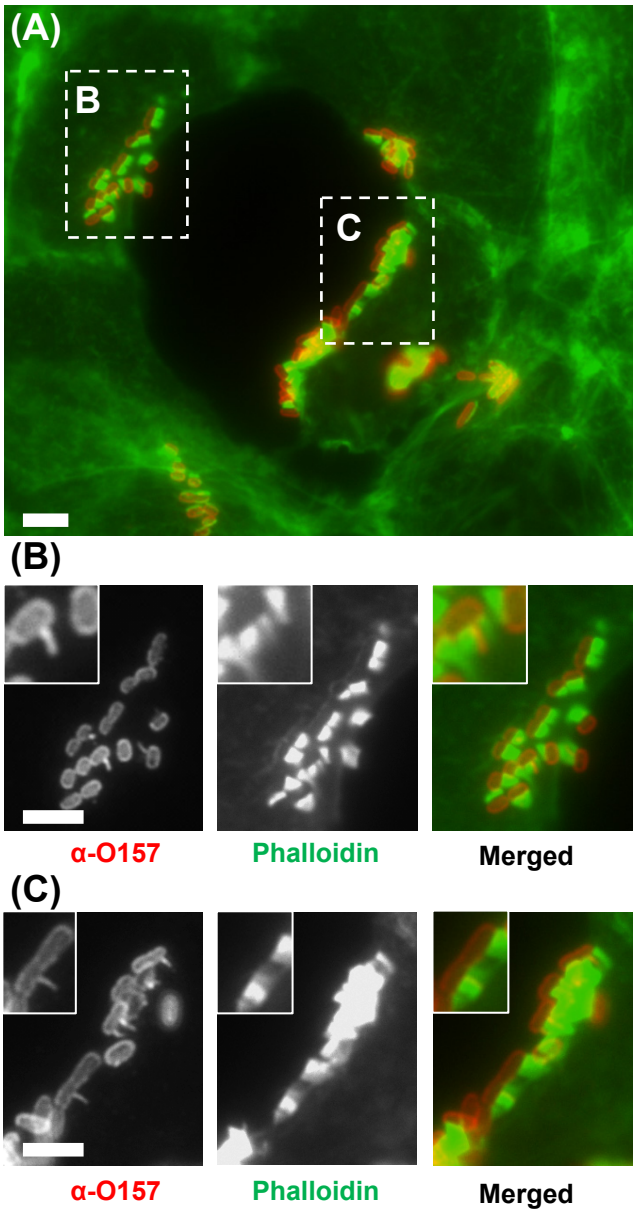

Figure 3.6. O157^{+} filaments are present within A/E lesions of embryonic bovine lung cells. **(A)** Whole-widefield micrograph with merged channels of intimately attached *E. coli* O157 micro-colonies (methods 2.7.2). **(B)** and **(C)** Magnified images of micro-colonies indicated in **(A)**. These images contain insets of one example where O157 positive filaments occlude actin pedestal staining. Widefield fluorescent microscopy was undertaken on *E. coli* O157:H7 micro-colonies on embryonic bovine lung cells, 3 h post-infection. The O157 strain (TUV93-0) used was labelled with a-O157 rabbit IgG (Mast Assure) and AlexaFluor568-conjugated a-rabbit IgG (Sigma). Actin was stained using FITC-conjugated phalloidin (Sigma). Images are representative of 1 experiment with 6 6 fields of view captured but similar results have been obtained in another 2 independent experiments by confocal microscopy. Micrographs were imaged using a Leica DMLB microscope by Xuefang Xu, and scale bars indicate 10 μm.

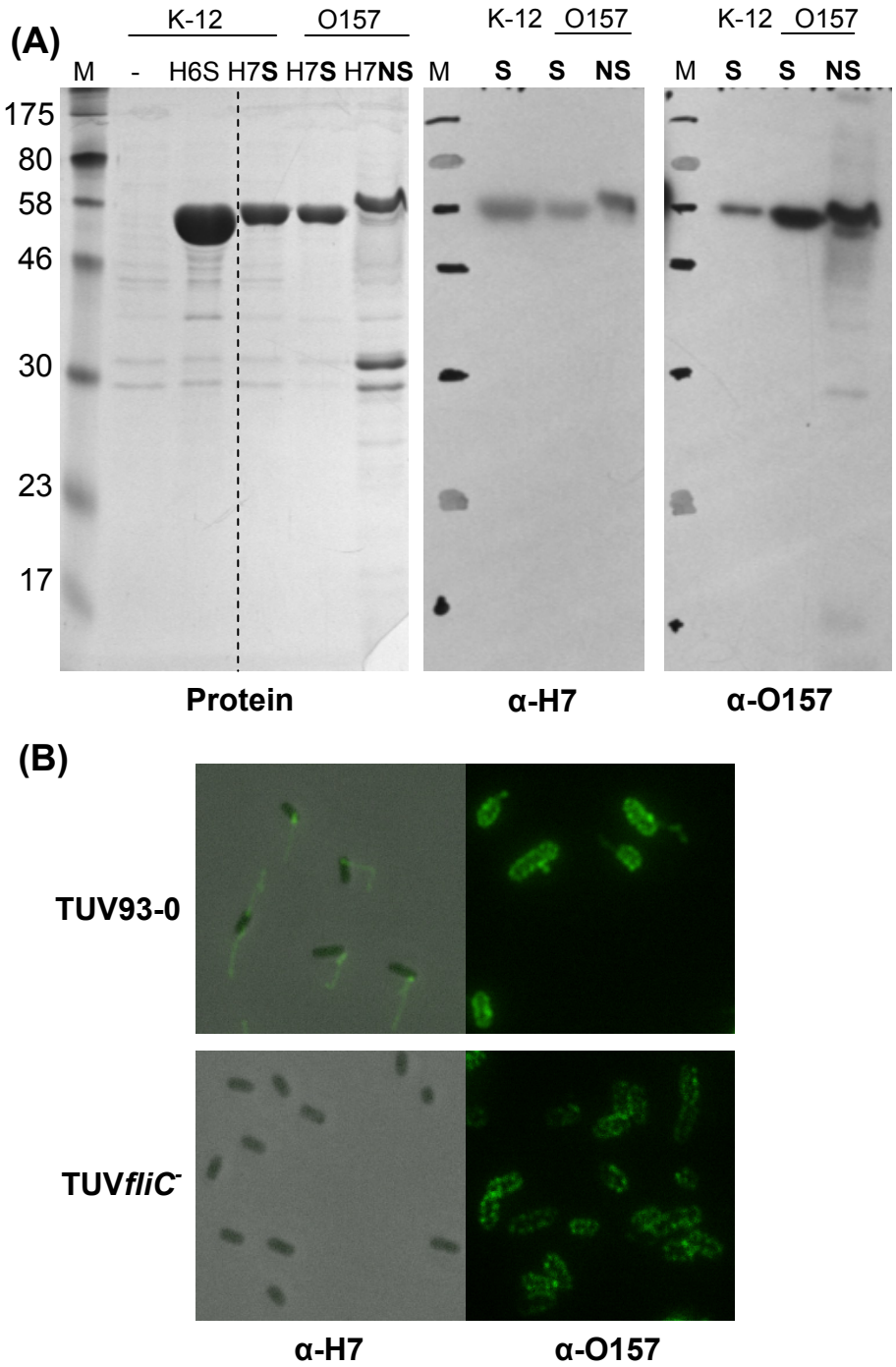

Figure 3.7. Detection of $FliC_{H7}$ flagella with O157 and H7 antibodies. **(A)** Detection of flagella purified from strains +/- O157 LPS by Western-blotting. Flagella were purified by shearing (S, methods 2.5.5) or acid depolymerisation (NS, methods 2.5.5) and added neat to 2x Laemmli sample buffer for SDS-PAGE; proteins to the right of the dashed line were Western-blotted. The $O157^-$ LPS (K-12) strain used was a *fliC* negative strain, JT1, containing pWSK29 (-), pWSKH6 ($FliC_{H6}$, H6, ~5µg) or pWSKH7 ($FliC_{H7}$, H7, ~2µg, table 2.1 and 2.2). The $O157^+$ LPS strain used was TUV93-0. Molecular weight markers (M) are annotated on the left. **(B)** Detection of flagella on *E. coli* O157:H7 by immunofluorescence (methods 2.7.1).

3.5.2 Role of $FliD_{H7}$ in flagella BTRE binding

To assess the role of $FliD_{H7}$ in H7 flagella binding to the BTRE, different components of the H7 flagella filament were cloned and purified. The *fliD*$_{H7}$ expression plasmid pBAD$FliD_{H7}$, which was used to purify recombinant His-tagged $FliD_{H7}$, partially complemented TUV*fliD*$^-$ strain (figure 3.8, methods section 2.9.2). This indicates that the His-tag does not interfere with $FliD_{H7}$ function. Figure 3.9 shows the flagella components that were purified. $FliC_{H7}$ from sheared-off H7 flagella ($FliC_{H7}$, methods 2.5.5), recombinant His-tagged $FliC_{H7}$ ($FLrH7_{1\text{-}585}$), its variable region ($VrH7_{180\text{-}496}$), its amino-terminal of $FliC_{H7}$ ($NTrH7_{1\text{-}179}$) and $FliD_{H7}$, are all of expected size and are recognised by α-H7 or α-His anti-serum as appropriate. The regions of $FliC_{H7}$ chosen for recombinant protein purification were based on a previously published scheme (McNeilly *et al.*, 2010b), where phenotypic differences of $FLrH7_{1\text{-}585}$, $VrH7_{180\text{-}496}$ or $NTrH7_{1\text{-}179}$ with $FliC_{H7}$ may indicate involvement of post-translational modifications, non-H7-specific regions and H7-specific regions respectively.

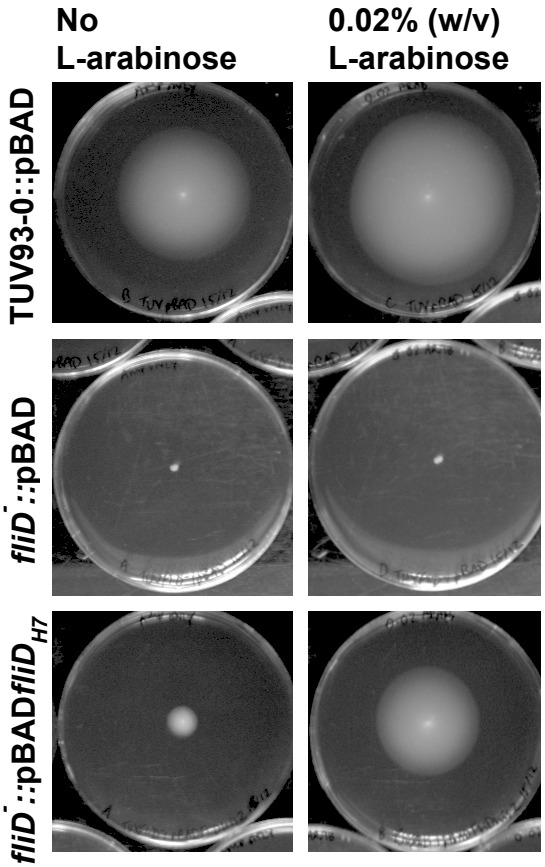

Figure 3.8. Complementation of TUV*fliD*$^-$ motility with *fliD*$_{H7}$. Plasmids indicated on the left were electroporated (methods 2.3.10) into the strain indicated. These were stab-inoculated into semi-solid agar (methods 2.9.2) + 50μg/ml amp and incubated at 28°C for 24 h then imaged. Images are representative of 4 replicates.

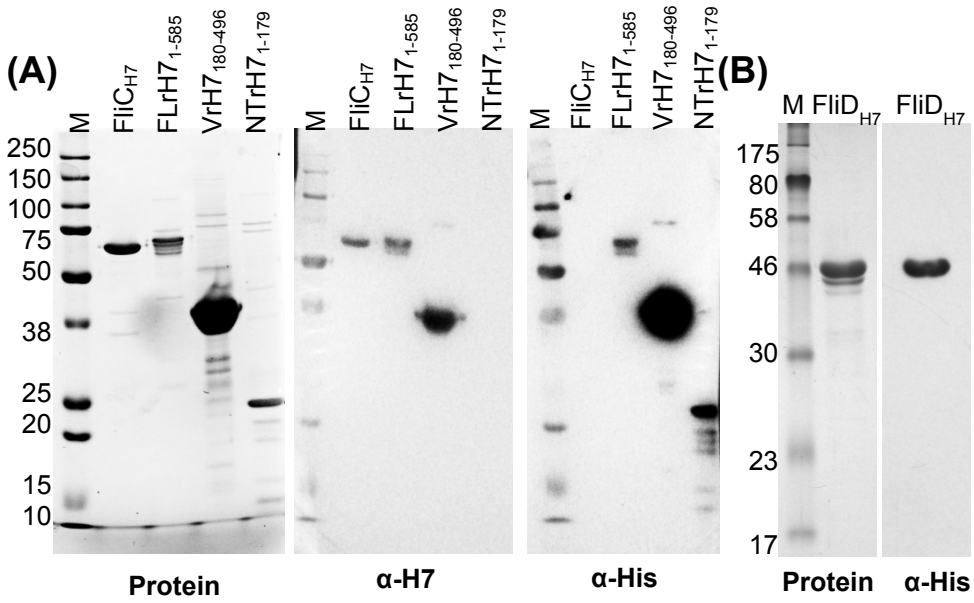

Figure 3.9. Western-blots of purified native FliC$_{H7}$, recombinant H7 fragments and FliD$_{H7}$ (methods 2.5.3 and 2.5.6). **(A)** Imperial protein stained SDS-PAGE gel of native sheared FliC$_{H7}$ (60kDa), FLrH7$_{1-585}$ (61kDa), VrH7$_{180-496}$ (38kDa), NTrH7$_{1-179}$ (20kDa) and their respective α-H7 and α-His Western-blots. **(B)** Coomassie stained SDS-PAGE gel of recombinant FliD$_{H7}$ (48kDa) and it's respective α-His Western-blot. Expected sizes are shown in brackets.

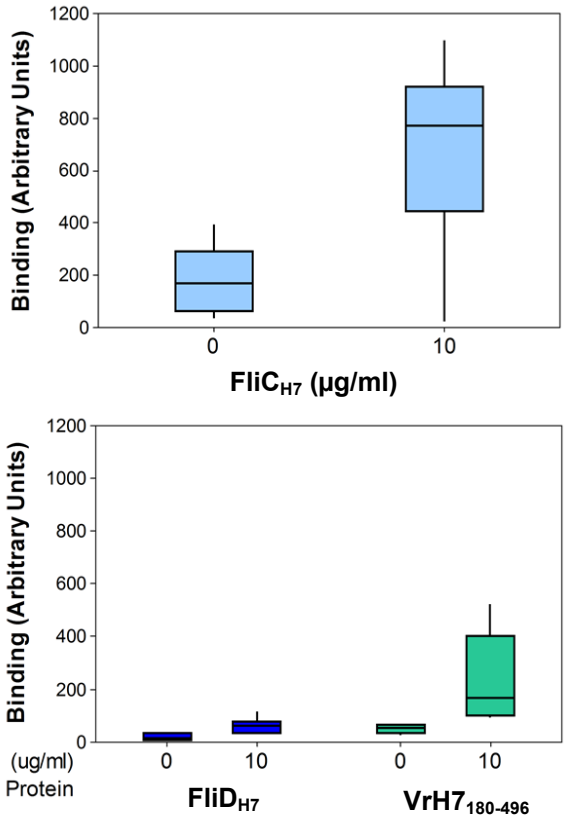

Figure 3.10. Binding of H7 flagellar proteins to primary BTRE cells. Purified FliC$_{H7}$ flagella and recombinant constituents were tested for their ability to adhere to the BTRE by far cell-based ELISAs (methods 2.9.1). Proteins were labelled by α-H7 rabbit IgG (Mast Assure, for sheared H7 flagella) or α-His mouse IgG (Invitrogen, for recombinant FliD$_{H7}$ and VrH7$_{180-496}$), then α-rabbit or mouse IgG-HRP respectively. Binding was detected by chemiluminescence and quantified by densitometry.

Purified flagella components were tested for their ability to bind to primary cultures of BTRE by far cell-based ELISA (methods 2.9.1). Figure 3.10 shows that after addition of 10 µg/ml of $FliC_{H7}$, $VrH7_{180-496}$ or $FliD_{H7}$ to primary BTRE cell cultures for 3 hours, these proteins were all detectable above background levels (0 µg/ml, a negative control of media alone). However, background levels were variable, between and within experiments. For example, there was overlap between $FliD_{H7}$ binding and $VrH7_{180-496}$ background levels. Additionally, the background levels in $FliC_{H7}$ experiments were more than protein binding in $VrH7_{180-496}$ experiments. This was likely due to plate to plate variation of BTRE primary cell cultures and the different types of antibodies used respectively.

Molecular binding efficiency indices were calculated to take into account differences in antibody detection and normalise binding according to the molar concentration of protein used, as the proteins vary in size (38-60kDa). The molecular binding efficiency indices were 19.69 for $FliC_{H7}$, 18.26 for $VrH7_{180-496}$ and 16.22 for $FliD_{H7}$. Sheared $FliC_{H7}$ flagella therefore appeared to bind the BTRE more effectively than its recombinant constituent parts. The data shown are of two direct repeats, but many more very similar experiments, testing the effect of cell permeabilisation and peroxidase treatment on protein binding detection (methods 2.9.1), were undertaken with equivalent results. The specificity of this binding has not yet been demonstrated, as all proteins tested appeared to adhere to the BTRE cell cultures. However, these results suggest that sheared $FliC_{H7}$ flagella, $VrH7_{180-496}$ and $FliD_{H7}$ are all physically capable of binding to primary cultures of BTRE.

To see if $FliD_{H7}$ is specifically involved in binding to the BTRE during *E. coli* O157:H7 colonisation, $FliD_{H7}$ antiserum was raised for use in binding inhibition assays (section 2.5.8). Recombinant $FliD_{H7}$ was used as a 3-dose vaccine by the Scottish National Blood Transfusion Service at the Pentlands Science Park. They then supplied rabbit sera taken pre-vaccination (pre-immune), one month after the first dose (bleed 1 or B1), the second dose (bleed 2 or B2) and the third dose (bleed 3 or B3).

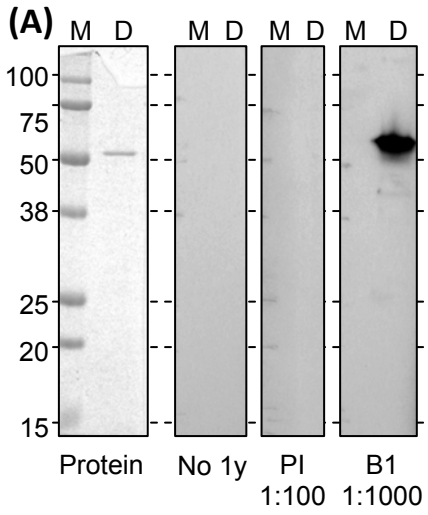

Figure 3.11. Validation of α-FliD$_{H7}$. **(A)** Western-blots of recombinant FliD$_{H7}$ probed with the α-rabbit IgG-HRP (R&D) alone (No 1y), pre-immune rabbit serum (PI) or bleed 1 of α-FliD$_{H7}$ (B1) at the titres indicated. **(B)** Indirect ELISAs of sera from the 3 bleeds with recombinant FliD$_{H7}$. Representative wells are shown at the top; below this the mean density of triplicates is plotted. Bleed 1 values are less comparable as they are imaged in an independent experiment (methods 2.9.1).

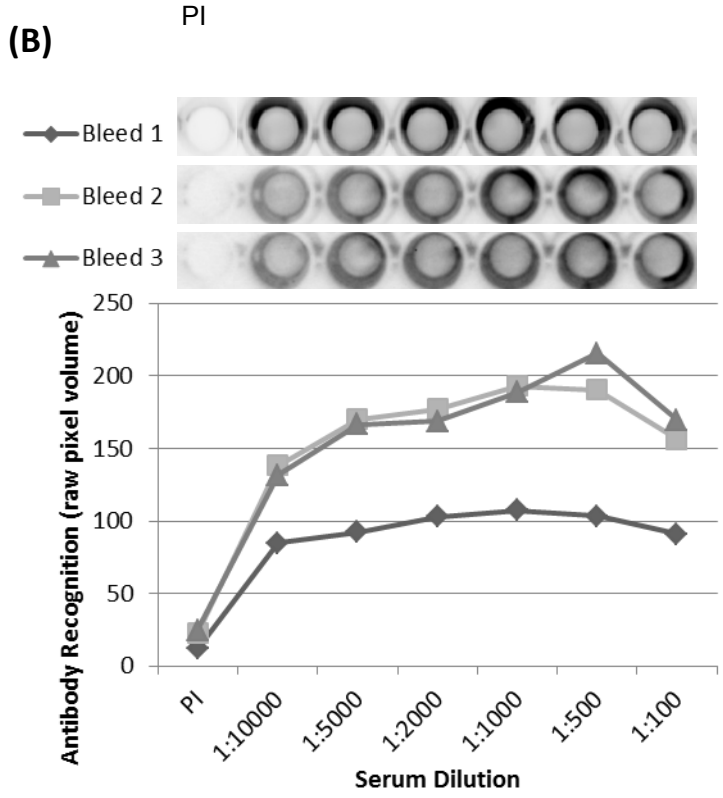

These sera were validated by testing their ability to bind to linear epitopes (figure 3.11(A)) and conformational epitopes (figure 3.11(B)) of recombinant FliD$_{H7}$. Pre-immune serum did not recognise denatured FliD$_{H7}$ at a dilution of 1:100, whereas bleed 1 did at a dilution of 1:1000 by western blot. As bleed 1 recognised linear epitopes of FliD$_{H7}$ adequately, it was assumed that subsequent bleeds would also do

so. At a dilution of 1:10 000, bleeds 1-3 recognised conformational $FliD_{H7}$ epitopes, whereas pre-immune serum did not, even at a dilution of 1:100, as shown by this ELISA. Pre-immune serum was therefore used as a control for any effects due to additional serum components in $FliD_{H7}$ antiserum in subsequent assays.

$FliD_{H7}$ anti-sera were then tested for their ability to inhibit *E. coli* O157:H7 motility. As can be seen in figure 3.12, motility of TUV93-0 after treatment with serum raised against recombinant $FliD_{H7}$ is less than with pre-immune serum. Additionally this motility inhibition is probably at least equivalent to that by commercial α-H7 rabbit IgG (methods 2.9.2). This data suggests that serum raised against recombinant $FliD_{H7}$ recognises native $FliD_{H7}$.

Figure 3.12 also suggests that bleed 1 and 3 sera may have different characteristics. Bleed 3 serum appears to have a greater inhibitory effect than bleed 1 serum. However, in combination with α-H7 antibodies, the opposite is the case. This may be artefactual, having restricted analysis of bleed 3 to technical replicates in the absence of biological replicates. However, it is in line with the generation of an adaptive antibody response. Bleed 3 serum is likely to contain mainly IgG, that would bind to $FliD_{H7}$ with higher affinity than the IgG and IgM in bleed 1 serum (Estes, 1996), and this could explain why bleed 3 is more effective than bleed 1 alone. Yet despite the high proportion of lower affinity IgM in bleed 1 serum, it is more effective in motility inhibition in combination with α-H7 rabbit IgG than bleed 3 serum is. Perhaps this is because IgM has more binding sites than IgG. The higher avidity of IgM may allow it to cross-link monomers in pentameric $FliD_{H7}$ caps. The combination of high affinity IgG from α-H7 antibodies with a higher proportion of high avidity IgM from bleed 1 serum may be more effective than just having lots of specific IgG, as in the case of α-H7 antibodies in combination with bleed 3 serum. With this in mind, bleed 3 was used for antibody inhibition studies, to make it more comparable with commercial α-H7 IgG.

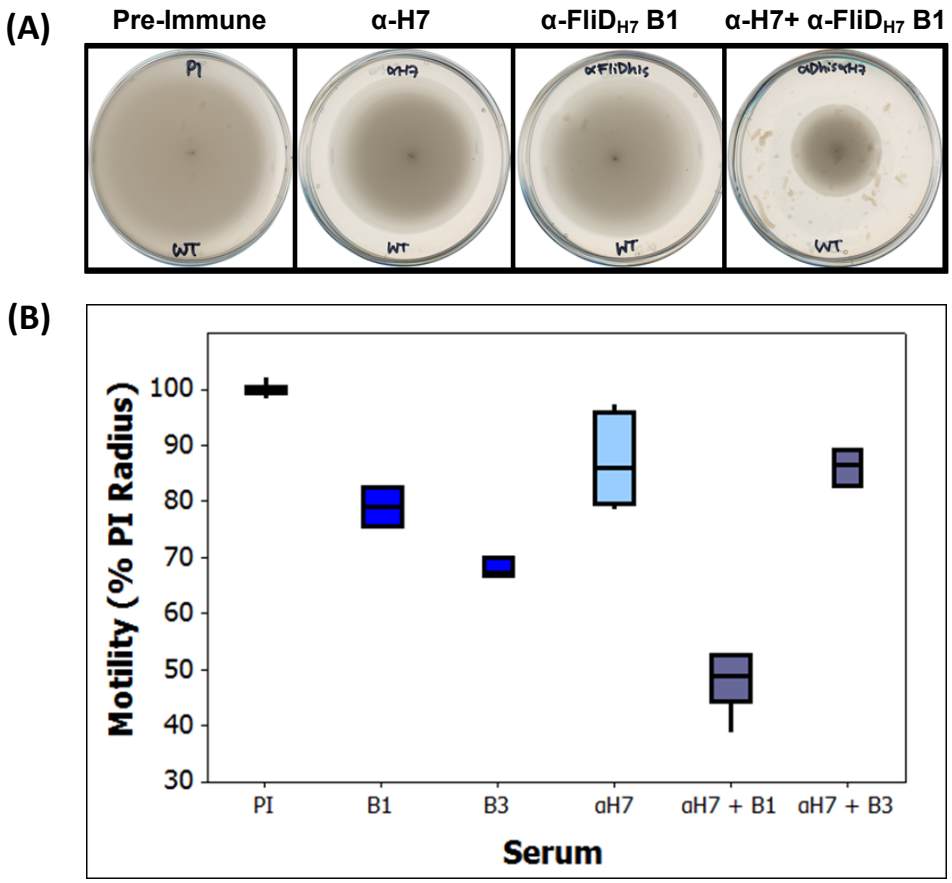

Figure 3.12. FliD$_{H7}$ antibody inhibition of *E. coli* O157:H7 motility. **(A)** Motility halos of TUV93-0 incubated with the sera indicated. Images are representative of triplicates. **(B)** Motility as a percentage of the halo radius of TUV93-0 incubated with pre-immune rabbit serum (PI). Bleed 1 (B1) and bleed 3 (B3) FliD$_{H7}$ sera were tested, with α-H7 as a control. TUV93-0 was stab-inoculated into semi-solid agar (section 2.9.2.1) containing a 1:1000 dilution of the rabbit sera indicated and incubated at 30°C for 22 h before imaging and radius measurement.

Pre-incubation of *E. coli* O157:H7 with FliD$_{H7}$ bleed 3 serum and α-H7 antibodies reduced BTRE binding, when compared to pre-immune serum controls (figure 3.13). This reduction was not dramatic, but neither was the previously published inhibition by α-H7 (Mahajan *et al.*, 2009). As α-FliD$_{H7}$ bleed 1 does not recognise denatured FliC$_{H7}$ (figure 3.14(A)), there is little reason to assume that the FliD$_{H7}$ bleed 3 serum is not specific for FliD$_{H7}$. These results from 2 independent experiments of 5 technical replicates indicate that the antibodies which bound to FliD$_{H7}$ inhibited its function, and this reduced *E. coli* O157:H7 binding to the BTRE. However, these

results do not discriminate between the $FliD_{H7}$ binding to the BTRE directly and downstream effects of $FliD_{H7}$ inhibition on $FliC_{H7}$ filament formation. However, as purified $FliD_{H7}$ is capable of BTRE binding, these results do suggest that $FliD_{H7}$ is involved in H7 flagella binding to the BTRE.

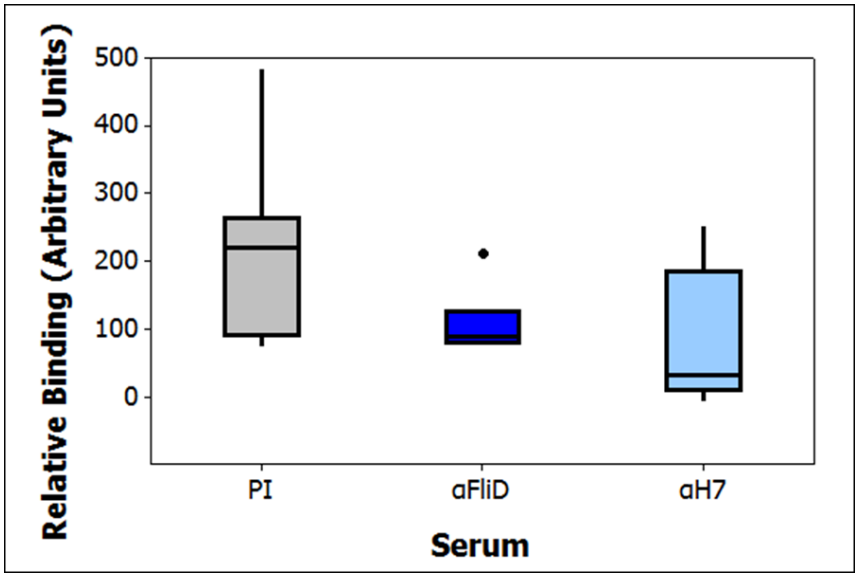

Figure 3.13. α-$FliD_{H7}$ inhibition of *E. coli* O157:H7 binding. Motility-enriched (section 2.2) TUV93-0 were incubated with a 1:10 dilution of the anti-serum/antibodies indicated, then used to infect confluent primary BTRE cells for 1h at 37°C 5% CO_2 85% humidity. Cells were washed and bacteria were labelled using α-O157 mouse IgG (AbD SeroTec) followed by α-mouse IgG-HRP (R&D). Binding was quantified using chemi-luminescence and densitometry (section 2.9.1.5). Outliers (•).

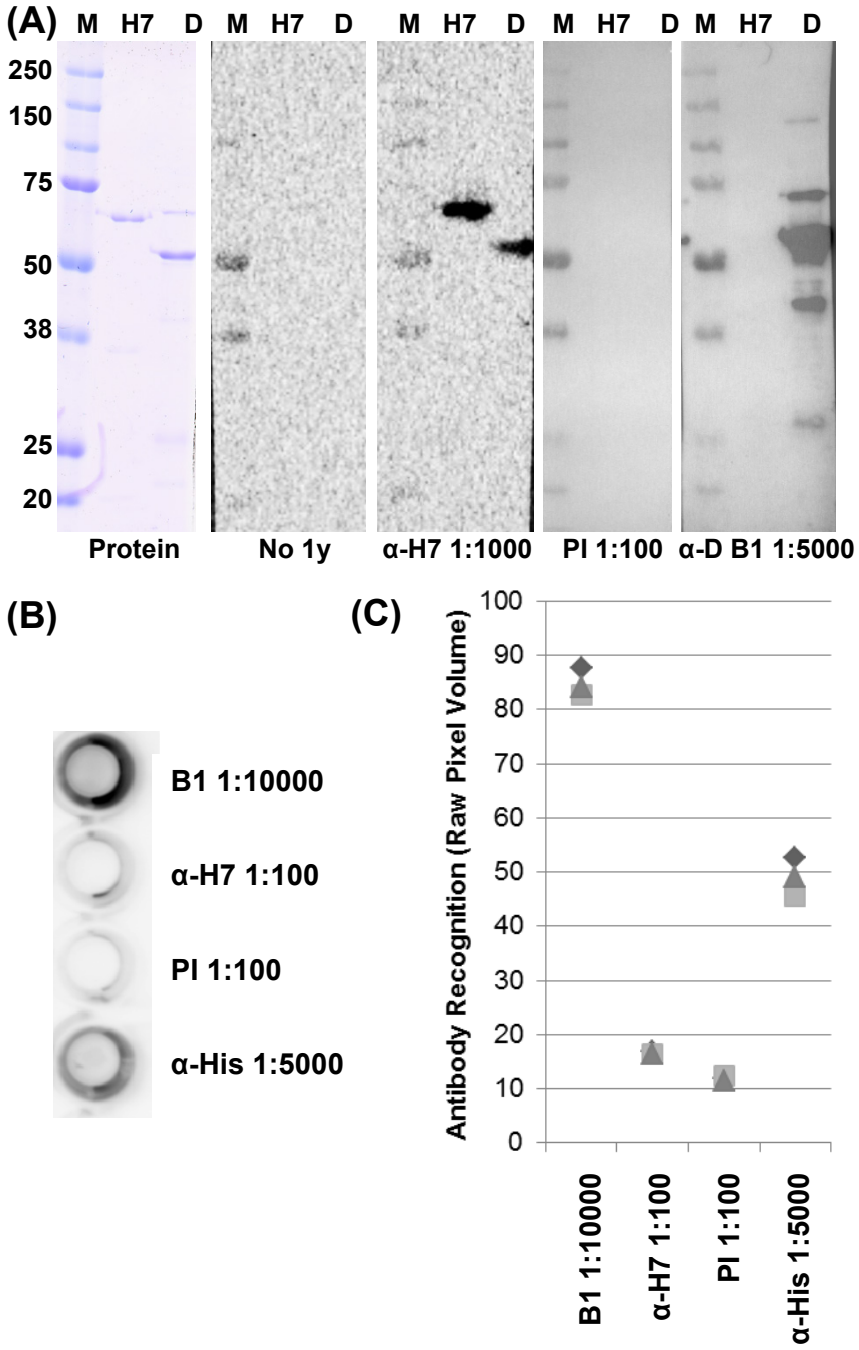

Figure 3.14. α-H7 antibodies recognise linear epitopes of $FliD_{H7}$. **(A)** Western-blots of sheared $FliC_{H7}$ flagella (H7) and recombinant $FliD_{H7}$ (D) probed with secondary antibody alone (α-rabbit IgG-HRP, No 1y), α-H7 rabbit IgG (mast assure), pre-immune rabbit serum (PI) and α-FliD bleed 1 serum (α-D B1) at the dilutions indicated, according to methods 2.5.3. **(B)** Representative wells from an indirect $FliD_{H7}$ ELISA (methods 2.9.1) detected by α-$FliD_{H7}$ bleed 1 (B1), α-H7 (mast assure), pre-immune rabbit serum (PI) and α-His (Invitrogen). **(C)** Densitometry of indirect $FliD_{H7}$ ELISA triplicates with primary antibodies indicated.

3.5.3 Implications of $FliD_{H7}$ binding on potential *E. coli* O157:H7 vaccine

If $FliD_{H7}$ was involved in binding to the BTRE, it would be worth investigating whether there is an antibody response towards it during *E. coli* O157:H7 challenge of cattle, and how current vaccine strategies affect this. For instance, does the bovine host normally recognise $FliD_{H7}$? Does vaccination with the immuno-dominant $FliC_{H7}$ epitope skew antibody responses away from or towards a $FliD_{H7}$-neutralising effect? Sera from a vaccine trial conducted by Tom McNeilly at Moredun Research Institute (McNeilly *et al.*, 2010a) were used to start to address these questions.

Sera obtained from Tom McNeilly represent two groups of seven calves from a larger four group trial that tested different vaccine preparations. One group of calves was intra-muscularly vaccinated with purified Tir, Intimin, EspA and $FliC_{H7}$ flagella before *E. coli* O157:H7 experimental challenge. The other group was the study control group, which was not vaccinated before the same experimental challenge.
Figure 3.15 shows Western-blots of recombinant $FliD_{H7}$ that were probed with sera taken pre- and post-challenge or pre- and post-vaccination. IgG in these sera was then detected with HRP-conjugated α-bovine IgG (AbD SeroTec). Experimental challenge does not appear to result in FliD-specific IgG (figure 3.15(A)). However, vaccination with purified T3S proteins and H7 flagella does result in $FliD_{H7}$-specific IgG (figure 3.15(B)). The same approach was applied for IgA, but H7-specific IgA was barely detectable despite known high H7-specific IgA titres, indicating that detection conditions were not optimal.

To see if raising FliD-specific IgG as a consequence of $FliC_{H7}$ flagella vaccination is species-specific, similar Western-blots were probed with H7 polyclonal rabbit antibodies from Mast Assure (figure 3.14(A)). This commercial α-H7 also contained IgG that recognised denatured recombinant $FliD_{H7}$, showing that this phenomenon was not bovine-specific. Interestingly, this recognition was confined to denatured linear epitopes of $FliD_{H7}$, not the native epitopes tested by ELISA (figure 3.14(B)). The bovine sera have not yet been tested for IgG-based $FliD_{H7}$ recognition by ELISA, so it is not known whether they can recognise native epitopes.

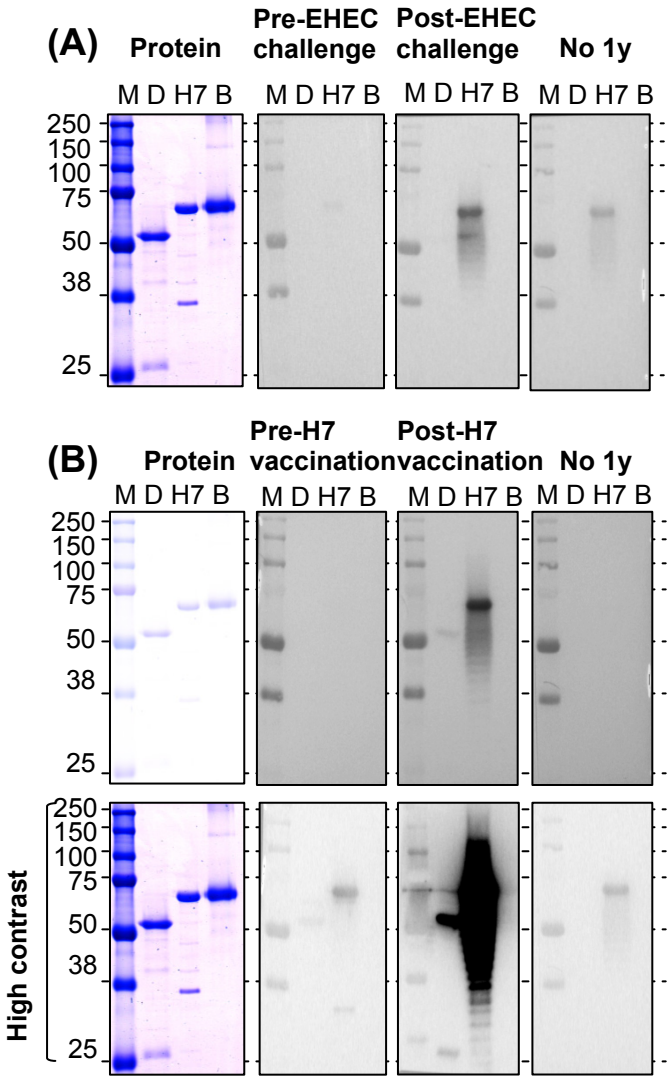

Figure 3.15. Recognition of recombinant $FliD_{H7}$ by bovine IgG from EHEC challenged calves. **(A)** Western-blots of $FliD_{H7}$ (D), $FliC_{H7}$ (H7) and BSA (B) probed with bovine serum pre- and post-challenge with *E. coli* O157:H7 and a secondary antibody control (α-bovine IgG-HRP (company), No 1y). **(B)** Western-blots of $FliD_{H7}$ (D), $FliC_{H7}$ (H7) and BSA (B) probed with bovine serum pre- and post-vaccination with purified H7, with a secondary antibody alone control as previously.

3.6 Discussion

Previous studies used microscopy and mutagenesis to assess the role of $FliC_{H7}$ flagella in *E. coli* O157:H7 binding to the BTRE. To address the precise role of

$FliD_{H7}$ in H7 flagella adhesion, microscopy is not specific enough as discussed below, due to the variation in adherence mechanisms. Additionally, mutagenesis cannot separate the specific binding capacities of $FliD_{H7}$ from its regulatory and structural role in $FliC_{H7}$ filament formation. Testing the BTRE binding inhibition of *E. coli* O157:H7 by purified flagella is also not specific enough, as the flagella preparations are likely to contain $FliC_{H7}$, $FliD_{H7}$ and other hook proteins. With this in mind, the BTRE binding capacity of individual flagellar components was assessed.

The intention was to test the specific quantitative binding of purified flagella, recombinant $FliD_{H7}$, $FliC_{H7}$ and its different domains ($VrH7_{180\text{-}496}$, $NTrH7_{1\text{-}179}$, $CTrH7_{497\text{-}585}$ as published by (McNeilly *et al.*, 2010b)) to the BTRE. $VrH7_{180\text{-}496}$ does not contain any $FliD_{H7}$ and recombinant $FliD_{H7}$ does not contain any $FliC_{H7}$. Binding of $VrH7_{180\text{-}496}$ and recombinant $FliD_{H7}$ would therefore confirm specific adherence of $FliC_{H7}$ or $FliD_{H7}$ respectively. The results in this chapter show that both recombinant $FliD_{H7}$ and $VrH7_{180\text{-}496}$ from H7 flagella can bind BTRE cells. Unfortunately the specificity of this is unknown. Based on previous data, the expectation was that purified $FliC_{H7}$ flagella would bind, as a positive control, and the $NTrH7_{1\text{-}179}$ and $CTrH7_{497\text{-}585}$ domains of $FLrH7_{1\text{-}585}$ would not bind, and serve as negative controls. However, there were setbacks in purifying $FLrH7_{1\text{-}585}$, $NTrH7_{1\text{-}179}$ and $CTrH7_{497\text{-}585}$ domains, partly due to receiving incorrect constructs. Given the time it would have taken to make and purify protein from correct constructs, a decision was made to qualitatively assess the binding capacity of the proteins already purified. However, the other $FliC_{H7}$ domains have since been purified and could be used in further binding studies with more biological replicates. In any case, both $FliC_{H7}$ and $FliD_{H7}$ were able to bind to the BTRE. If this is specific binding, both molecules are potential EHEC vaccine candidates, as neither are likely to contain TLR5 epitopes that hamper full protection with purified flagella.

It was hoped that the specific role of $FliD_{H7}$ in *E. coli* O157:H7 binding would become clearer with α-$FliD_{H7}$ inhibition binding studies. Adding $FliD_{H7}$ antiserum reduced *E. coli* O157:H7 BTRE binding to a level comparable with whole flagella antibodies. In hindsight however, it is difficult to tell from this whether this is due to

an inhibition of $FliC_{H7}$ filament formation, flagellar motility or $FliD_{H7}$ binding. A combination of fluorescence microscopy and scanning electron microscopy could be used to resolve this.

No $FliD_{H7}$-specific serum IgG was detected after experimental challenge with *E. coli* O157:H7 in the animal tested. Either $FliD_{H7}$ does not illicit specific antibodies or there may be a more local mucosal IgG or IgA response. Testing sera and mucosal scrapings from the BTRE by ELISA in more animals would indicate which alternative is the case, quantify any responses and show how common they are. Interestingly, vaccination with H7 flagella (predominantly $FliC_{H7}$) did raise $FliD_{H7}$-specific IgG, at least in the one calf and rabbit tested. It is possible that $FliD_{H7}$ was inadvertently present in the purified $FliC_{H7}$ flagella preparations used for vaccination. If this was the case, and $FliD_{H7}$ is involved in BTRE binding, it is already being used to prevent *E. coli* O157:H7 colonisation. This raises the question of how efficacious the Tir, Intimin and EspA vaccine would be with $FliD_{H7}$, in the absence of $FliC_{H7}$.

Having looked closely at the adherence of whole flagella to BTRE primary cell cultures, it was apparent that broadly speaking there were three types of adherence. These were lateral, perpendicular and penetrative adhesion, named as such for the direction of flagella curving relative to the host cell membrane. The mechanisms involved were not apparent by simple observation. This was due to the amount of variation; flagella were not all adhering at their tips or penetrating like a needle into host cells. From this it was not any more clear which parts of the flagella are involved, nor whether adhesion is based on the force of the flagella motor (MotAB), hydrophobicity, or involves particular receptors. Additionally, it was not possible due to technical and time restraints to image bacterial flagella penetrating eukaryotic cell membranes very successfully. The gold standard for this would be transmission electron microscopy. However, the logistics of attempting to image sections that capture and dissect the length of a 20 nm thick flagella filament from bacterial anchorage to host cell penetration are formidable.

Flagella are evolutionarily related to T3SS (Abby & Rocha, 2012) and contain a T3S export apparatus in the basal body to secrete flagellar components (Büttner, 2012). Like a T3SS, flagella have a central channel spanning the entire structure, with a cap at the distal end (Samatey, 2009). Also like *E. coli* O157:H7 T3SS needles which are capped by pore-forming proteins EspBD, $FliC_{H7}$ flagella are capped by $FliD_{H7}$. It is not known if FliD can be pore-forming, or whether it generically dissociates from FliC, as it does in entero-toxigenic *E. coli* (Roy *et al.*, 2009). Additionally, secretion of effector proteins through flagella into culture supernatants has been demonstrated, at least with *Campylobacter* secretion of Cia proteins (Konkel *et al.*, 2004). Taking this together with the penetration of H7 flagella into host cells, the idea of T3S of effector proteins through H7 flagella starts to gain credibility.

Penetration into host cells greatly increases the number of potential flagella interactants. In essence, the known interface between the host and H7 flagella is extended by this finding. FliC and FliD could be acting as effector proteins in their own right, independent of the T3S translocon, potentially affecting a number of host cell processes and its immune recognition. If this were the case, this further justifies defining the H7 binding epitope for use as part of a multi-component vaccine against *E. coli* O157:H7 in cattle.

3.7 References

Abby, S. S. & Rocha, E. P. C. (2012). The non-flagellar type III secretion system evolved from the bacterial flagellum and diversified into host-cell adapted systems. *PLoS genetics* **8**, e1002983.

Arora, S. K., Ritchings, B. W., Almira, E. C., Lory, S. & Ramphal, R. (1998). The *Pseudomonas aeruginosa* flagellar cap protein, FliD, is responsible for mucin adhesion. *Infection and immunity* **66**, 1000–7.

Büttner, D. (2012). Protein export according to schedule: architecture, assembly, and regulation of type III secretion systems from plant- and animal-pathogenic bacteria. *Microbiology and molecular biology reviews* **76**, 262–310.

Estes, D. M. (1996). Differentiation of B cells in the bovine. Role of cytokines in immunoglobulin isotype expression. *Veterinary immunology and immunopathology* **54**, 61–7.

Faulstich, H., Trischmann, H. & Mayer, D. (1983). Preparation of tetramethylrhodaminyl-phalloidin and uptake of the toxin into short-term cultured hepatocytes by endocytosis. *Experimental cell research* **144**, 73–82.

Faulstich, H., Zobeley, S., Rinnerthaler, G. & Small, J. V. (1988). Fluorescent phallotoxins as probes for filamentous actin. *Journal of muscle research and cell motility* **9**, 370–83.

Konkel, M. E., Klena, J. D., Rivera-Amill, V., Monteville, M. R., Biswas, D., Raphael, B. & Mickelson, J. (2004). Secretion of virulence proteins from *Campylobacter jejuni* is dependent on a functional flagellar export apparatus. *Journal of bacteriology* **186**, 3296–303.

Mahajan, A., Currie, C. G., Mackie, S., Tree, J., McAteer, S., McKendrick, I., McNeilly, T. N., Roe, A., La Ragione, R. M. & other authors. (2009). An investigation of the expression and adhesin function of H7 flagella in the

interaction of *Escherichia coli* O157 : H7 with bovine intestinal epithelium. *Cellular microbiology* **11**, 121–37.

McNeilly, T. N., Naylor, S. W., Mahajan, A., Mitchell, M. C., McAteer, S., Deane, D., Smith, D. G. E., Low, J. C., Gally, D. L. & Huntley, J. F. (2008). *Escherichia coli* O157:H7 colonization in cattle following systemic and mucosal immunization with purified H7 flagellin. *Infection and immunity* **76**, 2594–602.

McNeilly, T. N., Mitchell, M. C., Rosser, T., McAteer, S., Low, J. C., Smith, D. G. E., Huntley, J. F., Mahajan, A. & Gally, D. L. (2010a). Immunization of cattle with a combination of purified intimin-531, EspA and Tir significantly reduces shedding of *Escherichia coli* O157:H7 following oral challenge. *Vaccine* **28**, 1422–8.

McNeilly, T. N., Mitchell, M. C., Nisbet, A. J., McAteer, S., Erridge, C., Inglis, N. F., Smith, D. G. E., Low, J. C., Gally, D. L. & other authors. **(2010b).** IgA and IgG antibody responses following systemic immunization of cattle with native H7 flagellin differ in epitope recognition and capacity to neutralise TLR5 signalling. *Vaccine* **28**, 1412–21.

Roy, K., Hilliard, G. M., Hamilton, D. J., Luo, J., Ostmann, M. M. & Fleckenstein, J. M. (2009). Enterotoxigenic *Escherichia coli* EtpA mediates adhesion between flagella and host cells. *Nature* **457**, 594–8.

Samatey, F. A. (2009). Flagellum structure. In *Pili and flagella, current research and future trends*, 1st edn., pp. 137–153. Edited by K. F. Jarrell. Norfolk: Caister Academic Press.

Scharfman, A. & Arora, S. (2001). Recognition of Lewis x derivatives present on mucins by flagellar components of *Pseudomonas aeruginosa*. *Infection and immunity* **69**, 5243–5248.

Tasteyre, A., Barc, M. & Collignon, A. (2001). Role of FliC and FliD flagellar proteins of *Clostridium difficile* in adherence and gut colonization. *Infection and immunity* **69**, 7937–7940.

Yonekura, K. (2000). The bacterial flagellar cap as the rotary promoter of flagellin self-assembly. *Science* **290**, 2148–2152.

4 : Potential H7 flagella binding epitopes

4.1 $FliC_{H7}$ BTRE-binding epitopes

Given that H7 flagella may be playing a more complex role in adherence than previously thought, it's inclusion in a multi-component vaccine against *E. coli* O157:H7 in cattle is further justified. However, vaccination with $FliC_{H7}$ flagella is not always protective, due to the TLR5-neutralising antibodies it generates. Also, the role of $FliD_{H7}$ in flagella binding remains unclear. Therefore a closer examination of H7 flagella-based adhesion was necessary to tease apart H7 flagella binding epitopes and TLR5 recognition epitopes. This was done by comparing FliC sequences that are unlikely to contain BTRE binding epitopes with $FliC_{H7,}$ with the hope that this would shed some light on which $FliC_{H7}$ sequences could be required for BTRE binding.

To narrow down which binding epitopes are specific to $FliC_{H7}$, assumptions were made based on existing binding data. This binding data showed that $FliC_{H7}$ protein adhered to BTRE primary cell cultures, the assumption being that this was specific because $FliC_{H11}$ and $FliC_{H21}$ did not (Mahajan *et al.*, 2009). $fliC_{H6}$ did not fully complement wild-type O157:H7 BTRE cell binding in an isogenic $fliC_{H7}^{-}$ strain (Mahajan *et al.*, 2009). Therefore it was assumed that $FliC_{H6}$, $FliC_{H11}$ and $FliC_{H21}$ do not contain BTRE binding epitopes. In addition, $FliC_{H48}$ is from a non-pathogenic, lab-adapted strain of *E. coli* K-12. This strain was thought unlikely to be able to colonise the BTRE, so the $FliC_{H48}$ sequence was also included for comparative analysis.

As well as variation between FliC of different serotypes, diversity within the H7 allele of *fliC* has been reported (Reid *et al.*, 1999; Wang *et al.*, 2000) and this was also taken into account. However, there was not as much sequence divergence as might be expected, even at a nucleotide level, considering its wide distribution across *E. coli* of different serotypes. In a study by Wang et al. (2000), there were only 1 or 2 nucleotide differences between the ancestral O55:H7 strains and O157:H7 strains that they sequenced. They reported a total variation of 0.06 to 3.12% (Wang *et al.*, 2000). $FliC_{H7}$ from ZAP198 and TUV93-0, two O157:H7 strains that both adhere to the BTRE, have identical sequences.

4.1.1 Structural epitopes

Multiple protein sequence alignments do not take into account, in their making, the structural context of particular amino acids, nor do they provide this at the end. For example, insertions are less likely to occur in structurally constrained regions, such as α-helices and β-sheets, than in flexible and disordered loops (Kelley & Sternberg, 2009). Amino acid substitutions are also more likely to occur in surface exposed regions because there is less structural constraint for side chains and with pathogen extracellular proteins, generally a greater selective pressure due to their interactions with the host immune system (Hilleman, 2002).

A multiple structural alignment with the same FliC sequences was undertaken because it uses a structural template to impose higher gap penalties in structurally ordered regions. This results in an alignment that has a smaller total of larger insertions in loop regions, and their likely location in the protein. Currently the only solved structure of FliC is from *S.* Typhimurium ($FliC_{P1}$, PDB entry 1UCU, (Yonekura *et al.*, 2003)). Sequence threading of $FliC_{H7}$ through the 1UCU structure was useful to see if binding epitopes could be mapped, or whether a specific $FliC_{H7}$ structure would be needed to define structural epitopes.

4.2 $FliD_{H7}$ BTRE-binding epitopes

As shown in the previous chapter, $FliD_{H7}$ plays a role in H7 flagella-based adherence and specific adhesion was not ruled out. With this in mind, multiple FliD protein sequence alignments were carried out using the same methods, strains and reasoning as with FliC. Except that to date there is no solved structure for FliD, so a structural template sequence was not included.

4.3 Post-translational epitopes

To fully characterise the H7 flagella binding epitope, the possibility that $FliC_{H7}$ is post-translationally modified was also investigated. This is because there is a precedent for

post-translational modification of flagellins in Gram negative bacteria (see Logan, 2006 for a review). *Helicobacter pylori* and *Campylobacter jejuni* flagellin subunits are glycosylated by chromosomally expressed glycosylation islands (Schirm *et al.*, 2003; Thibault *et al.*, 2001). However, this may or may not relate to binding (Howard *et al.*, 2009).

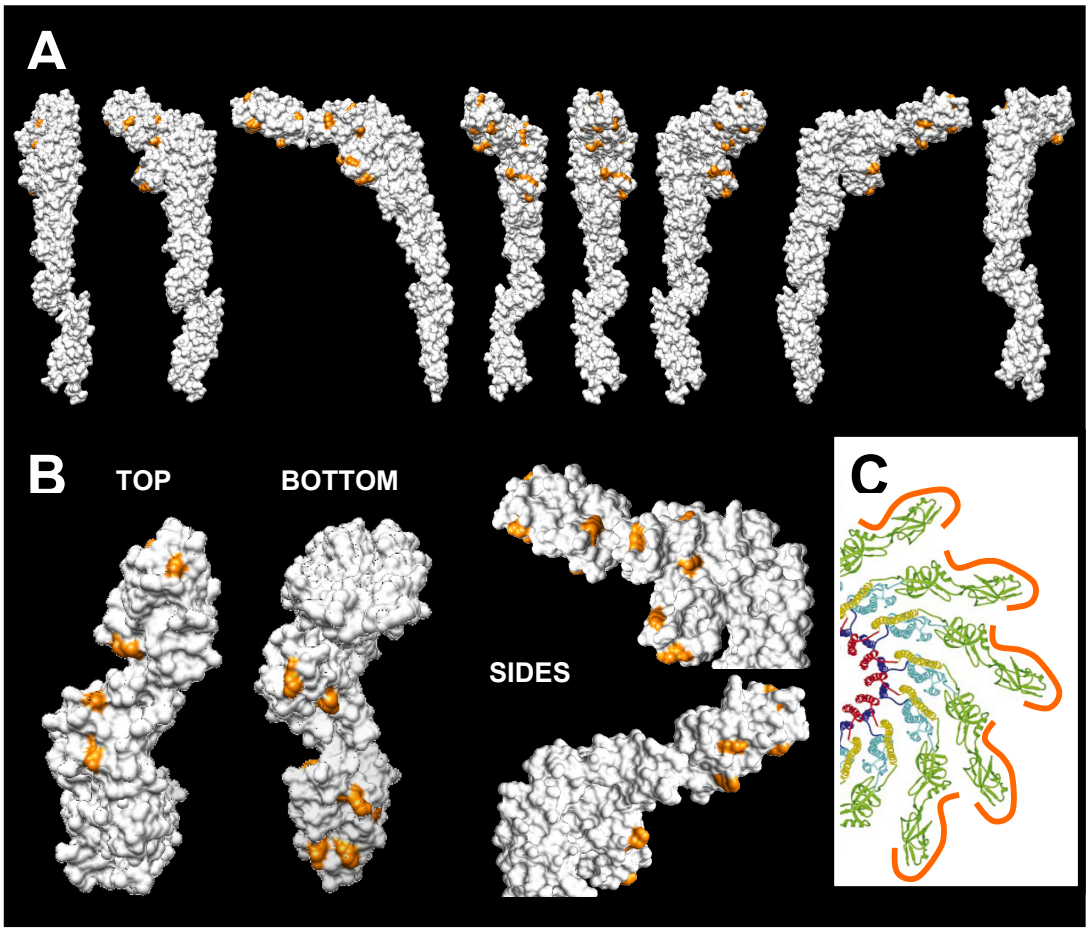

Figure 4.1. ε-methyl-lysines (orange) are located on the outside surface of $FliC_{P1}$ from *S.* Typhimurium. **A)** Rotational views of the whole FliC monomer show ε-methyl-lysines are located exclusively in the D2/D3 domains. **B)** Top, bottom and side views of the D2/D3 domain show that ε-methyl-lysines are not uniformly distributed, but are located more on the bottom than the top and one side more than the other. **C)** Methylated lysines, indicated approximately by orange line, are only the outside of the structural assembly of the filament (developed from Yonekura *et al.* 2003). Surface models were constructed using PDB entry 1UCU in USCF Chimera by individually labelling ε-methyl-lysines in orange.

S. Typhimurium flagellins are highly methylated by FliB (Tronick & Martinez, 1971). FliB specifically methylates surface exposed lysine residues on both $FliC_{P1}$ and $FljB_{P2}$ D2/D3 domains (Stocker & McDonough, 1961), as shown in figure 4.1 with $FliC_{P1}$. Methylation by FliB does not affect motility and its functional significance has not been determined (Burnens *et al.*, 1997). Attempts to understand the function of flagella methylation were made before it was discovered that flagella can act as adhesins. *E. coli* O157:H7 has multiple horizontally-acquired genomic regions that encode proteins of unknown function (Perna *et al.*, 2001), including a number of proteins with predicted glycosylation or methylation activity. Therefore there is the potential for post translational modification of $FliC_{H7}$ in *E. coli* O157:H7.

4.4 Aims

- To compare phenotypically relevant FliC and FliD protein sequences to identify H7-specific regions.
- To establish a structural context for $FliC_{H7}$ specific epitopes.
- To determine if $FliC_{H7}$ undergoes post-translational modification.

4.5 Results

4.5.1 FliC variation

A multiple sequence alignment (methods 1.4.2) of $FliC_{H7}$, $FliC_{H6}$, $FliC_{H48}$, $FliC_{H11}$, $FliC_{H21}$ and *S.* Typhimurium $FliC_{P1}$ showed that the amino (N) and carboxy (C) termini are both highly conserved, and the central region is very variable (figure 4.2 and table 4.1). This is highlighted in table 4.1; total sequence identity and similarity of the termini is approximately double that of the central region. This is in line with previous discussion about flagellins (section 1.5.1.1 and (Hakalehto *et al.*, 1997; Smith *et al.*, 2003)). Therefore, as the flagellins with different BTRE binding epitopes have highly conserved termini, BTRE-specific binding epitopes are most likely to be present in the central region of $FliC_{H7}$.

Table 4.1. Sequence identity and similarity of $FliC_{H6}$, $FliC_{H48}$, $FliC_{H11}$, $FliC_{H21}$ and *S.* Typhimurium $FliC_{P1}$ to $FliC_{H7}$ using the GONNET scoring matrix.

FliC	% Identity	% Similarity	% Identity of variable region	% Similarity of variable region
H6	53.6	62.7	20.0	34.7
H11	43.4	55.2	12.2	24.5
H21	42.5	55.7	13.5	26.6
H48	52.2	60.9	17.8	29.9
P1	40.7	55.5	12.6	26.2

Figure 4.2 and table 4.1 also show that $FliC_{H6}$ is the most closely related sequence to $FliC_{H7}$, followed by $FliCH_{48}$. $FliC_{H11}$ and $FliC_{H21}$ appear to be closely related to one another, but distinct from $FliC_{H6}$, $FliC_{H7}$ and $FliC_{H48}$ (figure 4.2). Because $FliC_{H6}$ is more similar to $FliC_{H7}$ while still retaining phenotypic binding differences, $FliC_{H11}$ and $FliC_{H21}$ were omitted from further alignments. $FliC_{P1}$ is the least identical sequence to $FliC_{H7}$ (table 4.1) and this trend is apparent when looking at the whole sequence or just the variable region.

Figure 4.2. Multiple sequence alignment of FliC from flagella with different BTRE adherence phenotypes (see table 4.1 and next page). Sequences from UniprotKB, see table 2.4 for details. Adherent (+), not adherent (-), not tested (NT). $FliC_{H7}$ (H7, +), $FliC_{H6}$ (H6, +/-), $FliC_{H48}$ (H48, NT), $FliC_{H11}$ (H11, -), and $FliC_{H21}$ (H21, -), with *S.* Typhimurium $FliC_{P1}$ (P1, NT). Residues are shaded if >60% similar. Residues are coloured according to property (green = small/hydrophobic, red = acidic, turquoise = aromatic, dark blue = basic, light blue = hydroxyl/amine). Alignments were carried out in MUSCLE and presented in BioEdit.

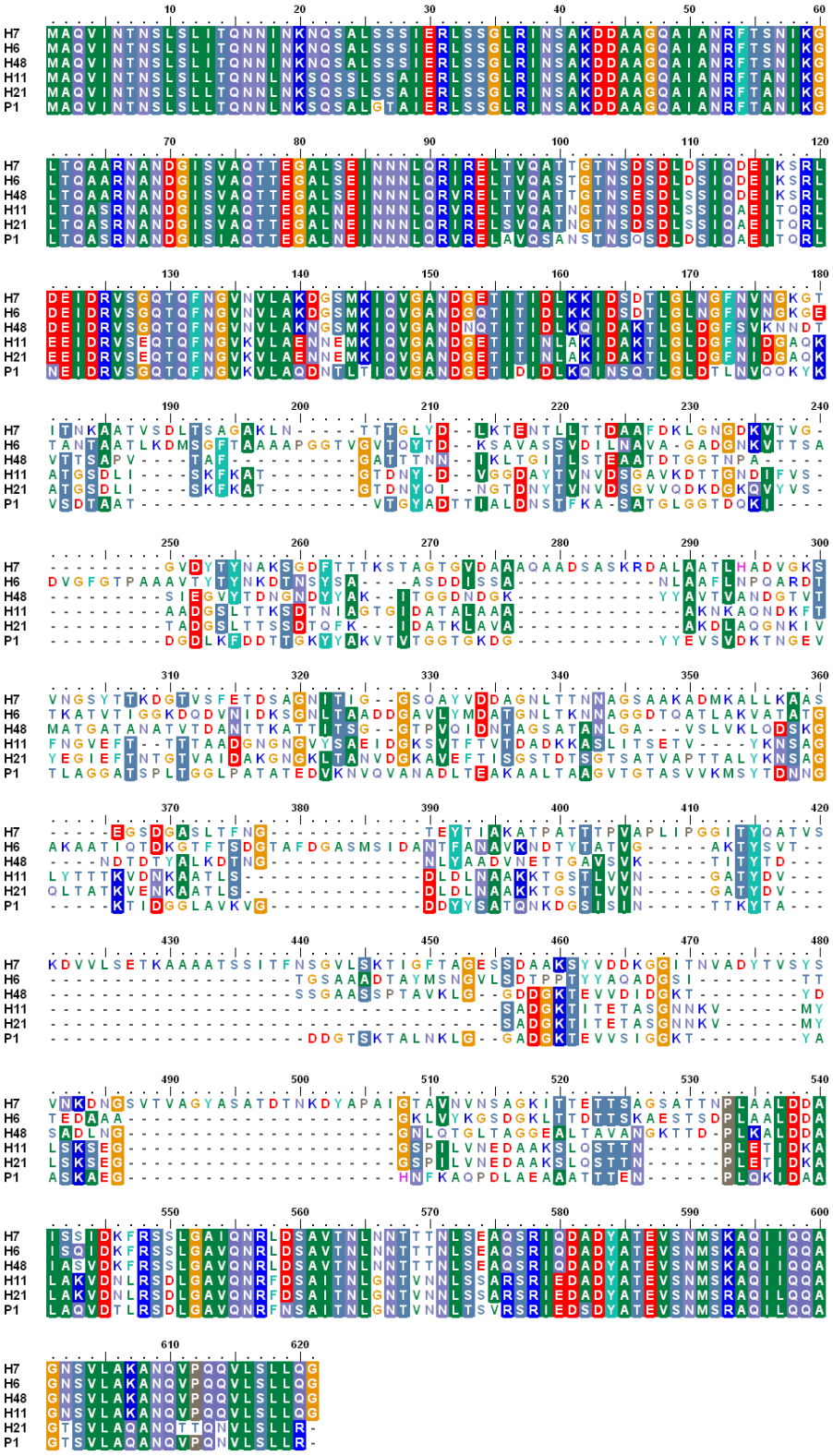
H7
H6
H48
H11
H21
P1

4.5.2 FliC$_{H7}$-specific structural epitopes

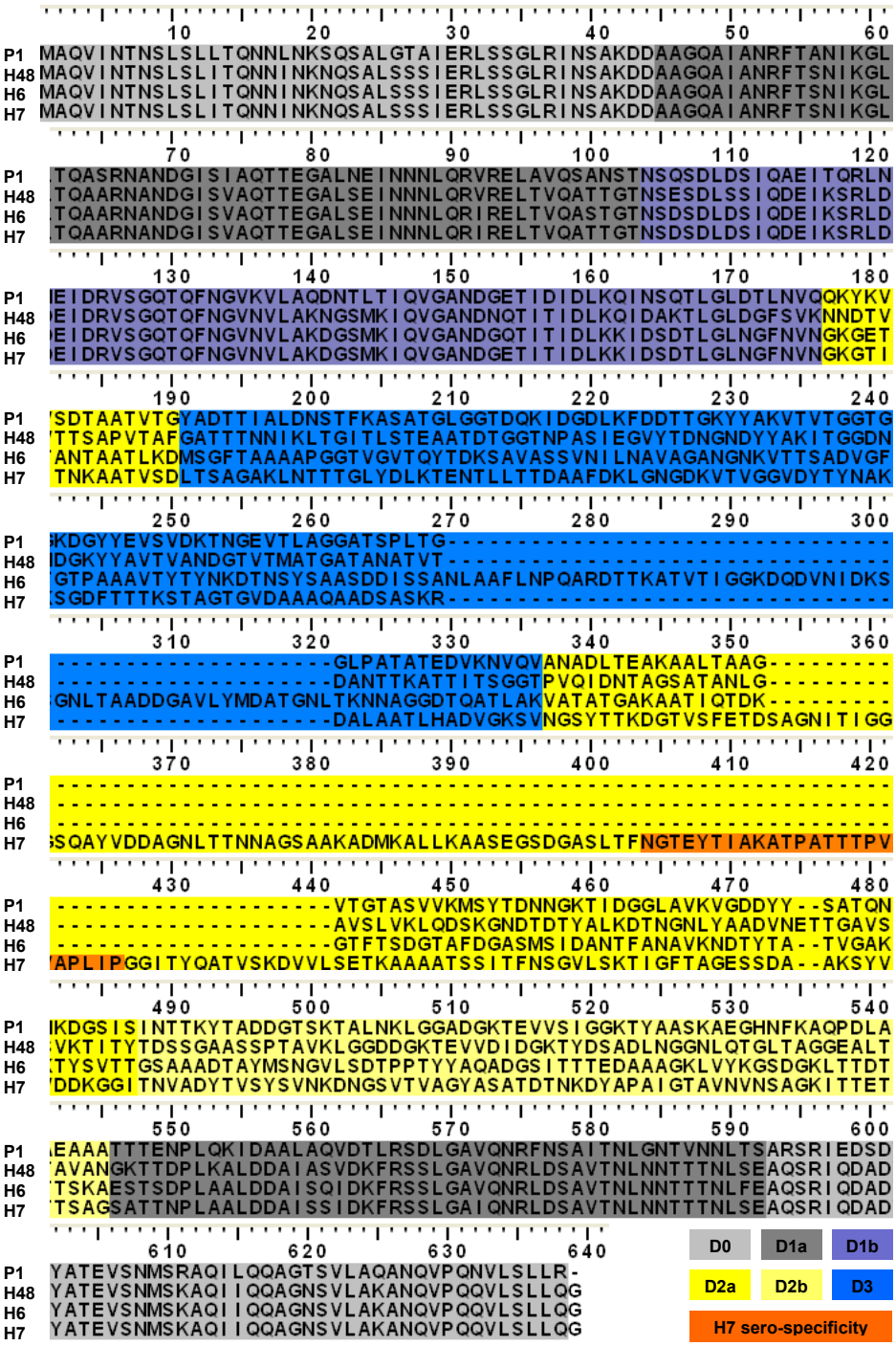

Figure 4.3. Multiple structural alignment of FliC$_{H6}$ (H6), FliC$_{H7}$ (H7) and FliC$_{H48}$ (H48) with *S.* Typhimurium SJW103 FliC$_{P1}$ (P1, PDB entry 1UCU). Pairwise alignments were carried out using the FFAS03 server, manually collated and presented in BioEdit. Structural domains are coloured as indicated (see bottom right and figure 4.4).

The structural alignment of $FliC_{H6}$, $FliC_{H7}$ and $FliC_{H48}$ with *S.* Typhimurium $FliC_{P1}$ is shown in figure 4.3. Table 4.2 details the specific structural domain boundaries for each FliC allele, predicted by the multiple structural alignment in figure 4.3. This alignment predicts far fewer insertions than in figure 4.2, but the insertions are still in the central portion of the sequence. Figure 4.3 shows that $FliC_{H6}$ has a predicted 51aa insertion in the D3 domain (270-321aa), and $FliC_{H7}$ has a predicted 88aa insertion and $FliC_{H48}$ has a predicted 2aa insertion, both in the carboxy-terminal D2a domain, (302-390aa and 331-2aa respectively). The $FliC_{H7}$ insertion contains an experimentally validated H7-specific linear epitope (Kwang *et al.*, 1996). This insertion is structurally unique, as no structural templates were found when searching FFAS03 databases with this 88aa sequence. Figure 4.4 illustrates where $FliC_{H6}$ and $FliC_{H7}$ insertions are in relation to the structural template, $FliC_{P1}$ (PDB entry 1UCU, (Yonekura *et al.*, 2003)). This gives a clear idea of where H7-specific BTRE binding epitopes are likely to be in the $FliC_{H7}$ monomer.

Table 4.2. Structural domain boundaries for $FliC_{H48,}$ $FliC_{H6}$ and $FliC_{H7}$ based on the multiple structural alignment in figure 4.3. Boundaries are shown for N-terminal and C-terminal portions of structural domains.

DOM	**H48**		**H6**		**H7**	
	N	**C**	**N**	**C**	**N**	**C**
D0	M1-D44	G453-G498	M1-D44	Q503-G548	M1-D44	Q540-G585
D1a	A45-T103	K406-A452	A45-T103	S456-A502	A45-T103	A493-A539
D1b	N104-K176	-	N104-N176	-	N104-N176	-
D2a	N177-F190	P285-G338	G177-D190	V337-V387	G177-D190	N285-K424
D2b	-	A339-G405	-	G389-E455	-	S425-S492
D3	G191-T284		M191-K336		L191-V284	

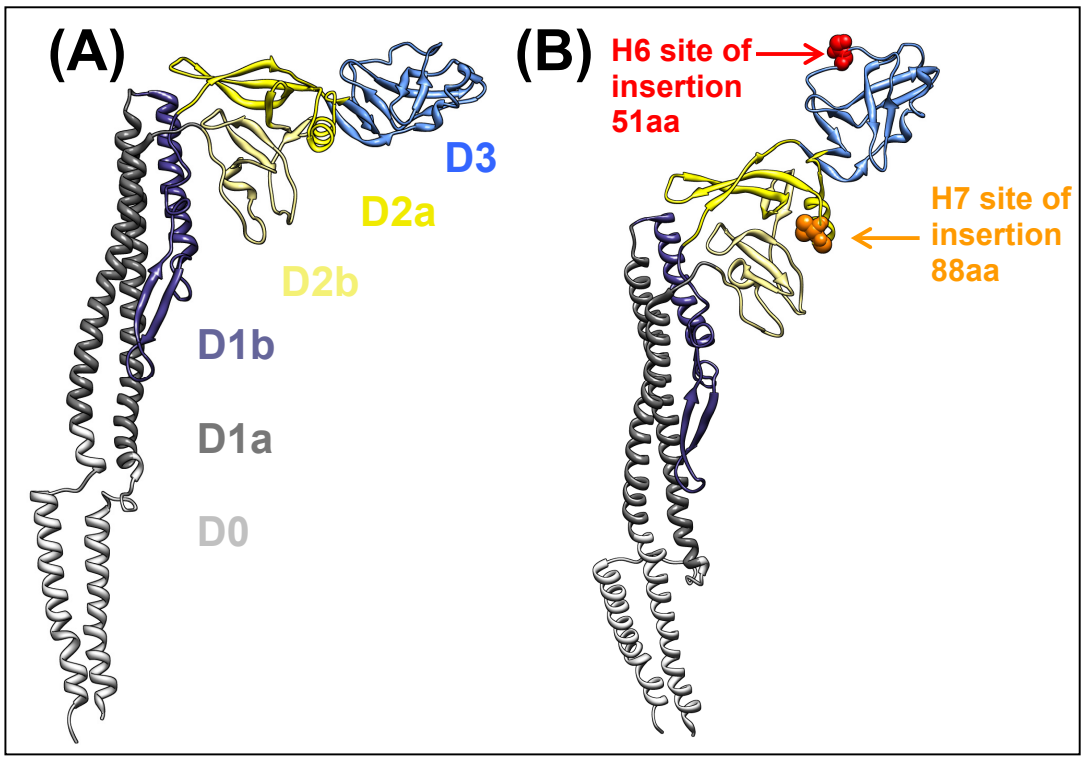

Figure 4.4. Structural organisation of FliC and position of predicted H6 and H7 insertion sites. **(A)** Electron cryomicroscopy structure of *S. Typhimurium* $FliC_{P1}$ from an (PDB entry 1UCU, (Yonekura *et al.*, 2003)) is coloured in UCSF Chimera according to structural domains as shown in figure 4.3. **(B)** Position of predicted H6 and H7 insertion sites in known structure for $FliC_{P1}$ based on multiple structural alignment in figure 4.3. Amino acids either side of insertion sites are highlighted as ball and stick structures in UCSF Chimera.

Apart from the main location in the monomer, the structural models of $FliC_{H6}$ and $FliC_{H7}$ do not give any structural information about the specific insertions. These models tell us that the sero-specific insertions are not in the same place, and where their similarity with $FliC_{P1}$ ends, but not their structural conformation. This information is particularly important if the insertions are likely to contain the binding epitopes. Therefore the known crystal structure for FliC is not similar enough to $FliC_{H7}$ to be useful in structural epitope discovery and modelling.

4.5.3 FliD variation

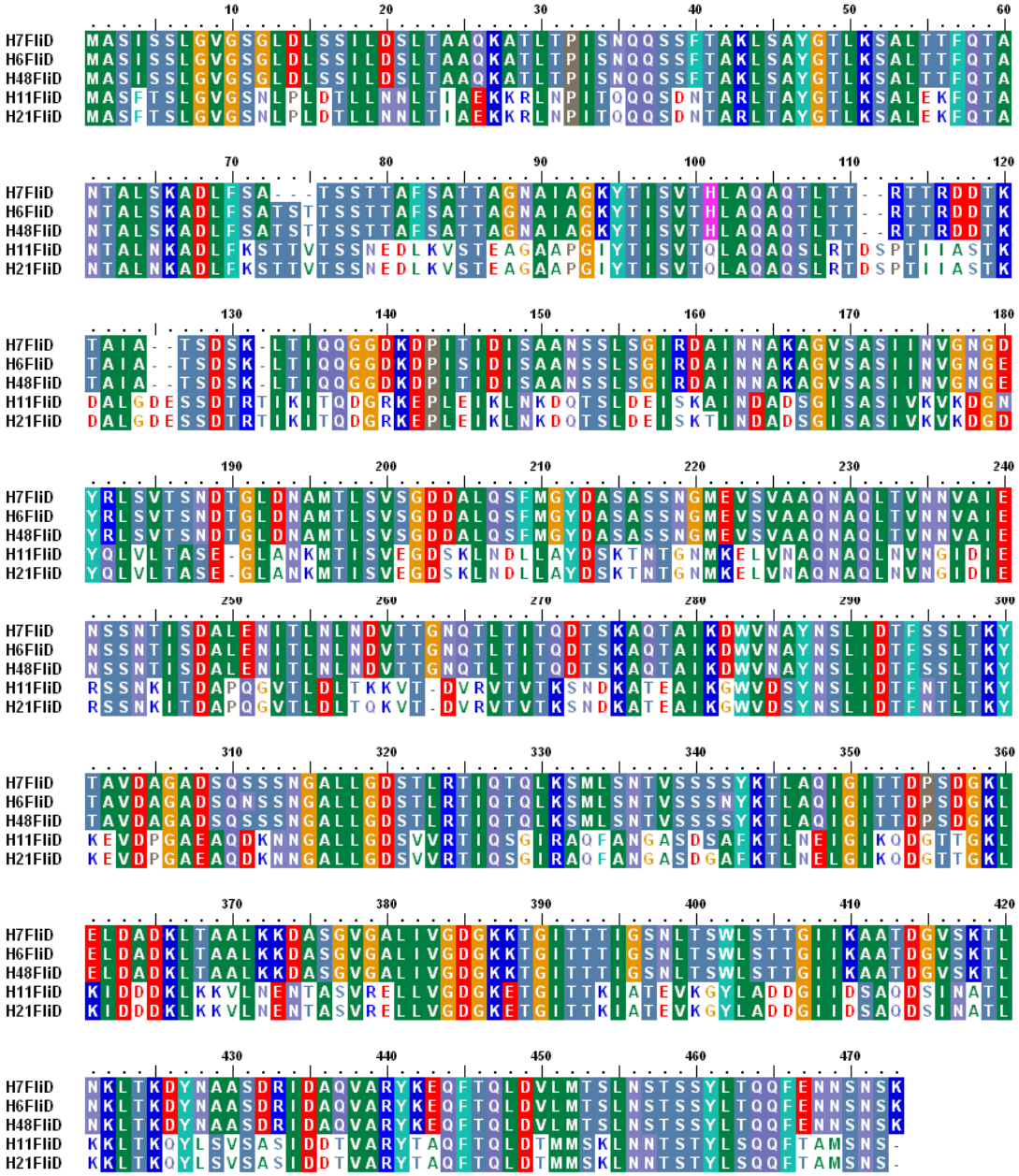

Figure 4.5. Multiple sequence alignment of FliD proteins from flagella with different BTRE adherence phenotypes. Sequences from UniprotKB, from strains detailed in table 2.4. Residues are shaded if ≥60% similar. Residues are coloured according to property as in figure 4.2. Alignments were carried out in MUSCLE and presented in BioEdit.

The FliD protein sequences were more conserved than the FliC sequences from the same strains (table 4.1, figure 4.5 and figure 4.6(A)). As with FliC, FliD from these strains formed the same two distinct groups of homology, (H6 with H7 and H48, and H11 with H21). $FliD_{H6}$ and $FliD_{H48}$ share 98-99% identity with $FliD_{H7}$, but $FliD_{H11}$ and $FliD_{H21}$ only share ~50% identity with $FliD_{H7}$, (71.5% similarity, see figure 4.6(A)). $FliD_{H11}$ and $FliD_{H21}$ are 98.9% identical and 99.8% similar with one another when using the same scoring matrix. Unlike with FliC, the variation between these two groups occurs along the whole length of the protein sequence (see figure 4.5).

(A)

FliD	% Identity	% Similarity
H6	98.5	99.3
H11	50.1	71.5
H21	49.7	71.5
H48	99.1	99.4

(B)

	FliC	FliD	BTRE binding
H7	100	100	++
H6	53.6	98.5	+/-
H48	52.2	99.1	?
H11	43.4	50.1	-
H21	42.5	49.7	-

Figure 4.6. Summary of FliD sequence and phenotype comparison. **(A)** Sequence identity and similarity of $FliD_{H6}$, $FliD_{H48}$, $FliD_{H11}$ and $FliD_{H21}$ to $FliD_{H7}$ using the GONNET scoring matrix. **(B)** Summary of FliC and FliD sequence identity to $FliC_{H7}$ and $FliD_{H7}$ (%) and flagella binding phenotype. Grey boxes <75% identity, blue boxes >75% identity.

Figure 4.6(B) puts the above sequence comparisons into context with the BTRE binding phenotype. H7 flagella bind to BTRE epithelial cells. Both FliC and FliD from H11 and H21 are less than 50% identical to the corresponding H7 sequences, but neither flagella bind to BTRE epithelial cells. Complementation of $fliC_{H7}^{-}$ with $fliC_{H6}$ leads to variably reduced bacterial binding compared to wild-type bacteria because these *fliC* sequences are only ~50% identical. However, in this experiment the FliD was $FliD_{H7}$, not $FliD_{H6}$,

resulting in chimeric flagella. If $FliD_{H7}$ is involved in this binding, this might account for the subtlety of differences observed.

4.5.4 Post-translational modification of $FliC_{H7}$

Investigating possible post-translational modifications of $FliC_{H7}$ became a priority when different purification methods gave different protein band patterns by SDS-PAGE (figure 4.7). All purification of $FliC_{H6}$ and $FliC_{H7}$ flagella was carried out using isogenic chromosomal *fliC* knock-ins (TUV*fliC*$_{H6F1}$ and TUV*fliC*$_{H7F1}$, methods 2.3.12). Aside from the proteins themselves, any low level contaminants and genetic content required for post-translational modification should be comparable in this context.

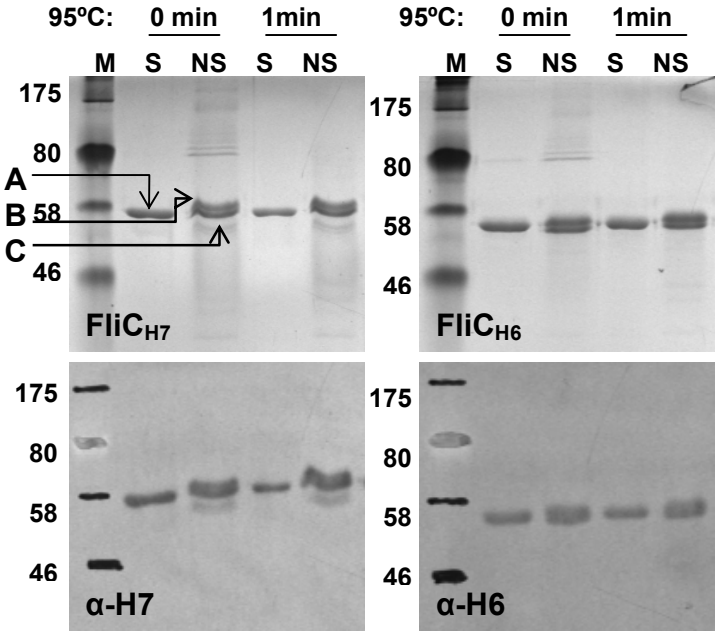

Figure 4.7. Differential migration during SDS-PAGE by $FliC_{H6}$ and $FliC_{H7}$ purified by shearing (S) and acid depolymerisation (NS) of TUV*fliC*$_{H6F1}$ and TUV*fliC*$_{H7F1}$ strains. Samples were incubated at 95ºC for the time indicated, prior to loading. Western blotting with specific antibodies is shown below. Molecular weights indicated on the left (M). Bands A, B and C were excised for mass spectrometry (methods 2.5.2 and 2.5.7).

Purification of flagella by shearing is a relatively mild method, carried out entirely in PBS and yields one ~58 kDa $H7^+$ band or one ~56 kDa $H6^+$ band by Western-blotting, $FliC_{H7}$ or $FliC_{H6}$ respectively (figure 4.7). Purification by acid depolymerisation is a harsher method; flagella filaments are depolymerised by reducing pH and the purified reassembled filaments are precipitated in ammonium sulphate (methods 2.5.5). This

purification resulted in faint smearing of protein bands when visualised with coomassie staining; as shown for 3 $H7^{+}$ bands and 2 $H6^{+}$ bands in figure 4.7. Both acid-depolymerised $FliC_{H6}$ and $FliC_{H7}$ samples have a band with a reduced electrophoretic mobility by SDS-PAGE. This may be because this species has a higher apparent molecular weight or an altered surface charge as a result of the acid treatment. Therefore this differential size shift may be evidence of post-translational modification of FliC in an O157 strain background.

On the basis that flagellin can be glycosylated (Logan, 2006), the $FliC_{H7}$ sequence was searched for N-linked and O-linked glycosylation motifs (see figure 4.8(A)). 8/9 ≥60% probability glycosylation sites were in the H7-specific insertion, as determined by structural alignments (figure 4.3). All 5 predicted O-linked glycosylation sites were within the H7-sero-specificity region, which also contained a motif with 65-70% likelihood for N-linked glycosylation (figure 4.8(A)).

Comparative analysis of the identified mass:charge peaks (m/z) from the different species of $FliC_{H7}$ excised only showed differential cleavages by trypsin. However, unidentified larger masses of particular sizes can indicate the presence of a post-translational modification. Also, unrepresented peptides in the sample coverage can be a result of post-translational modification preventing sample ionisation during the matrix-assisted laser de-ionisation (MALDI) procedure, or the presence of only a larger (modified) peptide species. As there were no apparent unassigned larger or missing peptide masses unique to sample B, unassigned m/z common to all samples were analysed for possible post-translational modifications.

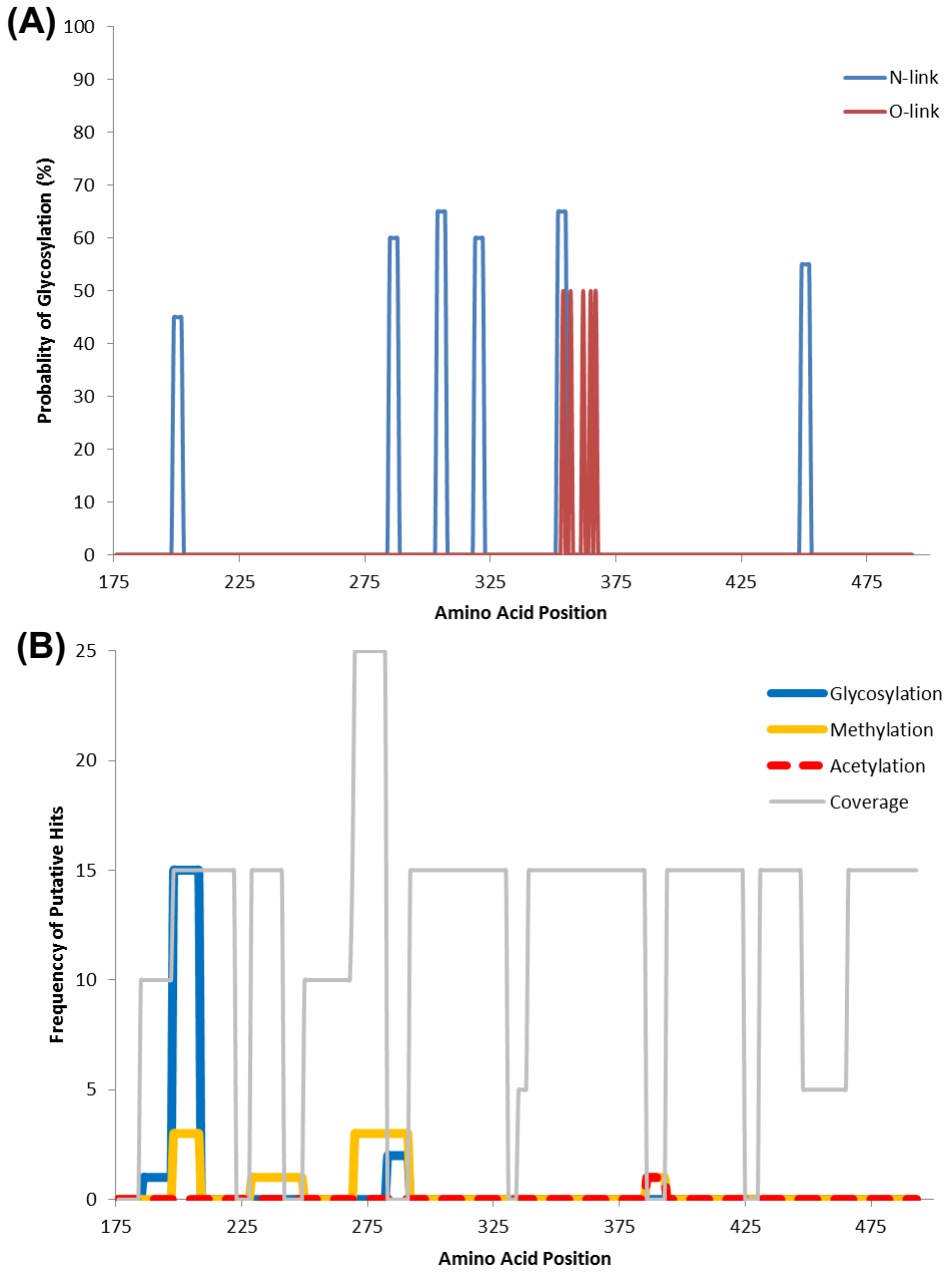

Figure 4.8. Predicted sites of post-translational modification in the $FliC_{H7}$ D2/D3 domain. **(A)** % likelihood of correctly predicted N and O linked glycosylation sites in $FliC_{H7}$ using NetNGlyc and NetOGlyc programs from expasy bioinformatics resource portal. **(B)** Potential PTMs indicated by analysis of MS peptide fragments. MASCOT was used to assign peptide identities for each sample; sequence coverage of D2/D3 domain from all samples is indicated by grey line. Total coverage frequency = units/5. Unassigned m/z were put through FindMod and GlycMod programs from expasy bioinformatics resource portal; frequency of total putative glycosylation, methylation and acetylation modifications are indicated by orange, blue and red lines respectively.

Figure 4.8(B) summarises this analysis of unidentified m/z and unrepresented peptides. Of the two N-linked glycosylation sites not ruled out by this research, the second site corresponds to an unrepresented region and a 60-65% probability prediction. This result is suggestive of glycosylation. However, glycosylation of sheared and acid-depolymerised $FliC_{H6}$ and $FliC_{H7}$ in an O157:H7 background was not detected by sodium metaperiodate labelling (see figure 4.9).

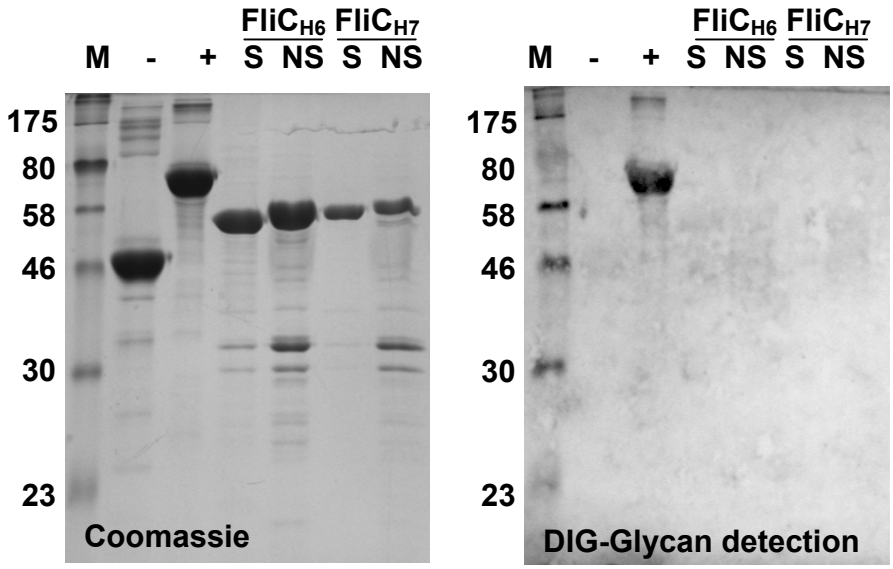

Figure 4.9. Detection of glycosylation of $FliC_{H6}$ and $FliC_{H7}$ with DIG-labelled sodium metaperiodate (methods 2.5.4). Samples were run on an 12-4% SDS-PAGE gel (left), western blotted onto nitrocellulose, and detected using a DIG-glycan detection kit (right, Roche). Creatinase from *E. coli* (-). Transferrin (+). Sheared flagella preparation (S). Acid depolymerised flagella preparation (NS).

There were no putative post-translational modifications in the $FliC_{H7}$ sero-specificity region (352-374, see figure 4.8(B), (Kwang *et al.*, 1996)). However, there was an m/z that could correspond to methylation or acetylation of a peptide in close proximity to the sero-specificity region. This peptide was otherwise unrepresented in the spectra. Accurate molecular weight determination of $FliC_{H7}$ purified by shearing was measured

at 59,823.6 Da, which is very similar to the predicted value minus the initiator methionine (59,822.3 Da) ruling this out under these conditions (figure 4.10).

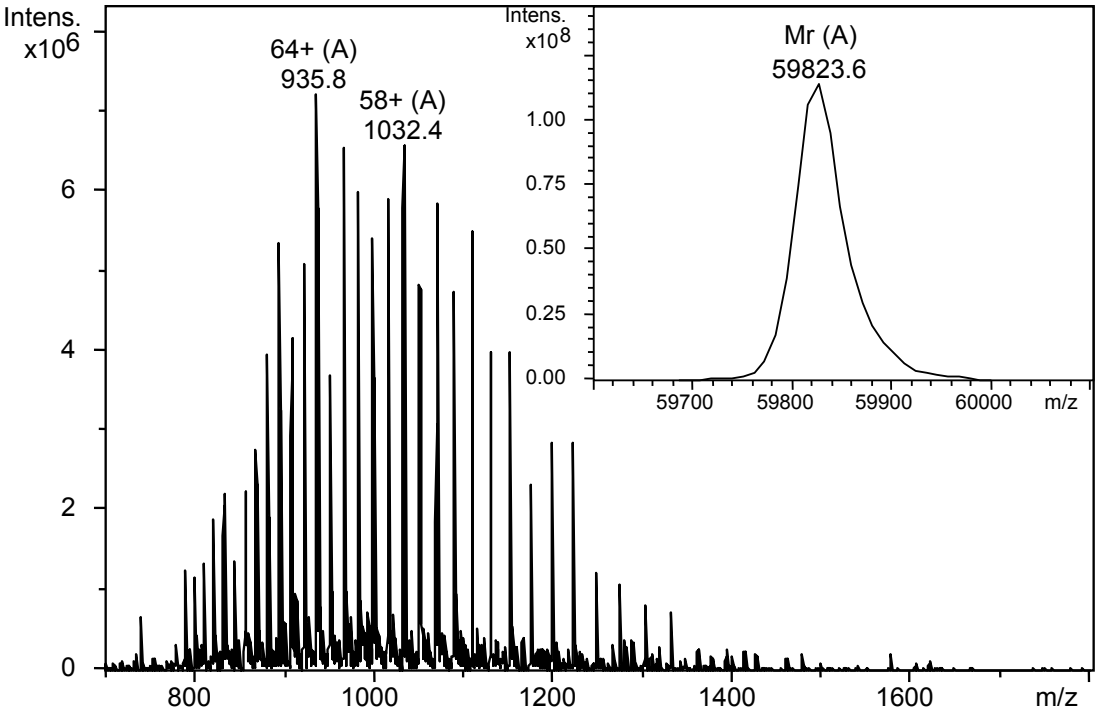

Figure 4.10. Mass spectrum and (inset) deconvoluted mass spectrum of sheared $FliC_{H7}$ from TUV93-0. $FliC_{H7}$ was analysed by online HPLC-MS by dedicated personnel in the facilities of Proteomics and Metabolomics at the Roslin Institute (methods 2.5.7). The measured mass of 59,823.6 Da is in good agreement with the theoretical mass predicted from the sequence of 59,822.3 Da (after removal of the N-terminal methionine).

4.6 Discussion

The principle aim of the above investigations was to gain a better understanding of what is specific about $FliC_{H7}$ and $FliD_{H7}$ that allows H7 flagella to bind to the BTRE. Both sets of phenotypically relevant FliC and FliD sequences showed similar groupings of homology. H6 and H48 sequences were most similar to H7, with H11 and H21 being similar to one another but distinct from H7. The areas of variation in FliC and FliD were different; FliD variation occurred along the full length of the protein, while FliC variation only took place in the central region. Therefore H7-specific FliD binding epitopes could be at discrete points throughout the protein sequence. However, as the

termini are highly conserved, H7-specific FliC binding epitopes could only be in the central domain of the sequence.

A multiple structural alignment of the H7-homologous FliC, using $FliC_{P1}$ from *S.* Typhimurium as a template, predicted discrete H6- and H7-specific insertions. The H7-specific insertion maps to the H7-sero-specificity region as determined by (Kwang *et al.*, 1996). This gives some confidence in the quality of the alignment and the prediction that 302-390aa in $FliC_{H7}$ contains the specific BTRE binding epitopes. However, the known structure of FliC or any other structures are not similar enough to $FliC_{H7}$ for accurate structural prediction of the binding epitopes.

The multiple structural alignment undertaken in this study has subsequently been used by the group in further Biotechnology and Biological Sciences Research Council (BBSRC)-funded research into uses of $FliC_{H7}$ flagella as a vaccine technology. This work is specifically looking at the mucosal adjuvancy of $FliC_{H7}$ flagella by introducing different antigenic epitopes into $FliC_{H7}$. This alignment has been useful as a guide for what changes the flagellin structure might tolerate, in addition to empirical data reviewed by Westerlund-Wikström (Westerlund-Wikström, 2000), and for knowing where specific regions are for mutagenesis.

To see if BTRE-specific binding epitopes in $FliC_{H7}$ were post-translationally modified, $FliC_{H7}$ was analysed using sequence and mass spectrometry. If post-translational modifications were to be part of a BTRE-specific binding epitope they would likely occur in the $FliC_{H7}$-specific insertion between 302-390aa. The most likely predictions of glycosylation did not occur within this region and there was no experimental evidence to confirm them. Methylation was predicted to occur within this region but was not detectable by any discrepancy in molecular weight under these conditions. Perhaps this is because glycosylation and methylation prediction software was developed using eukaryotic parameters. Differential migration of different $FliC_{H7}$ preparations by SDS-PAGE could be explained by degradation of $FliC_{H7}$ during or as a result of acid-

depolymerisation but not shearing. As acid-depolymerisation is a harsher method than shearing, this explanation is not unreasonable. Taken together, these results suggest that $FliC_{H7}$ is not post-translationally modified under these conditions.

As $FliC_{H7}$ does not appear to be post-translationally modified, the type of binding interaction is limited to being protein-based on the $FliC_{H7}$ flagella side, unless O157 LPS is associated with $FliC_{H7}$. This simplifies BTRE binding epitope discovery and engineering of recombinant epitopes for use in vaccines. Having predicted a region that may contain specific BTRE binding epitopes, experimental validation was necessary to confirm and refine this.

4.7 References

Burnens, A. P., Stanley, J., Sack, R., Hunziker, P., Brodard, I. & Nicolet, J. (1997). The flagellin N-methylase gene *fliB* and an adjacent serovar-specific IS200 element in *Salmonella typhimurium*. *Microbiology* **143**, 1539–47.

Hakalehto, E., Santa, H., Vepsalainen, J., Laatikainen, R. & Finne, J. (1997). Identification of a common structural motif in the disordered N-terminal region of bacterial flagellins - Evidence for a new class of fibril-forming peptides. *European journal of biochemistry* **250**, 19–29.

Hilleman, M. (2002). Realities and enigmas of human viral influenza: pathogenesis, epidemiology and control. *Vaccine* **20**, 3068–3087.

Howard, S. L., Jagannathan, A., Soo, E. C., Hui, J. P. M., Aubry, A. J., Ahmed, I., Karlyshev, A., Kelly, J. F., Jones, M. A. & other authors. **(2009).** *Campylobacter jejuni* glycosylation island important in cell charge, legionaminic acid biosynthesis, and colonization of chickens. *Infection and immunity* **77**, 2544–56.

Kelley, L. a & Sternberg, M. J. E. (2009). Protein structure prediction on the Web: a case study using the Phyre server. *Nature protocols* **4**, 363–71.

Kwang, J., Wilson, R., Yang, S. & He, Y. (1996). Mapping of the H7-serospecific domain of *Escherichia coli* flagellin. *Clinical and diagnostic laboratory immunology* **3**, 523–6.

Logan, S. M. (2006). Flagellar glycosylation - a new component of the motility repertoire? *Microbiology* **152**, 1249–62.

Mahajan, A., Currie, C. G., Mackie, S., Tree, J., McAteer, S., McKendrick, I., McNeilly, T. N., Roe, A., La Ragione, R. M. & other authors. **(2009).** An investigation of the expression and adhesin function of H7 flagella in the interaction of *Escherichia coli* O157 : H7 with bovine intestinal epithelium. *Cellular microbiology* **11**, 121–37.

Perna, N. T., Plunkett, G., Burland, V., Mau, B., Glasner, J. D., Rose, D. J., Mayhew, G. F., Evans, P. S., Gregor, J. & other authors. **(2001).** Genome sequence of enterohaemorrhagic *Escherichia coli* O157:H7. *Nature* **409**, 529–33.

Reid, S. D., Selander, R. K. & Whittam, T. S. (1999). Sequence diversity of flagellin (*fliC*) alleles in pathogenic *Escherichia coli*. *Journal of bacteriology* **181**, 153–60.

Schirm, M., Soo, E. C., Aubry, A. J., Austin, J., Thibault, P. & Logan, S. M. (2003). Structural, genetic and functional characterization of the flagellin glycosylation process in *Helicobacter pylori*. *Molecular microbiology* **48**, 1579–92.

Smith, K. D., Andersen-Nissen, E., Hayashi, F., Strobe, K., Bergman, M. a, Barrett, S. L. R., Cookson, B. T. & Aderem, A. (2003). Toll-like receptor 5 recognizes a conserved site on flagellin required for protofilament formation and bacterial motility. *Nature immunology* **4**, 1247–53.

Stocker, B. & McDonough, M. (1961). A gene determining presence or absence of epsilon-N-methyl-lysine in *Salmonella* flagellar protein. *Nature* **189**, 556–558.

Thibault, P., Logan, S. M., Kelly, J. F., Brisson, J. R., Ewing, C. P., Trust, T. J. & Guerry, P. (2001). Identification of the carbohydrate moieties and glycosylation motifs in *Campylobacter jejuni* flagellin. *Journal of biological chemistry* **276**, 34862–70.

Tronick, S. R. & Martinez, R. J. (1971). Methylation of the flagellin of *Salmonella typhimurium*. *Journal of bacteriology* **105**, 211–9.

Wang, L., Rothemund, D., Curd, H. & Reeves, P. R. (2000). Sequence diversity of the *Escherichia coli* H7 *fliC* genes: implication for a DNA-based typing scheme for *E. coli* O157:H7. *Journal of clinical microbiology* **38**, 1786–90.

Westerlund-Wikström, B. (2000). Peptide display on bacterial flagella: principles and applications. *International journal of medical microbiology* **290**, 223–30.

Yonekura, K., Maki-Yonekura, S. & Namba, K. (2003). Complete atomic model of the bacterial flagellar filament by electron cryomicroscopy. *Nature* **424**, 643–50.

5 : Flagella receptors in the BTRE

5.1 Definition of $FliC_{H7}$ binding epitopes by mutagenesis

The overarching aim of this study is to produce an improved H7-based vaccine component that raises neutralising antibodies against $FliC_{H7}$ flagella BTRE-binding epitopes but not TLR5-activation epitopes. To do this, it is useful to know the location of BTRE-specific binding epitopes in $FliC_{H7}$. The previous chapter detailed the predictions made about where they might be. However, looking at the effect of defined *fliC* mutations on EHEC binding phenotypes is required to confirm these predictions.

A cloning strategy that allows *E. coli* O157:H7 to express chimeric flagella at wild-type levels would be ideal for testing defined $fliC_{H7}$ mutations. This is because mutants complemented with *fliC* expression plasmids can over-express flagella. Flagella over-expression leads to bundling and clumping of bacteria and consequently altered binding. This can even be the case with low copy number plasmids containing the wild-type promoter region. Therefore the preferred method was to introduce different alleles into the $fliC_{H7}$ locus. To start with, introduction of different *fliC* H-antigen types would be attempted to test and confirm the allelic exchange methodology (section 2.3.12). With this in mind, a $fliC_{H7}$ knock-out was made, and used to make chromosomal complements with different *fliC*.

The main difficulty with making a chromosomal $fliC_{H7}$ complement that expresses flagella at wild-type levels is that the regions involved are highly conserved. The small changes necessary to introduce restriction sites can disrupt the mRNA structure and reduce $fliC_{H7}$ flagella expression. Figure 5.1 shows the effect that changing 3 bp in the $fliC_{H7}$ promoter region has had on flagella expression; flagella are short and bacteria are less motile, despite the $fliC_{H7}$ sequence being the same in all other respects. However, a strategy was developed that was successful in introducing different *fliC* serotypes into the $fliC_{H7}$ locus (methods 2.4.1, figure 2.3 and appendix

1). This strategy is now being used by the group to introduce more subtle changes in *fliC*$_{H7}$. These strains will then be used to test key FliC$_{H7}$ residues involved in binding and host receptor recognition, in a project funded by the BBSRC.

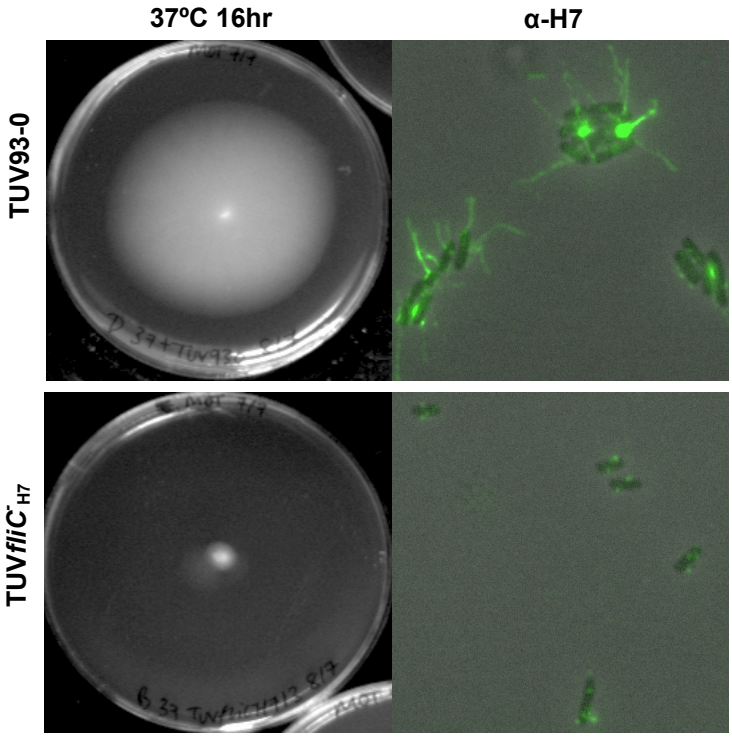

Figure 5.1. Flagella expression of wild-type *E. coli* O157:H7 (TUV93-0) compared to initial *fliC*$_{H7}$ complement (TUV*fliC*$^{-}_{H7}$). This was assayed by motility in semi-solid agar (left, methods 2.9.2) and wide-field fluorescent microscopy (right, methods 2.7.1).

Having created *fliC* chimeras, it was possible to directly compare the *fliC*$_{H6}$ and *fliC*$_{H7}$ binding epitopes in phenotypic assays. FliC$_{H6}$ and FliC$_{H7}$ specific binding assays published by (Erdem *et al.*, 2007) were used as a starting point. They reported that FliC$_{H6}$ and FliC$_{H7}$ flagella filaments and monomers bind to mucin I and mucin II crude preparations from Sigma (not to be confused with binding to specific mucins MucI and MucII). FliC$_{H7}$ flagella binding to mucin II was detectable by dot-blot at lower levels of mucin II compared to FliC$_{H6}$ flagella filaments. This was not the case with FliC$_{H6}$ and FliC$_{H7}$ monomers, implying that FliC$_{H7}$ flagella filaments had a greater binding avidity than FliC$_{H6}$ flagella for mucin II. This published interaction

was used as the basis for an ELISA, where mucin II was used to coat plates, and strain binding was detected using α-O157 antibodies.

The results from a pilot mucin II binding α-O157 ELISA are shown in figure 5.2. More TUV93-0 and TUV*fliC*$_{H7F}$ binding was detected compared to TUV*fliC*$^{-}$ and TUV*fliC*$_{H6F}$. This suggests that there is a measurable difference and perhaps some specificity between $FliC_{H6}$ and $FliC_{H7}$ binding to mucin II in this ELISA. However, this experiment has only been attempted once, without verifying flagella expression levels, so more work would have to be done to ensure this is the case.

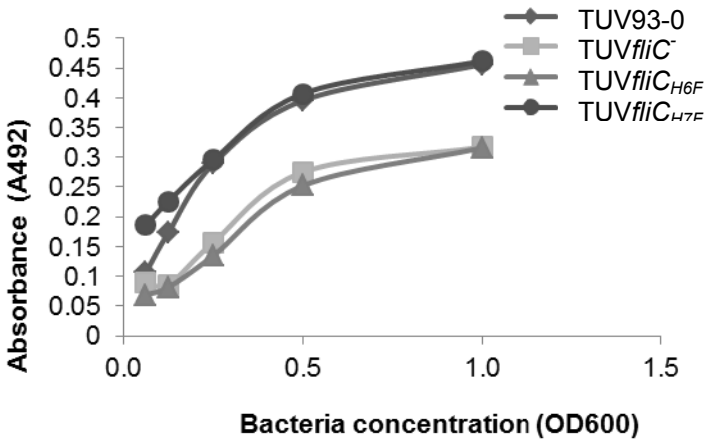

Figure 5.2. Role of $FliC_{H7}$ flagella in *E. coli* O157 strains binding to crude mucin II by ELISA (methods 2.9.12). TUV93-0 is an *E. coli* O157:H7 strain, TUV*fliC*$^{-}$ is its isogenic *fliC*$_{H7}$ mutant. TUV*fliC*$_{H6F}$ and TUV*fliC*$_{H7F}$ are isogenic chromosomal *fliC* complements of TUV*fliC*$^{-}$ (methods 2.3.12, appendix 1).

There are a number of advantages to putting different functional *fliC* alleles into the same strain background. Firstly, this allows the direct comparison of the contribution of different *fliC* alleles to *E. coli* O157 BTRE colonisation, without over-expression and antibiotic issues associated with plasmid-based complementation. Secondly, it allows the use of whole bacteria as a binding substrate in simplified binding assays, as the strains are otherwise isogenic. Also, having such strains is a good source of different flagella that is relatively easy to purify and can be compared with the confidence that additional 'contaminating' components are similar, for example in TLR5 stimulation assays. For binding assays, levels of other proteins such as $FliD_{H7}$, should also be comparable. Finally, the system is highly adaptable. All that is

required is the *fliC* allele coding sequence between two BamHI sites. This means that this system could be used for very detailed mutagenesis, and the results can be examined at a protein and whole bacteria level.

Despite these advantages, this approach is not practical without a binding assay that can discriminate between $FliC_{H6}$ and $FliC_{H7}$ binding epitopes. Mucin II may act as a specific binding substrate for $FliC_{H7}$ flagella, but this binding assay had its issues. Commercial mucin preparations are highly variable and homogenous re-suspension is difficult to achieve. Also, without quantifying flagella expression in the strains tested, no definite conclusions from binding differences could be made.

A measurably clear and specific assay was needed to map $FliC_{H7}$ binding epitopes. With this and the above issues in mind, it became clear that a change in approach was required. $FliC_{H7}$ flagella are known to bind to the BTRE. The BTRE is therefore a source of potential $FliC_{H7}$ receptors. Using purified $FliC_{H7}$ receptors as substrates in binding assays would reduce the variability associated with crude preparations.

5.2 Aims

- To generate candidate $FliC_{H7}$ and $FliD_{H7}$ binding partners from the BTRE.
- To confirm *in vitro* binding interactions of candidates with $FliC_{H7}$ flagella and investigate how generic this is.
- To develop a binding assay to map H7-specific BTRE-binding epitopes in $FliC_{H7}$ and $FliD_{H7}$.

5.3 Results

5.3.1 Generation of $FliC_{H7}$ flagella receptor candidates from the BTRE

To generate some candidates for BTRE $FliC_{H7}$ flagella receptors, far-co-immunoprecipitation of BTRE cell lysates with sheared $FliC_{H7}$ flagella was carried out. However, as can be seen in figure 5.3, there was no difference between beads

linked to α-H7/$FliC_{H7}$ compared to the same beads without $FliC_{H7}$ by SDS-PAGE. This is probably because the antibody recognition site in $FliC_{H7}$ is likely to be in the same region as BTRE binding epitopes. $FliC_{H7}$ would therefore be unable to bind BTRE proteins because the binding sites would be occupied by α-H7 unless they were able to displace this high-affinity interaction.

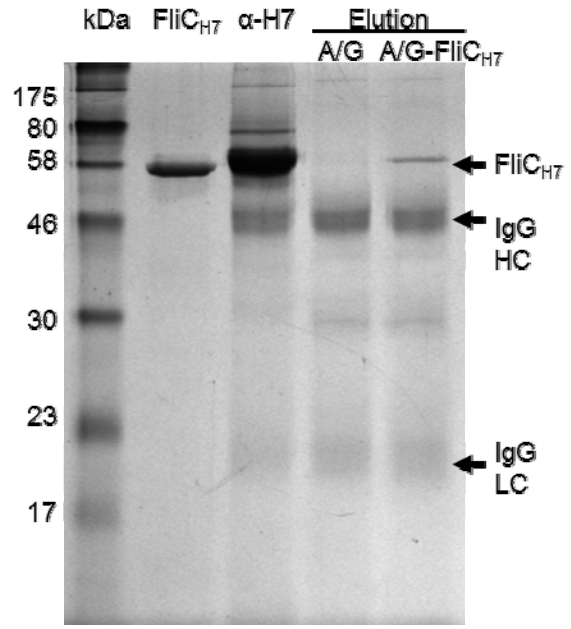

Figure 5.3. SDS-PAGE analysis of samples from co-immunoprecipitation of α-H7 and sheared $FliC_{H7}$ flagella with BTRE cell lysates (A/G-$FliC_{H7}$, methods 2.5.2 and 2.9.3). Pre-cleared protein A/G beads with α-H7 alone were used as a negative control (A/G). IgG heavy chain (IgG HC), IgG light chain (IgG LC).

To avoid this, $FliC_{H7}$ flagella were instead linked to cyanogen-bromide (CnBr) activated sepharose beads. Cross-linking occurs at free amine groups and so cross-linking to the beads occurs more randomly, allowing $FliC_{H7}$ flagella and the binding epitopes to be presented in a variety of ways. In this case though, the cross-linking efficiency of $FliC_{H7}$ flagella to the beads was very low. However, a faint $FliC_{H7}$-

specific band was detectable at high contrast after imaging the protein-stained 12% SDS-PAGE gel (Figure 5.4). This band was excised from the gel and analysed by mass-spectrometry at Moredun Research Institute. This identified the cell-lysate equivalent band as bovine β-actin (ACTB1), a component of bovine cytoskeletal actin.

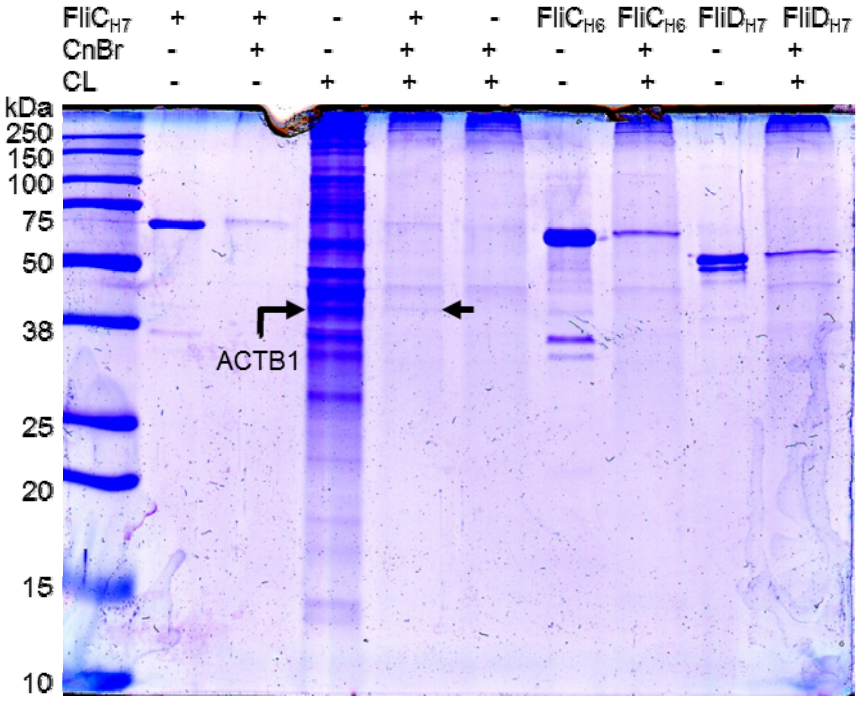

Figure 5.4. SDS-PAGE analysis of pull-down with BTRE cell lysates (CL, methods 2.9.4) with sheared $FliC_{H6}$ or $FliC_{H7}$ flagella or recombinant $FliD_{H7}$ linked CnBr beads. Pre-cleared empty beads were used as a negative control. Arrows indicate protein bands that were excised and the one identified as β-Actin (ACTB1) by mass spectrometry (methods 2.9.4 and 2.5.7).

To confirm this finding, far-Western blots were carried out with purified human platelet actin (Cytoskeleton Inc., figure 5.5). Actin from platelets is a mixture of β and γ cytoskeletal isotypes, which are highly conserved between cows and humans. Probing Western-blots of this actin with sheared $FliC_{H6}$ and $FliC_{H7}$ flagella and recombinant $FliD_{H7}$ showed that none of these bound to actin in this setting, but to gelsolin instead. This may be due to a binding interaction that is conformation

specific, so undetectable where actin is denatured. However, it could also be because actin was pulled down indirectly. $FliC_{H7}$ flagella could have bound an actin binding protein that pulled down actin with it, as indicated by the gelsolin binding. Actin is a large component of the cytoskeleton and would therefore be far more detectable because of its sheer quantity in the cell lysate.

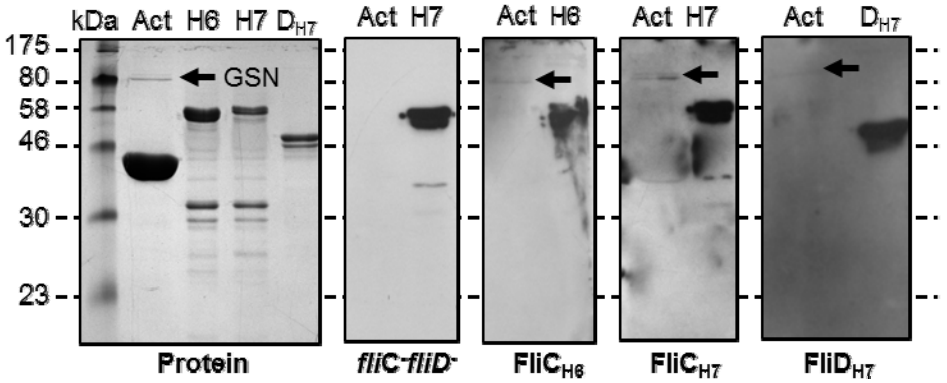

Figure 5.5. Far-Western blots of $FliC_{H6}$ and $FliC_{H7}$ flagella and recombinant $FliD_{H7}$ (D_{H7}) with βγ actin (Act, methods 2.5.3.1). $FliC_{H6}$ and $FliC_{H7}$ flagella used were purified by acid depolymerisation. The same protocol was applied to TUV*fliC*⁻*fliD*⁻ (*fliC*⁻*fliD*⁻) as a negative control. $FliC_{H6}$ was detected with α-H6, $FliC_{H7}$ and *fliC*⁻*fliD*⁻ were detected with α-H7, both followed by α-rabbit IgG-HRP. $FliD_{H7}$ was detected with α-His followed by α-mouse IgG-HRP. Bands indicated by arrows were excised and identified by peptide-mass fingerprinting at Moredun Research Institute as Gelsolin (GSN).

To generate more receptor candidates, far-Western blots of BTRE cell lysates were carried out and probed with sheared $FliC_{H7}$ flagella (figure 5.6(B)) and recombinant $FliD_{H7}$ (figure 5.6(C)). This resulted in similar non-specific binding patterns, but both also had a high intensity band between 17-24 kDa. As there were a lot of proteins at that size (figure 5.6(A)), the experiment was repeated using 20% SDS-PAGE gels instead of 12%. This reduced the number of proteins present in one band, and therefore the number of potential false-positive identifications. It also gave a more accurate indication of molecular weight due to the higher resolution of smaller proteins. Figure 5.7 shows that doing this split the high intensity band into at least 2 strong bands for $FliC_{H7}$ flagella. These bands are present for $FliD_{H7}$ too, but at a

lower intensity. Removal of N-linked sugars by PNGase-F or O-linked sugars by O-Glycosidase appeared to make these bands more intense and sharp, particularly for $FliD_{H7}$. This was also the case with lysates from tunicamycin treated cells (data not shown). Together, this indicates that $FliC_{H7}$ flagella and $FliD_{H7}$ are interacting with the protein component of that band, not any glycan present.

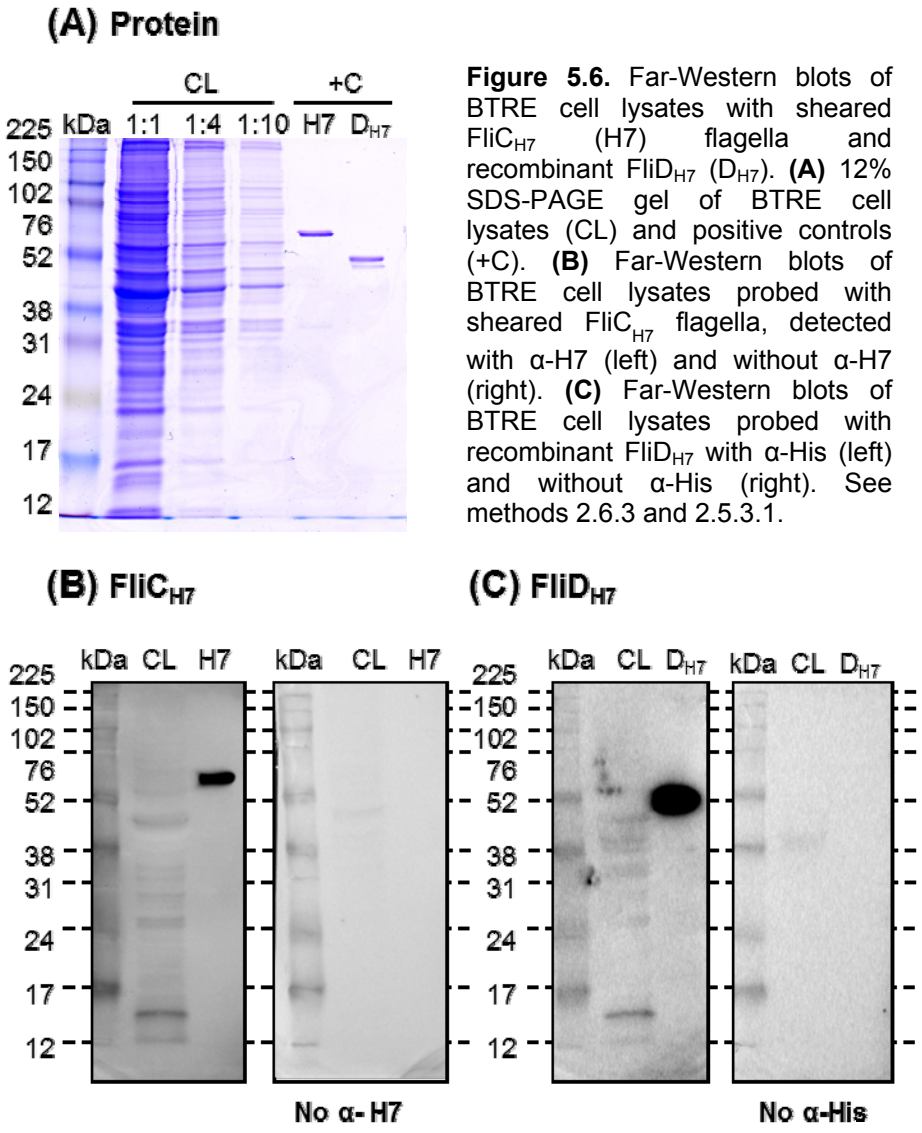

Figure 5.6. Far-Western blots of BTRE cell lysates with sheared $FliC_{H7}$ (H7) flagella and recombinant $FliD_{H7}$ (D_{H7}). **(A)** 12% SDS-PAGE gel of BTRE cell lysates (CL) and positive controls (+C). **(B)** Far-Western blots of BTRE cell lysates probed with sheared $FliC_{H7}$ flagella, detected with α-H7 (left) and without α-H7 (right). **(C)** Far-Western blots of BTRE cell lysates probed with recombinant $FliD_{H7}$ with α-His (left) and without α-His (right). See methods 2.6.3 and 2.5.3.1.

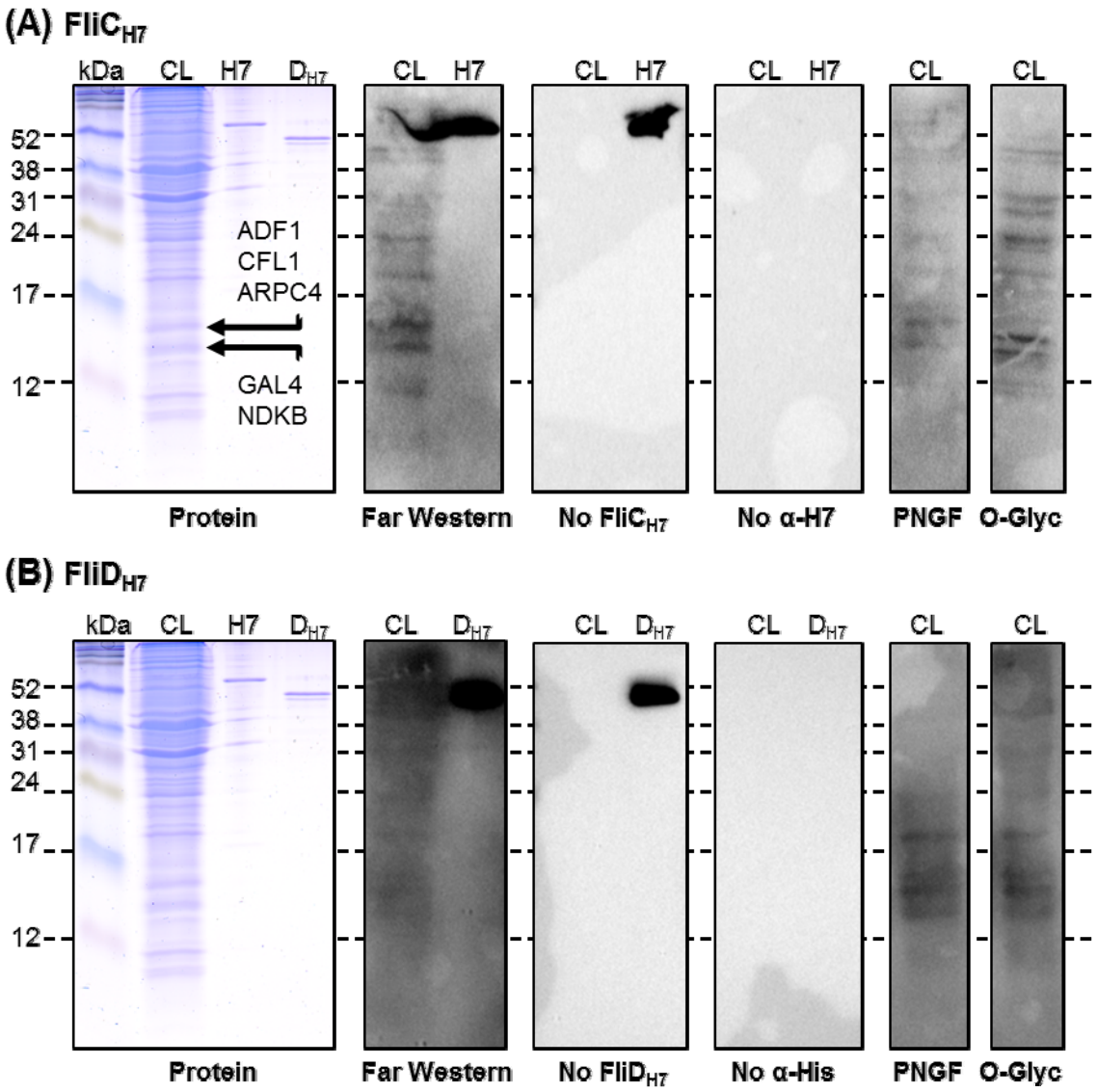

Figure 5.7. Far-Western blots of BTRE cell lysates (CL) using 20% SDS-PAGE gels to further resolve low molecular weight bands, +/- N and O-linked sugars. **(A)** Far-Western blots probed with sheared FliC$_{H7}$ flagella (H7) with no protein and no α-H7 controls, with PNGase-F (PNGF, New England Biolabs) and O-Glycosidase (O-Glyc, New England Biolabs) treatment to remove N-linked or O-linked glycans in-situ as indicated. **(B)** Far-Western blots probed with recombinant FliD$_{H7}$ (D$_{H7}$), as with **(A)**. Indicated bands were excised from 2 different cell lysates and identified as ADP-ribosylation factor 1 (ADF1), cofilin-1(CFL1), arp2/3 complex subunit 4 (ARPC4) and galectin-4, nucleoside diphosphate kinase B (NDKB) by tandem mass spectrometry peptide mass fingerprinting at Moredun Research Institute.

The two strongest bands in figure 5.7 (indicated by arrows) were carefully overlaid and identified on the SDS-PAGE gel, excised and analysed by tandem-mass spectrometry at Moredun Research Institute (section 2.5.7). This was done more than once, with at least two different cell lysates to reduce error in band excision. The upper band was identified as containing cofilin-1 (CFL1), ADP-ribosyltransferase 1 (ADF1) and arp2/3 complex subunit 4 (ARPC4). The lower band contained galectin-4 and nucleoside di-phosphate kinase B (NDKB). From these experiments a list of potential BTRE receptors has been generated: gelsolin, cofilin-1, ARPC4, galectin-4 and nucleoside di-phosphate kinase B. These are all actin-binding proteins.

5.3.2 Confirmation of $FliC_{H7}$ flagella BTRE receptors

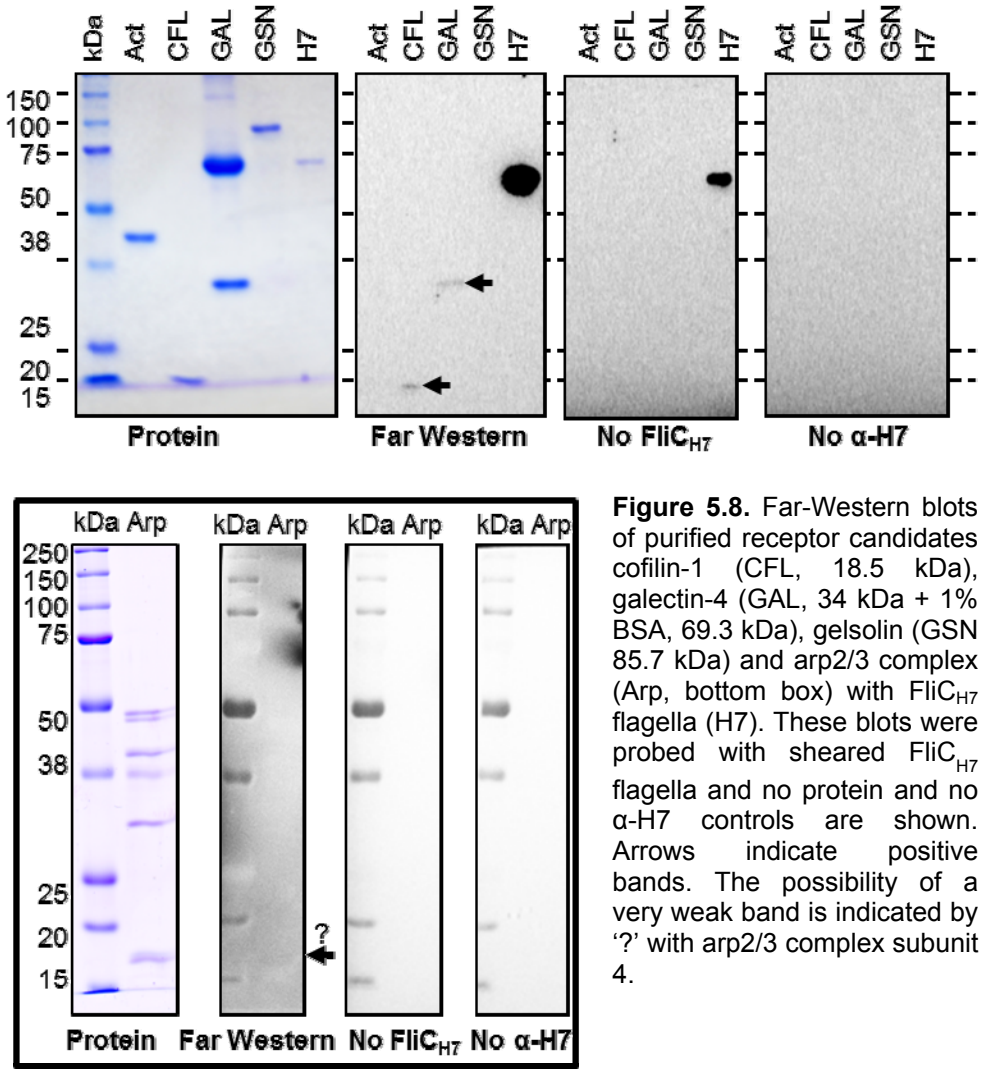

Figure 5.8. Far-Western blots of purified receptor candidates cofilin-1 (CFL, 18.5 kDa), galectin-4 (GAL, 34 kDa + 1% BSA, 69.3 kDa), gelsolin (GSN 85.7 kDa) and arp2/3 complex (Arp, bottom box) with $FliC_{H7}$ flagella (H7). These blots were probed with sheared $FliC_{H7}$ flagella and no protein and no α-H7 controls are shown. Arrows indicate positive bands. The possibility of a very weak band is indicated by '?' with arp2/3 complex subunit 4.

The first step was to see if these candidates were the proteins being bound to in figure 5.6 and 5.7. To do this, far-Westerns with available purified proteins were undertaken. ADF1 was unavailable at the time and NDKB was also not purchased as there were many isotypes with alternative splice-forms which would have been impractical to test.

As seen in figure 5.8, $FliC_{H7}$ flagella bound to recombinant human cofilin-1 and recombinant human galectin-4. There may be a very faint band for ARPC4, but it was not included in further tests in the light of more promising candidates. $FliD_{H7}$ was not shown to bind to any of these purified candidates by far-Western blot (figure 5.9). This indicates that $FliD_{H7}$ binding in figure 5.7 was non-specific.

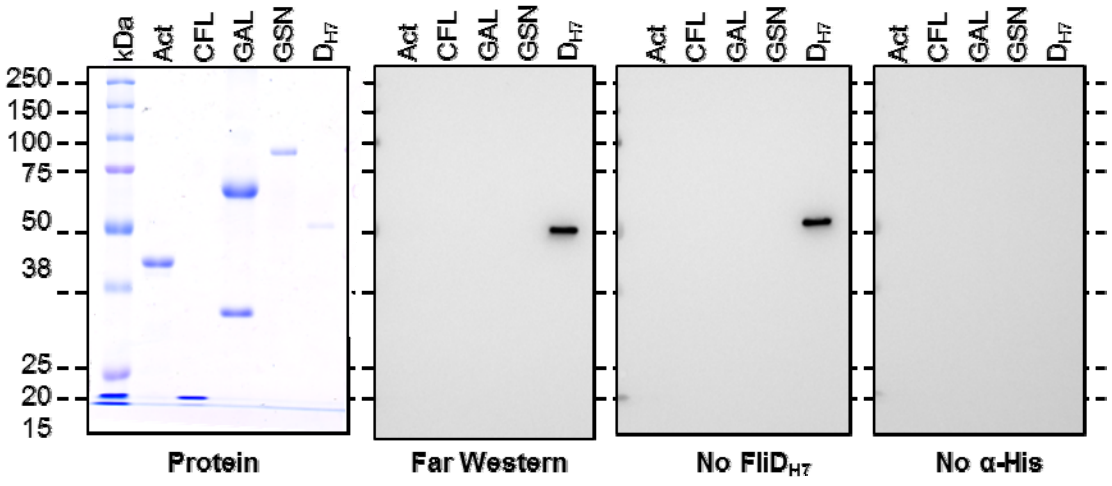

Figure 5.9. Far-Western blots of purified receptor candidates cofilin-1 (CFL, 18.5 kDa), galectin-4 (GAL, 34 kDa + 1% BSA, 69.3 kDa) and gelsolin (GSN 85.7 kDa) probed with $FliD_{H7}$ (D_{H7}). No protein and no α-His controls are shown.

Figure 5.10 shows Western-blots confirming the presence of cofilin-1 at ~18 kDa and galectin-4 at ~17 kDa in the cell lysates. This is important as the full-length galectin-4 is 36 kDa, but it was detected at ~17 kDa, probably due to degradation during lysate preparation or storage. Galectin-4 was first discovered as a 17 kDa C-terminal fragment in rat intestine extracts (Leffler *et al.*, 1989), the N-terminal having been lost by degradation due to sample handling. It is therefore likely that

$FliC_{H7}$ flagella bound cofilin-1 in the upper band and galectin-4 in the lower band in the far-Western blot with BTRE cell lysates.

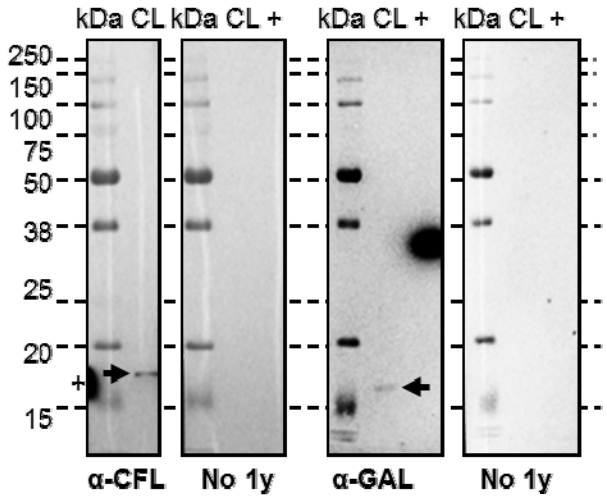

Figure 5.10. Western-blots of BTRE cell lysates (CL) to confirm the presence of cofilin-1 with α-cofilin-1 (α-CFL) and galectin-4 with α-galectin-4 (α-GAL, arrows).

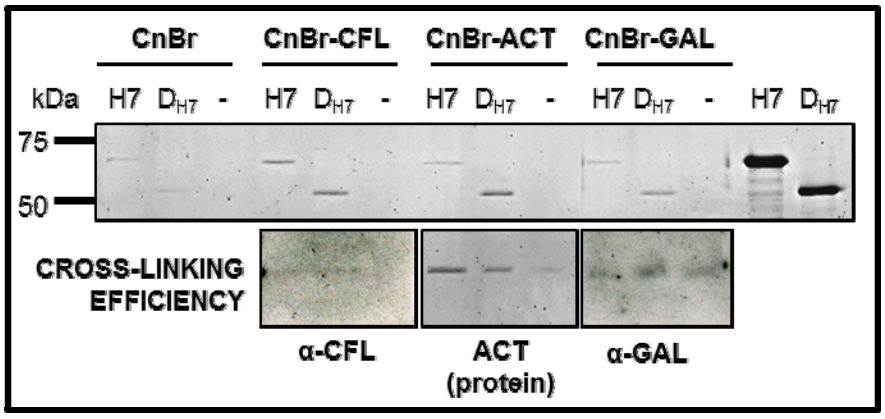

Figure 5.11. Pull-downs of sheared $FliC_{H7}$ flagella (H7) and recombinant $FliD_{H7}$ (D_{H7}) with cofilin-1 (CFL), βγ-Actin (ACT) and galectin-4 (GAL) linked CnBr beads. Empty beads and actin-linked beads were used as negative controls. Coating efficiency of the candidate receptors with the CnBr beads by Western blot (unless stated) is represented in the lower panel.

Pull-downs and ELISAs were carried out with purified cofilin-1 and galectin-4 to see if their interaction with $FliC_{H7}$ flagella was genuine. Actin was used as a negative control. The cross-linking efficiencies of purified candidate proteins to the CnBr-

activated sepharose beads were variable (figure 5.11, lower panel), with actin most efficient and detectable by protein staining, and cofilin-1 barely detectable by Western-blot with specific antibodies. Galectin-4 was not detectable by protein staining, but was easily detectable as 2 species by Western-blot (36 kDa, and 17 kDa shown). However, even with cofilin-1 barely detectable on the beads, the amount of $FliC_{H7}$ flagella and $FliD_{H7}$ that was recovered is quite remarkable. This is particularly the case as $FliD_{H7}$ did not appear to bind to denatured cofilin-1. As this experiment was not quantitative, ELISAs were performed to better test the binding interactions of these proteins with one another.

ELISAs confirmed that $FliC_{H7}$ flagella specifically bind to cofilin-1. $FliC_{H7}$ flagella bound to galectin-4 at lower levels and bound to actin at much lower levels still (figure 5.12(A)). $FliD_{H7}$ also bound to cofilin-1, at seemingly lower levels, and galectin-4 comparably, but not at all to actin (figure 5.12(C)). This indicates that $FliD_{H7}$ interacts with native cofilin-1 and galectin-4.

It is difficult to make precise quantitative comparisons between flagella proteins tested given that different antibody pairings were used. Data were normalised to the positive and negative detection controls (methods 2.9.1). Quantification by densitometry is not so accurate that the discrepancies still present after normalisation would make much difference to the analysis. With this caveat in mind though, statistical analysis was only carried out between candidate proteins binding to the same flagella protein, and all other comparisons are qualitative.

Flagella from other entero-pathogenic bacteria were tested, to see how generic these binding interactions might be, or whether they were $FliC_{H7}$ flagella-specific. $FliC_{H6}$ flagella from entero-pathogenic *E. coli* O126:H6 also bound to cofilin-1, very slightly to actin and not at all to galectin-4 (figure 5.12(B)). Interestingly, phase-1 ($FliC_{P1}$, figure 5.12(D)) and phase 2 ($FljB_{P2}$, figure 5.12(E)) flagella from *S.*

Typhimurium both bound at low levels to cofilin-1 and galectin-4, but very highly to actin, showing the opposite phenotype to the *E. coli* flagella proteins tested.

Looking at the coat only controls in figure 5.12, where no receptor candidate was coated to the well, a certain amount of background binding is apparent with $FliC_{H7}$, $FliC_{P1}$ and $FljB_{P2}$ flagella. This is despite using Carbo-free blocking (VectorLabs, methods 2.5.3) and stringent conditions (0.1% Tween-20). However, binding is dose-dependent, and some receptors show very efficient blocking of binding, for example, cofilin-1 for $FliC_{P1}$ flagella binding. Also, $FliC_{H7}$ flagella and $FliD_{H7}$ binding to cofilin-1 correlates with results from other assays.

Figure 5.12. Far-ELISAs of flagella proteins from enteropathogenic bacteria binding to $FliC_{H7}$-BTRE receptor candidates (methods 2.9.1.4). Actin (ACT), cofilin-1 (CFL) and galectin-4 (GAL) were coated to ELISA plates, and probed with **(A)** $FliC_{H7}$ from TUV*fliC*$_{H7}$, **(B)** $FliC_{H6}$ from TUV*fliC*$_{H6}$, **(C)** recombinant $FliD_{H7}$ **(D)** $FliC_{P1}$ from *S.* Typhimurium SL1344Δ*fljB* and **(E)** $FljB_{P2}$ from *S.* Typhimurium SL1344Δ*fliC*. Flagellins were purified as sheared flagella. Left panels show a representative example of an ELISA, with detection controls of the probe coated to the plate, with primary antibody (+) and without (-). Right panels show the final results. Statistical analysis involved pairwise comparisons with actin; P≤0.05 (*), p ≤0.001 (**) p ≤0.0001 (***).

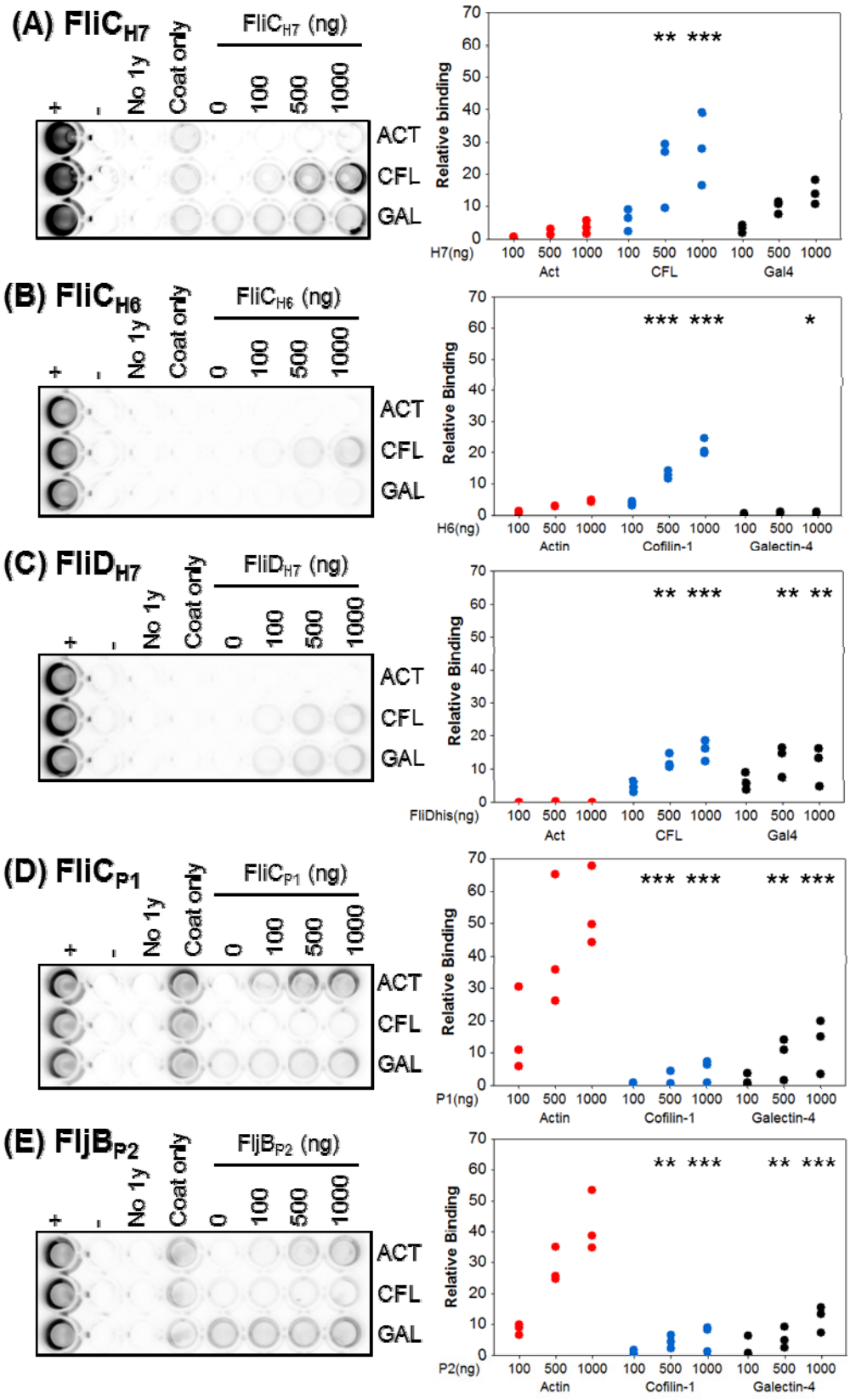
(A) FliC$_{H7}$
FliC$_{H7}$ (ng)
+
-
No 1y
Coat only
0
100
500
1000
ACT
CFL
GAL
Relative binding
** ***
H7(ng)
Act
CFL
Gal4
(B) FliC$_{H6}$
FliC$_{H6}$ (ng)
*** ***
*
H6(ng)
Actin
Cofilin-1
Galectin-4
(C) FliD$_{H7}$
FliD$_{H7}$ (ng)
** ***
** **
FliDhis(ng)
(D) FliC$_{P1}$
FliC$_{P1}$ (ng)
*** ***
** ***
P1(ng)
(E) FljB$_{P2}$
FljB$_{P2}$ (ng)
** ***
** ***
P2(ng)
Relative Binding

5.4 Discussion

The expectation was that $FliC_{H7}$ flagella receptors from the BTRE would be extracellular, yet initial results identified predominantly intracellular receptor candidates. Only galectin-4 is extracellular, and only for some of the time, when it is secreted out of cells and associated with membrane-bound proteins (Leffler *et al.*, 1989). These initial results were quite subtle and may have been discounted as artefactual were it not for previous observations of flagella penetration into host cells (figure 3.3-3.6). For instance, the lack of extracellular proteins may have related to the method cell lysate preparation by freeze-thaw cycles (methods 2.6.3).

Using freeze-thaw cycles to extract cellular proteins may have depleted membrane proteins from cell lysates. This is because after five freeze-thaw cycles, cell membranes from the lysates were removed by centrifugation. However, cell lysis is likely to cause some dissociation of membrane proteins before fractionation. Therefore membrane proteins may still be present, but in reduced amounts. Recovery of surface-associated proteins that are not membrane-anchored, such as galectin-4, should not be affected by this method of cell lysis. It is unknown but the cofilin-1 detected by far-Western could initially have been associated with the cytosolic leaflet of the cell membrane via a phosphatidylinositol 4,5-bisphosphate anchor (Zhan *et al.*, 2003).

Confidence was gained in the initial results by the fact that under the conditions tested, all $FliC_{H7}$ flagella candidate receptors were actin-binding proteins. Not only that, but they appear to be proteins that skew the actin dynamics towards lamellipodia and filopodia formation (figure 5.13). This is intriguing, given that *E. coli* O157:H7 are already known to alter actin dynamics in this way to create actin pedestals. These results were also reinforced by the ELISA data. These experiments not only validated candidate binding interactions, but showed that this type of interaction was more generic. Flagella were shown to bind to eukaryotic cytoskeletal proteins with four types of flagella from species of two different genera.

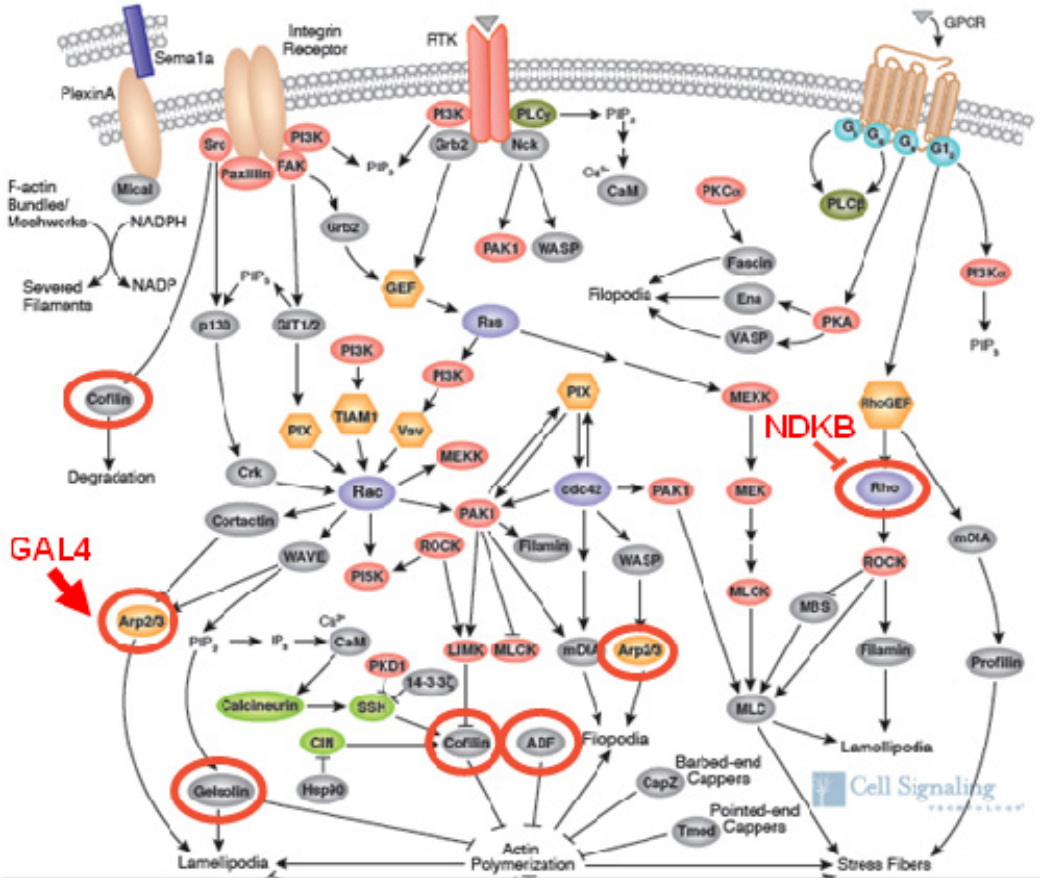

Figure 5.13. Regulation of actin dynamics by actin-binding receptor candidates. Receptor candidates are highlighted in red on an actin dynamics regulation reference pathway altered from Cell Signalling.

$FliC_{H7}$ flagella binding to cofilin-1 and galectin-4 was shown by far-Western, pull-down and ELISA (figure 5.8, 5.11 and 5.12 respectively). $FliD_{H7}$ binding to cofilin-1 and galectin-4 was shown by pull-down and ELISA, but was negative by far-Western (figure 5.11, 5.12 and 5.9). This confirmed that $FliD_{H7}$ binding to initial far-Western blots of BTRE cell lysates (figure 5.6) was non-specific. Perhaps $FliD_{H7}$ only binds conformational epitopes that were not present on a Western-blot. The actin binding phenotype of $FliC_{H7}$ flagella and $FliD_{H7}$ was less clear. $FliC_{H7}$ flagella were shown to bind to actin by ELISA, but probably not by pull-down, whereas $FliD_{H7}$ was shown

to bind to actin by pull-down, but this was not confirmed by ELISA. Candidate protein coating levels in the ELISAs were much more consistent than cross-linking efficiencies were for pull-downs and therefore more easily comparable. As actin was very efficiently cross-linked to the beads, a positive result with $FliD_{H7}$ by pull-down, where it is negative by ELISA, may simply indicate non-specific binding to a highly abundant protein.

$FliC_{H6}$ flagella had a very similar binding phenotype to $FliC_{H7}$ flagella by ELISA, though more experiments are warranted to confirm this. The only difference between $FliC_{H6}$ and $FliC_{H7}$ flagella binding by ELISA was that $FliC_{H6}$ flagella did not bind to galectin-4. This indicates, unsurprisingly, as cofilin-1 is ubiquitously expressed (Vartiainen *et al.*, 2002), that cofilin-1 is not the BTRE-specific receptor for $FliC_{H7}$ flagella. Unless galectin-4 is the BTRE-specific receptor in this case, this binding assay cannot be used for BTRE-specific epitope mapping of $FliC_{H7}$. More work is necessary to see if galectin-4 is the BTRE-specific receptor for $FliC_{H7}$ flagella.

Flagella from *S.* Typhimurium were also tested for their ability to bind actin, cofilin-1 and galectin-4, to see how generic these binding interactions might be. These flagella were also able to bind to these intracellular proteins. However, they did have a different binding phenotype compared to $FliC_{H7}$ and $FliC_{H6}$ flagella from *E. coli*. *Salmonella* flagella were able to bind actin directly, at higher levels than cofilin-1 or galectin-4. This finding lead colleagues Johanna Elvidge and Amin Tahoun to observe by confocal microscopy the coincidence of $FliC_{P1}$ and $FljB_{P2}$ flagella with cytoskeletal actin in human, porcine and bovine epithelial cells. *Salmonella* flagella bind directly to actin, while *E. coli* flagella appear to bind to an actin-binding protein more than to actin. This is particularly interesting, given the different lifestyles of invading *S.* Typhimurium and attaching and effacing *E. coli.* Further biochemical and phenotypic tests are needed to confirm these binding interactions, but a theme appears to have emerged in which bacterial flagella interact with the eukaryotic cytoskeleton.

The work detailed in this chapter has confirmed $FliC_{H7}$ flagella binding to some candidates in defined conditions, but has not ruled out binding interactions with the other candidates in different conditions. That aside, $FliC_{H7}$ flagella are able to interact with cofilin-1 and this protein is intracellular. $FliC_{H7}$ flagella have been observed inside host cells, in areas coincident with BTRE cell actin (chapter 3), have pulled down actin from BTRE cell lysates (figure 5.4) and don't seem to bind to cytoplasmic actin as well as cofilin-1 (figure 5.12). Taken together, this indicates that the $FliC_{H7}$ flagella interaction with cofilin-1 may be biologically relevant.

5.5 References

Erdem, A. L., Avelino, F., Xicohtencatl-Cortes, J. & Girón, J. a. **(2007).** Host protein binding and adhesive properties of H6 and H7 flagella of attaching and effacing *Escherichia coli*. *Journal of bacteriology* **189**, 7426–35.

Leffler, H., Masiarz, F. R. & Barondes, S. H. (1989). Soluble lactose-binding vertebrate lectins: a growing family. *Biochemistry* **28**, 9222–9.

Vartiainen, M. K., Mustonen, T., Mattila, P. K., Ojala, P. J., Thesleff, I., Partanen, J. & Lappalainen, P. (2002). The three mouse actin-depolymerizing factor/cofilins evolved to fulfill cell-type-specific requirements for actin dynamics. *Molecular biology of the cell* **13**, 183–94.

Zhan, Q., Bamburg, J. R. & Badwey, J. A. (2003). Products of phosphoinositide specific phospholipase C can trigger dephosphorylation of cofilin in chemoattractant stimulated neutrophils. *Cell motility and the cytoskeleton* **54**, 1–15.

6 : Flagella interactions with cytoskeletal proteins

The type of proteins found to bind to flagella in the previous chapter was intriguing, and raises a number of questions. This is because the eukaryotic cytoskeleton is such a complex, responsive and highly regulated system that it is hard to imagine bacterial flagella binding to its components without affecting its homeostasis in some way. So, what sort of effects could the penetrating flagella be having on the cytoskeleton? Perhaps cytoskeletal proteins have an effect on the bacterial flagella. It is possible that either could be beneficial to bacterial colonisation or host innate pathogen recognition.

6.1 Effect of cofilin-1 on $FliC_{H7}$ flagella

$FliC_{H7}$ flagella bind to cofilin-1. However, it is not known how this occurs. Both $FliC_{H7}$ flagella and $FliD_{H7}$ were able to bind to cofilin-1, so it is likely that both are involved. It is possible that $FliC_{H7}$ is more involved than $FliD_{H7}$, as it is present in higher quantities. Also, unlike $FliC_{H7}$ flagella filaments, $FliD_{H7}$ did not bind to linear epitopes of cofilin-1. Sheared flagella preparations are a mixture of filaments, with and without FliD caps, and FliC monomers. It may be that the repeating epitopes of an intact $FliC_{H7}$ flagella filament were required to detect cofilin-1 binding, but it is also possible that the binding being detected was just $FliC_{H7}$ monomer.

Perhaps cofilin-1 is interacting with $FliC_{H7}$ flagella as it would interact with actin. Like actin, $FliC_{H7}$ flagella are filamentous. Cofilin-1 can bind, depolymerise and sever actin filaments (Bobkov *et al.*, 2006). It can also bind actin monomers (Andrianantoandro & Pollard, 2006). It may be that cofilin-1 binds to $FliC_{H7}$ flagella filaments, affects their stability and consequently the amount of $FliC_{H7}$ monomer. This is particularly relevant, as FliC monomers are detected by flagella pattern recognition receptors with a much greater sensitivity than FliC filaments (Andersen-Nissen *et al.*, 2007). Or cofilin-1 could be binding directly to $FliC_{H7}$ monomers, either sequestering them, or conversely, delivering them to pattern recognition receptors.

6.2 Effect of $FliC_{H7}$ flagella on the actin cytoskeleton

By interacting with cofilin-1, $FliC_{H7}$ flagella may be indirectly affecting actin dynamics. This could be passively, simply by reducing the amount of locally available cofilin-1 to interact with actin by sequestration. However, $FliC_{H7}$ flagella could play a more active role, by making cofilin-1 more readily available to interact with actin, as a scaffold protein might. It is difficult to predict what effects either of these modes of action would have on actin dynamics, as the role of cofilin-1 varies depending on its stoichiometry with actin (Andrianantoandro & Pollard, 2006). At equimolar ratios, cofilin-1 binds and stabilises actin filaments. When there is more actin than cofilin-1, cofilin-1 severs filaments, creating more faster-growing (+) ends, with a net result of actin polymerisation or depolymerisation, depending on the complement of other host factors (Van Troys *et al.*, 2008). When there is more cofilin-1 than actin, cofilin-1 coats actin filaments and nucleates monomeric actin; the net result is actin polymerisation (Andrianantoandro & Pollard, 2006). Of course, $FliC_{H7}$ flagella may interact with actin directly as suggested by ELISAs in the previous chapter. This could also potentially alter actin dynamics.

Results from the previous chapter indicate that other flagella may be able to interact with cytoskeletal proteins. The same questions about actin dynamics that have been posed about $FliC_{H7}$ flagella interactions with cofilin-1 and actin are also applicable to $FliC_{H6}$ flagella and *Salmonella* $FliC_{P1}$ and $FljB_{P2}$ flagella. In trying to answer these questions, it will be possible to confirm whether these flagella bind actin and cofilin-1 or not.

6.3 Aims

- To see whether cofilin-1 binds to $FliC_{H7}$ monomers or flagella filaments.
- To see if cofilin-1 affects $FliC_{H7}$ flagella filament stability.
- To see if $FliC_{H7}$ flagella and other types of flagella can affect actin dynamics directly or indirectly.

6.4 Results

6.4.1 Characterisation of cofilin-1 binding to $FliC_{H7}$ flagella and flagellin

To see which component of $FliC_{H7}$ flagella cofilin-1 binds to, sheared $FliC_{H7}$ flagella preparations needed to be separated into filament and monomer fractions. Whole flagella filaments are bigger than flagellin monomers, so ultra-centrifugation was used to pellet $FliC_{H7}$ flagella filaments, while $FliC_{H7}$ monomers were retained in the supernatant. Cofilin-1 is smaller than $FliC_{H7}$ (18 kDa < 60 kDa); at the centrifugal force used and in the absence of any other proteins, it remains in the supernatant. This is an ideal basis for co-sedimentation studies; if the smaller protein binds the larger protein complex, it would be recovered in the pellet fraction.

The activity of cofilin-1 is very pH dependent; at pH 6.8 cofilin-1 primarily exhibits actin binding activity, whereas at pH 8.0 cofilin-1 mainly severs actin (Pavlov & Muhlrad, 2006). However, incubation of equimolar concentrations of cofilin-1 and $FliC_{H7}$ flagella preparations at either pH 6.8 or pH 8.0 did not alter the sedimentation of cofilin-1 (figure 6.1, left lower panel). It was instead apparent that cofilin-1 altered the sedimentation properties of $FliC_{H7}$ flagella, so that more was present in supernatant fractions at pH 8.0 (figure 6.1).

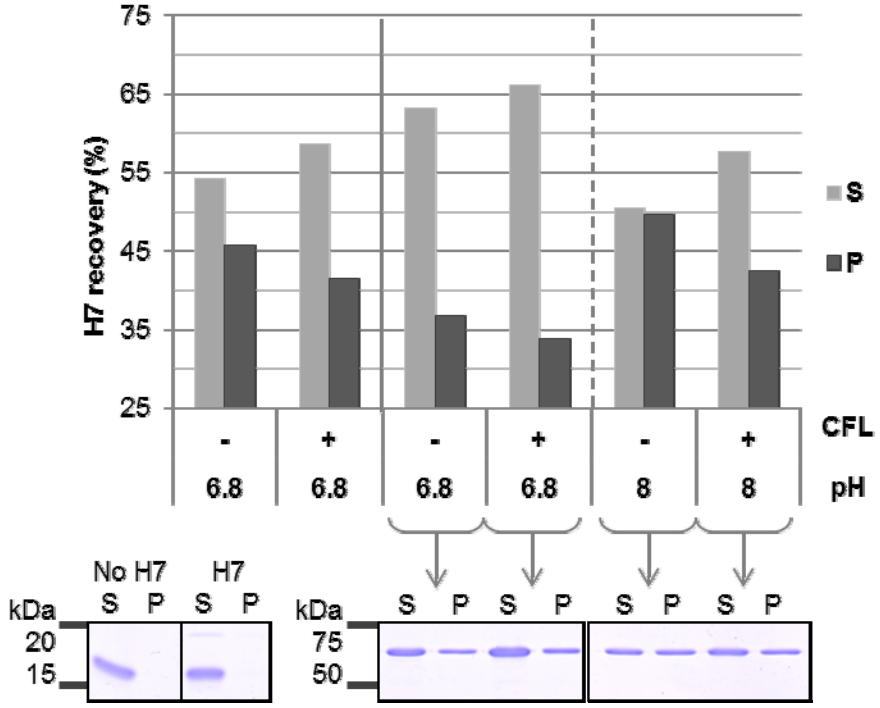

Figure 6.1. Effect of cofilin-1 on $FliC_{H7}$ flagella by co-sedimentation assay (methods 2.9.5). Equimolar amounts of $FliC_{H7}$ flagella (H7) and cofilin-1 (CFL) were incubated and ultra-centrifuged. Equivalent amounts of resulting supernatants (S) and pellets (P) were analysed by 12% SDS-PAGE and densitometry. The lower panel shows the cofilin-1 bands on the left (18kDa) and the $FliC_{H7}$ bands on the right (60kDa) in an SDS-PAGE gel that were analysed for the experiment directly above it. $FliC_{H7}$ recovery in each fraction is represented as a % of total $FliC_{H7}$ in the specific reactions. The vertical solid line separates reactions which are independent experiments – the dashed line separates reactions which were performed in parallel.

To see if the cofilin-1 would have the same effect on native $FliC_{H7}$ flagella, co-sedimentation of cofilin-1 was undertaken with live *E. coli* O157:H7 (figure 6.2). Again, no cofilin-1 was detected in pellet fractions. In all but one of these experiments, addition of cofilin-1 resulted in a reduction in bacteria-associated flagella. This is particularly apparent at pH 8.0, the pH that enhances cofilin-1 severing of actin (Bernstein *et al.*, 2000). Perhaps cofilin-1 is severing $FliC_{H7}$ flagella. This is in-line with the results from figure 6.1, which also show an increase in supernatant $FliC_{H7}$. These results rule out a high affinity interaction of cofilin-1 with $FliC_{H7}$ flagella filaments, as there was no co-sedimentation. However, they do

indicate that cofilin-1 may affect the stability of $FliC_{H7}$ flagella filaments, either by transient interactions with the filaments, or by interacting with $FliC_{H7}$ monomers.

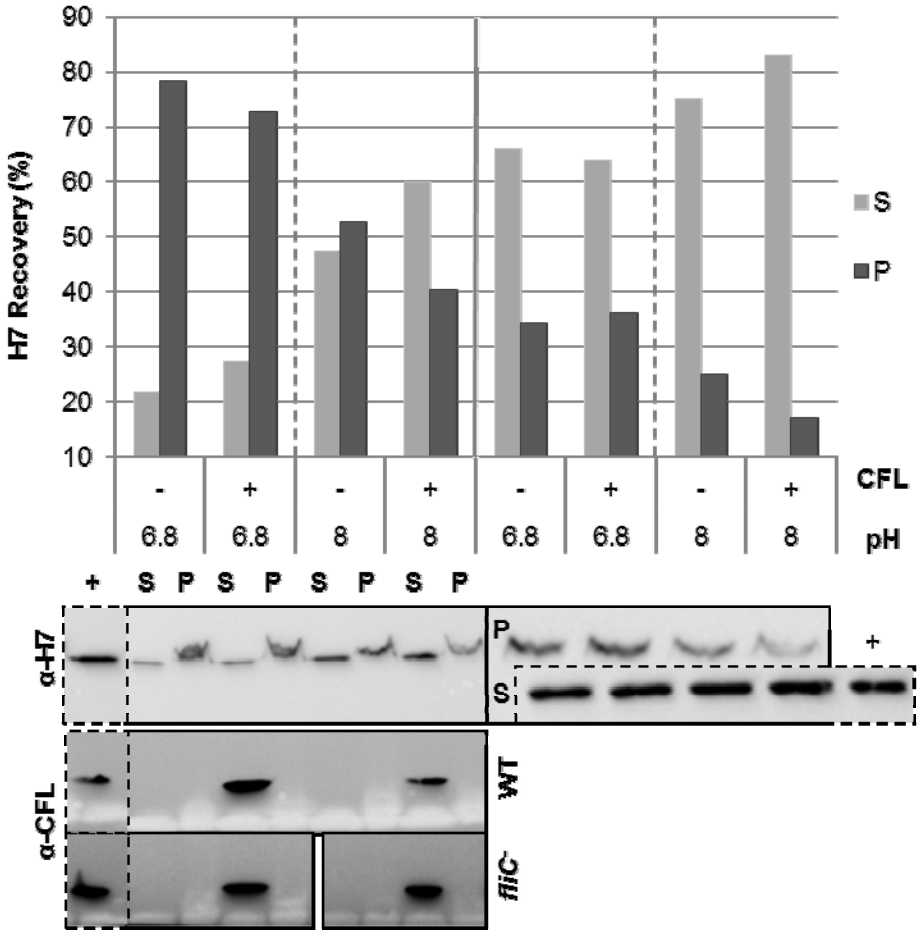

Figure 6.2. Effect of cofilin-1 on bacteria-associated $FliC_{H7}$ flagella. *E. coli* O157:H7 (WT, TUV93-0; *fliC*$^-$, TUV*fliC*$^-$) were incubated with cofilin-1 (CFL) and pelleted by centrifugation (methods 2.9.5). Equivalent supernatant (S) and pellet (P) fractions were analysed by Western-blotting (lower panels) and then densitometry (upper panel). TUV93-0 cultures with cofilin-1 added but not centrifuged were used as a positive control (+) for western blots. $FliC_{H7}$ (H7) recovery was expressed as a percentage of total $FliC_{H7}$ from TUV93-0 detected by α-H7 in each experiment. In the top panel, the vertical solid line separates reactions which are independent experiments – the dashed lines separate reactions which were performed in parallel.

6.4.2 Effect of cofilin-1 on $FliC_{H7}$ flagella

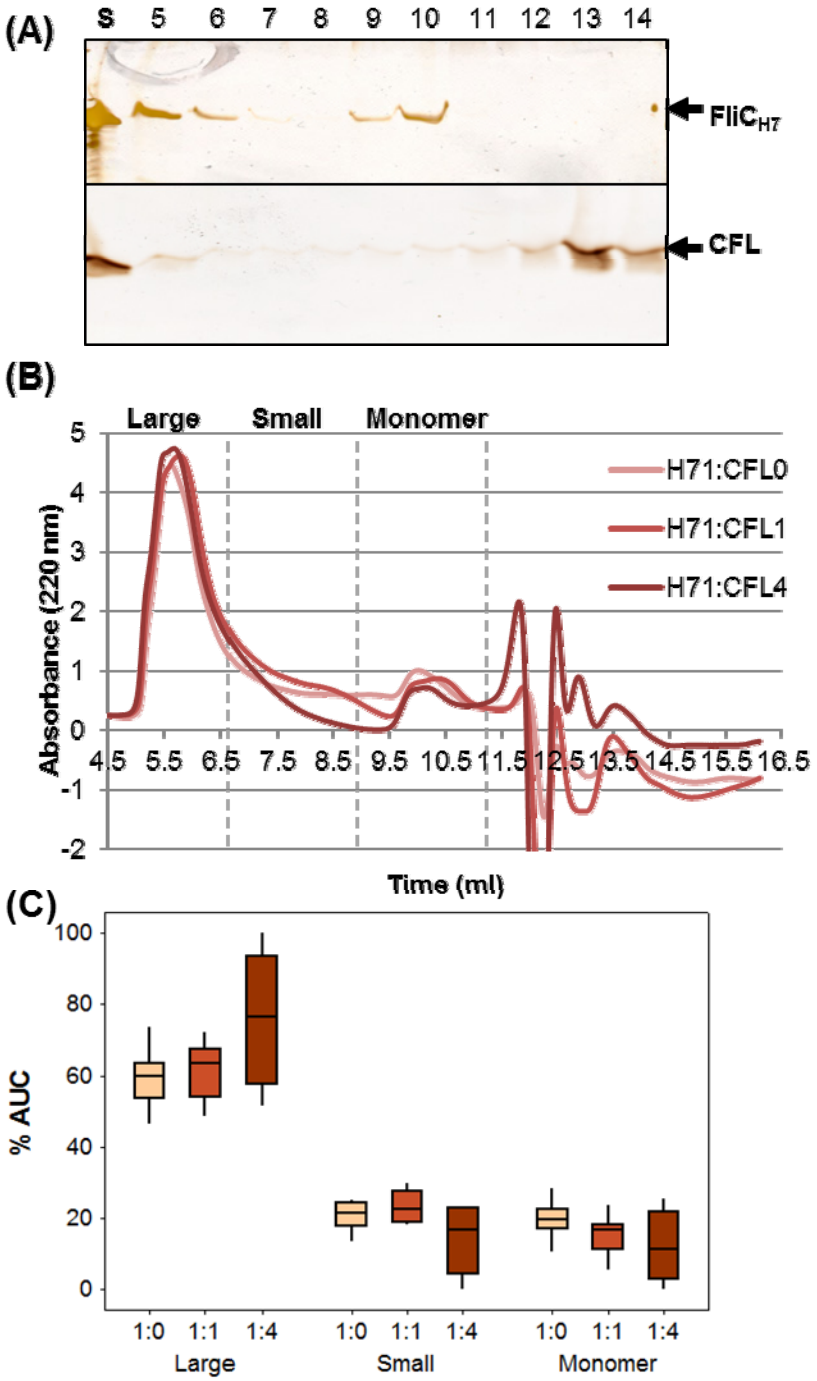

Figure 6.3. Cumulative effect of cofilin-1 on $FliC_{H7}$ flagella at pH 8.0 by size exclusion chromatography (methods 2.9.6). **(A)** Elution profiles of $FliC_{H7}$ flagella (upper panel) and cofilin-1 (CFL, lower panel) size-exclusion chromatography separate test-runs during buffer optimisation. 1 ml elution fractions were collected and analysed by 12% SDS-PAGE and silver staining (methods 2.5.2). Sample run (S). **(B)** Size-exclusion traces of 3 molar ratios of $FliC_{H7}$ (H7) to cofilin-1 (CFL) as indicated. Traces represent the mean of 10 tests. These traces were normalised to each other at the column void volume (4.5 ml) and then the lowest absorbance value was used as a baseline of 0. **(C)** Boxplot of the % area under curve (AUC) of large and small $FliC_{H7}$ filaments and monomers as indicated in **(B)**.

Size-exclusion chromatography separates proteins by size; the time it takes proteins to run through a column matrix is related to the inverse of their size. This method was carried out in an attempt to clarify how cofilin-1 was interacting with $FliC_{H7}$ flagella filaments and monomers. However, 200mM NaCl was required to run cofilin-1 through the column without it binding to the resin (methods 2.9.6). Co-elution of cofilin-1 with $FliC_{H7}$ was not detected by silver staining of SDS-PAGE gels. This is probably because the high salt concentration inhibited interactions between $FliC_{H7}$ and cofilin-1 in the column and therefore co-elution.

Without this clear indicator of which H7 component cofilin-1 was interacting with, the $FliC_{H7}$ elution profile was instead analysed to see how cofilin-1 was affecting $FliC_{H7}$ flagella stability (figure 6.3). Figure 6.3(A) shows the size exclusion profiles of $FliC_{H7}$ and Cofilin-1 when run alone through a 15 ml column (methods 2.9.6). $FliC_{H7}$ elutes at 5-7 ml and 8-9 ml. It is likely that the first elution fractions are $FliC_{H7}$ flagella filaments, while the second lot are $FliC_{H7}$ monomers. Cofilin-1 elutes mainly at 13 ml.

Figure 6.3(B) shows the mean of ten A_{220} nm traces of $FliC_{H7}$ flagella incubated with cofilin-1 at 1:0, 1:1 and 1:4 molar ratios. The first two peaks in the 1:0 trace agree with previous $FliC_{H7}$ flagella elution profiles, showing that these peaks correspond to $FliC_{H7}$. The elution of cofilin-1 is likely to correspond to the peak at 12.5 ml, but it is difficult to confirm this due to the sensitivity of absorbance at 220nm for buffer salts, which also appear to be eluting at that point (figure 2.5).

If cofilin-1 was severing $FliC_{H7}$ filaments, as indicated by figure 6.1 and 6.2, a reduction in the area of the $FliC_{H7}$ filament peak when cofilin-1 was added would be observed. However, this was not the case. If anything, cofilin-1 seemed to cause more of the filament peak to elute a little earlier and have less of a tail. Qualitatively, cofilin-1 seemed to cause a subtle trend towards filament stabilisation. Figure 6.3(C) shows this data divided into large filaments, small filaments and monomers, and expressed as a percentage of the total area under curve (AUC) of each sample. There

was a trend for the largest filaments to increase in % AUC, and the smallest filaments and monomers to decrease in % AUC with increasing amounts of cofilin-1. According to Kruskal-Wallis analyses, these trends caused by cofilin-1 were not statistically significant for large filaments or monomers (df=2, h=3.68, p=0.16 and df=2, h=4.68, p=0.10 respectively) but were for smaller filaments (df=2, h=6.36, p=0.04).

The ten column runs of each molar ratio were measured in series, directly after cofilin-1 was added to $FliC_{H7}$ flagella in each case. As such, these experiments can be considered as time courses, measured at 30 minute intervals. Figure 6.4 shows the same data from figure 6.3(C), over time. Without cofilin-1, the state of $FliC_{H7}$ flagella appears to oscillate slightly between 50% large filaments/30% monomers, and 60-70% large filaments/10-20% monomers (figure 6.4(A)). This cycle appears to take approximately 90 minutes. When cofilin-1 is added 1:1, this pattern becomes extended, taking 150 minutes, with generally less monomer present (figure 6.4(B)). The pattern is most marked however, at a 1:4 molar ratio (figure 6.4(C)). $FliC_{H7}$ filaments and monomers oscillate over the same period of 90 minutes, but from 50% large filaments/20% monomer to nearly 100% large filaments/0% monomer. This cycle appears to reduce over time, which maybe suggestive of an oscillation towards equilibrium. The experiments would have to be repeated to ensure this was the case, but the 1:4 ratio results do suggest that cofilin-1 affects the steady-state equilibrium of $FliC_{H7}$ flagella filaments and monomers.

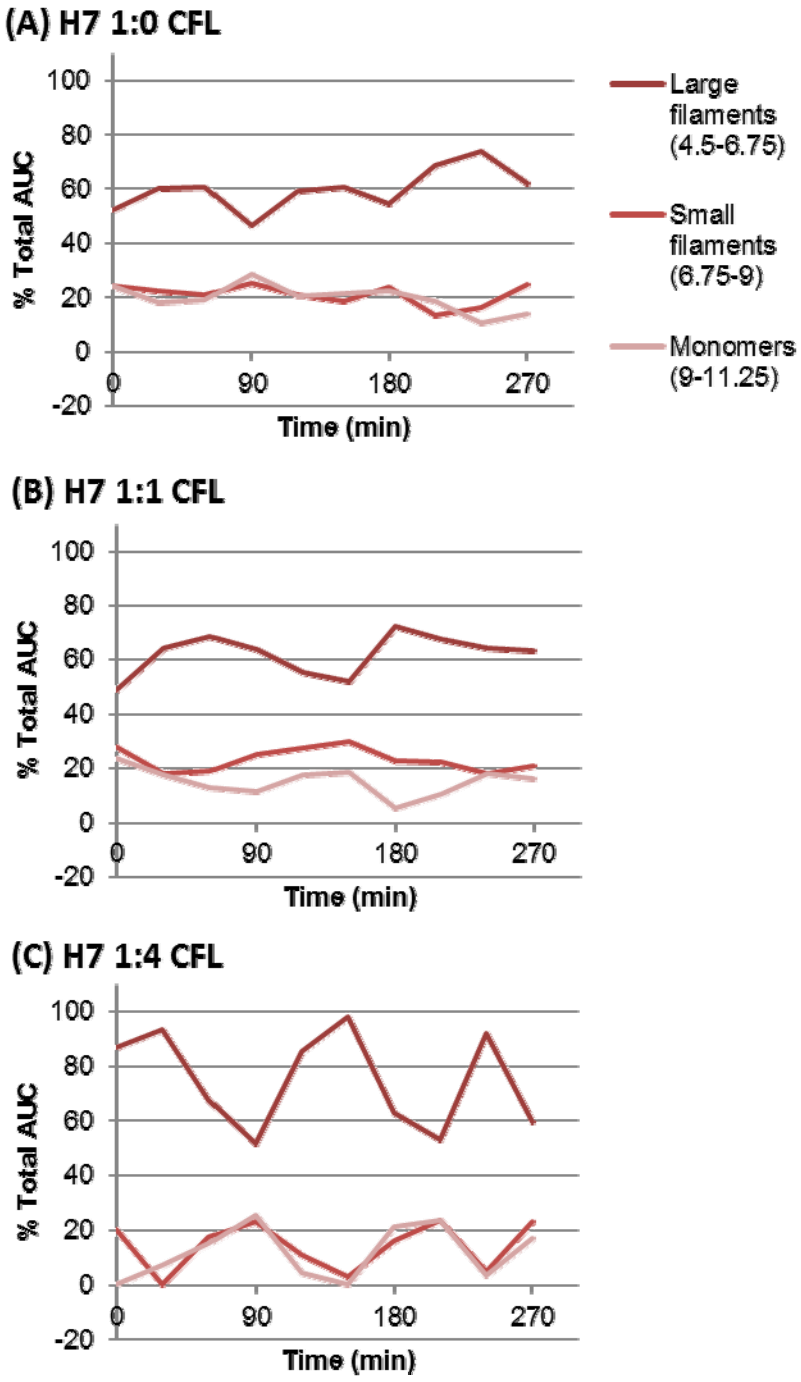

Figure 6.4. Effect of cofilin-1 (CFL) on $FliC_{H7}$ flagella (H7) over time by size exclusion chromatography (methods 2.9.6). Samples in figure 6.3(C) were run in series, every 30 minutes so the % total AUC from the 3 molar ratios **(A)** H7 1:0 CFL, **(B)** H7 1:1 CFL and **(C)** H7 1:4 CFL, were analysed over time.

6.4.3 Effect of flagella on actin dynamics

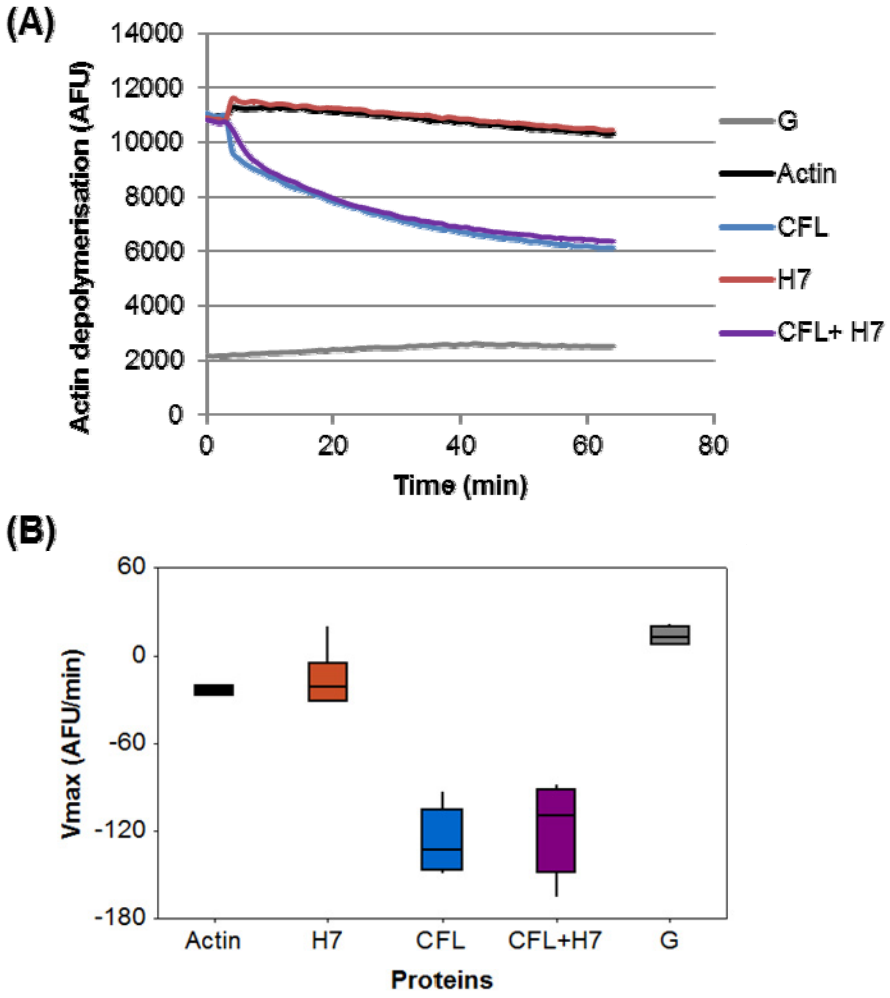

Figure 6.5. Effect of $FliC_{H7}$ flagella on actin depolymerisation +/- cofilin-1 (methods 2.9.8). **(A)** Change in pyrene-fluorescence over time of just G-buffer (G), pyrene-rabbit muscle F-actin 1:5 human platelet F-actin (Actin, ~5uM), with cofilin-1 added (CFL, ~0.5uM) or $FliC_{H7}$ flagella (H7, ~1uM) or both (CFL+H7). **(B)** Maximum velocity of actin depolymerisation (V_{max}, methods 2.9.7.3) as detailed in **(A)**.

$FliC_{H7}$ flagella may be able to affect actin dynamics through its interaction with cofilin-1. Cofilin-1 is primarily known for its depolymerising and severing action upon actin. Actin depolymerisation assays were therefore carried out to test this hypothesis. Figure 6.5(A) shows an average graph of 2 independent experiments with

3 technical replicates. Addition of $FliC_{H7}$ flagella to F-actin or F-actin with cofilin-1 appeared to have little or no effect. To ensure $FliC_{H7}$ flagella were not reducing the initial velocity of cofilin-1 depolymerisation, maximum velocities (V_{max}) for each replicate were analysed (figure 6.5(B), methods 2.9.7.3). The more negative the V_{max} value, the higher the velocity of depolymerisation. Though more work is needed to verify this, there were no obvious differences in rate between adding and not adding $FliC_{H7}$ flagella to F-actin or F-actin with cofilin-1.

Cofilin-1 severing of actin filaments can also enhance the rate of actin polymerisation in sub-optimal polymerisation conditions, by increasing the number of faster-growing (+) ends (Frantz *et al.*, 2008). With this in mind, $FliC_{H7}$ flagella might affect the polymerisation function of cofilin-1 on actin. However, to investigate this it was necessary to look at the effect of $FliC_{H7}$ flagella on actin polymerisation rate by itself. In doing this, it was sensible to compare $FliC_{H7}$ flagella with $FliC_{H6}$, $FliC_{P1}$ and $FljB_{P2}$ flagella to see how generic any effects might be. This has the added benefit of validating previous actin binding results in the previous chapter.

$FliC_{H6}$, $FliC_{H7}$, $FliC_{P1}$ and $FljB_{P2}$ flagella all appear to increase the rate of actin polymerisation. Figure 6.6 shows one example of this with different concentrations of flagella. Qualitatively, $FljB_{P2}$ flagella appear to be most effective at this, followed by $FliC_{P1}$ flagella, $FliC_{H7}$ flagella then $FliC_{H6}$ flagella. This is seems to be dose-dependent, apart from with $FliC_{H6}$, where the effect on actin polymerisation rate may be limited. To assess these effects more directly, the V_{max} of experiments were analysed (figure 6.7). $FliC_{H7}$, $FliC_{P1}$ and $FljB_{P2}$ flagella had equivalent effects on actin polymerisation rates, and $FliC_{H6}$ had less of an effect. These experiments would have to be repeated a number of times to see if there are any differences in actin polymerisation rates caused between $FliC_{H7}$, $FliC_{P1}$ and $FljB_{P2}$ flagella.

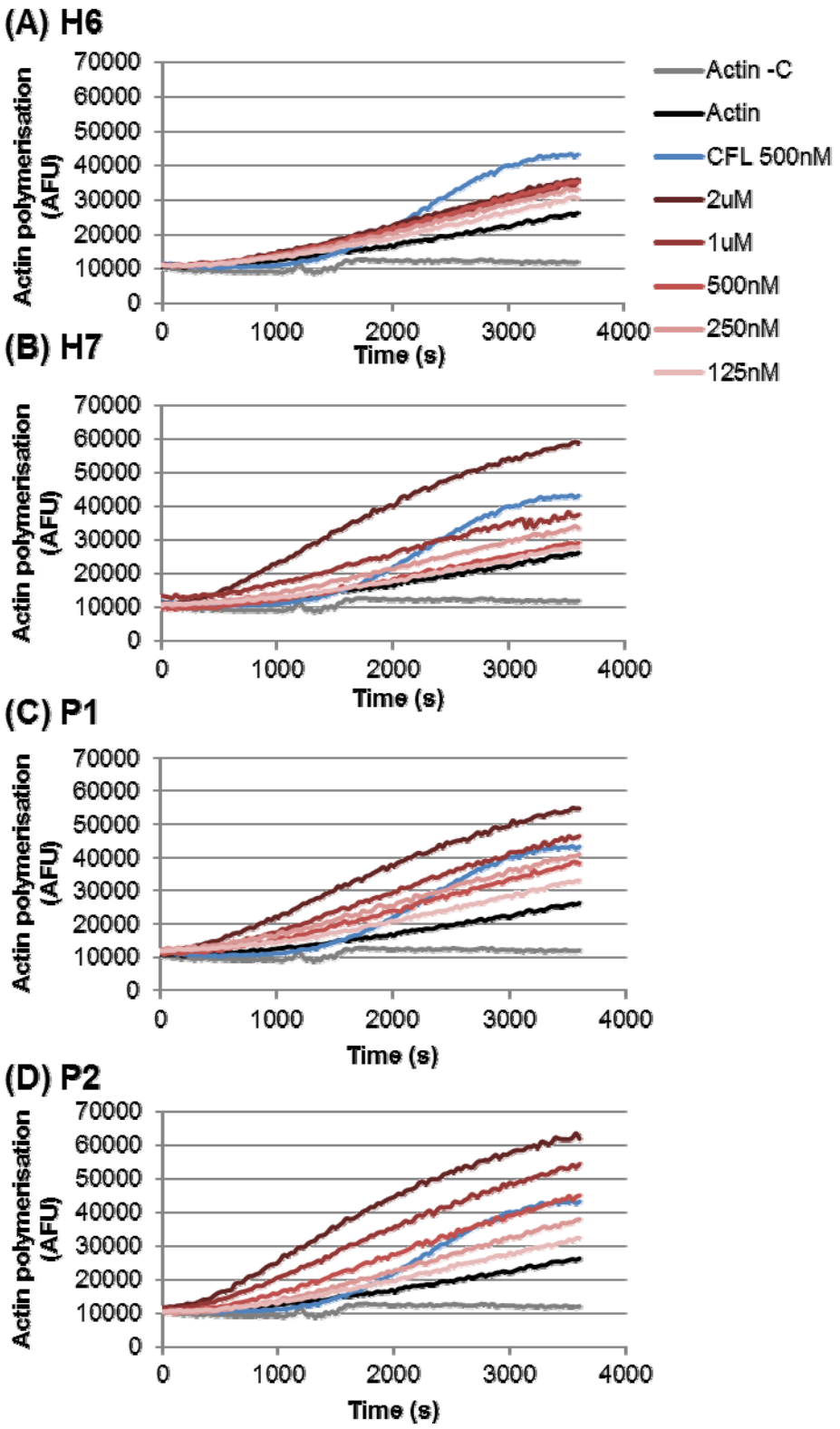

Figure 6.6. Titration of sheared $FliC_{H6}$ (H6), $FliC_{H7}$ (H7), $FliC_{P1}$ (P1) and $FljB_{P2}$ (P2) flagella effects on actin polymerisation (methods 2.9.7). Serial dilutions of flagella (red) or Cofilin-1 positive control (CFL, blue) were added to 1 µM pyrene-conjugated rabbit skeletal actin (Cytoskeleton Inc., black), polymerisation buffer was added, and fluorescence was measured every 30s for 1h. Polymerisation buffer was not added to Actin -C (grey). Data were normalised for the polymerisation ability of the G-actin preparation as it was collected, by applying a gain that was measured that day to all wells.

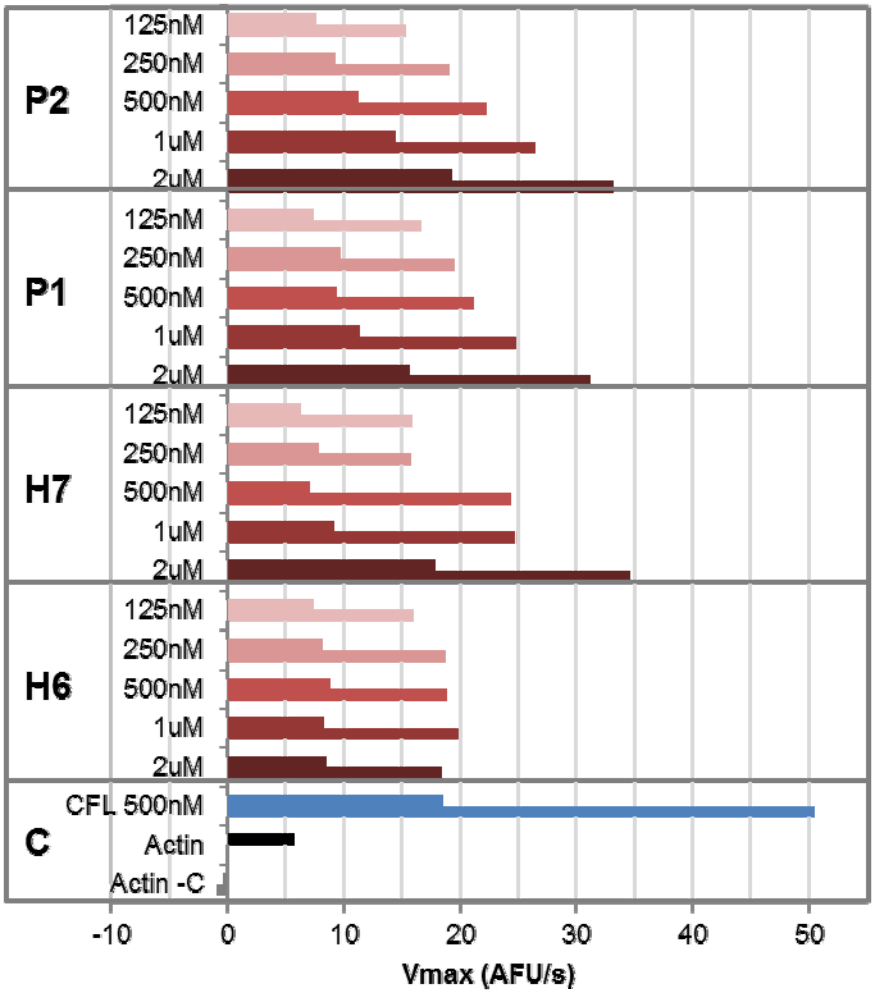

Figure 6.7. Effect of sheared $FliC_{H6}$ (H6), $FliC_{H7}$ (H7), $FliC_{P1}$ (P1) and $FljB_{P2}$ (P2) flagella titration on maximum velocity (V_{max}) of actin polymerisation. Molar concentrations used are indicated. Data is representative of 2 polymerisation experiments (methods 2.9.7). The differences between experiments can be explained by the 75% and 90% gains, applied in error. Controls (C) include cofilin-1 (CFL) as a positive control and actin with polymerisation buffer (Actin) or no polymerisation buffer added (Actin -C) as negative controls.

A separate set of experiments were used to investigate whether interactions between flagella and cofilin-1 affect their individual effects on actin polymerisation (figure 6.8). Adding sub-optimal doses of sheared $FliC_{H6}$ ($df=4$, $t=5.15$, $p=0.004$), $FliC_{H7}$ ($df=4$, $t=7.82$, $p=0.0002$), $FliC_{P1}$ ($df=4$, $t=9.90$, $p<0.0001$) or $FljB_{P2}$ ($df=4$, $t=10.84$, $p<0.0001$) flagella to G-actin still resulted in a V_{max} significantly different from that of G-actin alone (0μM). This confirms results from figure 6.7.

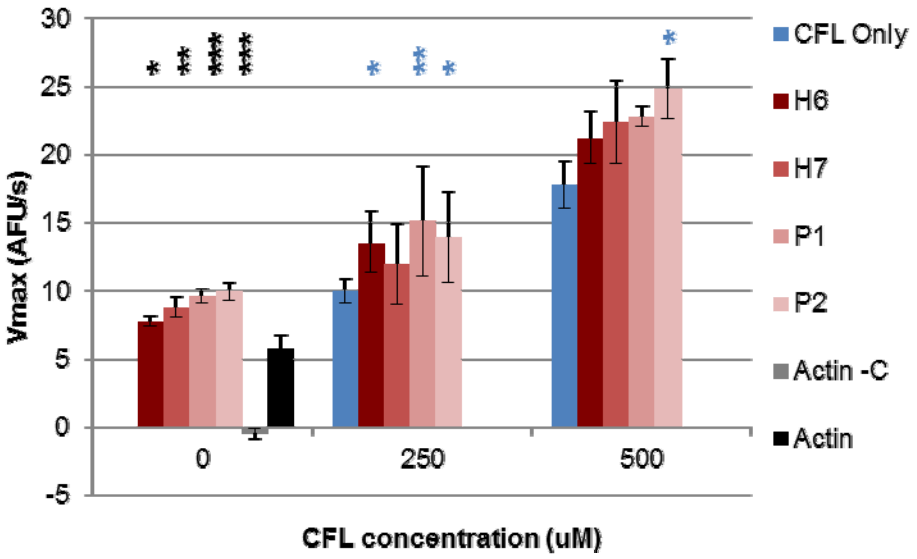

Figure 6.8. Effect of flagella on actin polymerisation +/- cofilin-1 (CFL). Sub-optimal concentrations of sheared $FliC_{H6}$ (H6), $FliC_{H7}$ (H7), $FliC_{P1}$ (P1) and $FljB_{P2}$ (P2) flagella (250uM) were tested at 1:0 (0), 1:1 (250) and 1:2 (500) molar ratios of cofilin-1 (CFL) according to methods 2.9.7. Error bars represent 95% confidence intervals (n=3). Statistical analysis was carried out using GLM Tukey pairwise comparisons where $p<0.05$(*), $p<0.001$(**) and $p<0.0001$(***). Pairwise comparisons were with actin with polymerisation buffer (Actin, *) or cofilin-1 only (CFL only, *). Actin with no polymerisation buffer (Actin –C) was used as a negative control.

It is unclear whether increases in rate of actin polymerisation with cofilin-1 and $FliC_{P1}$ or $FljB_{P2}$ flagella were additive, due to the independent effects of flagella and cofilin-1 on actin, or synergistic, due to the effect of flagella-cofilin-1 complexes on actin. At a sub-optimal dose of cofilin-1 (250µM), addition of sheared $FliC_{H6}$, $FliC_{P1}$ or $FljB_{P2}$ flagella, but not $FliC_{H7}$ flagella, caused a significant increase in V_{max} compared to cofilin-1 alone. This may be due to experimental variation, but it is also possible that cofilin-1 is less effective with $FliC_{H7}$ flagella at increasing the rate of actin polymerisation than it is with other flagella. Perhaps it is their interaction with one another that causes this. $FliC_{H6}$ flagella were also shown by ELISA to bind to

cofilin-1 and actin at roughly equivalent levels to $FliC_{H7}$ flagella. However, in combination with cofilin-1 and actin, $FliC_{H6}$ flagella did not show the same effect as $FliC_{H7}$ flagella. If anything, addition of cofilin-1 has made the effects of $FliC_{H6}$ flagella on actin polymerisation, which alone were fairly limited, more equivalent to $FliC_{P1}$ or $FliC_{P2}$ flagella under the same conditions.

6.5 Discussion

The aims of this chapter were to establish whether cofilin-1 binds to $FliC_{H7}$ flagella filaments or monomers, what sort of effect this has on $FliC_{H7}$ flagella and whether $FliC_{H7}$ flagella affect cofilin-1 function in actin dynamics. It was also to see if $FliC_{H6}$, $FliC_{H7}$, $FliC_{P1}$ and $FljB_{P2}$ flagella alone could affect actin dynamics and in doing so, confirm any actin binding interactions.

Co-sedimentation studies showed no clear or direct evidence that cofilin-1 binds to $FliC_{H7}$ filaments. To be unable to detect cofilin-1 in pellets even by Western-blotting, any interaction with $FliC_{H7}$ filaments would have to be transient. However, the proportion of $FliC_{H7}$ that was retained in the supernatant was increased when cofilin-1 was present. So rather than $FliC_{H7}$ flagella influencing cofilin-1 sedimentation, cofilin-1 was influencing $FliC_{H7}$ flagella sedimentation. Assuming that ultra-centrifugation separates flagella into filaments in the pellet and monomers in the supernatant, cofilin-1 is either interacting transiently with $FliC_{H7}$ filaments and depolymerising them, or binding to monomers in such a way that affects their incorporation into filaments.

The assumption of this co-sedimentation assay is that ultra-centrifugation separates $FliC_{H7}$ flagella preparations into filaments and monomers. However, under these conditions this has not been tested. This is a limitation of this assay; it may be that only larger $FliC_{H7}$ filaments are being pelleted, in which case all that can be concluded is that cofilin-1 does not interact detectably with large $FliC_{H7}$ filaments. Co-sedimentation of cofilin-1 with $FliC_{H7}$ flagella-expressing *E. coli* O157:H7 was carried out in an attempt to resolve this issue. In this system, flagella are separated into those attached to bacteria and those that are not. Despite not detectably

associating with it, cofilin-1 somehow reduced the amount of bacteria-associated $FliC_{H7}$ flagella. As this is consistent with the co-sedimentation studies undertaken with purified flagella, this is likely to be $FliC_{H7}$-dependent.

Size-exclusion data also indicates that interaction with cofilin-1 affects $FliC_{H7}$ filament stability. However, the data can be interpreted differently, depending on whether total or temporal effects are examined. In contrast to co-sedimentation assays, the overall effect of cofilin-1 indicates a trend towards filament stability that is not statistically significant, apart from the effects on smaller filaments. However, looked at over time, this data indicates an increase in $FliC_{H7}$ flagella polymerisation and depolymerisation dynamics. If this were the case, this is more in-line with results from co-sedimentation assays, suggesting that cofilin-1 alters the dynamic equilibrium of $FliC_{H7}$ flagella filaments by binding to $FliC_{H7}$ monomers. This effect is likely to be most visible on smaller filaments, as changes in total length are proportionally larger, which was the case in these experiments.

Fluorescence microscopy could also be used to examine whether cofilin-1 binds to $FliC_{H7}$ flagella filaments, monomers or both. This was attempted, but all the antibodies available at that time exhibited non-specific binding. This issue has consequently been resolved with different antibodies and microscopy is currently being undertaken by Amin Tahoun, a post-doctoral researcher. TLR5-stimulation assays could then be used to assess how cofilin-1 alters the bio-availability of $FliC_{H7}$ monomers. However, these experiments are all in artificial conditions; it would be interesting to use *fliC*$_{H7}$ transfection studies to see if cofilin-1 interactions with $FliC_{H7}$ flagella affect *in vivo* NLRC4 inflammasome activation. Such a finding raises interesting possibilities, as this may affect the innate recognition of $FliC_{H7}$ flagellin.

For the first time, bacterial flagella have been shown to enhance actin polymerisation rates *in vitro*. That cofilin-1 was not required for $FliC_{H7}$ flagella to do this was unexpected, because previous ELISA data indicated that actin binding, though detectable, was much less than cofilin-1 binding. However, ELISAs were done in very different buffer conditions. Also, the actin used in polymerisation experiments

was purified G-actin in solution, rather than the actin being coated onto ELISA plates, which was probably mostly F-actin. While these experiments don't show that bacterial flagella can enhance actin polymerisation in cells, they demonstrate that it is physically possible. Cell-transfection studies are required to see if this effect actually occurs and what the role of cofilin-1 might be in cells.

Results from experiments undertaken to see if bacterial flagella affected cofilin-1 dependent increases in actin polymerisation rate were unclear. With 3 interactants it was difficult to judge which interactions were affecting actin polymerisation rates. Adding $FliC_{P1}$ or $FljB_{P2}$ flagella to cofilin-1 did significantly increase the actin polymerisation rate compared with cofilin-1 alone, but was it was unclear whether this was additive or synergistic. Interactions between $FliC_{H7}$ flagella and cofilin-1 were possibly preventing one or the other from interacting with actin. Interactions between $FliC_{H6}$ flagella and cofilin-1 may have enabled $FliC_{H6}$ flagella to interact more effectively with actin. More detailed mapping of binding sites and using mutagenesis would be useful in validating these results and picking out which protein is contributing, when and how.

The effect of flagella on actin dynamics has some degree of specificity to it that implies a mode of action. For example, $FliC_{H7}$ flagella affected the rate of actin polymerisation but did not appear to change the rate of actin depolymerisation, with or without cofilin-1. Therefore, $FliC_{H7}$ flagella did not alter F-actin dynamics, whereas it did affect G-actin dynamics. $FliC_{H7}$ flagella and other flagella tested, increase the overall rate of G-actin polymerisation without altering the duration of the lag phase, unlike cofilin-1, which does. Instead they do this by increasing the maximum velocity of actin polymerisation. The specificity showed with $FliC_{H7}$ flagella points towards how they and other flagella may be causing this effect on actin polymerisation. It implies that flagella are not involved in actin nucleation, but perhaps act as G-actin binding proteins, that increase the affinity of G-actin for F-actin in a manner analogous to Profilin. The effect of other flagella on actin depolymerisation would have to be tested and assays that distinguish between F and G-actin binding undertaken to investigate this.

It is also conceivable that flagellin could play a dual role in relation to actin and cofilin-1 binding. One function does not necessarily rule out another. For instance, $FliC_{H7}$ flagella could be acting as a bacterial effector protein targeting actin dynamics, while the host protects its bacterial invader from flagellin recognition and inflammation through interaction with cofilin-1.

6.6 References

Andersen-Nissen, E., Smith, K. D., Bonneau, R., Strong, R. K. & Aderem, A. (2007). A conserved surface on Toll-like receptor 5 recognizes bacterial flagellin. *Journal of experimental medicine* **204**, 393–403.

Andrianantoandro, E. & Pollard, T. D. (2006). Mechanism of actin filament turnover by severing and nucleation at different concentrations of ADF/cofilin. *Molecular cell* **24**, 13–23.

Bernstein, B. W., Painter, W. B., Chen, H., Minamide, L. S., Abe, H. & Bamburg, J. R. (2000). Intracellular pH modulation of ADF/cofilin proteins. *Cell motility and the cytoskeleton* **47**, 319–36.

Bobkov, A. A., Muhlrad, A., Pavlov, D. A., Kokabi, K., Yilmaz, A. & Reisler, E. (2006). Cooperative effects of cofilin (ADF) on actin structure suggest allosteric mechanism of cofilin function. *Journal of molecular biology* **356**, 325–34.

Frantz, C., Barreiro, G., Dominguez, L., Chen, X., Eddy, R., Condeelis, J., Kelly, M. J. S., Jacobson, M. P. & Barber, D. L. (2008). Cofilin is a pH sensor for actin free barbed end formation: role of phosphoinositide binding. *Journal of cell biology* **183**, 865–79.

Pavlov, D. & Muhlrad, A. (2006). Severing of F-actin by yeast cofilin is pH-independent. *Cell motility and the cytoskeleton* **63**, 533–542.

Van Troys, M., Huyck, L., Leyman, S., Dhaese, S., Vandekerkhove, J. & Ampe, C. (2008). Ins and outs of ADF/cofilin activity and regulation. *European journal of cell biology* **87**, 649–67.

7 : Conclusions

7.1 Summary

This thesis has focussed on the interactions of $FliC_{H7}$ flagella with the BTR, with two purposes in mind. The first was, from a practical standpoint, to find specific $FliC_{H7}$ flagella binding epitopes that are distinct from TLR5-activation epitopes for use as vaccine antigens. The structurally variable region of $FliC_{H7}$ is a predicted 88aa insertion, which is not post-translationally modified. Because this region is variable, it is unlikely to contain TLR5-activation epitopes. Both the recombinant variable region of $FliC_{H7}$ ($VrH7_{180\text{-}496}$) and recombinant $FliD_{H7}$ contained BTRE binding epitopes. Despite attempts with $FliD_{H7}$, further tests are still required to see if these binding epitopes are specific. If $VrH7_{180\text{-}496}$ and recombinant $FliD_{H7}$ do contain specific BTR binding epitopes, these two easily purified proteins become promising H7 antigen-based vaccine candidates, for use in cattle.

The second purpose of investigating $FliC_{H7}$ flagella interactions with the BTR was to better understand the role of flagella in the pathogenesis of EHEC, and perhaps more broadly, in enteric pathogen infection. $FliC_{H7}$ flagella were shown to bind across, through and probably inside host-cell surfaces. This raised the possibility that penetrating flagella could be involved in actin pedestal formation. Further studies revealed potential interactions between $FliC_{H7}$ flagella and a number of actin-binding proteins, including cofilin-1. $FliC_{H7}$ flagella also increased actin polymerisation rates, but probably not actin depolymerisation rates, *in vitro*, in the absence of cofilin-1. Furthermore, this effect on actin polymerisation rates was not restricted to $FliC_{H7}$ flagella, but was also shown for EPEC $FliC_{H6}$ flagella, and *Salmonella* $FliC_{P1}$ and $FljB_{P2}$ flagella. If these previously unknown functions are in the future shown to occur in the context of bacterial colonisation, this study may have revealed a novel mechanism of flagella-mediated bacterial pathogenesis among entero-pathogens.

This study did not uncover many clues to the biological relevance of the $FliC_{H7}$ flagella interaction with cofilin-1. It is not likely to alter effects on cofilin-1-dependent actin depolymerisation, though more work is needed to ascertain this is the case for a range of stoichiometric and pH conditions. Cofilin-1 may alter $FliC_{H7}$ flagella filament stability, though how this could occur without detectable interactions with $FliC_{H7}$ flagella filaments remains to be seen. This study proposed that the dynamics between filaments and monomers are changed as a result of cofilin-1 binding $FliC_{H7}$ monomers, and therefore may affect innate detection of $FliC_{H7}$.

7.2 Proposed model of the role of $FliC_{H7}$ flagella in EHEC colonisation

Figure 7.1 summarises the current thinking based on the results from this thesis. In this model, the role of $FliC_{H7}$ flagella changes over time. To begin with, $FliC_{H7}$ flagella allow chemotaxis to the BTRE, and initial adherence. If this adherence is penetrative, $FliC_{H7}$ flagella affect actin dynamics. The potential inflammation that would be caused by this is dampened by $FliC_{H7}$ interactions with cofilin-1. With time, flagella expression is down-regulated, but the actin recruited under EHEC by penetrating $FliC_{H7}$ flagella can then be remodelled into A/E lesions more efficiently. The possibility EHEC uses its $FliC_{H7}$ flagella to secrete T3S effector proteins at an earlier time point has been considered, but as yet there is no direct evidence for this.

Such is the model, though convincing evidence of all aspects of it occurring at the BTR is still some way off. An understanding of the mechanism of actin polymerisation by different flagella would give more weight to this model. For this, investigating the conditions in which this occurs artificially and in cells is necessary. Also, more definitive evidence for the effect of cofilin-1 on flagellin monomer availability is required. Additionally, it is still unknown if the NLRC4 inflammasome plays a role in innate recognition of $FliC_{H7}$ flagella in BTR epithelial cells, or if apical TLR5 expression occurs at this particular site.

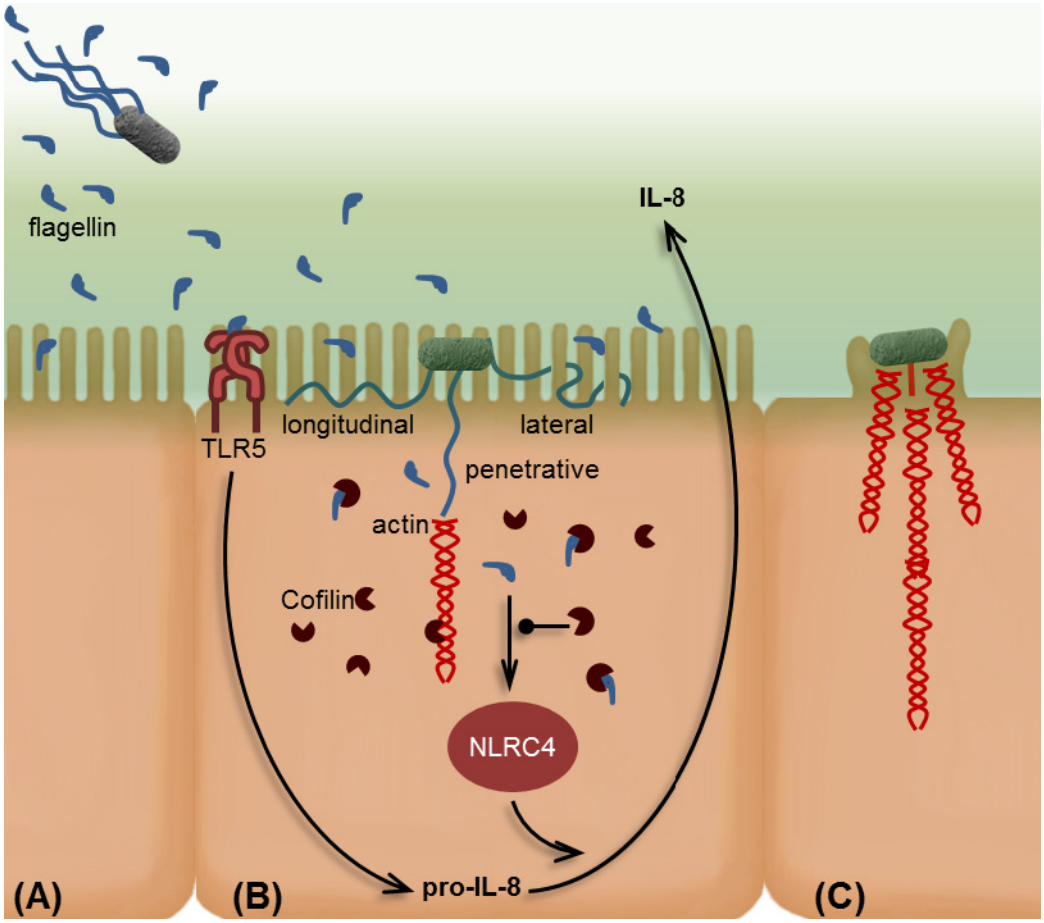

Figure 7.1. Proposed model for the temporal roles of $FliC_{H7}$ flagella in EHEC colonisation of cattle. **(A)** Bacteria use swimming motility to penetrate the mucus layer. $FliC_{H7}$ flagella expression leads to release of $FliC_{H7}$ monomers. **(B)** $FliC_{H7}$ activates TLR5 signalling, resulting in pro-IL-8 expression. EHEC initially bind to the BTRE via longitudinal, lateral or penetrative flagellar adhesion. Penetrative adhesion allows intracellular flagella to trigger actin polymerisation, setting up A/E lesion formation. Cofilin-1 prevents NLRC4 inflammasome activation by free $FliC_{H7}$, which would otherwise result in cleavage of pro-IL-8 and secretion of mature IL-8. **(C)** Flagella are down-regulated as T3S is up-regulated, allowing a more intimate attachment and continued actin rearrangement to take place.

7.3 Conclusions

In addition to motility and initial attachment, this study has revealed two surprising new functions of flagella from EHEC O157:H7. These are penetration into host cells and polymerisation of actin. If these functions are relevant in cellular models of infection, flagella become a very logical choice for use in EHEC O157:H7 vaccines in cattle. This study has also shown that two recombinant flagellar proteins, $FliD_{H7}$ and $VrH7_{180\text{-}496}$, can bind to BTRE. As these are unlikely to contain TLR5-binding epitopes, they may provide protection against EHEC colonisation of cattle, as part of existing multi-component T3S protein vaccines.

Appendix 1: Validation of strains and plasmids

A1.1 Validation of *fliC* expression plasmids

Restriction digest validation of expression plasmids detailed in table 2.2 and section 2.3.13 is shown below (figure A1.1). This confirms the presence of *fliC* (~2kb) or *fliD* (~1.5kb) coding sequence inserts and correct restriction sites. These plasmids were also shown to complement motility deficient *fliC* and *fliD* mutants (figure A1.2 and figure 3.8).

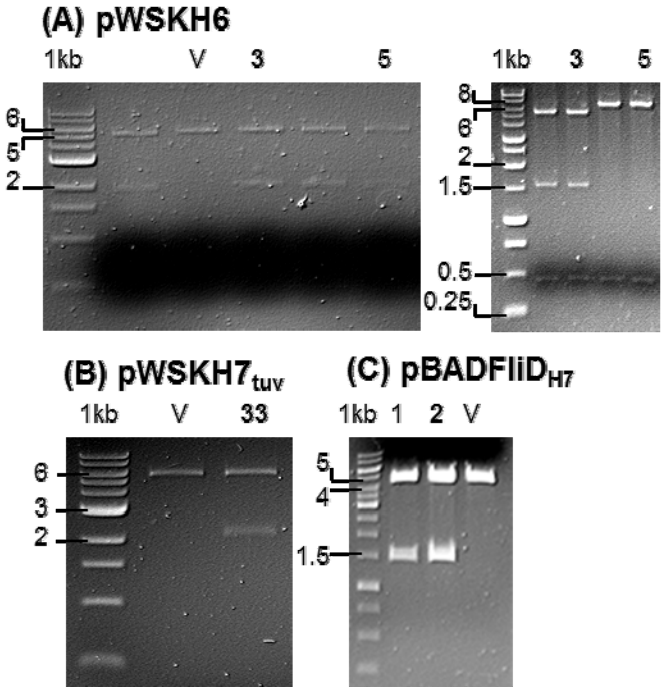

Figure A1.1. Restriction confirmation of expression vector construction and insert orientation screening. V= empty vector (pWSK29 or pBAD/*Myc*-His A). Clones in bold used for further study. **(A)** Left panel: BamHI digest of pWSKH6 clones to confirm insertion of $fliC_{H6}$ and its native promoter. Right panel: PstI restriction mapping of pWSKH6 to determine orientation. Both orientations shown; 3 and 5 indicate the clone numbers from each direction taken forward for sequencing and stab motility tests. **(B)** BamHI/SalI double digest of $pWSKH7_{tuv}$ to confirm directional insertion of $fliC_{H7}$ with its native promoter. **(C)** NcoI/SacI double digest of $pBADFliD_{H7}$ to confirm directional insertion of $fliD_{H7}$ with its native promoter.

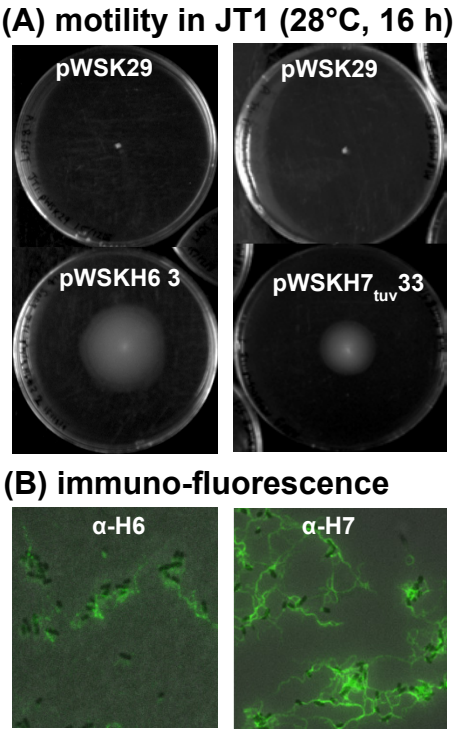

Figure A1.2. Complementation of flagella expression in JT1, a Tn10::*fliC* strain, by pWSKH6 and pWSKH7$_{tuv}$. **(A)** Complementation with expression plasmids compared to empty plasmid (pWSK29), as shown by motility assay (methods 2.9.2). **(B)** Immuno-fluorescence of JT1 containing pWSKH6 (α-H6) or pWSKH7$_{tuv}$ (α-H7) from the outer region of motility halos (methods 2.2 and 2.7.1).

A1.2 Validation of TUVΔ*fliC* and TUV*fliC*$^-$

A1.2.1 Exchange plasmids

Engineering the exchange plasmids (table 2.2 and figure 2.3) correctly is critical to successful allelic exchange (methods 2.3.12). Figure A1.3(B) shows the restriction digest confirmation of pIBXH7$_{tuv}$, which was the allelic exchange vector used to make TUVΔ*fliC* from TUV93-0 (table 2.1). The *sacB-kan*^{r} cassette insert (~4kb) has been cut out of the plasmid backbone (~6kb). The plasmid backbone in this figure, is pIBXSK$_{tuv}$, which is validated in figure A1.3(A). pIBXSK$_{tuv}$ is the allelic exchange vector used to make TUV*fliC*$^-$ from TUVΔ*fliC* (table 2.1). Figure A1.3(A) shows the restriction digest confirmation of the second *fliC*$_{H7}$ flanking region in this vector, H7downD (figure 2.3). This is visible in figure A1.3(A) as a 600bp band on SalI/BamHI digest or comparative size increase on BamHI digest. The first *fliC*$_{H7}$ flanking region, H7upB, is visible as a size increase in the plasmid backbone (>5kb) on SalI/BamHI digest compared to just pIB307 (V, 4.2kb).

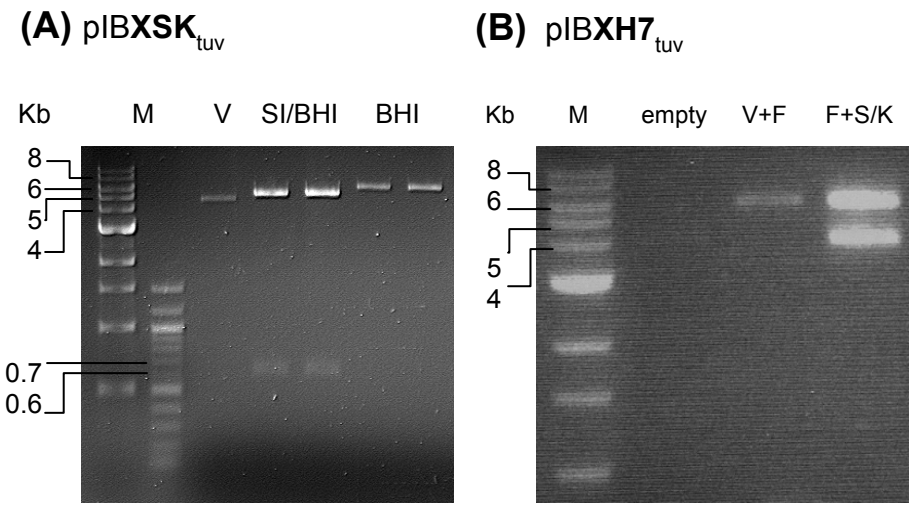

Figure A1.3. Restriction confirmation of allelic exchange vector construction for *fliC*$_{H7}$ knock-outs. **(A)** BamHI digest of pIBXH7$_{tuv}$ (F+S/K) to confirm insert of gel purified *sacB::kan*^{r} cassette (S/K). pIBXSK$_{tuv}$ (vector and flanks, V+F). **(B)** SacI/BamHI and BamHI digests of pIBXSK$_{tuv}$ to confirm insert of 2nd flank and presence of 1st flank. pIB307 (empty vector, V). Samples were digested with the enzymes specified (New England Biolabs), loaded into a 0.7%

A1.2.2 Intermediate strain TUVΔ*fliC*

After allelic exchange of TUV93-0 with pIBXH7$_{tuv}$, clones were screened as detailed in methods 2.3.12.1. The results from kan^{r}, cam^{s} clones (that do not contain the exchange plasmid but do contain the exchanged cassette) screened by PCR for the presence of *fliC*$_{H7}$ and *sacB* are shown in figure A1.4. Clone 10 was *fliC*$^{-}$, *sacB*$^{+}$ and non-motile. The mutation in clone 10 was non-polar, as the motility was restored by plasmid complementation (figure A1.4(D)). Therefore TUVΔ*fliC*10 was used as the intermediate strain for further allelic exchanges in this study and in further work. An important point to note in figure A1.4(D) is the typical variation of TUV93-0 (WTp) in motility assay.

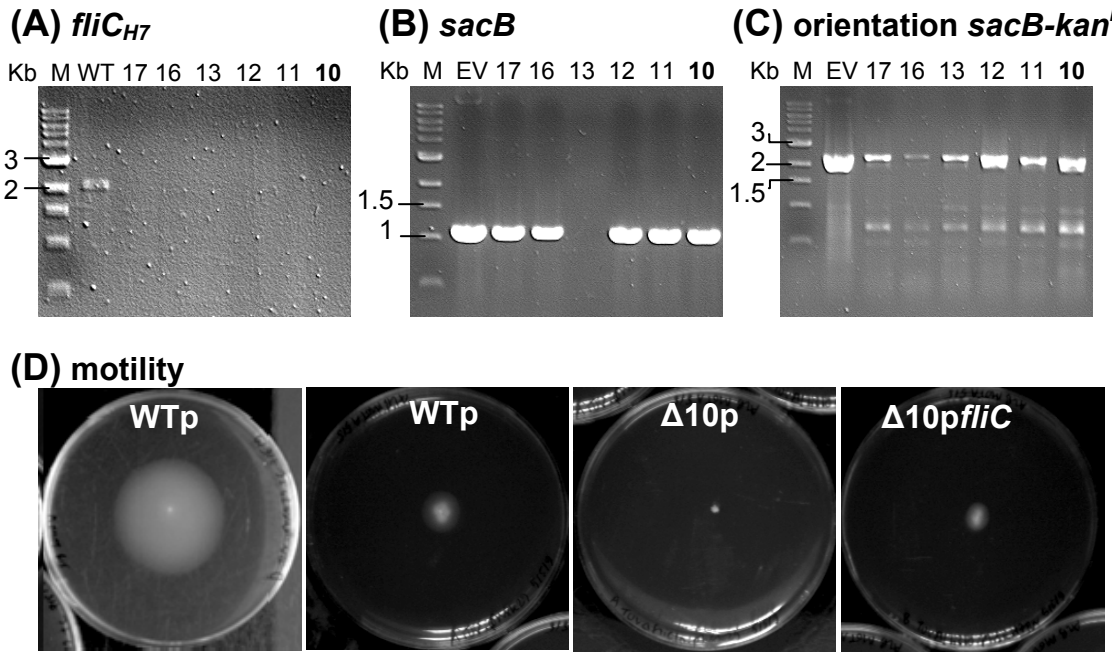

Figure A1.4. Validation of TUVΔ*fliC*. Clone 10 (bold) was used as the intermediate strain. WT= TUV93-0, EV= exchange vector pIBXH7$_{tuv}$, a positive control. **(A)** The absence *fliC*$_{H7}$ (~2.1kb) was screened by PCR using Ct-FliC-SalI - Nt-FliC-BamHI2 primers. **(B)** The presence of *sacB* (1.2kb) was screened by PCR for with SacB-5 - SacB-3 primers. **(C)** The orientation of the *sacB::kan*^{r} cassette was screened by PCR using two sets of primers: a product with 5'H7upF.SacI - SacB-3 is the same orientation as pIBXH7$_{tuv}$ (EV), shown. PCR was done using Quick-Load *Taq* 2x master mix (New England Biolabs) as detailed in methods 2.3.4. **(D)** Motility of TUVΔ*fliC*10 (Δ10) compared to TUV93-0 (WT) and complementation by pWSKH7$_{tuv}$ (p*fliC*) in 0.3% agar after 28ºC for 24 hr (methods 2.9.2); this assay vector controlled with pWSK29 (p). Primers detailed in table 2.3.

A1.2.3 Isogenic strain TUV*fliC*$^-$

Allelic exchange was carried out between TUVΔ*fliC*10 and pIBXSK$_{tuv}$ and screened according to section 2.3.12.2 to make an isogenic *fliC*$_{H7}$ deletion. PCR validation of some of the kan^s, cam^s clones (that do not contain either the exchange plasmid or the cassette) is shown in figure A1.5. In particular, figure A1.5(B) shows the size of the mutated region in the parent strain (~3kb), pIBXSK$_{tuv}$ (~1.2kb), pIBXH7$_{tuv}$ (~5.2kb) and the 4 clones tested (~1.2kb). These sizes are as expected if they were to contain the *fliC*$_{H7}$ region, just the flanking regions, and the flanking regions and the *sacB-kan*^{r} cassette respectively. The clones tested match pIBXSK$_{tuv}$ as expected. They do not contain ~1.8 or 4kb between the two flanking regions cloned into pIBXSK$_{tuv}$,

confirming the absence of *fliC*$_{H7}$ or the *sacB-kan*^{r} cassette between the *fliC*$_{H7}$ flanking regions.

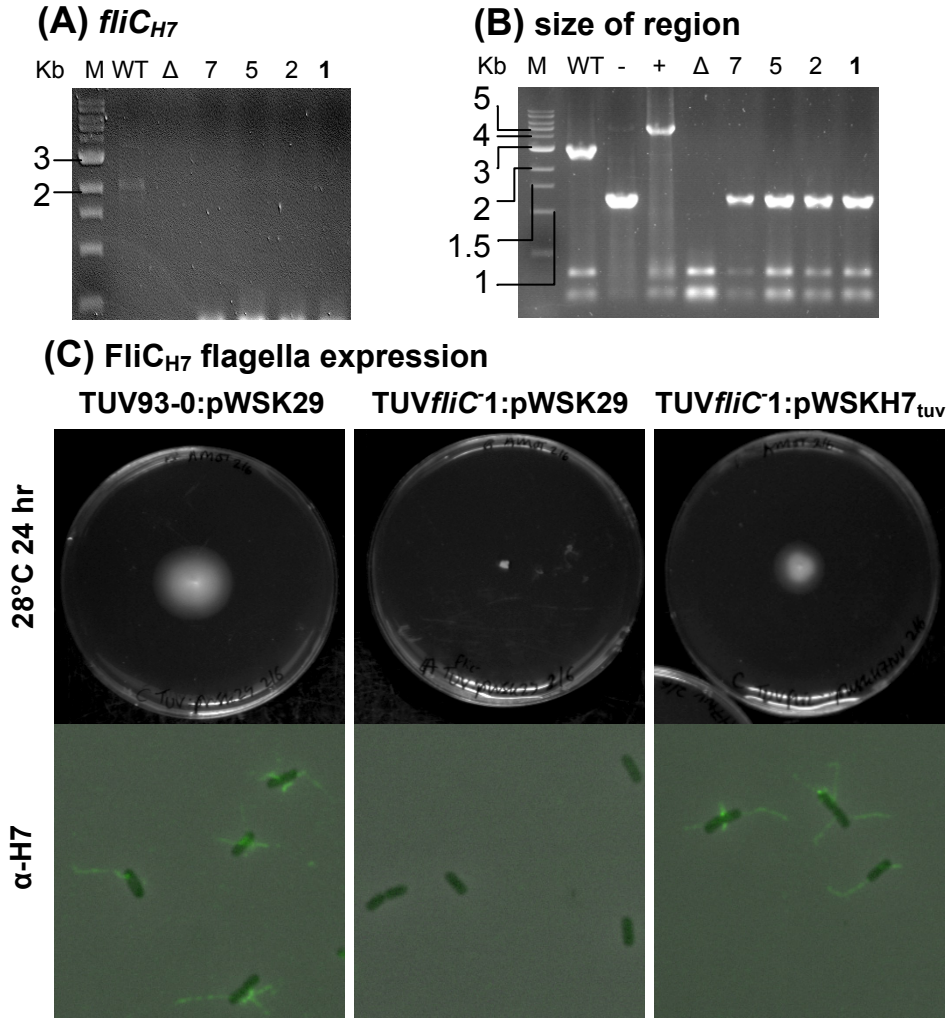

Figure A1.5. Validation of TUV*fliC*$^{-}$. Clone 1 (bold) was used as the *fliC*$_{H7}$ clean deletion strain in this study. + = pIBXH7$_{tuv}$, - = pIBXSK$_{tuv}$. **(A)** The absence *fliC*$_{H7}$ (~2.1kb when present) was screened by PCR with Ct-FliC-SalI - Nt-FliC-BamHI2 primers. **B)** The size of the region between the external primers was screened by PCR with 5'H7upF.SacI – 3'H7downR.SalI primers. PCR was done using Quick-Load *Taq* 2x master mix (New England Biolabs) as detailed in methods 2.3.4. **C)** Flagella expression of clone 1 compared to TUV93-0, with and without plasmid complementation as assessed by motility assay and immunofluorescence as indicated (methods 2.9.2 and 2.7.1). Primers detailed in table 2.3

One result from figure A1.5 differs from what was predicted. The PCR reaction of the intermediate strain TUVΔ*fliC*10 in figure A1.5(B) has no specific product. Theoretically this PCR should yield a 5kb product, but the reaction may have failed.

This is likely to be the case as previous screening of TUVΔ*fliC* shows this clone to contain the *sacB-kan*^{r} cassette in the same orientation as pIBXH7$_{tuv}$ at the *fliC*$_{H7}$ locus (figure A1.4(C)). TUV*fliC*$^{-}$1, highlighted in figure A1.5, was non-motile and *fliC*$^{-}$, with few base pairs in between the *fliC*$_{H7}$ flanking regions. Again this mutation was non-polar, as complementation was possible with *fliC*$_{H7}$-containing plasmids (section A1.1, figure A1.5(C) and data not shown). As such, TUV*fliC*$^{-}$1 was used as the TUV*fliC*$^{-}$ strain in this study.

A1.3 Validation of *fliC* knock-ins

A1.3.1 TUV*fliC*$^{-}_{H7}$

Using the same strategy as above, a *fliC*$_{H7}$ knock-in was designed (section 2.3.12.2, figure 2.3). However, by making TUVΔ*fliC*10 with pIBXH7$_{tuv}$, this strain's *fliC* Shine-Dalgarno sequence was disrupted by the introduced BamHI site. A new exchange vector of similar design to pIBXH7$_{tuv}$ was made, which instead of having the *sacB-kan*^{r} cassette between the flanking regions, contained the *fliC*$_{H7}$ coding sequence. This was called pIBH7KI. pIBH7KI contained a different upstream flanking region that repaired the sequence in TUVΔ*fliC*10 and maintained start codon spacing. Allelic exchange was successful with pIBH7KI; *fliC*$_{H7}$ was inserted in the correct orientation of that region, and the strain no longer contained *sacB* (figure A1.6).

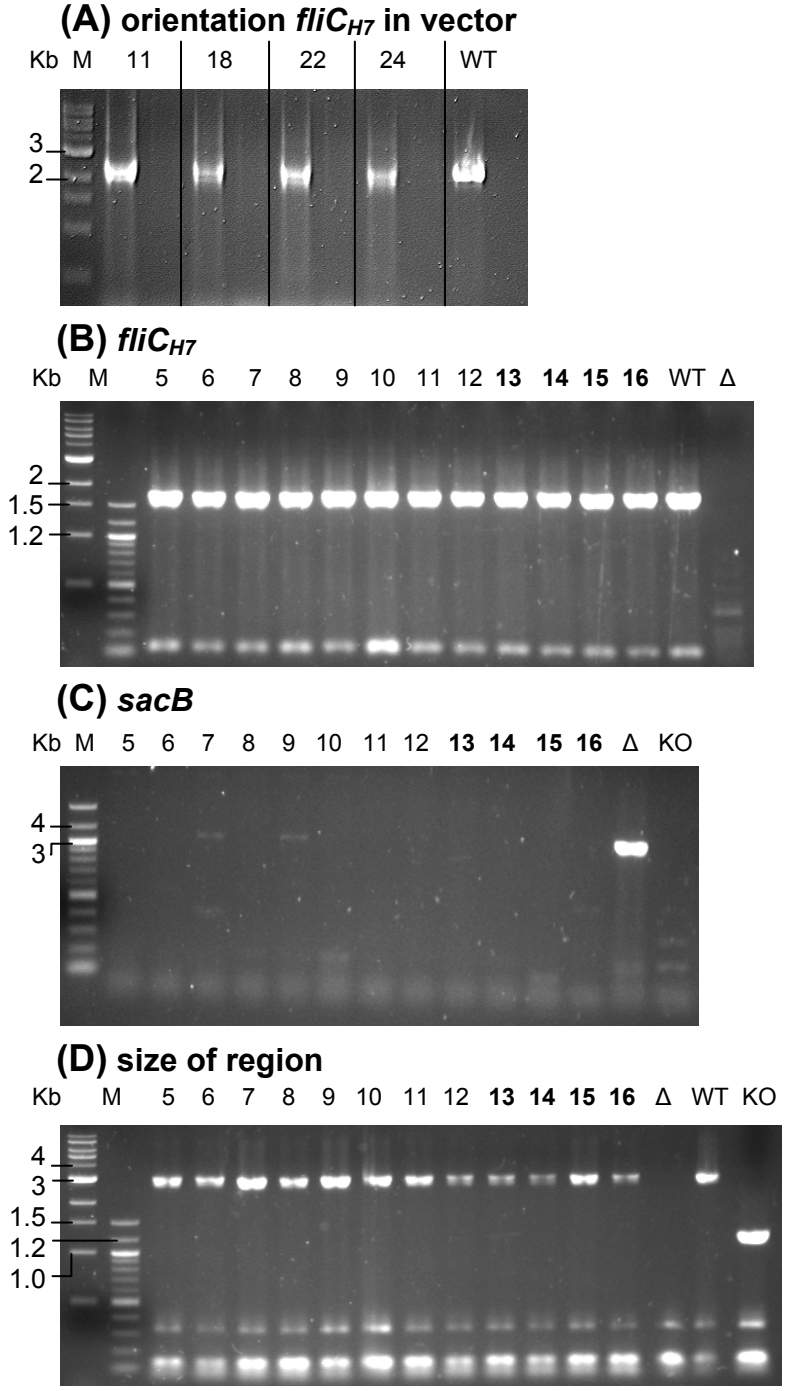

Figure A1.6. Validation of TUV*fliC*$^{-}_{H7}$. Clones 13-16 (bold) were used in phenotypic assays. **(A)** Orientation screening by PCR (methods 2.3.4) of pIBH7KI using H7upF.SacI/ 3NtH7F.BamHI primers on the right, and 3'H7downR.SalI/ 3'NtH7F.BamHI on the left. WT= TUV93-0 genomic DNA. **(B)** The presence of *fliC*$_{H7}$ was screened for by PCR using 5'CtH7R.BamHI/ 3'NtH7F.BamHI primers. **(C)** The absence of *sacB* was screened for by PCR with SacB-5/ SacB-3 primers. **(D)** The size of the region between the external primers was screened by PCR with 5'H7upF.SacI/ 3'H7downR.SalI primers. Primers detailed in table 2.3.

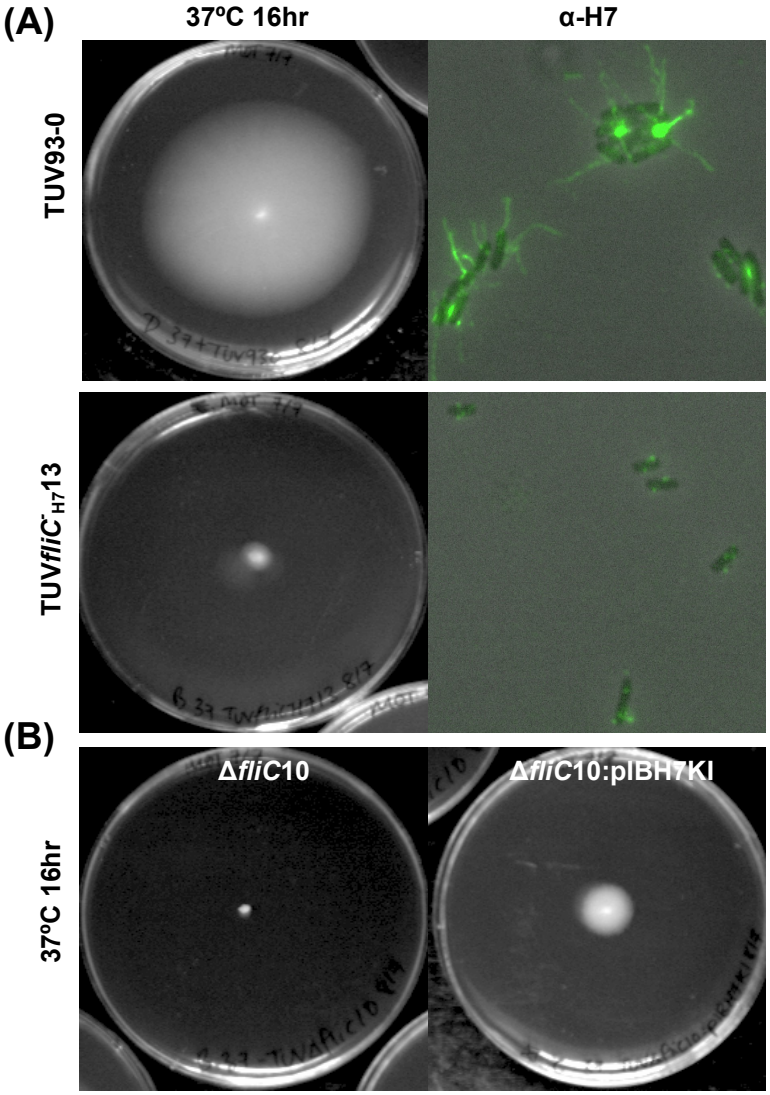

Figure A1.7. Flagella expression of TUV*fliC*$^{-}_{H7}$ clone 13 assessed by motility and immunofluorescence (methods 2.9.2 and 2.7.1). Clones 13-16 were tested and clone 13 is representative. **(A)** Comparison of flagella expression between TUV93-0 with a TUV*fliC*$^{-}_{H7}$ knock-in strain. **(B)** Parent of TUV*fliC*$^{-}_{H7}$13, TUVΔ*fliC*10 (Δ*fliC*10) and plasmid complementation by exchange vector.

Despite a successful chromosomal complementation of *fliC*, flagella expression of the $fliC_{H7}$ knock-in strains was very poor compared to the wild-type (figure A1.7). Motility of the $fliC_{H7}$ knock-in strains was restored compared to the intermediate

strain, but very obviously weak and flagella appeared to be much shorter by immunofluorescence (figure A1.7(A)). To rule out any problem with the *fliC*$_{H7}$ transferred by the allelic exchange, motility complementation of the intermediate strain TUVΔ*fliC*10 with the exchange plasmid was assessed (figure A1.7(B)). The motility halos were slightly larger than the *fliC*$_{H7}$ knock-in strains tested and more dense and consistent in shape. This indicates that the *fliC*$_{H7}$ exchanged is functional but that expression levels are compromised, possibly by the changes in the *fliC*$_{H7}$ promoter caused by introducing a BamHI site, as indicated by RNA modelling (section 2.4.1, figure 2.4).

A1.3.2 TUV*fliC*$_{H6F}$ and TUV*fliC*$_{H7F}$

A1.3.2.1 Exchange plasmids

New allelic exchange vectors for insertion of *fliC*$_{H6}$ and *fliC*$_{H7}$ were made based on the RNA modelling that contained upstream F flanking regions (table 2.2, figure 2.4). Both *fliC*$_{H6F}$ and *fliC*$_{H7F}$ vectors were made in parallel and used in allelic exchange with TUVΔ*fliC*10.

Figure A1.8 shows validation at each step in the construction of pIBH6KIF and pIBH7KIF. The insertion of the first flanking region, H7upB, for both of these vectors is confirmed in figure A1.8(A), as the ~600bp insert is cut out of pIB307 (~4.2kb). The F flanking region, H7downF, was then cloned into this plasmid, as shown in figure A1.8(B). Again this is confirmed by a ~600bp insert cut out of a plasmid that runs level with the plasmid made in figure A1.8(A) at ~5kb. Figure A1.8(C) shows the restriction digest confirmations of the final cloning to make pIBH6KIF and pIBH7KIF. *fliC*$_{H6}$ and *fliC*$_{H7}$ coding sequences are ~1.5 kb; *fliC*$_{H7}$ is actually larger than this, but the samples have run at an angle so the size estimation is inaccurate. The plasmid backbone is >5kb and runs to the same size as the the F24 plasmid featured in figure A1.8(B), run in figure A1.7(C) on the far left. As the *fliC* coding sequences are not cloned in any particular direction, clones were screened for the orientation that would allow expression (figure A1.8(D)-(E)). A ~1.5kb product

indicates the desired orientation. pIBH6KIF clone 17 (bold) and pIBH7KIF clone 6 were used in allelic exchange with TUVΔ*fliC*10 to make the new *fliC* knock-ins.

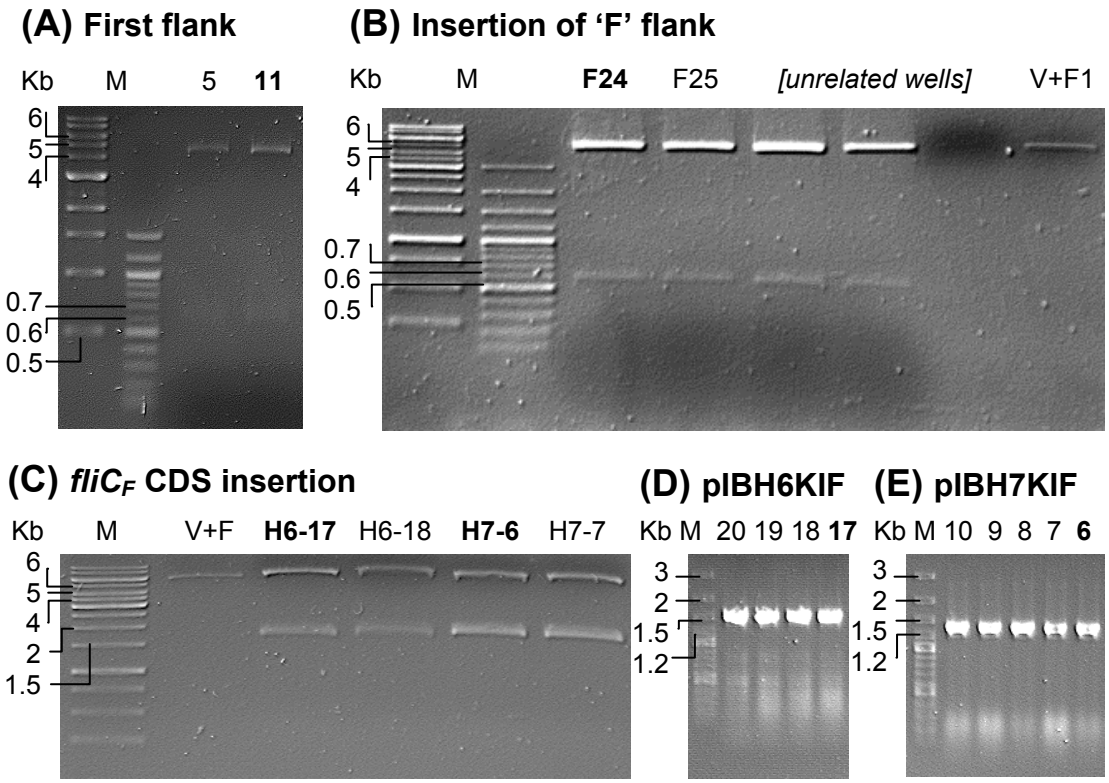

Figure A1.8. Validation of allelic exchange vectors used to make $fliC_{H6F}$ and $fliC_{H7F}$ knock-ins. **(A)** SalI/BamHI restriction digest confirmation of the H7upB flanking region insertion (used clone 11, bold). **(B)** SacI/BamHI restriction confirmation of the H7downF flanking region insertion (used clone 24 of the F flank). V+F1= vector plus first flanking region, H7upB. **(C)** BamHI restriction digest confirmation of the $fliC_{H6}$ and $fliC_{H7}$ insertion into plasmids containing F flanking regions. V+F= allelic exchange vector containing F flanking regions. **(D)** Orientation screening of $fliC_{H6F}$ by PCR using the PIBF – H6Nt4 primer pair. A ~1.5kb product indicates the correct orientation for expression. **(E)** Orientation screening of $fliC_{H7F}$ by PCR using the H7Ct4 – PIBR primer pair. A ~1.5kb product indicates the correct orientation for expression. Samples were digested with the enzymes specified (New England Biolabs), loaded into a 0.7% agarose/safe-view gel, electrophoresed at 90 V for 35 min and imaged with a UV gel-doc system (methods 2.3.4, 2.3.5, 2.3.1). Primers detailed in table 2.3 and figure 2.3.

A1.3.2.2 TUV*fliC*$_{H6F}$ and TUV*fliC*$_{H7F}$ knock-in strains

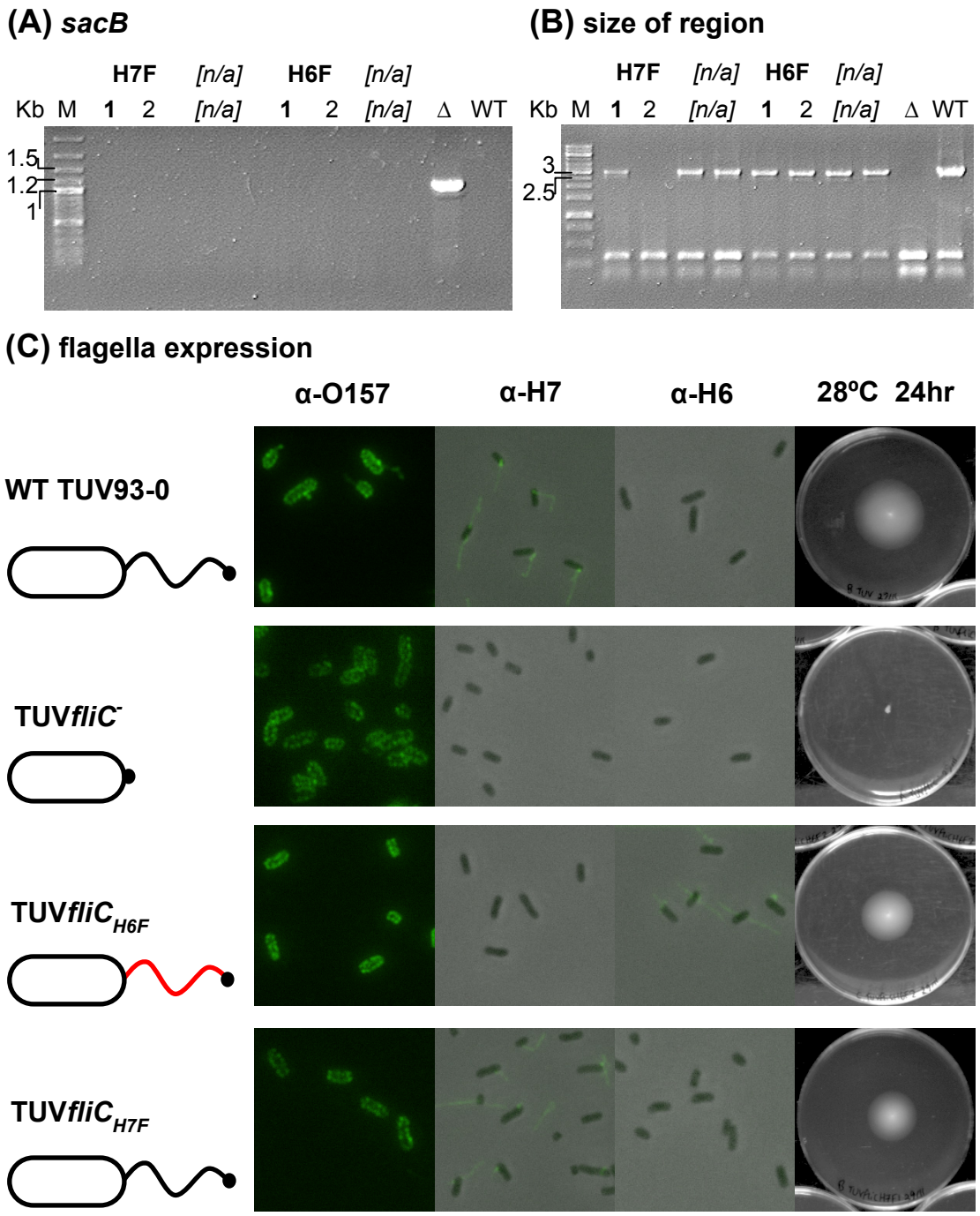

Figure A1.9. Validation of TUV*fliC*$_{H6F}$ and TUV*fliC*$_{H7F}$. **(A)** PCR screening for the absence of *sacB* using SacB-5 - SacB-3 primers. **(B)** PCR screening to compare the size of the manipulated region to TUV93-0 (WT) and TUVΔ*fliC* using 5'H7upF.SacI – 3'H7downR.SalI primers. Clones highlighted in bold were used for further study. *[n/a]* describes wells unrelated to this study. **(C)** Flagella expression and sero-specificity of TUV*fliC*$_{H6F}$1 and TUV*fliC*$_{H7F}$1. PCR, immunofluorescence and motility assays were done as in methods 2.3.4, 2.7.1 and 2.9.2 respectively. Primers detailed in table 2.3.

Not only were the allelic exchanges successful, but motility was restored in all strains tested. Figure A1.9 shows how the *fliC*$_{H6F}$ and *fliC*$_{H7F}$ knock-in strains were validated. *sacB* from the *sacB-kan*^{r} cassette was not detected by PCR (figure A1.9(A)), and the *fliC* region was the same size as in the wild-type TUV93-0 by PCR (figure A1.9(B); again the TUVΔ*fliC*10 PCR reaction across the larger region containing the *sacB-kan*^{r} cassette appears to have failed). Also, strains were all sero-typed by immunofluorescence as O157 (figure A1.9(C)). The wild-type strain and *fliC*$_{H7F}$ knock-in were also H7^{+} and H6^{-}, while the *fliC*$_{H6F}$ knock-in was H7^{-} and H6^{+}. The *fliC*$^{-}$ strain was neither H7^{+} nor H6^{+}. Flagella filaments of knock-in strains were not short as with the previous method, but fully formed. Figure A1.9(C) also shows that the motility of the *fliC* knock-ins, while not quite as much as the wild-type, was at least comparable.

A1.4 Validation of TUVΔ*fliD* and TUV*fliD*$^{-}$

A1.4.1 Exchange plasmids

Figure A1.10 shows restriction digest confirmation of each insert that was cloned into the exchange plasmids (figure 2.2) to make *fliD*$_{H7}$ mutants. pIBXFliD was used to make TUVΔ*fliD* from TUV93-0 and pIBXSKFliD was used to make TUV*fliD*$^{-}$ from TUVΔ*fliD*. The ~0.6kb *fliD* flanking region FliDdown has been cut out of the 4.2kb pIB307 backbone in figure A1.10(A). The ~0.6kb *fliD* flanking region FliDup has been cut out of the 5kb pIB307+FliDdown backbone in figure A1.10(B), which is visibly larger than pIB307 alone (V), confirming the construction of pIBXSKFliD. Figure A1.10(C) shows the restriction digest confirming the insertion of the *sacB::kan*^{r} cassette (3.8kb) into pIBXSKFliD (V+F, 5.6kb) to make pIBXFliD.

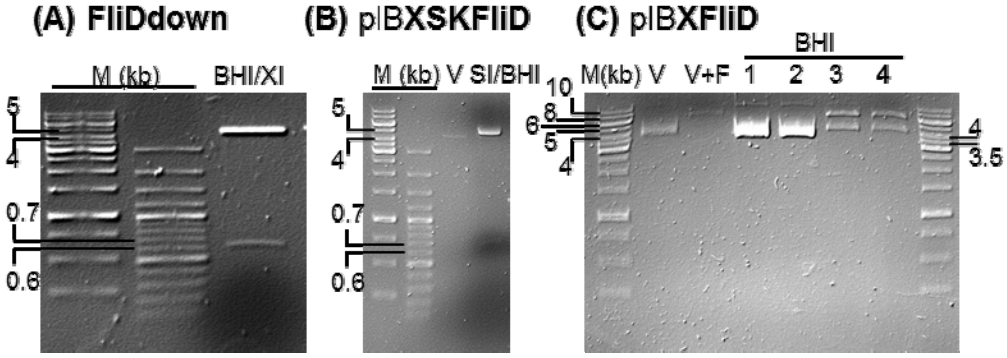

Figure A1.10. Restriction digest confirmation of inserts in exchange plasmids used to make TUVΔ*fliD* (pIBXFliD) and TUV*fliC*$^{-}$ (pIBXSKFliD). **A)** BamHI/XbaI digest of pIB307 containing FliDdown flanking region (BHI/XI) to confirm its insertion. **(B)** SacI/BamHI digest of pIBXSK$_{tuv}$ (SI/BHI) to confirm insert of 2nd flank, FliDup, and presence of 1st flank compared to pIB307 (empty vector, V). **(C)** BamHI digests of pIBXFliD (BHI) to confirm the insertion of gel purified *sacB::kan*^{r} cassette into pIBXSK$_{tuv}$ (vector and flanks, V+F). Samples were digested with the enzymes specified (New England Biolabs), loaded into a 0.7% agarose/safe-view gel, electrophoresed at 90 V for 35 min and imaged with a Bio-Rad 1000 UV gel-doc system (methods 2.3.1 and 2.3.5).

A1.4.2 Intermediate strain TUVΔ*fliD*

After allelic exchange of TUV93-0 with pIBXFliD, clones were screened as detailed in methods 2.3.12.1. The results from kan^{r}, cam^{s} clones screened by PCR for the presence of *sacB* and the correct sized *fliD*$_{H7}$ region are shown in figure A1.11. Clone 1 was *sacB*$^{+}$ (figure A1.11(A)) and had a *fliD*$_{H7}$ region of ~5kb instead of ~2kb (figure A1.11(B)) and was non-motile (figure A1.11(C)). The mutation in clone 10 was non-polar, as the motility was restored by plasmid complementation (data not shown). Therefore TUVΔ*fliD*1 was used as the intermediate strain for further allelic exchanges in this study.

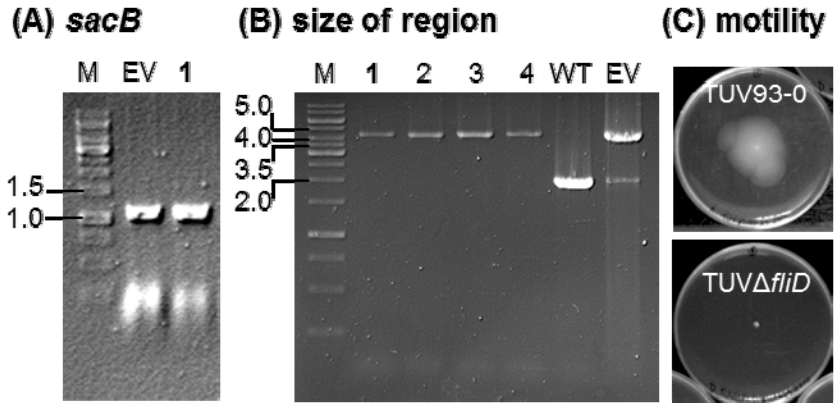

Figure A1.11. Validation of TUVΔ*fliD*. Clone 1 (bold) was used as the intermediate strain. WT= TUV93-0, EV= exchange vector pIBXFliD, a positive control. **(A)** The presence of *sacB* (1.2kb) was screened by PCR for with SacB-5 - SacB-3 primers. **(B)** The size of the altered region was screened by PCR using FliDupF.SacI – FliDdownR.XbaI primers. The region is the same size as pIBXFliD (EV), shown. PCR was done using Quick-Load *Taq* 2x master mix (New England Biolabs) as detailed in methods 2.3.4. **(C)** Motility of TUVΔ*fliC*1 compared to TUV93-0 in 0.3% agar after 28ºC for 24 hr (methods 2.9.2). Primers detailed in table 2.3.

A1.4.3 Isogenic strain TUV*fliD*$^{-}$

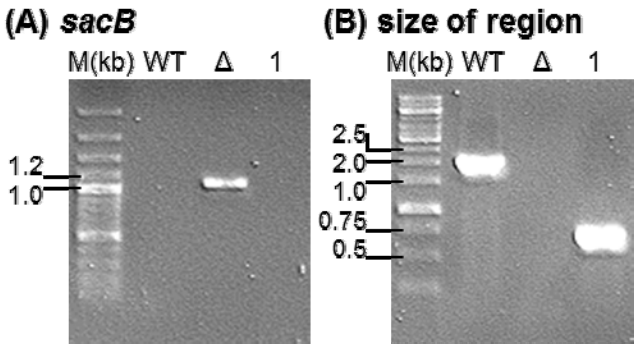

Figure A1.12. Validation of TUV*fliD*$^{-}$ clone 1 (1). **(A)** PCR screening for the absence of *sacB* using SacB-5 - SacB-3 primers. TUV93-0 (WT) was a positive control and TUVΔ*fliD* (Δ) was a negative control. **(B)** PCR screening to compare the size of the manipulated region to TUV93-0 (WT) and TUVΔ*fliD* (Δ) using 5'NtFliDHISF – FliDdownR.XbaI primers. PCR was undertaken as in methods 2.3.4 and motility validation is shown in figure 3.8. Primers detailed in table 2.3.

Allelic exchange was carried out between TUVΔ*fliD*1 and pIBXSKFliD and screened according to section 2.3.12.2 to make an isogenic $fliD_{H7}$ deletion, TUV*fliD*$^{-}$. PCR validation of some of the kan^{s}, cam^{s} clones, as was done with TUV*fliC*$^{-}$ is

shown in figure A1.12. Figure A1.12(A) shows that TUVΔ*fliD*1 is *sacB*$^{+}$ and TUV93-0 and TUV*fliD*$^{-}$1 is not. Figure A1.12(B) shows the size of the mutated region in TUV93-0 (WT, ~2kb) and TUV*fliD*$^{-}$1 (1, ~0.6kb). These sizes are as expected if they were to contain the $fliD_{H7}$ and FliDdown or just FliDdown respectively. Once again, the screening PCR for the intermediate strain has failed, as in figure A1.5(B), presumably for similar reasons. However, the size of the $fliD_{H7}$ region in TUV*fliD*$^{-}$1 and its lack of motility (figure 3.8), confirms the absence of $fliD_{H7}$ or the *sacB-kan*^{r} cassette next to a $fliD_{H7}$ flanking region. TUV*fliD*$^{-}$1 was therefore used as TUV*fliD*$^{-}$ for further study.

A1.5 *E. coli* O157 PCR screening of mutant strains

The mutant strains made in this study and validated in this appendix were screened with O157-specific primers by PCR as described in table 2.3 and sections 2.3.4 and 2.3.12. In the conditions tested, these primers yield a 259bp product, but only with DNA from *E. coli* O157 strains. Figure A1.13 shows that all strains screened had a 200-300bp product, indicating that they are *E. coli* O157.

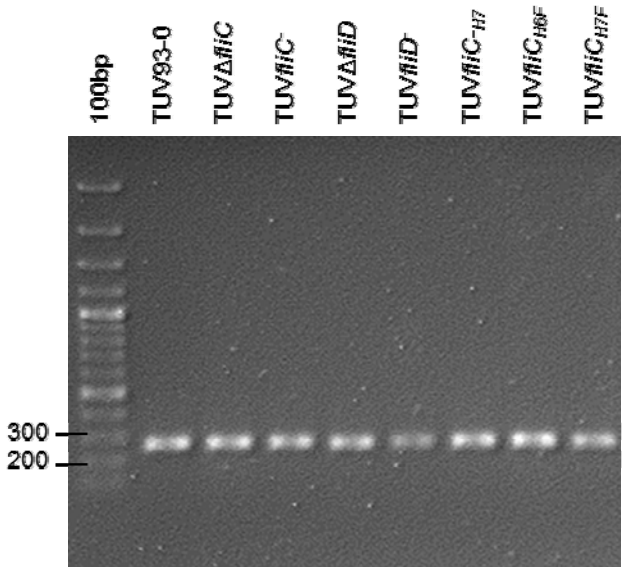

Figure A1.13. Agarose electrophoresis of an O157-specific PCR screen of cell-lysates from strains made in this study.